



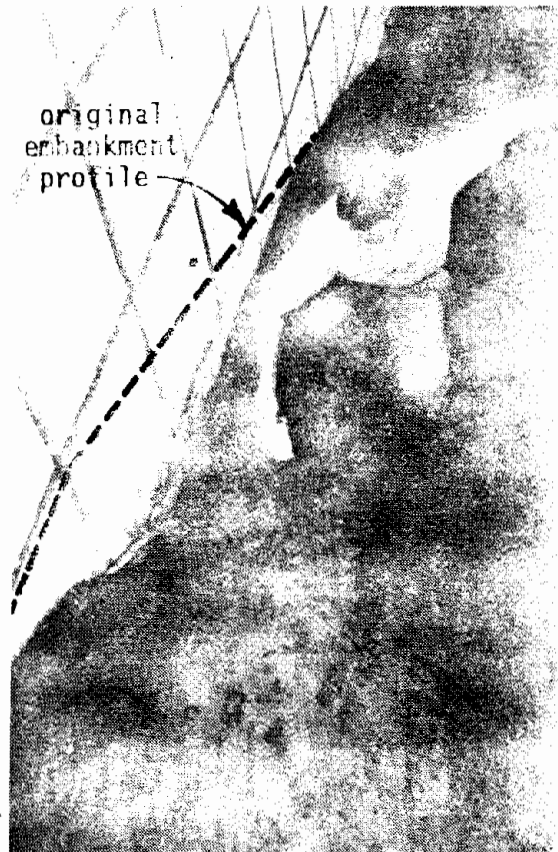
U.S. Department
of Transportation

Federal Highway
Administration

Cosponsored by:

U.S. Dept. of Interior
Bureau of Reclamation
Denver, Co. 80225

MINIMIZING EMBANKMENT DAMAGE DURING OVERTOPPING FLOW



Research, Development, and Technology
Turner-Fairbank Highway Research Center
6300 Georgetown Pike
McLean, Virginia 22101-2296

Publication no. FHWA-RD-88-181
November 1988

REPRODUCED BY
U.S. DEPARTMENT OF COMMERCE
NATIONAL TECHNICAL
INFORMATION SERVICE
SPRINGFIELD, VA 22161

1. Report No. FHWA-RD-88-181		2. Government Accession No. PB90-266107		3. Recipient's Catalog No. FHWA-RD-88-181	
4. Title and Subtitle MINIMIZING EMBANKMENT DAMAGE DURING OVERTOPPING FLOW				5. Report Date November 1988	
				6. Performing Organization Code	
7. Author(s) Paul E. Clopper Yung-Hai Chen				8. Performing Organization Report No.	
9. Performing Organization Name and Address Simons, Li & Associates, Inc. 3555 Stanford Road P.O. Box 1816 Fort Collins, CO 80522				10. Work Unit No. (TRAIS) NCP 3D32062	
				11. Contract or Grant No. DTFH61-85-C-00131	
12. Sponsoring Agency Name and Address Office of Engineering & Highway Operations R & D Federal Highway Administration 6300 Georgetown Pike McLean, VA 22101-2296				13. Type of Report and Period Covered Final Report Oct 1985 - Aug 1988	
				14. Sponsoring Agency Code	
15. Supplementary Notes Contracting Officer's Technical Representative: J. Sterling Jones Co-Sponsoring Agency: U.S. Department of the Interior (HNR-10) Bureau of Reclamation Denver Federal Center, Denver, CO					
16. Abstract The hydraulic and erosional characteristics of overtopping flow are examined. Methods of protecting earth embankments of dams, levees, and roadways from damage during overtopping flow are investigated. Nineteen full-scale tests of bare earth embankments (unprotected) were conducted to derive baseline erosion rate relationships. Thirty-eight full-scale hydraulic tests examined the performance of selected commercially available embankment protection systems under various hydraulic conditions. Failure modes and hydraulic stresses at the the failure threshold were determined and compared to results from other investigators. Design and installation considerations are presented which address observed failure modes.					
17. Key Words overtopping, embankment, erosion, erosion protection systems, hydraulics, shear stress, channels, spillways, floods			18. Distribution Statement No restrictions. This document is available to the public through the National Technical Information Service (NTIS), Springfield, VA 22161		
19. Security Classif. (of this report) Unclassified		20. Security Classif. (of this page) Unclassified		21. No. of Pages 228	22. Price

SI* (MODERN METRIC) CONVERSION FACTORS

APPROXIMATE CONVERSIONS TO SI UNITS

Symbol	When You Know	Multiply By	To Find	Symbol
--------	---------------	-------------	---------	--------

LENGTH

in	inches	25.4	millimetres	mm
ft	feet	0.305	metres	m
yd	yards	0.914	metres	m
mi	miles	1.61	kilometres	km

AREA

in ²	square inches	645.2	millimetres squared	mm ²
ft ²	square feet	0.093	metres squared	m ²
yd ²	square yards	0.836	metres squared	m ²
ac	acres	0.405	hectares	ha
mi ²	square miles	2.59	kilometres squared	km ²

VOLUME

fl oz	fluid ounces	29.57	millilitres	mL
gal	gallons	3.785	litres	L
ft ³	cubic feet	0.028	metres cubed	m ³
yd ³	cubic yards	0.765	metres cubed	m ³

NOTE: Volumes greater than 1000 L shall be shown in m³.

MASS

oz	ounces	28.35	grams	g
lb	pounds	0.454	kilograms	kg
T	short tons (2000 lb)	0.907	megagrams	Mg

TEMPERATURE (exact)

°F	Fahrenheit temperature	5(F-32)/9	Celsius temperature	°C
----	------------------------	-----------	---------------------	----

APPROXIMATE CONVERSIONS FROM SI UNITS

Symbol	When You Know	Multiply By	To Find	Symbol
--------	---------------	-------------	---------	--------

LENGTH

mm	millimetres	0.039	inches	in
m	metres	3.28	feet	ft
m	metres	1.09	yards	yd
km	kilometres	0.621	miles	mi

AREA

mm ²	millimetres squared	0.0016	square inches	in ²
m ²	metres squared	10.764	square feet	ft ²
ha	hectares	2.47	acres	ac
km ²	kilometres squared	0.386	square miles	mi ²

VOLUME

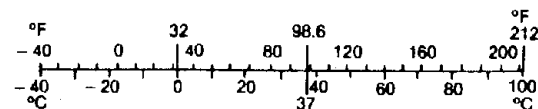
mL	millilitres	0.034	fluid ounces	fl oz
L	litres	0.264	gallons	gal
m ³	metres cubed	35.315	cubic feet	ft ³
m ³	metres cubed	1.308	cubic yards	yd ³

MASS

g	grams	0.035	ounces	oz
kg	kilograms	2.205	pounds	lb
Mg	megagrams	1.102	short tons (2000 lb)	T

TEMPERATURE (exact)

°C	Celsius temperature	1.8C + 32	Fahrenheit temperature	°F
----	---------------------	-----------	------------------------	----



* SI is the symbol for the International System of Measurement

(Revised April 1989)

TABLE OF CONTENTS

Page

INTRODUCTION

1. Description of Problem	1
2. Project Objectives	2
3. Organization of Report	4

REVIEW OF EXISTING INFORMATION PERTAINING TO OVERTOPPING FLOW AND EROSION PROTECTION

1. Hydraulic Characteristics of Overtopping Flow	5
a. Discharge Equations for Flow Over an Embankment	6
b. Flow Regimes	8
(1) Zone One - Subcritical Flow Over Embankment Crest	8
(2) Zone Two - Supercritical Flow Over The Embankment Crest	9
(3) Zone Three - Supercritical Flow On The Downstream Slope of the Embankment	9
c. Pressure and Velocity	9
d. Shear Stress and Stream Power	12
2. Erosional Characteristics of Overtopping Flow	16
a. Erosion Process	16
b. Embankment Erosion Zones	18
3. Case Studies of Dam, Levees, and Road Embankment Overtopping Events	21
4. Behavior of Embankments and Protection Systems	21
a. Vegetation	27
b. Geotextile	31
c. Chemical	39
d. Cements	40
e. Concrete Blocks	42
f. Gabions	44
g. Riprap	45
h. Bare Soil Embankments	46
5. Summary of Protection Systems	47
a. Vegetation	49
b. Geotextile	49
c. Chemical	49

TABLE OF CONTENTS (continued)

	<u>Page</u>
d. Cements	54
e. Concrete Blocks	54
f. Gabions	56
g. Riprap	56

DESCRIPTION OF FULL-SCALE EMBANKMENT TESTING PROGRAM

1. General	61
2. Data Collection Procedure	63
3. Documentation of Test Conditions and Qualitative Assessment of Performance	64
a. Test Series 1: Type II Soil (CL)	70
(1) Embankment Construction and Installation	73
(2) Description of Hydraulic Test Conditions	73
(3) Qualitative Description of Type II Soil Performance	73
b. Test Series 2: Type I Soil (SM-SC)	74
(1) Embankment Construction and Installation	74
(2) Description of Hydraulic Test Conditions	77
(3) Qualitative Description of Type I Soil Performance	77
c. Test Series 3: Soil Cement	78
(1) Installation of Protection System	78
(2) Description of Hydraulic Test Conditions	80
(3) Qualitative Description of Soil Cement Performance	85
d. Test Series 4: Gabion Mattresses	85
(1) Installation of Protection System	85
(2) Description of Hydraulic Test Conditions	87
(3) Qualitative Description of Gabion Mattresses Performance	90
e. Test Series 5: Geoweb	92
(1) Installation of Protection System	92
(2) Description of Hydraulic Test Conditions	94
(3) Qualitative Description of Geoweb Performance	94

TABLE OF CONTENTS (continued)

	<u>Page</u>
f. Test Series 6: Enkamat (7020)	98
(1) Installation of Protection System	98
(2) Description of Hydraulic Test Conditions	99
(3) Qualitative Description of Enkamat Performance	102
g. Test Series 7: Enkamat (7020) With Asphalt	102
(1) Installation of Protection System	102
(2) Description of Hydraulic Test Conditions	104
(3) Qualitative Description of Enkamat-With-Asphalt Performance	108
h. Test Series 8: Cable-tied Concrete Block Mattresses	108
(1) Description of the Armorflex Product	112
(2) Installation of the Armorflex System	112
(3) Description of Armorflex Hydraulic Test Conditions	114
(4) Description of the Petraflex-Vick System	114
(5) Installation of the Petraflex-Vick Product	116
(6) Description of Petraflex-Vick Hydraulic Test Conditions	117
(7) Description of the Dycel Product	120
(8) Installation of the Dycel System	120
(9) Description of Dycel Hydraulic Test Conditions	121
(10) Qualitative Description of Cable-Tied Concrete Block Mattress Performance	121

RESULTS OF FULL-SCALE EMBANKMENT TESTING PROGRAM

1. Determination of Test Discharges	130
2. Computation of Hydraulic Parameters	130
3. Analysis Methodology for Freefall Conditions	131
a. Computation of Bed Shear Stress	132
b. Computation of Flow Resistance	134
4. Results for Freefall Conditions	134
a. Bare Soil Embankments	136
b. Embankment Protection Measures	148
(1) Soil Cement	153
(2) Gabion Mattresses	153
(3) Geoweb	157

TABLE OF CONTENTS (continued)

	<u>Page</u>
(4) Enkamat	158
(5) Enkamat with Asphalt	158
(6) Articulating Concrete-Block Revetment Systems	158
5. Uplift Forces and the Subatmospheric Pressure Zone	159
COMPARISON OF CURRENT TEST PROGRAM RESULTS TO OTHER INVESTIGATIONS	
1. General	172
2. Nonreinforced Grass Protection	173
3. Soil Cement ProtectionSystems	174
4. Gabion Mattress Protection Systems	175
5. Geoweb ProtectionSystems	176
6. Enkamat ProtectionSystems	178
7. Enkamat-with-Asphalt Protection Systems	179
8. Concrete Block Protection Systems	180
a. Dycel Blocks	181
b. Armorflex Blocks	181
c. Petraflex-VickBlocks	182
9. Summary and Conclusions	183
DESIGN AND INSTALLATION CONSIDERATIONS	
1. Hydraulic Considerations	186
2. Installation Considerations	193
3. Cost Considerations	199
GLOSSARY OF TERMS	203
REFERENCES	207

LIST OF FIGURES

<u>Figure</u>	<u>Page</u>
1. Progressive stages of unprotected embankment erosion under freefall and high tailwater conditions	3
2. Discharge coefficients for flow over roadway embankment	7
3. Hydraulic flow regimes and overtopping flow zones	10
4. Comparison of theoretical nappe geometry versus rigid embankment for determination of subatmospheric pressure zone	13
5. Theoretical pressure distribution on downstream slope corresponding to a 4-ft (1.2m) overtopping flow	14
6. Variation of the theoretical maximum negative pressure developed during various overtopping depths of flow	14
7. Retardance curves and vegetal classifications	29
8. Typical failure mechanisms exhibited by vegetative linings	32
9. Recommended limiting values for erosion resistance of plain and reinforced grass	35
10. Profile of hydraulic testing facility	62
11. Partial listing of EMBANK data and results for test 49	65
12. Embankment, water-surface, and energy grade line profiles for test 49	66
13. Partial listing of VEL268 data for test 49.	67
14. Moisture-density curve for the type II soil	71
15. Grain-size distribution curve for the type II soil	72
16. Moisture-density curve for the type I soil	75
17. Grain-size distribution curve for the type I soil	76

LIST OF FIGURES (continued)

<u>Figure</u>	<u>Page</u>
18. Grain-size distribution curve for the soil cement aggregate	79
19. Sketch of the soil cement embankment (3H:1V slope)	81
20. Profile of the soil cement embankment (3H:1V slope)	82
21. Profile of the soil cement embankment (2H:1V slope)	83
22. Typical soil cement installation	84
23. Sketch of 6-in (15.2 cm) gabion mattress and lid	86
24. Sketch of typical 6-in (15.2 cm) gabion mattress system	88
25. Typical 6-in (15.2 cm) mattress installation	89
26. Failure of the gabion mattress system for test 24	91
27. Geoweb grid confinement system	93
28. Sketch of the geoweb protection system	95
29. Washed river rock [1 to 2 in (2.5 to 5.0 cm) diameter] used to fill the geoweb cells	96
30. Geoweb protection system with Tenax netting in place	97
31. Sketch of Enkamat 7020 protection system	100
32. Enkamat 7020 embankment protection system	101
33. Grain size distribution curve for the asphalt aggregate	103
34. Sketch of Enkamat 7020 with 3-in (7.6 cm) asphalt cover	105
35. Sketch of Enkamat 7020 with 1-in (2.5 cm) asphalt cover	106
36. Enkamat with 1-in (2.5 cm) asphalt cover embankment protection system	107
37. Failure of the enkamat with 1-in (2.5 cm) asphalt cover protection system	109
38. Sketches of the three types of concrete blocks tested	111

LIST OF FIGURES (continued)

<u>Figure</u>	<u>Page</u>
39. Typical concrete block revetment system configuration	113
40. Completed Armorflex embankment protection system prior to placement of crushed rock in fill	115
41. Anchoring system for the Petraflex-Vick revetment	118
42. Completed Petraflex-Vick concrete block embankment protection system	119
43. Completed Dycel concrete block embankment protection system	122
44. Anchoring system for the Dycel 100 revetment	123
45. Dycel block system after failure, showing displacement of individual blocks	125
46. Dycel block system after failure, showing deformation of embankment	126
47. Localized failure exhibited by the Armorflex system	127
48. Petraflex-Vick concrete block mattress after testing	129
49. Control volume for test 49	133
50. Typical control volume with momentum equation parameters	135
51. Bed shear versus unit discharge for bare soil freefall tests	138
52. Flow velocity versus unit discharges for bare soil freefall tests	139
53. Flow depth versus unit discharges for bare soil freefall tests	140
54. Erosion pattern for the test 29 bare soil embankment under freefall conditions	142
55. Erosion pattern for the test 33 bare soil embankment under tail water conditions	143
56. Hourly erosion rates for tests 29 and 33	145

LIST OF FIGURES (continued)

<u>Figure</u>	<u>Page</u>
57. Erosion pattern for the test 54 bare soil embankment, loosely compacted, under freefall conditions	146
58. Detachment rate regression equations for soil types I and II	149
59. Bed shear versus unit discharge for protection system freefall tests	154
60. Flow velocity versus unit discharge for protection system freefall tests	155
61. Flow depth versus unit discharges for protection system freefall tests	156
62. Profile of water nappe and theoretical subatmospheric pressure zone	161
63. Theoretical pressure variation with distance from crest for 4-ft (1.2 m) overtopping depth	163
64. Theoretical maximum negative pressure variation with overtopping depth	163
65. Theoretical negative pressure profile for test 49	164
66. Pressure transducer readings taken during test 46A	165
67. Pressure transducer readings taken during test 52	166
68. Pressure transducer readings taken at station 40 during test 47	168
69. Typical tailwater conditions	194
70. Typical crest details for selected protection systems	196
71. Typical cross section through protected waterway showing side termination options	198
72. Examples of typical toe termination details	200

LIST OF TABLES

<u>Table</u>	<u>Page</u>
1. Maximum permissible velocities recommended by Fortier and Scobey and the corresponding unit-tractive-force values converted by the U.S. Bureau of Reclamation	17
2. Existing embankment erosion equations	19
3. Overtopping events at dam and levee embankments	22
4. Overtopping events at roadway embankments	25
5. Summary of characteristics of CIRIA tested geotextile protection systems	37
6. Summary of CIRIA tests on geotextile-reinforced steep-grassed channels	38
7. Summary of results of USBR's overtopping flow tests	48
8. Maximum permissible velocities for vegetative linings	50
9. Maximum permissible shear stresses for vegetative linings	51
10. Manning's roughness coefficients for selected geotextiles	52
11. Permissible shear stresses for selected geotextiles	53
12. Permissible shear stresses for cement-stabilized soil	55
13. Summary of characteristics of CIRIA-tested concrete protection systems	57
14. Summary of CIRIA tests on concrete-reinforced grass channels	58
15. Permissible shear stress for gravel and rock riprap	60
16. Summary of hydraulic test conditions	68
17. Shear stress and bed roughness analysis results for bare soil embankments under freefall conditions	137
18. Measured erosion rates for bare soil embankment tests	144
19. Comparison of FHWA phase I and FHWA phase II soil characteristics and detachment rate equations parameters	150
20. Shear stress and bed roughness analysis results for soil cement, gabion mattress, and geoweb protection systems under freefall conditions	151

LIST OF TABLES (continued)

<u>Table</u>		<u>Page</u>
21.	Shear stress and bed roughness analysis results for enkamat with asphalt and concrete-block mattress protection systems under freefall conditions	152
22.	Subatmospheric pressure analysis for enkamat with asphalt and concrete-block mattress protection systems under freefall conditions	169
23.	Summary of critical velocity and shear stress for various protection measures	185
24.	Recommended values of the Manning's roughness coefficient for various protection systems during overtopping flow	188
25.	Recommended values of the Darcy friction factor" f" for various protection systems during overtopping flow	190
26.	Limiting values of shear stress observed for the FHWA embankment testing program for various protection systems	191
27.	Representative costs of various protection systems	202

INTRODUCTION

1. Description of Problem

Erosion as a result of overtopping flow has been identified as a principal cause of failure of earth embankments. When an embankment is expected to overtop during a flood event, most members of the water resources engineering profession assume that severe damage or even total failure will result. In the case of roadway embankments, this usually implies that roads will be taken out of service for some period of time while costly repairs are made. In the case of dam and levee embankments, where serious property damage or loss of life may occur in the event of failure, this assumption has led to a general rule that embankments must not be allowed to overtop.

When hydrologic and hydraulic analyses indicate that a potential for overtopping exists, the typical approach to mitigation usually involves costly modifications to spillways, raising the embankment, modifying reservoir operating rules, or a combination of these measures. The U.S. Bureau of Reclamation has estimated that over 57,000 dam embankments in the United States alone could potentially experience overtopping. The number of miles of roadway and levee embankments which could be threatened by overtopping has not been estimated, but certainly can be considered significant in terms of the economic burden associated with repair and maintenance of this aspect of the nation's infrastructure.

If embankments could be modified in a cost-effective way to allow safe overtopping along a portion of their length, economic benefits could be realized on a national scale. During recent years, a number of Federal agencies and private consulting firms in the United States and in at least one foreign country have conducted research activities on the processes of embankment damage during overtopping flow and on methods of protecting embankments when overtopping occurs.

Unprotected embankments exhibit erosional rates and patterns which are governed by soil type and compaction, embankment geometry, depth and velocity

of overtopping flow, and the presence or absence of downstream tailwater. Local surface discontinuities such as trees or shrubs, embankment/foundation intersection, or embankment groin areas tend to accelerate the initiation and propagation of erosion through a change in momentum, increased turbulence, and concentration of flow. In general, embankment erosion under freefall (low tailwater) conditions is more severe than when high tailwater is present, all other factors being equal. This is because the high tailwater pool provides some dissipation of energy on the downstream slope. Erosion patterns are qualitatively different for these two cases as well. As indicated in figure 1, erosion under the freefall condition tends to initiate at the embankment toe, and progressively works upstream as a headcut. Given sufficient duration and overtopping flow depth, this process may ultimately result in a serious breach of the embankment. Also shown in figure 1 is the erosion pattern typically produced during overtopping with high tailwater. In this case, erosion tends to initiate at the downstream shoulder, propagating both up and downstream with time. A total embankment breach is not necessarily an inevitable outcome of this condition as a balance of forces may become established whereby the embankment profile becomes stable.

2. Project Objectives

The objectives of this project were as follows:

- Collect available information on the various aspects of overtopping flow, including theoretical developments, results of research by other investigators for both bare earth and protected embankments, and field observations.
- Conduct full-scale tests of bare earth embankments and protected embankments to obtain a qualitative understanding of failure mechanisms, and to provide a quantitative assessment of hydraulic conditions at either the failure threshold of the protection systems or the maximum capacity of the testing facility, whichever was less.
- Compare results of testing program to experiences documented by other researchers.
- Identify data gaps.
- Based on the above objectives, develop, where possible, preliminary design recommendations for the protection of embankments against erosion induced by overtopping flow.

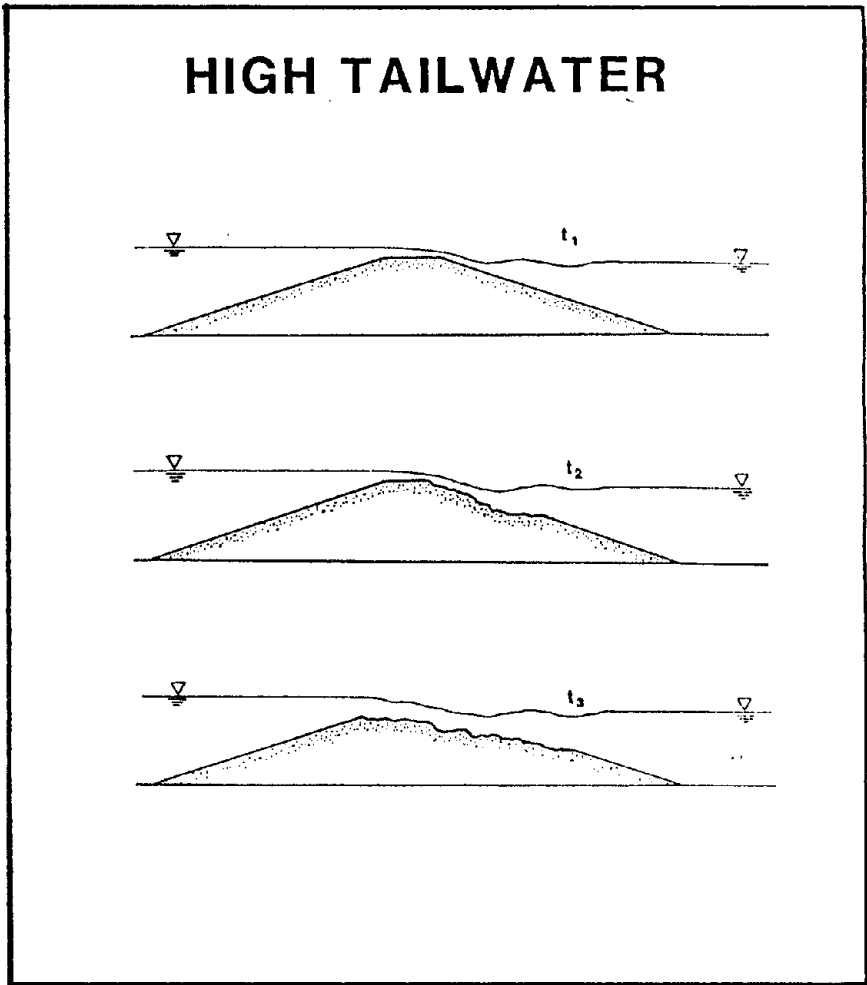
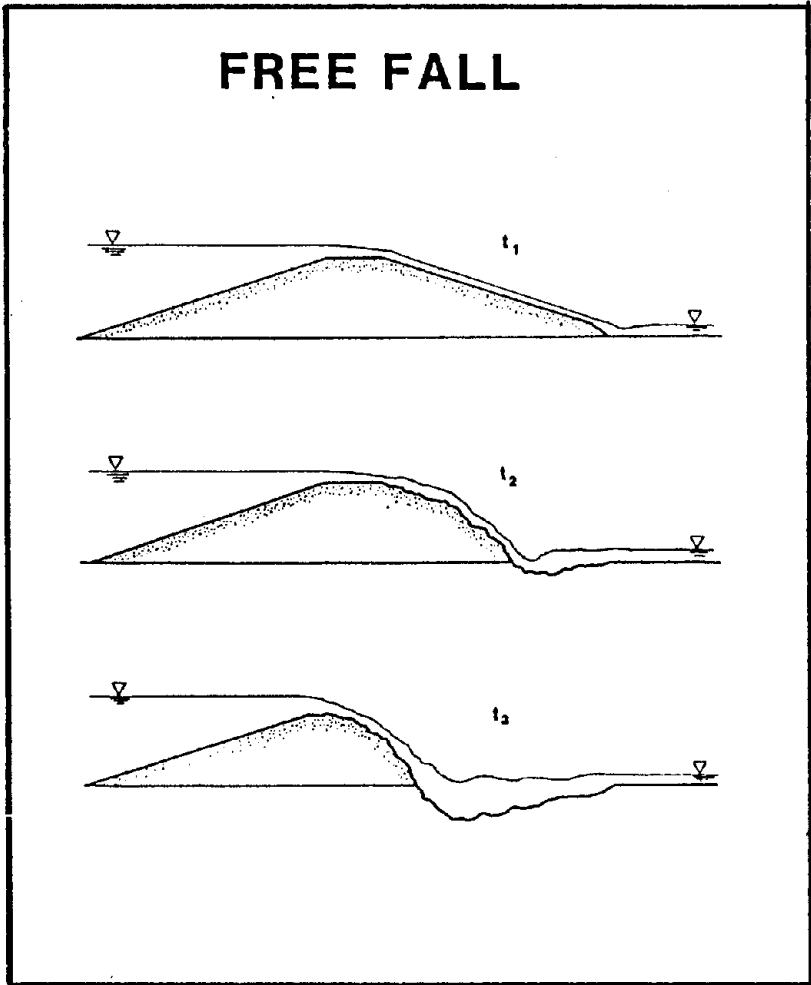


Figure 1. Progressive stages of unprotected embankment erosion under freefall and high tailwater conditions.

- Obtain representative unit cost data for each of the protection systems investigated.

3. Organization of Report

This report begins with a summary of previous findings relating to the hydraulic characteristics of overtopping flow, the initiation and progression of erosion damage to unprotected embankments, and the documented performance of systems designed to protect against such damage.

The next section documents, in detail, the performance of the full-scale hydraulic tests conducted under the current contract (DTFH61-85-00131). This includes a description of the test facility and test methodology, documentation of embankment construction procedures and installation of protection systems, description of data collection procedures, and a qualitative discussion of the performance of each protection system investigated.

The subsequent section details the analysis methodology utilized to determine hydraulic parameters and stress levels from the test data. Included in this section are summary tables of the test results and rates of soil loss for the bare soil embankment tests.

The following section provides a comparison of the test results with the experience obtained in other investigations. Failure mechanisms and threshold hydraulic stress levels are compared and contrasted based on system installation details, presence or absence of vegetation, and method of testing. Where differences exist which cannot be reconciled with existing data, the data gap is noted with recommendations for additional study.

Recommendations for design and installation guidelines are also provided. These are presented within the context of the foregoing developments and are based on theoretical considerations, results of controlled experimental research, and field experience.

REVIEW OF EXISTING INFORMATION PERTAINING TO OVERTOPPING FLOW AND EROSION PROTECTION

This section presents a review of available information relating to the hydraulic and erosion characteristics of overtopping flow, and methods designed to prevent, minimize, or delay embankment damage when overtopping occurs. The emphasis of the literature review portion of this section deals with recent research activities pertaining to steep slope applications. In addition, a summary of documented overtopping events which have occurred at dams, levees, and roadways is presented.

1. Hydraulic Characteristics of Overtopping Flow

An understanding of the hydraulics of water flowing over an embankment provides a basis for defining the mechanics of the erosion process. Several studies have been conducted in the past concerning this topic. Perhaps the most comprehensive material is found in the USGS water supply paper by Kindsvater.⁽¹⁾ The purpose of his research was to determine the discharge characteristics of embankment-shaped weirs so the USGS could make more accurate estimates of flood discharges. Various flow patterns have been observed as water flows over an embankment. These flow patterns were classified in Kindsvater as (1) free-plunging flow, (2) free surface flow, and (3) submerged flow.⁽¹⁾

For the low-tailwater condition known as free flow, critical depth occurs on the embankment crest, and the discharge is dependent upon the upstream head. At higher tailwater levels, when the flow depth over the crest is greater than the critical depth, the discharge is controlled by both the tailwater and the headwater. Under conditions of tailwater control, the flow is said to be submerged. With a rising tailwater level, the change from free flow to submerged flow occurs rather abruptly. The flow pattern antecedent to the transition is described as incipient submergence.

Free flow is subclassified into plunging flow and surface flow. Plunging flow occurs when the jet plunges under the tailwater surface, producing a submerged hydraulic jump on the downstream slope. Surface flow

occurs when the jet separates from the crest surface at the downstream shoulder and "rides" over the tailwater surface. Whereas free flow can be either a plunging or a surface flow, submerged flow is always a surface flow.

A detailed summary of Kindsvater's paper is presented in the Federal Highway Administration Report, "Development of a Methodology for Estimating Embankment Damage Due to Flood Overtopping."(1,2)

a. Discharge Equations for Flow Over an Embankment

The widely used form of the equation that computes discharge over an embankment for the free-flow condition is

$$q = C H_1^{3/2} \quad (1)$$

where q is the discharge per unit width, C is a coefficient that has been determined experimentally, and H_1 is the total head above the embankment crest as defined in figure 2. Using Kindsvater's data for a smooth roadway surface, Bradley presented figure 2 to determine the discharge coefficient.(1,3) To determine the discharge flowing over a roadway, with a width (W), first enter chart B (figure 2) with H_1/W and obtain the free-flow coefficient of discharge C . Should the value of H_1/W be less than 0.15, it is suggested that C be read from chart A of the same figure. If submergence is present (i.e., if t/H_1 is larger than 0.7), enter chart C with the proper value of submergence in percent and scale off the submergence factor C_s/C . The resulting discharge is calculated by substituting values in the equation:

$$Q = C L H_1^{3/2} \frac{C_s}{C} \quad (2)$$

where L represents the length of inundated roadway, H_1 is the total upstream head measured with respect to the crown of the roadway, and C and C_s are coefficients of discharge for free and submerged flow, respectively. Where the depth of overflow varies along the roadway, it is advisable to separate the inundated portion into segments and compute the discharge over each reach separately.

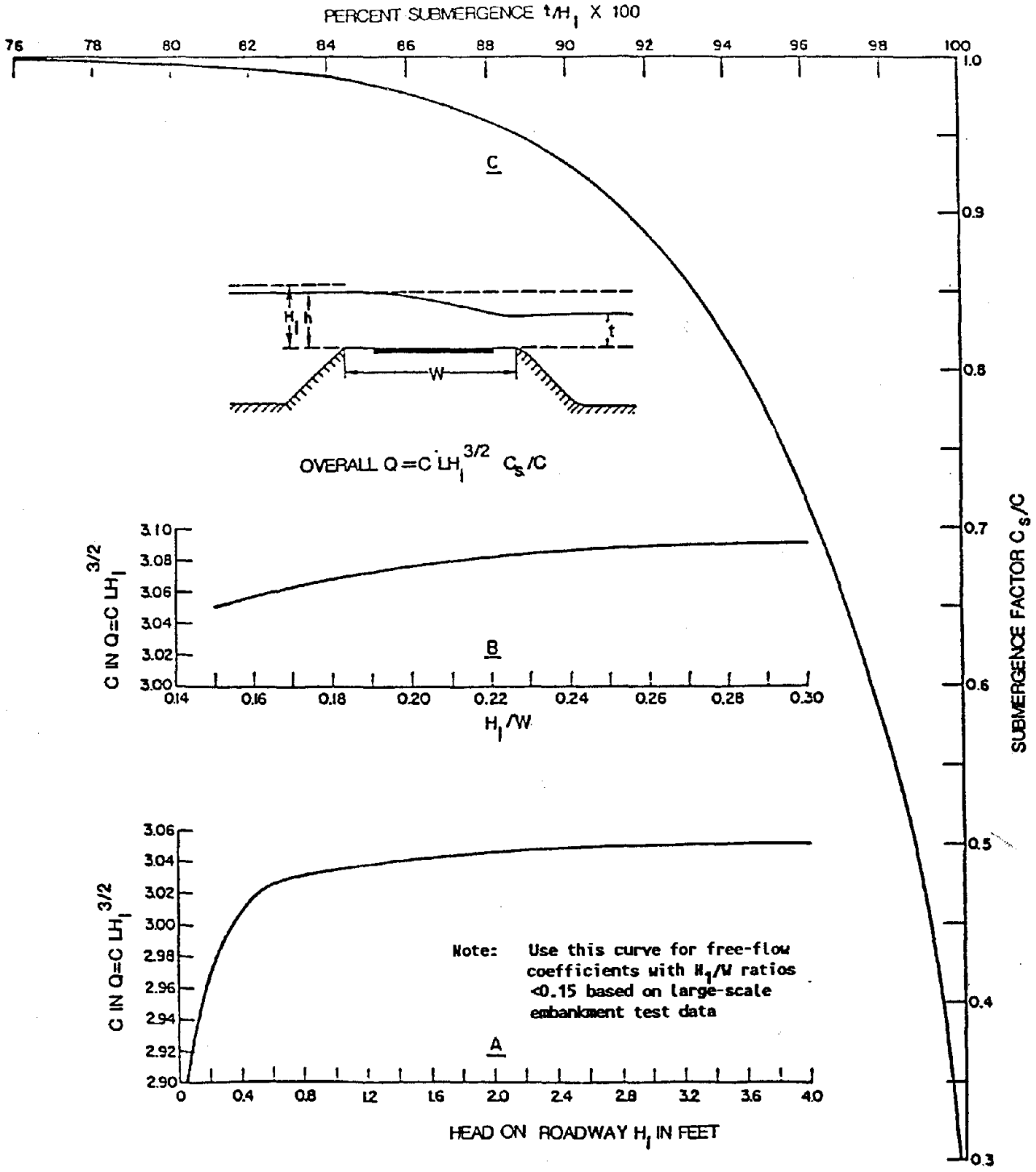


Figure 2. Discharge coefficients for flow over roadway embankment.(3)

Based on experimental results, it was found that the embankment sideslope is insignificant in its effect on the unit discharge. However, the embankment slope does influence the velocity of flow and the hydraulic characteristics of horizontal axis stationary rollers which develop on the downstream side of the embankment.

b. Flow Regimes

Flow overtopping an embankment with little or no tailwater goes through three zones: (1) from a static energy head to a combination of static and dynamic head, flow proceeds from the calm reservoir to a subcritical velocity over the upstream portion of the embankment crest; (2) through critical depth on the crest resulting in supercritical flow across the remainder of the embankment crest to the intersection with the downstream embankment slope; and (3) supercritical turbulent flow on the downstream slope. Figure 3 provides a definition sketch of these regimes. A detailed discussion of hydraulics in each of the three zones is presented in the next three paragraphs.

(1) Zone One - Subcritical Flow Over Embankment Crest. The first zone of flow exhibits a water-surface elevation approximately equal to the reservoir level drawn down by the amount due to the velocity head, $V^2/2g$. By definition, this drawdown at critical depth will be equal to one-third of the overtopping head H_1 plus friction losses across the crest, however, losses in this zone are usually negligible.

The location of critical depth on the embankment crest is dependent upon the crest profile. When the crest is rounded, the point of critical depth will be near the crest center line. When the crest has an adverse slope in the downstream direction, the location of critical depth will be near the downstream edge of the crest. When the crest has a positive slope in the downstream direction, the point of critical depth will be near the upstream edge of the crest. The exact location of critical depth will also vary with overtopping head; the location of critical depth will shift upstream with an increase in overtopping head.

(2) Zone Two - Supercritical Flow Over The Embankment Crest. The second zone of flow occurs across the portion of the crest downstream of the location of critical depth, and is characterized by supercritical flow. As in the first zone, the length of this zone is dependent on crest design. There is very little change in flow depth and velocity in this zone due to the short distance. The stage in zone 2 can be related to critical flow depth and velocity at the upstream limit of zone 2 (figure 3). Critical depth at this point will be equal to two-thirds of the overtopping head H_1 and the corresponding velocity will be equal to $(gy_c)^{1/2}$ where g is the acceleration due to gravity and y_c is equal to critical depth.

(3) Zone Three - Supercritical Flow On The Downstream Slope of the Embankment. The third zone is along the downstream slope of the embankment. This flow condition will be supercritical due to the steepness of the embankment face and highly turbulent due to surface roughness. There will be a gradual increase in air entrainment down the slope; and flow will become fully entrained with air and exhibit a white water appearance if the sloped surface is rough and of sufficient length. Corrections need to be made for slope angle and air entrainment. Flow depth must be corrected for the influence of slope angle in calculation of gravitational forces. This correction is made with the cosine of the slope angle, i.e., $h = y \cos \theta$; unit weight and depth of the air entrained water should be used in all velocity and shear stress computations.

c. Pressure and Velocity

Uplift pressure can result in failures of embankments with paved crests. If the head across the embankment is large enough, the resulting uplift pressures on the paved surface can be sufficient to lift the pavement off the embankment crest. This has been described as rafting and it is a good demonstration of flotation due to uplift forces which may be the result of the reservoir head penetrating beneath the pavement (or any impermeable layer). The maximum possible uplift can be determined by assuming that uplift beneath the pavement equals the overtopping head H_1 without seepage losses (e.g., an open crack or coarse drain fill layer could transmit full head) with the maximum downward load on the pavement from the weight of water

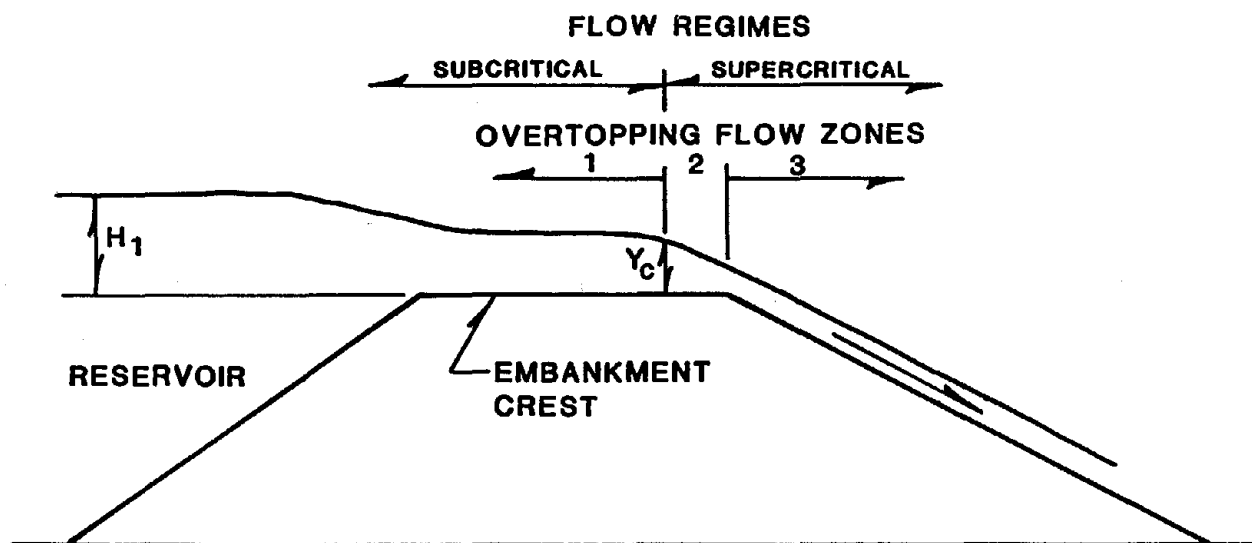


Figure 3. Hydraulic flow regimes and overtopping flow zones.

at critical flow depth (two-thirds of the overtopping head). Therefore, the maximum potential uplift under an impermeable layer can be equal to the velocity head $(H_1 - 2/3 H_1) = H_1/3$, which is equal to the velocity head at critical depth. Similarly, seepage through the downstream face of the embankment can decrease the stability of the embankment material.

Embankment erosion is dependent upon the flow velocity, which varies according to the headwater and tailwater depths. When the tailwater depth does not affect the discharge across the embankment, critical velocity can be computed as approximately equal to $(2/3gH_1)^{1/2}$. In zone 3 the terminal velocity achieved where uniform flow has established can be calculated using the embankment geometry and Manning's velocity equation. A computer model, EMBANK, developed in FHWA's earlier study, calculates the water-surface profile, velocities, and shear stresses during an overtopping flow event at user-determined stations along the profile.⁽²⁾ The user is allowed to enter various geometries, soil types, and time-varying head- and tailwater depths. The model also updates embankment geometry based on estimated erosion rates after each time step.

Another factor which should be considered in the hydraulic analysis of overtopping flow is the zone of negative pressure which can develop on the downstream embankment slope. Flow along the embankment crest develops considerable momentum in the horizontal direction. This momentum will continue to carry the flow out over the downstream slope for a distance which is a function of the embankment geometry and the velocity of the flow. This effect can be idealized graphically by superimposing the proper ogee crest shape onto the embankment profile. The ogee shape approximates the lower nappe boundary for free overflow, and can therefore be used to estimate the extent and magnitude of the negative pressure zone. However, standard ogee crest nomographs do not strictly apply to the geometry of a typical embankment section, which has a long horizontal approach prior to the downstream slope. Considering this, the situation can be reanalyzed using the equations of projectile motion, which results in the following relationship:

$$y = \left(\frac{-g}{2V_o^2} \right) x^2 \quad (3)$$

where V_0 is the velocity of flow in the horizontal direction at the point of slope transition, and x and y are cartesian coordinates with origin at the point of slope transition. Figure 4 illustrates the development of the subatmospheric pressure region on the embankment slope. Analysis performed using equation 3 results in figures 5 and 6, which provide numerical estimates very similar to graphical analyses using ogee crest nomographs. The conclusions drawn from this analysis are as follows:

- The steeper the embankment slope, the more severe the magnitude of negative pressure and the greater the distance over which it acts.
- The greater the overtopping head, the greater the magnitude of negative pressure.

d. Shear Stress and Stream Power

When embankments are overtopped by floodwaters, erosion can be significant due to high velocities on the downstream face of the embankment. When the shear stress exerted by the flow exceeds the critical shear stress of the embankment soil, erosion begins. Shear stress increases with an increase in velocity, and velocity depends on head- and tailwater conditions. Shear stress in the zone of subcritical flow (zone 1) is typically less than critical; therefore, serious erosion does not usually occur on the upstream portion of the embankment crest. This conclusion has been verified based on observations of overtopped dam crests and earthen auxiliary spillways, as well as controlled experimental conditions.

For the supercritical region on the embankment crest (zone 2), the tractive stress level is equal to $\gamma y S$, where γ is the unit weight of water, y is the flow depth (which also equals the hydraulic radius for a wide channel), and S is the energy slope. Tractive stress levels in this region can be highly variable because the energy slope can be quite variable. A simple situation to evaluate the possible stress level is to assume that the crest of an embankment has a crown that is 0.5 ft (0.15 m) higher at the center than the shoulders, and the crest width is 26 ft (7.9 m). The crowned slope away from the center crown will be 0.5/13 or 0.038. The

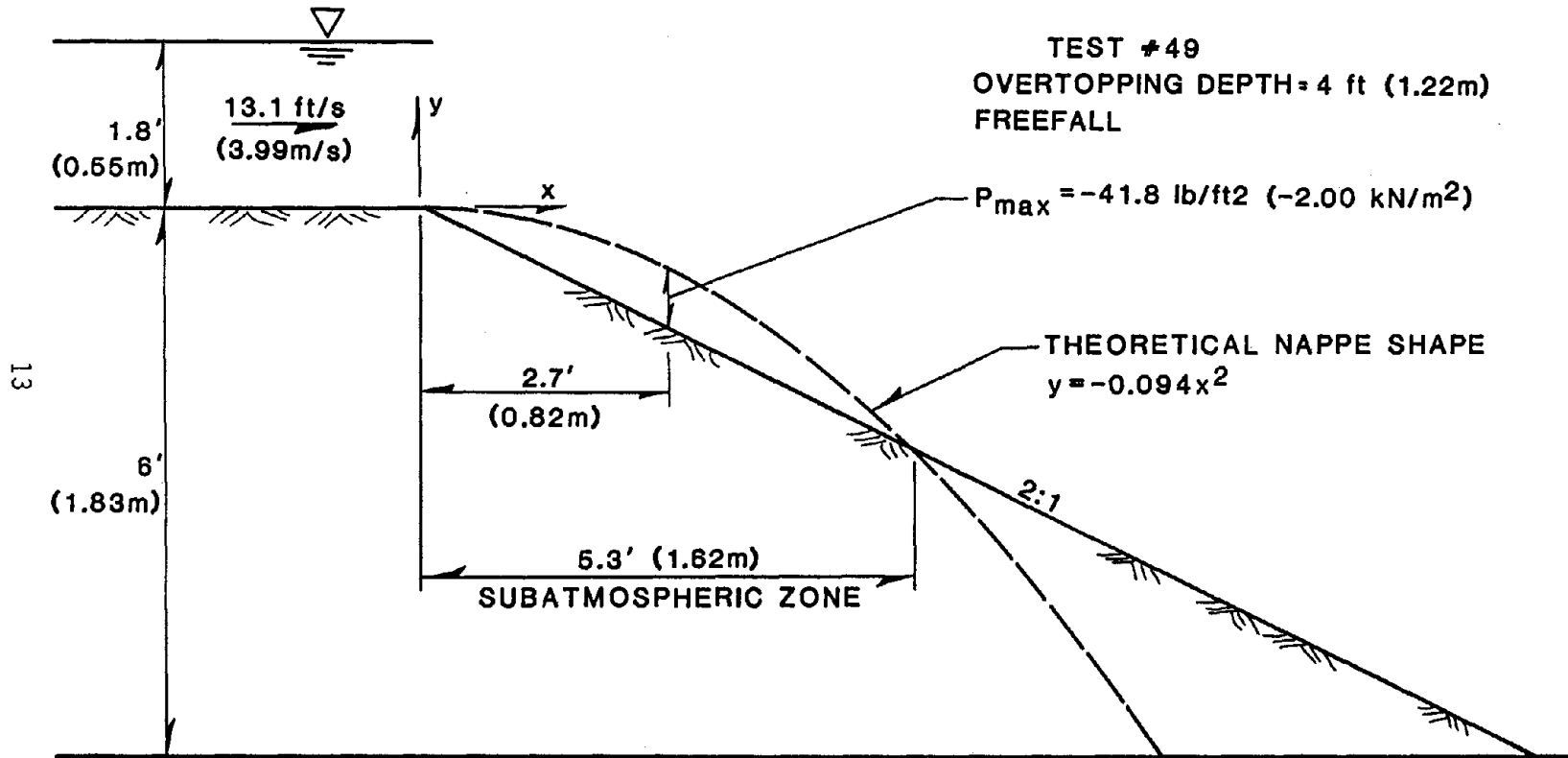


Figure 4. Comparison of theoretical nappe geometry versus rigid embankment for determination of subatmospheric pressure zone.

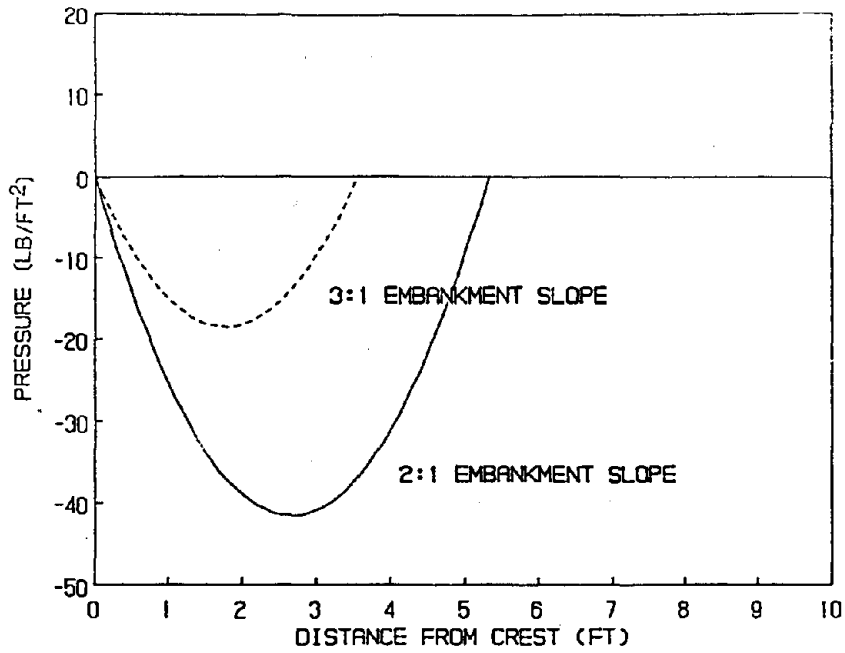


Figure 5. Theoretical pressure distribution on downstream slope corresponding to a 4-ft (1.22-m) overtopping flow.

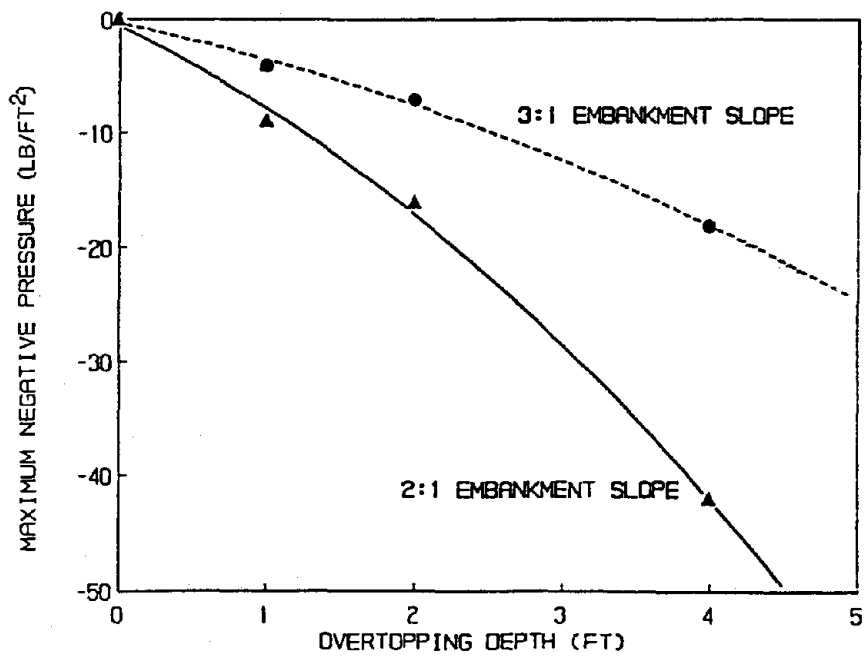


Figure 6. Variation of the theoretical maximum negative pressure developed during various overtopping depths of flow.

minimum stress level for this crest shape (assuming uniform flow at critical depth), will be equal to $62.4(2/3 H_1)(0.038)$ or $1.6 H_1$ lb/ft² [$0.25 H_1$ (m) kPa]. For an overtopping depth of 1.0 ft (0.3 m), this would exceed the critical tractive stress for most soils. Even though tractive stresses are high, the distance over which they occur can be very limited, depending on the configuration of the embankment crest. However, this illustrates that erosion in zone 2 can be expected to be initiated at the downstream edge of the crest near the point of slope transition.

Supercritical flow on the downstream slope of an embankment (zone 3) produces the largest tractive stresses, however, tractive stress methods for analysis of erosion rates are difficult to apply. This is because shortly after erosion initiates, surface discontinuities occur, resulting in a progressively more complex flow field. Prior to the occurrence of surface discontinuities, computed tractive stresses should be valid. Two modifications must be made to the tractive stress equation to account for the steep embankment slope and air entrainment. The flow depth correction is made by multiplying the depth, in the vertical plane, by the cosine of the slope angle, i.e., $h = y(\cos \theta)$. The tractive stress equation becomes $\tau = \gamma y S (\cos \theta)$, where the unit weight and depth of the air entrained water are used if appropriate conditions exist. For even moderate overtopping depths, the resulting shear stress on the downstream embankment slope can be quite large. For example, a 2-ft (0.61 m) overtopping head produces a uniform flow depth of approximately 0.8 ft (0.24 m) on a 3H:1V embankment slope, which yields an effective bed shear stress of 15.8 lb/ft² (0.76 kN/m²).

In research by Yang, the concept of dimensionless unit stream power is introduced.⁽⁴⁾ Dimensionless unit stream power is defined as the product of the average flow velocity and energy slope divided by the mean terminal fall velocity of sediment particles. Yang concluded that the transport of cohesionless bed load was strongly correlated with dimensionless unit stream power, and that this parameter was a better predictor of bed-load transport than methods based on tractive stress. However, cohesive soils were not included in this investigation.

2. Erosional Characteristics of Overtopping Flow

a. Erosion Process

When embankments are overtopped by flood waters, erosion damage can be significant due to high velocities on the downstream side of the embankment. When the shear stress exerted by the flow exceeds the critical shear stress of the embankment material, erosion begins. Shear stress increases with the increase in velocity, and velocity depends on the headwater and tailwater conditions. Another important parameter is the erodibility of the soil. Cohesive soils or soils with larger particles are more resistant to erosion compared to noncohesive, fine-grained soils. Finally, the duration of overtopping affects the total volume of material which is ultimately removed.

Critical (or maximum permissible) shear stress and velocity are defined by the threshold values above which erosion is initiated. Table 1 presents the maximum permissible velocities and unit tractive force values for various classifications of soil. For noncohesive soils, the following relationship can be used to estimate the critical shear stress:

$$\tau_c = 0.05 (\gamma_s - \gamma) D_{50} \quad (4)$$

where γ_s and γ are the unit weights of soil and water, respectively, and D_{50} is the median particle size of the soil.

Several relations for determining critical shear stress have been developed for cohesive soil. Typically these relations rely on some measure of the soil plasticity to characterize the resistance to erosion. Plasticity is defined as the ability of a material to change shape continuously under the influence of an applied stress and to retain the new shape after removal of the stress. Plasticity index (PI) is defined as the difference between the soil's liquid and plastic limits as determined by Atterberg tests. In the study of hydraulic erosive forces required to initiate motion of cohesive soils in open channels, Smerdon and Beasley found that the critical shear

Table 1. Maximum permissible velocities recommended by Fortier and Scobey and the corresponding unit-tractive-force values converted by the U.S. Bureau of Reclamation (for straight channels of small slope, after aging). (90)

Material	Clear Water		Water Transporting Colloidal Silts	
	V_c ft/s	τ_c^* lb/ft ²	V_c ft/s	τ_c^* lb/ft ²
Fine sand, colloidal	1.50	0.027	2.50	0.075
Sandy loam, noncolloidal	1.75	0.037	2.50	0.075
Silt loam, noncolloidal	2.00	0.048	3.00	0.11
Alluvial silts, noncolloidal	2.00	0.048	3.50	0.15
Ordinary firm loam	2.50	0.075	3.50	0.15
Volcanic ash	2.50	0.075	3.50	0.15
Stiff clay, very colloidal	3.75	0.26	5.00	0.46
Alluvial silts, colloidal	3.75	0.26	5.00	0.46
Shales and hardpans	6.0	0.67	6.00	0.67
Fine gravel	2.50	0.075	5.00	0.32
Graded loam to cobbles when noncolloidal	3.75	0.38	5.00	0.66
Graded silts to cobbles when colloidal	4.00	0.43	5.50	0.80
Coarse gravel, noncolloidal	4.00	0.30	6.00	0.67
Cobbles and shingles	5.00	0.91	5.50	1.10

Note V_c converted to τ_c by the equation: $\tau_c = \frac{\gamma V_c^2 n^2}{2.22 R^{1/3}}$

where: τ_c = critical shear stress (lb/ft²) ft/s x 0.3048 = m/s
 V_c = critical velocity (ft/s)
 n = Manning's roughness coefficient lb/ft² x 47.87 = N/m²
 R = hydraulic radius (ft)
 γ = density (lb/ft³)

stress of cohesive soil correlated well with plasticity index. The general relationship is a power function in the form of:

$$\tau_c = a(\text{PI})^b \quad (5)$$

where PI is the Atterberg plasticity index, and a and b are fitted parameters which vary for different soil types.^(5,6) Studies have shown that values for a and b vary from 0.0034 to 0.019 and 0.58 to 0.84, respectively.

A comprehensive literature review of previous studies of embankment erosion and several equations which relate embankment erosion rates to shear stress can be found in the FHWA report entitled, "Development of a Methodology for Estimating Embankment Damage Due to Flood Overtopping."⁽²⁾ Embankment erosion equations developed for two soil types used in the FHWA study and for a noncohesive soil tested by McWhorter et al.⁽⁷⁾ are given as:

- For embankments made from highly cohesive soils such as clay ($\text{PI} \geq 10$)
 $E = 0.000086 (\tau - \tau_c)^{0.91}$
- For embankments made from low-cohesive soils such as sandy clay ($\text{PI} \leq 5$)
 $E = 0.00022 (\tau - \tau_c)^{0.43}$
- For embankments made from noncohesive sand/gravel soil
 $E = 0.00324 (\tau - \tau_c)^{1.3}$

where E is the erosion rate in $\text{ft}^3/\text{s-ft}^2$, and τ and τ_c are effective shear and critical shear stress, respectively, in lb/ft^2 . These equations are used by the computer model EMBANK which was developed for the FHWA study to calculate the volume of embankment erosion.⁽²⁾ Alternate forms of erosion equations developed by other researchers are presented in table 2 for comparison.

b. Embankment Erosion Zones

There are three erosion zones associated with flow over an embankment, corresponding to the hydraulic flow regimes presented in figure 3. In zone

Table 2. Existing embankment erosion equations.

Author(s)	Equation	Comments
1. Wiggert & Contractor ⁽⁸⁾	$E = \alpha V^\beta$	This equation was derived specifically for embankment erosion due to flood overtopping, where E = the erosion rate in tons/day/ft of the roadway and V = mean flow velocity on the downstream slope in ft/s. The given values of $\alpha = 0.25$ and $\beta = 3.8$ represent a compromise between cohesive and noncohesive soils.
2. Cristofano ⁽⁹⁾	$\frac{Q_s}{Q_w} = K e^{-x}$	This equation computes rate of erosion for earth dam failures due to overtopping where Q_s = erosion rate in ft ³ /s, Q_w = overtopping flow discharge in ft ³ /s, K = constant, $x = (b/H) \tan \phi_d$, b = base length of the breach in ft, H = hydraulic head in ft, and ϕ_d = angle of friction.
3. Ariathurai and Arulanandan ⁽¹⁰⁾	$E = M \left(\frac{\tau}{\tau_c} - 1 \right)$	This equation computes erosion of cohesive soil, where M = erosion rate constant, ranging from 0.00012 to 0.0012 lb/ft ² /s; τ = shear stress, and τ_c = critical shear stress.
4. Chee ⁽¹¹⁾	$\frac{q_s}{q_c} = \frac{1}{(60)} K_1 K_2 K_3 K_4 \left[g \left(\frac{d-0.5H}{2} \right) \right]^{1/20}$ $\left[\frac{1}{(S-1)} \right]^2 \left(\frac{D}{d} \right)^{1/8}$	This equation computes erosion rates for erodible fuse-plug dams, where q_s = erosion rate per unit width in ft ³ /s-ft; D = water depth upstream of the dam in ft; q_c = critical water discharge per unit width in ft ³ /s-ft; for D, height of dam in ft, d = mean grain size in ft; S_s = specific gravity of grain, and K = coefficients.
5. Agricultural research lab	$E = K (\tau - \tau_c)^a$	This equation computes detachment rate for erosion of cohesive soils where E = erosion rate in ft ³ /s-ft ² , τ = effective shear stress in lb/ft ² , and τ_c = critical shear stress in lb/ft ² .

1 the flow begins with near-zero velocity in the reservoir and extends across the crest until the flow depth reaches critical depth. Observations of overtopped dam crests and earth auxiliary spillways has shown that erosion generally does not occur on the crest within this zone of subcritical flow.

Zone 2 extends from the location of critical depth to the downstream edge of the embankment crest; the length of this erosion zone is dependent on the crest geometry. Erosion in this zone can vary from minor to significant damage, depending on the total upstream head. Generally, the downstream edge of this zone is where the crest will begin to erode, and this erosion will propagate upstream with time.

The erosion process for zone 3 tends to initiate at a point of slope discontinuity, such as the toe of the embankment. However, depending on the slope of the embankment, soil type, and the depth of tailwater, the initial erosion may occur anywhere. After the first break in the embankment surface, a small scour hole develops. Tailwater elevation and soil properties control the process of scour hole growth. When there are no tailwater effects the scour hole will advance upstream. The stability of the upstream edge of the scour hole is directly related to the strength of the soil supporting it and the erosion resistance of the soil at the bottom of the scour hole.

In addition, as the scour hole deepens, erosion can propagate laterally as well as upstream. This results from the scour hole "capturing" water from the side as well as upstream. Flow out of the scour hole removes the eroded soil unless the outlet to the scour hole becomes submerged by tailwater. As the scour hole enlarges and propagates upslope, the upstream edge rapidly increases in height due to the steep geometry of the embankment slope. When the scour hole and the outflow are submerged by tailwater, erosion is greatly reduced since the energy level change is very small due to the small differences in inflow and outflow energy heads.

3. Case Studies of Dam, Levees, and Road Embankment Overtopping Events

Case histories of embankment dams, levees, and roadways which have been overtopped provide researchers with a general understanding of the performance of a wide variety of embankments under overtopping conditions. A summary of documented overtopping events is presented in tables 3 and 4. A more comprehensive summary of the case studies listed in table 4 can be found in the FHWA report.(2)

4. Behavior of Embankments and Protection Systems

This section presents findings compiled from available literature on the performance of various types of embankment protection systems. The objective of this task is to identify published or unpublished data sets relevant to the performance of various types of protection specifically pertaining to either overtopping or steep-slope conditions. To expedite the literature search process the types of embankment protection systems were separated into the following categories:

- Vegetation - various types of vegetation (typically grasses) established on the embankment surface.
- Geotextile - a wide range of synthetic fabrics, mats, or larger-scale cells that can be installed on an embankment surface and either filled or vegetated.
- Chemical - products that are used to bind soil particles together or alter the chemical characteristics of the soil to make the soil less erodible.
- Cements - used to form either a soil cement or roller-compacted concrete embankment protection using traditional earthmoving equipment.
- Concrete Block Systems - specially shaped, precast concrete blocks which are designed to mechanically interlock in the plane of the embankment slope (plan-bonded), vertically (stack-bonded), or both. Blocks are placed on a geotextile fabric or on bedding material. Systems which are cabled together can be placed as a mattress, whereas noncabled systems must be placed block by block using hand labor.

Table 3. Overtopping events at dam and levee embankments.

Embankment 1	Approximate Height ft 2	Material 3	Maximum O.T. Depth ft 4	Duration, Hours 5	Extent Damage ¹ 6
R.D. Bailey cofferdam ^c	60	well graded sand & sand- stone	6.5	4 ³	B
Bloomington cofferdam	30	clayey sand gravel	0.5	1 ³	B
B. Everett Jordan cofferdam	30	silty-clay	1	>24	O
Little Blue River levee	15	clay (vegetated)	1	12 ⁴	O/B
Jacksonport levee	15	clay	1-2	1 week	O
Rocky Run Dam	20	loess	1.5	5	MD
Rocky Run protection levee	9	loess	2	6	MD
Elm Fork	36	clay (vegetated)	0.4	3	MD
Colorado M-1	38	SC-CL (vegetated)	1.3	2-4	O
Retarding S-1	23		0.75	2-4	O
Structures W-1 ⁴	49		3	1-2	MD
Upper Elk River Nos. 37, 41, 42, and Big Caney No. 39 (5)(4 dams)	39-47	clay & gravel	0.3 - 2.5	1-4	O
Rainbow	47	clay	0.2	121	B

Table 3. Overtopping events at dam and levee embankments (continued).

Embankment 1	Approximate Height ft 2	Material 3	Maximum O.T. Depth ft 4	Duration, Hours 5	Extent, Damage 6
W. Fork P. Remove Cr. Site 2	35	lean clay, gravel, & silty sand	1.2	<2	0
W. Fork Pt. Remove Cr. Site 4	50	lean clay gravel & silty sand	1	<2	0
East Willow Cr. W/S, Str. D-2	28	lean clay	1.5 - 2.0	1.0+	0
Bogue Cr., Dam No. Y-30-57	18	lean clay	0.6	<1	0
Deep Cr. W/S, Dam 30A	39	lean clay, silt, silt sand & sandy clay	0 - 0.6	<1	0
Randall RC&D CA-191-BH	22	lean clay	1.0	<12	0
Klinkner (Westfork Kickappo W)	28	silt-lean clay	2.1	2	0
Oros	100	zoned earth & rockfill	2.7	12 - 18 ³	B
Armando de Salles	110	earth fill	4	0.3 ³	B

Table 3. Overtopping events at dam and levee embankments (continued).

Embankment 1	Approximate Height ft 2	Material 3	Maximum O.T. Depth ft 4	Duration, Hours 5	Extent Damage ¹ 6
Euclides de Cumba	200	earth fill	4	7.5 ³	0
McCarty	54	sandy clay	unknown	"few" ³ <24	B

¹Damage Code: B - Breached
 MD - Moderate Damage
 O - Minor or No Damage

ft x 0.3048 = m

²Breaching would have occurred more quickly if the crest width had not been approximately 400 feet (122 m).

³Elapsed overtopping time until breaching.

⁴During 1977 overtopping, no breaching; during 1982 overtopping, breaching after 12 hours.

⁵High tailwater greatly increased the time to breach for a severe event.

Table 4. Overtopping events at roadway embankments.(2)

Roadway 1	Embankment		Peak Overtopping Conditions		Extent of Damage 6
	Height ft 2	Material 3	Maximum Depth ft 4	Duration, Hours 5	
1. Castor River at Zalma, St. Hwy 51, Bollinger County, MO	4	Sandy, low- cohesive	3.0	26	0
2. Little Black River near Grandin Cty Hwy K, Ripley Cty, MO	10	Sandy-clay	3.6	9	0
3. Illinois Bayou near Scottsville, AR, at AR St. Hwy 164	10	Sandy-silt noncohesive	4.0	12	0
4. Earth Road in Granite Reservoir, WY	4	d ₅₀ =2.7 mm noncohesive	1.0	10	B
5. WY St. Hwy 487 at Sand Cr. near Shirley Basin	10	D ₅₀ =0.4 MM PI = 10	1.0	42	B
6. Taft Hill Rd at Cache la Poudre River in Fort Collins, CO	8	Sandy, low cohesive	0.5	30	MD
7. Gila River at U.S. Hwy. 70 (Bylas Bridge)	6	Sandy-Silt D ₅₀ =0.4 mm	3.4	38	B

Table 4. Overtopping events at roadway embankments (continued).(2)

Roadway 1	Embankment		Peak Overtopping Conditions		Extent of Damage 6
	Height ft 2	Material 3	Maximum Depth ft 4	Duration, Hours 5	
8. Gila River at St. Hwy. 87 near Sacaton, AZ (milepost 148)	5	Sandy D ₅₀ =0.50 mm low cohesive	3.4	60	B
9. Peak Canyon at Interstate Hwy 19 near Nogales, AZ (milepost 14)	5	Sandy D ₅₀ =0.30 mm low cohesive	1.8	--	MD
10. Prairie Ave., Cheyenne, WY	5	Sandy clay D ₅₀ =0.90 mm PI = 4.3	2.5	3	MD
11. Windmill Rd, Cheyenne, WY	5	Sandy silt D ₅₀ =1.0 mm	3.0	3	MD

Damage Code B - Breached
 MD - Moderate Damage
 0 - Minor or No Damage

ft x 0.3048 = m

- Gabions - uniformly graded stone placed in wire mesh cells on the embankment surface.
- Riprap - well-graded stone of a specified mean diameter placed on the embankment surface to a specified thickness.

The literature was surveyed for application of these systems to steep-slope conditions. Applications specific to embankment overtopping are not common, however, use of these protection systems for stabilization of steep waterways (such as earthen spillways), or for bank stabilization is more frequently cited in the literature.

As a point of reference, the basis for current lining design methodologies are the fundamental papers by Fortier and Scobey, and Lane.(12,13) This work continues to provide the basic approach for stable channel design based on permissible velocity or permissible tractive force.

a. Vegetation

The literature on the hydraulics of grass-lined waterways is substantial. The primary emphasis of the reported research pertains to the resistance to flow of vegetative-lined channels. Values of permissible velocity or shear stress are less frequently reported. A consistent set of failure criteria or a description of dominant failure modes are seldom available from the literature. This is due in large part to the complexity of the hydraulic characteristics of vegetative linings. The physical properties of vegetation such as the stiffness, cover density, form, and rooting patterns vary significantly depending on soil, climate, and species of vegetation. The task of classifying hydraulic data in a meaningful and useful way has been the objective of most of the basic research to date. Beginning with basic studies by Cox, Cox and Palmer, Ree, and Ree and Palmer the basic performance data on grass linings were compiled and categorized.(14,15,16,17) Data specific to steep-channel conditions have been gathered by Cox, Eastgate, Yong, Yong and Stone, and Ree et al.(18,19,20,21,22) These data consist of estimates of stage, discharge, and

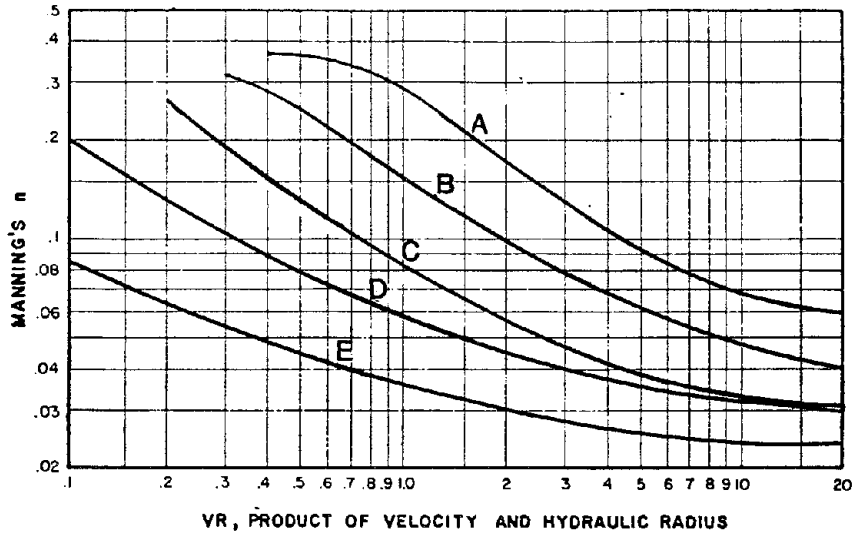
erosion damage that occurred during flood releases on vegetated spillways. These data sets are small and basically qualitative.

Further refinements of the flow-resistance characteristics of channels with a vegetated lining have been presented by Kouwen and Unny, McCool, Thomas and Robertson, Kao and Barfield, Kouwen and Li, Kouwen et al., and Temple. (23,24,25,26,27,28,29) The data base for the hydraulic resistance of vegetation is extensive and is derived largely from the work by Cox, Palmer, and Ree. (16,17) The well-known family of retardance curves first published by the USDA Soil Conservation Service was derived from these data and is shown in figure 7. (30) Reanalysis of these data sets addressing the biomechanical aspects of vegetative covers have been accomplished largely by Kouwen (with Unny and Li) and Temple. (23,27,29) The results are quantitative procedures for the determination of hydraulic resistance of vegetation based on measurable characteristics such as density of cover and flexural stiffness of the plant.

Testing of maximum permissible hydraulic conditions for vegetative-lined channels is generally limited. Permissible values for velocity or shear stress were developed using the data collected by Cox, Ree, and Palmer in the 1940s. (15,16) Design procedures incorporating these data were first developed by the SCS in 1947 and revised in 1954. (30) Temple has since revised this procedure to incorporate his research of flow-resistance characteristics of vegetation. (31)

A typical failure mode of vegetative linings is due to scour at the base of individual plants. Since the velocity distribution is nearly uniform through vegetation, the shear at the soil surface is equal to the change in velocity in this flow region. If the shear stress at the soil surface exceeds the permissible shear stress for the soil, erosion will be initiated. Temple has developed a procedure to design grass-lined channels based on an evaluation of the effective shear stress at the soil surface. (32) The effective shear stress is calculated from the following equation

$$\tau_e = \tau_o (1 - Cf) (ns/n)^2 \quad (6)$$



Retardance	Cover	Condition
A Very high	Weeping love grass	Excellent stand, tall (av 30 in.)
	Yellow bluestem ischaemum	Excellent stand, tall (av 36 in.)
B High	Kudzu	Very dense growth, uncut
	Bermuda grass	Good stand, tall (av 12 in.)
	Native grass mixture (little blue-stem, blue grama, and other long and short Midwest grasses)	Good stand, unmowed
	Weeping love grass	Good stand, tall (av 24 in.)
	Lespedeza sericea	Good stand, not woody, tall (av. 19 in.)
	Alfalfa	Good stand, uncut (av 11 in.)
	Weeping love grass	Good stand, mowed (av 13 in.)
	Kudzu	Dense growth, uncut
C Moderate	Blue grama	Good stand, uncut (av 13 in.)
	Crab grass	Fair stand, uncut (10 to 48 in.)
	Bermuda grass	Good stand, mowed (av 6 in.)
	Common lespedeza	Good stand, uncut (av 11 in.)
	Grass-legume mixture—summer (orchard grass, redtop, Italian rye grass, and common lespedeza)	Good stand, uncut (6 to 8 in.)
	Centipede grass	Very dense cover (av 6 in.)
D Low	Kentucky bluegrass	Good stand, headed (6 to 12 in.)
	Bermuda grass	Good stand, cut to 2.5 in. height
	Common lespedeza	Excellent stand, uncut (av 4.5 in.)
	Buffalo grass	Good stand, uncut (3 to 6 in.)
	Grass-legume mixture—fall, spring (orchard grass, redtop, Italian rye grass, and common lespedeza)	Good stand, uncut (4 to 5 in.)
E Very low	Lespedeza sericea	After cutting to 2 in. height, very good stand before cutting
	Bermuda grass	Good stand, cut to 1.5 in. height
	Bermuda grass	Burned stubble

Figure 7. Retardance curves and vegetal classifications. (31)

where τ_e is the effective shear stress at the soil surface, τ_0 is the average bed-shear stress, C_f is the vegetative cover factor, n_s is the Manning roughness coefficient for the soil surface, and n is the total Manning roughness coefficient. Values of C_f for types of vegetation are given by Temple, n_s is assumed to be a constant value of 0.0156, and n is found from Temple's form of the resistance for submerged grass-lined channels. Alternative forms of the resistance equation for vegetative linings could also be used with this method. Permissible shear stress for noncohesive and cohesive soils are given by equations 4 and 5, respectively, and typical values are reported in table 1.

Temple et al. have also developed an allowable stress design method for grass-lined channels.⁽³³⁾ The procedure was developed based on large scale laboratory test data compiled over the past 50 years. The design method uses the effective stress on the soil to predict incipient failure of the vegetal surface due to erosion of the supporting soil matrix. In 1986 the USDA Agricultural Research Service (ARS) was attempting to modify this method to predict the time to failure for vegetal linings subjected to shear stresses greater than the allowable stress for stable channel design.

A 1986 study conducted by the United Kingdom's Construction Industry Research and Information Association (CIRIA) involved the establishment, management, and performance of steep channels lined with grass and reinforced grass systems.⁽³⁴⁾ CIRIA's research culminated in a comprehensive design manual "Design of Reinforced Grass Waterways."⁽³⁴⁾ In this manual, CIRIA outlines four functions that vegetation provides while preventing erosion:

- Vegetation provides ground cover. In particular the protection of the soil surface is improved when the grass is laid down by the drag of high velocity, unidirectional flow.
- The root structure reinforces soil adjacent to the surface by forming a composite soil/root mat which has more resistance to erosion and higher shear strength than the soil alone.
- The root structure anchors the composite soil/root mat into the underlying subsoil.

- The vegetation above the ground may reduce the erosive velocity at the soil surface by interfering with the surface-water flow.

Erosion of vegetated surfaces by flowing water occurs in several different ways. Two failure modes are localized failure of individual plants and large-scale stripping and bulging of the soil/root mat, as shown in figure 8. The CIRIA study documented that steady erosion occurred in a well-grassed channel after 5-1/4 hours of testing at 9.2 ft/s (2.8 m/s).

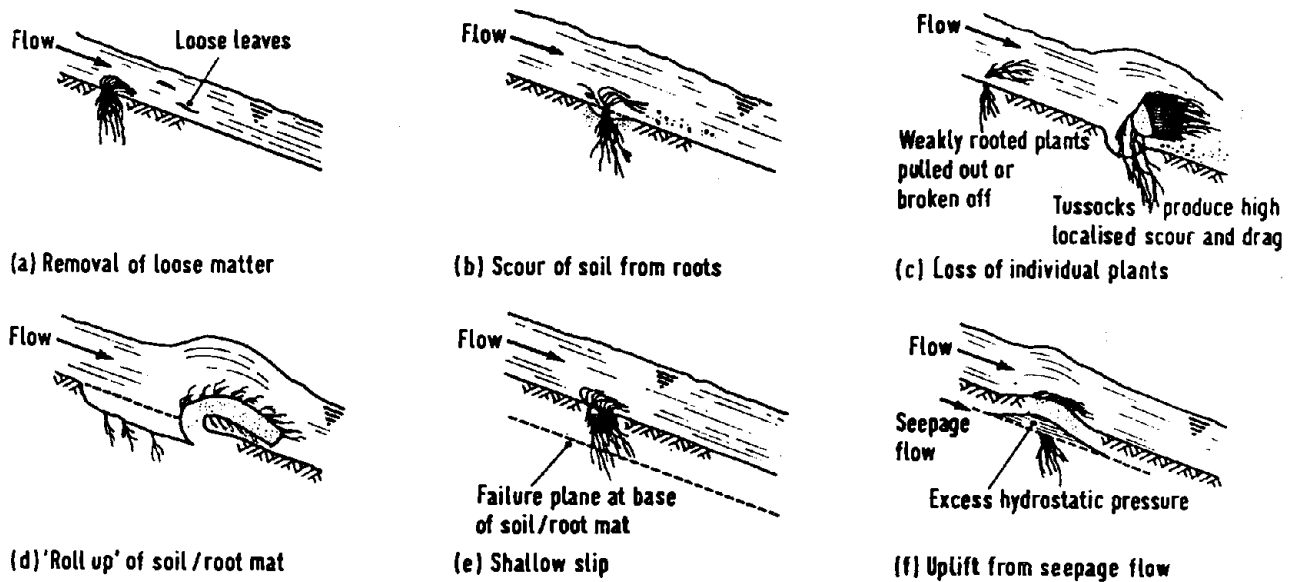
Once the unprotected soil is exposed to flowing water, it is eroded rapidly. In a steep waterway, erosion usually begins by downcutting and gully formation. Similarly, erosion gullies are likely to form if any surface features exist which cause a local concentration of the flow. The gully then propagates back up the slope by headcutting. Conditions are relatively unpredictable and erosion can be rapid due to local concentration of flow.

While vegetation has been shown to be effective in improving embankment stability, it is unsuitable in arid areas where uniform establishment of dense, well-rooted vegetation cannot be guaranteed.

b. Geotextile

Geotextile materials available for embankment protection are either woven fabrics, meshes, or mats. Geotextiles can be classified in three categories:

- Two-dimensional. Woven meshes and fabrics, using natural or synthetic (polymer) fibers, through which grass is allowed to grow.
- Three-dimensional open. Synthetic mats which are filled with topsoil and seeded.
- Three-dimensional filled. Synthetic mat or grid confinement systems filled with asphalt or rock.



- (a) When flow first occurs, any loose vegetation is removed by the drag force of the flowing water.
- (b) Locally, flow may slow down and scour soil away round the roots of a plant, thereby weakening its anchorage until the plant itself is removed by the drag force of the flow.
- (c) Individual grass plants with poorly developed root structures are either pulled out of the soil or broken off at the roots. Flowing water causes higher drag forces on plants which present a substantial profile to the flow, in comparison with those which are laid flat.
- (d) progressive rolling up due to high local drag forces at the leading edge of the mat.
- (e) Shallow surface slip.
- (f) Net uplift pressure arising from excessive seepage flow.

Figure 8. Typical failure mechanisms exhibited by vegetative linings. (34)

For a geotextile-reinforced system to be effective, it is essential that flow along the subsoil is restricted, either by establishing a dense geotextile/soil/root mat or by direct geotextile protection. Likewise, the longevity of the geotextile system is dependent on the environment within which the system is installed. Damage could occur due to vandalism, fire, damage by human and livestock traffic, or snagging of the geotextile during grass cutting. Geotextile systems designed to enhance the vegetative root mat are necessarily at risk during the period of grass establishment, and must be inspected and maintained to ensure that adequate grass growth is established (i.e., no bare patches) and that the geotextile does not begin to bridge over small rills which may develop in the subsoil during the establishment period. After 2 or 3 years, plant growth usually covers the geotextile adequately with surface roots and litter, given proper maintenance.

The majority of the data on the hydraulic performance of geotextile channel linings in the U.S. is provided in studies conducted for FHWA as described in the following paragraphs.(7,35)

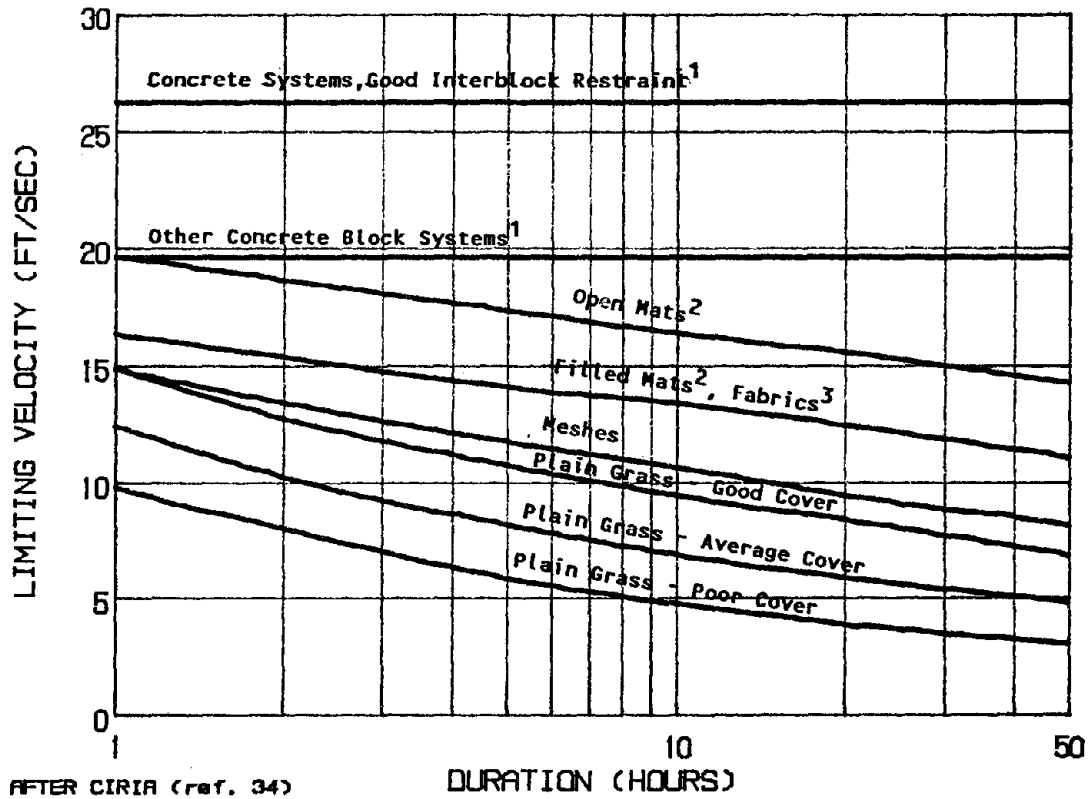
A study by McWorter et al. assessed the performance of 13 different geotextile linings, in three different channel shapes, comprised of 11 different soils.(7) A total of 150 separate runs were made with an average of 10 measurements per run. The majority of the runs were made in a 2-ft wide, rectangular flume.

Research by Cox et al. collected additional information on the performance of jute net, fiberglass mat, and wood excelsior mat, all of which were studied by McWorter, and in addition assessed the performance of fiberglass roving tacked with asphalt emulsion.(35) The tests were conducted in a 150-ft (46 m) flume with a triangular channel section with 4:1 sideslopes at a gradient of 4.8 percent. Results of the excelsior and jute tests were found to be consistent with McWorter's findings. The bulk of the data from this study focused on the performance of fiberglass roving. Additional flume tests were conducted for fiberglass roving to determine the roughness characteristics. The test channel was 72 ft (22 m) long with a trapezoidal section 1.5 ft (0.46 m) wide and 1:1 sideslopes at a gradient of 3.0 percent.

A study by the USGS hydraulics laboratory in Bay St. Louis, Mississippi, assessed the performance of 10 temporary ditch linings.⁽³⁶⁾ A 50-ft (15 m), tilting flume was used for the study that provided channel gradients of up to 12 percent with a trapezoidal section with a 1.0-ft (0.3 m) width and 3:1 sideslopes. Discharges in the flume could be varied up to 10.0 ft³/s. Two soil types were used, classified as erodible and nonerodible.

The FHWA analyzed existing performance data for widely used flexible channel linings from the above data sets.⁽³⁷⁾ They found that the flow resistance for flexible linings follows a semilogarithmic form. They also tabulated permissible shear stress values for various lining types. Hewlett et al. present permissible velocities for reinforced grass channels.⁽³⁴⁾ These curves are shown in figure 9 as a function of time with about a 50 percent reduction in permissible velocity in 24 hours. There are, however, no experimental data presented to support these curves. Hewlett et al. also reports Manning's n values for mat-reinforced vegetation of 0.035 for spillways of 10:1 slope and 0.025 for 2:1 slopes, and that these values are independent of vegetative cover type and density.

Several researchers have compiled performance records of field installation for a variety of geotextile protection products. The performance of fiberglass roving is reported by Cox et al. and Williams.^(35,39) These studies provide estimates of Manning's roughness coefficient and permissible shear stress for single and double thickness applications. A number of field studies have been conducted on the performance of enkamat. Hewlett et al. reported field data for enkamat performance for a small spillway in Sussex, England (2 to 3 m/s), and at a storm sewage bypass at Milton Keynes, England (1 m/s).⁽³⁸⁾ The North Dakota and Pennsylvania Departments of Transportation (DOT) studies document that enkamat performs well up to a velocity of 10 ft/s (3.1 m/s) or a shear stress of approximately 1.8 lb/ft² (0.086 kN/m²).^(40,41) Kemic summarizes the North Dakota and Pennsylvania data and presents field measurements by the Texas DOT and Texas SCS showing field shear stress conditions which ranged from 1.6 to 1.9 lb/ft² (0.077 to 0.091 kN/m²) with a maximum shear stress of 4.1 lb/ft² (0.196 kN/m²), and acceptable performance of the mat.⁽⁴²⁾



- Notes:
1. Minimum superficial mass 28 lb/ft² (135 kg/m²).
 2. Minimum nominal thickness 0.8 inch (20 mm).
 3. Installed within 0.8 inch (20 mm) of soil surface, or in conjunction with a surface mesh.
 4. These graphs should only be used for erosion resistance to unidirectional flow. Values are based on available experience and information at the date of this report.
 5. All reinforced grass values assume well established, good grass cover.
 6. Other criteria (such as short-term protection, ease of installation and management, susceptibility to vandalism, etc...) must be considered in choice of reinforcement.

Figure 9. Recommended limiting values for erosion resistance of plain and reinforced grass.(34)

A study for the FHWA and the U. S. Forest Service (USFS) investigated enkamat and geoweb geotextile protection systems for embankments subject to overtopping flows.⁽²⁾ Two soils forming the embankments were tested and included soil classified as clay (CL) and sandy clay (SC). Flood overtopping conditions included overtopping depths from 0.5 to 4 ft (0.15 to 1.2 m), discharges ranging from 1 to 25 ft³/s/ft (0.09 to 2.33 m³/s/m), and tailwater conditions ranging from 10 percent water-surface drop to complete free fall. Enkamat protective fabric performed well for overtopping depths less than 1 ft. Geoweb performed poorly because the 1- to 2-in (25 to 50 mm) gravel which filled the geoweb cells was quickly eroded thereby subjecting the embankment to direct erosion.

CIRIA research included testing of four geotextile fabrics (Lotrak, Netlon, Enkamat 7220, and Enkamat A20) which were well grassed prior to testing. The protection systems were installed in steep (2.5H:1V), 82 ft (25 m) long trapezoidal channels. The systems were tested at varying flows up to and including failure or maximum velocity of 26 ft/s (7.9 m/s) at a discharge of 40 ft³/s (1.1 m³/s). In general, the geotextile products were successful in that channels with geotextile protection failed at higher velocities than the control channel which was lined with grass only. In addition, rates of erosion in poorly grassed areas were reduced and local failures at the root-soil interface were prevented. A summary of the characteristics of geotextiles tested by CIRIA is presented in table 5. The results of the geotextile-lined channel performance are presented in table 6. A complete description of this research is contained in the CIRIA publication, "Guide to the Design of Reinforced Grass Waterways."⁽³⁴⁾

Several investigations by Federal and State agencies have produced a substantial base of information on the performance of a variety of geotextile meshes and mats (White, McNitt, Arkansas Department of Transportation, and Missouri Department of Transportation).^(43,44,45,46) These investigations focused on the use of commercially available geotextiles in roadway cut-and-fill slope stabilization projects and in streambank protection, and did not specifically address either steeply sloped waterways or overtopping conditions.

Table 5. Summary of characteristics of CIRIA tested geotextile protection systems.

Geotextile	Description	Thickness, in	Weight, oz/ft ²
Lotrak MT 22/16	Woven Synthetic Fabric	0.020	0.39
Netlon CE 131	Polyethylene Mesh	0.205	2.16
Enkamat 7220	Nylon Mesh	0.709	13.1
Enkamat A20	Nylon Mesh Filled With Bitumen Bound Gravel Chippings	9.84	65.5

in x 25.4 = mm

oz/ft² x 306 = G/m²

Table 6. Summary of CIRIA tests on geotextile-reinforced steep-grassed channels.(34)

Channel (1)	Run Numbers (2)	Date (3)	Duration (hour) (4)	Discharge ft ³ /s (5)	Velocity at Ch.15m ft/s (6)	Performance (7)	
Lotrak	1,2,3	6/20/86	0.75, 1, 3.50	2.4	9.8	Good	
	4,5,6	6/20/86	0.75, 1.50, 3	7.8	13.5	Good	
	7a	7/10/86	5 min	14.5	19.0	Good	
	7b,8,9	7/10/86	0.75, 1.50, 3	10.2	16.7	Signs of Stress	
	10,11,12	7/21/86	0.75, 1.50, 2	15.2	20.0	Stressed	
	12b	7/24/86	0.75	20.2	21.7	Failed	
Netlon	1,2,3	6/11/86	0.75, 1.50, 3	2.4	9.8	Good	
	4	6/25/86	0.75	7.0	14.8	Good	
	5,6,6a	6/25/86	2	8.7	15.7	Good	
	6	6/25/86	2.50	10.7	17.1	Good	
	7,8,9	7/11/86	1, 1.50, 2.75	12.4	18.4	Signs of Stress	
	10a	7/24/86	1.25	25.9	23.0	--	
	10b	7/24/86	1.25	37.8	27.0	Failed	
Enkamat 7220	1a	6/06/86	0.25	1.9	8.5	Good	
	1b	6/06/86	0.50	3.9	9.8	Good	
	2	6/06/86	1.50	2.5	9.2	Good	
	3	6/06/86	3	2.0	8.9	Good	
	4,5,6	6/23/86	0.75, 1.50, 3	6.7	12.5	Signs of Stress	
	7	7/09/86	0.75	15.5	19.0	Signs of Stress	
	8,9	7/09/86	1.50, 3	12.7	17.1	Signs of Stress	
	10	7/17/86	1.50	21.9	23.0	Failed	
	Enkamat A20	1,2,3	6/13/86	0.75, 1.50, 3	6.2	12.8	Good
		4,5	6/26/86	0.75, 1.50	16.2	18.0	Good
6		7/07/86	1	18.4	18.7	Failure No. 1	
7a		6/10/86	0.25	12.7	16.7	Good	
7b		6/10/86	1	17.3	18.4	Good	
7c		6/10/86	1	19.2	19.0	Good	
7d		6/10/86	10 min	28.1	21.3	Failure No. 2	

- Notes: 1. Flow velocities are the mean depth averaged values in the middle half of the channel.
 2. *Interpolated velocities.
 3. "Damage" refers to loss of soil and grass voids, not loss of subsoil which was the criterion for failure.
 4. "Velocity at Ch.15 m" refers to the velocity of flow at a point in the channel 15m (49 ft) downslope from the crest.

$$\text{ft}^3/\text{s} \times 0.0283 = \text{m}^3/\text{s}$$

$$\text{ft}/\text{s} \times 0.3048 = \text{m}/\text{s}$$

c. Chemical

Studies have been conducted on a variety of chemicals for stabilization of soils against erosion. Burgess Kay has produced a number of studies addressing the suitability of chemical products for use as mulch binders or for stabilizing a soil surface.^(47,48) Kay provides a useful classification of chemical products as either natural organic substances (which included Bio Binder, Ecology Control M-Binder, Kelgum, Petroset SB, Terratack I, Terratack III, and Verdyol Super) or synthetic emulsions (which included polyvinyl acetate homopolymers or vinyl acrylic copolymers (PVA) products and styrene butadiene (SBA) products). Kay evaluated the performance of the products under simulated rainfall. The results provide a qualitative comparison of product performance. Kay also tested the performance of chemical products at varying dilution rate, requirements for proper curing, effect on plant germination, and freeze damage.

Key articles by Kay include studies conducted (Goodman, Gabriels and DeBoodt, and Sultan and Liu) on chemical soil stabilizers subjected to rainfall.^(49,50,51) The rainfall erosion tests conducted by Sultan and Liu provided a relative comparison of the erodibility of nine stabilizers applied to two soil samples: one clay and one sand.⁽⁵¹⁾ Formula 125, Petroset-SB and cement were identified as the most promising stabilizers based on cost and effectiveness. Subsequent work by Sultan for the Arizona DOT studied the use of chemical stabilizers for dust control and tire-erosion control.^(52,53,54,55) Forty-six commercially available chemicals were studied and screened. Testing was directed at simulating wind erosion and abrasive forces due to traffic and environmental durability. Eleven chemicals were selected for large-scale field application, five of these were tested primarily for dust control on unpaved roads; the remaining were tested on areas not subjected to traffic. Forsyth also tested chemical stabilization of soils for control of dust and traffic erosion.⁽⁵⁶⁾ Asphalt emulsion was used to stabilize sands and lime was used to harden expansive clays.

Morrison and Simmons undertook a very comprehensive study for the Bureau of Reclamation on the chemical stabilization of soils.⁽⁵⁷⁾ Thirty

chemical products were evaluated based on tests for compressive strength, water erosion, wind erosion, penetration, and weathering. Water erosion was tested by centering a 0.04-in (1 mm) jet of water directly above the specimen at a distance of 2.5 in (63.5 mm) from the top surface. The jet was operated at a pressure of 5 psi (34.5 kN/m²) for up to 6 hours [giving a jet velocity of about 20 ft/s (6.1 m/s)]. The performance requirement was for less than a 1 percent loss of soil by weight. Based on all screening tests conducted PVA and vinyl acrylic copolymer emulsions products performed well for erosion control.

Elastomeric emulsion or urethane stabilizer was recommended for binding gravel together to form a riprap substitute. Long-term stabilization tests indicate that asphalt, elastomeric, and urethane products remain stable over a long period of time. Asphalt showed no erosion for 70 months of outdoor exposure testing and a gravel sample treated with urethane showed no erosion after 2 years of testing in a laboratory wave tank.

d. Cements

Cement treatments to stabilize soils include adding lime (CaO) to a clay soil, creating a mix of soil and cement to form soil cement, or using a select mix of sand, gravel, and cement for roller-compacted concrete. Native soils may often be used in the soil cement mixture, whereas roller-compacted concrete usually requires a higher proportion of cement and correspondingly lesser amounts of silts and clays to achieve a higher compressive strength. The primary source of testing of soil cement has been by the Bureau of Reclamation for dam facing and was initially substituted for riprap as a more cost-effective protection measure. Initial results on the use of a soil cement were reported by the Bureau of Reclamation for the Glen Elder Dam, indicating that a mix of 12 percent asphaltic cement plus 1.0 percent hydrate lime provided good erosion resistance against wave action.⁽⁵⁸⁾ Much of the Bureau's experience with soil cement was summarized by DeGroot whose report documents durability and strength of soil-cement installations at seven dams.⁽⁵⁹⁾ DeGroot did not conduct tests on the durability of soil cement to water erosion.

Specific design experience is reported by a number of users (Nussbaum and Colley, Davis et al., Duval and Alexander, Holtz and Hansen, and the Portland Cement Association).^(60,61,62,63,64,65) Key factors in the construction of soil-cement protection are achieving the proper degree of bonding between individual layers and properly compacting the soil cement. Holtz and Hansen give a brief history of the use of soil cement for slope protection on dams, dikes, and embankments.⁽⁶³⁾ They report that the performance of these structures, with properly designed and well-compacted soil cement, has been excellent. Little or no maintenance is typically required. Phase I of the FHWA embankment overtopping study tested soil cement, a zero slump mixture of soil, sand, and 11 percent cement, by dry weight.⁽²⁾ The soil cement was placed and mechanically compacted parallel to the embankment slope (2H:1V). The embankment with soil cement protection was subjected to overtopping conditions which included overtopping depths from 0.5 to 4 ft (0.15 to 1.2 m), discharges ranging from 1 to 25 ft³/s/ft (0.09 to 2.33 m³/s/m), and tailwater conditions ranging from 10 percent water-surface drop to complete free fall. No erosion of the soil cement or embankment material was observed in the tests. However, long-term weathering effects and potential toe erosion were not considered in this study.

The erodibility of cement-stabilized soils has been evaluated by Litton and Lohnes.^(66,67) Their testing involved directing a jet of water onto the surface of a treated sample and measuring the weight loss in the sample over a specified period of time. Estimates of permissible shear stress or velocity cannot be reliably made from these measurements. These studies provide only a qualitative comparison among various soil-cement mixtures.

Quantitative measurements of the critical shear stress for cement stabilized sandy soils are given by Akky.⁽⁶⁸⁾ They also noted a positive correlation between the critical shear stress and the unconfined compressive strength for unweathered samples. The grain distribution of the sand tested was characterized by a D₅₀ of 1.0 mm and a gradation coefficient, G, of 5 to 6. Samples were prepared with cement contents ranging from 1 to 3 percent. Marked reduction in erosion resistance was noted after 12 freeze-thaw cycles.

The properties of no-slump, roller-compacted concrete have been evaluated at WES by Saucier.⁽⁶⁹⁾ Erosion tests were conducted by directing a high-velocity [30 to 35 ft/s (9.1 to 10.7 m/s)] jet of water onto the surface of a prepared sample. Very little erosion occurred on the samples tested over a 14-hour period.

The addition of lime to a clay soil increases the unconfined compressive strength and will increase the erosion resistance. The addition of lime is especially useful for expansive soils or dispersive clay soils. Slaked lime (Ca(OH)_2) added at the rate of 1 to 3 percent of the dry weight of the soil is a typical application. Purdue University conducted a number of studies to evaluate the use of lime to reduce soil erodibility due to rainfall (Diamond; Kawamura et al., Machan, and Machan et al.).^(70,71,72,73)

Lime treatment of dams has been reported by the Bureau of Reclamation and the Corps of Engineers (Perry, and McDaniel and Decker).^(74,75) The results indicate that the dispersive character of the soil could be eliminated with the addition of 2 percent hydrated lime, Ca(OH)_2 . Lime being used to stabilize an irrigation canal is reported by Howard and Bara.⁽⁷⁶⁾

e. Concrete Blocks

CIRIA lists a number of concrete block products that can be used for revetment.^(34,38) They make the distinction between products that mechanically interlock versus products that are secured together with cables. The type of concrete reinforcement systems chosen for installation depends on the site. Interlocking blocks may be appropriate in restricted areas where access is limited, whereas, cable-tied blocks and in situ concrete require reasonable access for installation. Cable-tied blocks are usually installed in a series of factory assembled mats. In situ concrete systems may be most practical on large sites with access to a local or mobile batch plant, or where the geometry of the embankment does not facilitate the use of precast concrete blocks.

A review of the literature indicates that the predominant use of concrete blocks is in breakwater structures and coastal shore protection. The Corps of Engineers Waterways Experiment Station (WES), Delft Hydraulics Laboratory, and Tetra Tech, Inc. have conducted a variety of tests to assess the stability and durability of concrete block products.(77,78,79) The significant forces analyzed for coastal protection result from wave impact. Studies have shown that the low-impact strength of concrete can cause a rapid deterioration of the structure in a coastal environment. Additionally, noncabled blocks were susceptible to progressive block dislodgement following failure at a point, leading to severe slope destabilization. Both cabled and noncabled blocks performed best when tightly packed, and the interstices filled with gravel and cobbles.

CIRIA tested five types of concrete block products (Dycel, Petraflex, Armorflex, Dymex, and Grasscrete) in a high-velocity, steep-slope channel application.(34,38) All these concrete products provide a heavy protective surface layer of concrete containing cells which were filled with soil and grassed. The cell opening, depending on the product, varies from 25 to 75 percent of the total surface area. These products can be divided into three groups according to the type of interlocking systems. Dymex is an example of mechanically interlocking blocks; Armorflex, Dycel, and Petraflex can be connected together using flexible cables. Grasscrete is a system which requires casting the concrete in situ and then removing the forms and filling the voids with soil and grass. In CIRIA's tests, four of the five concrete products could not be failed at the maximum flow capacity of the testing facility. The maximum flow capacity was equivalent to an overtopping head of approximately 2.5 ft (0.76 m) or a discharge intensity of 10.7 ft³/s/ft (1.0 m³/sec/m). During long-duration tests at maximum discharge, some of the soil and grass were eroded from the block cells, but none of the subsoil was eroded, which was CIRIA's criterion for failure.

The use of block-type linings for streambank erosion control has been evaluated by Styron.(77) Aluminum and steel panels were also tested as bank protection with the conclusion that erosion can occur beneath the panel and that filters are therefore necessary to prevent erosion of the streambank.

Styron noted that the panels must be anchored securely to prevent movement. Keown conducted a study at WES to evaluate filter requirements for a variety of bank protection products, including cable-tied concrete blocks.⁽⁸⁰⁾ This study noted that, in a high turbulence environment, filter materials can be subjected to adverse fluctuating pressures that can lead to erosion of the streambank. Granular filters beneath the block system are recommended for these conditions and additional revetment thickness may be required to keep the filter in a low-turbulence environment.

f. Gabions

Gabions and Reno mattresses are rock-filled wire baskets which have been used for controlling erosion and stabilizing embankments for more than 100 years. Due to the large variety of gabion applications, studies of gabion performance have necessarily encompassed many areas. Research on the performance of gabions in an overtopping environment is limited, but recent studies have indicated that gabion mattresses can provide effective protection.

The use of gabions as erosion protection for channel bank stabilization has been very successful. However, until two recent studies by Powledge and Dodge and the FHWA, little work had been done on the performance of gabions for overtopping protection.^(81,2) The FHWA tested gabion embankment protection using a 6 ft (1.8 m) high embankment, 10- to 22-ft (3.0 to 6.7 m) crest width, and 3 ft (0.9 m) in length, with slopes of 2H:1V and 3H:1V. The gabions were constructed of wire mesh with dimensions of 3 ft wide by 8 ft long by 6 in (0.9 by 2.4 m by 152 mm) thick and filled with 3- to 6-in (75 to 152 mm) rock. The gabions were subjected to overtopping depths from 0.5 to 4 ft (0.15 to 1.2 m), discharges ranging from 1 to 25 ft³/s/ft (0.09 to 2.33 m³/s/m), and tailwater conditions ranging from 10 percent water-surface drop to freefall. Gabions performed well for the above conditions, but deformation of the wire baskets and shifting of the rockfill was observed. No erosion of the embankment material occurred, although the underlying filter fabric was exposed after the rocks within each compartment were displaced.

The USBR gabion tests by Powledge and Dodge were performed in a laboratory flume on embankment slopes of 4:1 and 6:1.⁽⁸¹⁾ The gabions modeled represented 4-in (102 mm) mesh cells filled with angular rock up to a 12 in (305 mm) maximum diameter overlying a filter bed. During these tests, there was no indication that dislodgement by overtopping flow was imminent. For the 4:1 embankment slope the main erosion was initiated near the downstream limit of the gabion mattresses. For the 6:1 slope, the main scour hole developed at a scaled distance of 45 ft (13.7 m) downstream of the protection. The 4:1 embankment slope resulted in approximately five times the scour volume as the 6:1 sideslope, with a scour hole about two times deeper. It should be noted that the scour described in this discussion refers to areas of unprotected embankment downstream from the gabions. The gabions themselves experienced deformation and rock migration within the individual compartments as in the FHWA tests, but did not fail.

g. Riprap

Research was started in 1983 by the Bureau of Reclamation to study the development of cost-effective modifications to small embankment dams which would allow them to withstand overtopping.⁽⁸¹⁾ A laboratory-scale flume, 3 ft wide by 4 ft high by 30 ft long (0.9 by 1.2 by 9.2 m) was used. A length scale of 1:15 was selected for the model soil embankment. The embankment was constructed with clayey sand to represent a prototype embankment 32 ft (9.9 m) high. The model riprap protection system consisted of model riprap representing 6- to 24-in (152 to 610 mm) diameter rock for prototype scale placed on a 6H:1V slope. The scaled velocities for this test reached magnitudes in excess of 30 ft/s (9.2 m/s), and the riprap material failed immediately. It should be noted that most riprap design methods do not account for the combination of high velocity, steep slopes, and shallow flow; however, results from German investigations have provided preliminary modifications to include the effects of air entrainment and packing factor on riprap stability.^(82,83) These studies have developed a relationship to determine air entrainment as a function of slope angle, relative depth, and rugosity. The decrease in effective viscosity and weight due to air entrainment was shown to increase riprap stability for a given unit discharge

and packing factor. However, scale relationships used to derive these results were unclear and additional research is necessary to determine if riprap is a viable embankment protection alternative for overtopping conditions.

h. Bare Soil Embankments

Several recent studies have addressed the performance and erosional characteristics of earthen embankments subjected to overtopping flow. (84,85,86,87,88) Centrifuge modeling was performed at the University of Colorado at Boulder in 1983 for WES. Two types of embankments were tested, crushed rock and soil. Erosion data and contour maps were developed for each eroded surface. The crushed rock embankment eroded and failed, while the earthen embankment eroded, but did not breach.

The second centrifuge study compared controlled overtopping performance of a 6 ft (1.8 m) high prototype and evaluated the hydraulic parameters of overtopping flow. Although the eroded volume of embankment material compared well between model and prototype, the erosion profiles did not agree. Model to prototype relationships for the hydraulics of overtopping flow and embankment erosion rates were developed. (86,88)

The third University of Colorado study modeled specific and general prototypes and compared the performance of two- and three-dimensional models for the same embankment. Relationships established in the previous study were quantified by specific prototype modeling. Three-dimensional models tended to more accurately portray overtopping performance of the prototypes. (86,88)

In 1983, the Bureau of Reclamation tested cohesive soil embankment models in their laboratory-scale flume. (89) The embankments were constructed with clayey sand with a plasticity index of 9 percent. The embankments were initially tested with a sideslope of 6H:1V, the slope was increased to 4H:1V for subsequent tests because the 6H:1V slope was very stable. No reliable sediment-transport time nor velocity scaling relationships could be

established, therefore, these tests were considered qualitative in nature, generally indicating which treatments performed well relative to the bare-soil control, rather than determining how much better, in a quantitative sense.

Two USBR tests of bare soil embankments indicated that increasing the standard Proctor compaction density from 95 to 102 percent results in one-half the erosion when similar protective measures were tested. The results of the USBR tests are summarized in table 7.


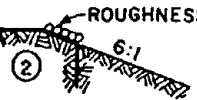


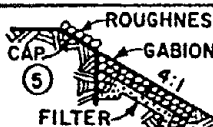
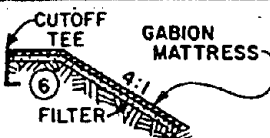



The ARS studies on the erosional failure processes of grass-lined earthen emergency spillways has resulted in information pertaining to the erosion rate of cohesive soils at stress levels consistent with headcut development and propagation. (31,32,33)

Six channels, each 3 ft (0.9 m) wide and 100 ft (30.5 m) long, were used in the ARS tests. The channel slopes ranged from 0.5 to 3.0 percent. The unit discharges ranged from 0.17 to 4.3 ft³/s/ft [0.016 to 0.4 (m³/s)/m] and were limited to durations that eroded depths of less than 0.5 ft (0.15 m). The 1986 tests involved two soil types. The soils were compacted with a sheepsfoot roller to densities consistent with field conditions for constructed embankments. Future tests will involve a broader range of soil conditions and variations in the test procedures and facilities.

5. Summary of Protection Systems

The performance of a variety of embankment protection systems has been reviewed. Information available on the performance of these systems indicates that characteristic failure mechanisms can be associated with each system, with a particular set of hydraulic stresses at the failure threshold. However, most of the information available for protection systems must be considered qualitative in nature, that is, most of the tests conducted provide only a relative comparison of products tested in the study. The

Table 7. Summary of results of USBR's overtopping flow tests. (81)

Schematic Sketch and Run Numbers	Unit Discharge ft ³ /s/ft	Time (hrs) *	Erosion Of Available Volume Of Material Percent	Total Volume Of Model Erosion ft ³
	40	1	15.8	9.13
	40	1	7.2	4.13
	40	1	13.4	7.71
	40	1 5	2.4 4.6	1.38 2.67
	40	1	11.7	4.11
	40	1 5	3.8 8.4	1.58 3.50
	40	1 5	9.1 14.1	3.82 5.90
	87	1 5	6.5 6.5	2.57 2.57
	87	1	12.7	5.31

*Prototype scaling of time
17 minutes ≈ 1 hour
77 minutes ≈ 5 hours

$$\text{ft}^3/\text{s}/\text{ft} \times 0.0929 = \text{m}^3/\text{s}/\text{m}$$

$$\text{ft}^3 \times 0.0283 = \text{m}^3$$

current state of information on protective systems as classified at the beginning of this report is as follows:

a. Vegetation

At the present time data and procedures exist for determining the resistance to flow. The nature of vegetative lining failure is complex and sufficient data have not been gathered to fully describe the phenomenon. Temple has proposed a conceptual model of scour of vegetation and a design procedure.^(32,33) The procedure involves determination of the effective shear stress at the soil surface and comparing that quantity to the permissible shear stress of the soil. Full-scale overtopping research by CIRIA has resulted in procedures for designing reinforced grassed waterways on steep slopes.⁽³⁴⁾ Their design guide provides a comprehensive treatment of the establishment, management, performance, and failure modes of several types of reinforced grassed systems. The ARS is also conducting further study on the erosion of vegetative linings on steep channels that will enable a further refinement of analysis procedures. Current values of permissible velocities and shear stresses are given in tables 8 and 9, respectively.

b. Geotextile

The laboratory work that has been conducted by FHWA is sufficient to describe the hydraulic performance of a variety of geotextile channel linings. Permissible shear stress values for a number of products have been summarized in its report.⁽³⁷⁾ These values can also be converted to permissible velocity using Manning's equation. Manning's n values for selected geotextiles are given in table 10. Current published values for permissible shear stress are given in table 11.

c. Chemical

The testing of chemical stabilization of soil indicates that a range of products exist that might have performance and durability characteristics

Table 8. Maximum permissible velocities for vegetative linings. (27,28)

Cover	Slope Range (%)	Permissible Velocity,	
		Erosion-Resistant Soils ft/s	Easily-Eroded Soils ft/s
Bermuda Grass	0-5	8	6
	5-10	7	5
	>10	6	4
Buffalo Grass, Kentucky Bluegrass, Smooth Brome, Blue Grama	0-5	7	5
	5-10	6	4
	>10	5	3
Grass Mixture	0-5	5	4
	5-10	4	3
	Do not use on slopes steeper than 10%.		
Lespedeza Sericea, Weeping Love Grass, Ischaemum (yellow bluestem), Kudzu, Alfalfa, Crabgrass	0-5	3.5	2.5
	Do not use on slopes steeper than 5% except for sideslopes in a combination channel.		
Annual-used on mild slopes or as temporary protection until permanent covers are established, common lespedeza, Sudan Grass	0-5	3.5	2.5
	Use on slopes steeper than 5% is not recommended.		

ft/s x 0.3048 = m/s

Table 9. Maximum permissible shear stresses for vegetative linings.(37)

Class	Cover	Condition	Critical Shear Stress (lb/ft ²)
A	Weeping lovegrass	Excellent stand, tall (average 30") (76 cm)	3.70
	Yellow bluestem Ischaemum	Excellent stand, tall (average 36") (91 cm)	
B	Kudzu	Very dense growth, uncut	2.10
	Bermuda grass	Good stand, tall (average 12") (30 cm)	
	Native grass mixture (little bluestem, blue- stem, blue gamma, and other long and short midwest grasses).....	Good stand, unmowed	
	Weeping lovegrass	Good stand, tall (average 24") (61 cm)	
	Lespedeza sericea	Good stand, not woody, tall (average 19") (48 cm)	
	Alfalfa	Good stand, uncut (average 11") (28 cm)	
	Weeping lovegrass	Good stand, unmowed (average 13") (33 cm)	
C	Kudzu	Dense growth, uncut	1.00
	Blue gamma	Good stand, uncut (average 13") (28 cm)	
	Crabgrass	Fair stand, uncut (10 to 48") (25 to 120 cm)	
	Bermuda grass	Good stand, mowed (average 6") (15 cm)	
	Common lespedeza	Good stand, uncut (average 11") (28 cm)	
D	Grass-legume mixture-- summer (orchard grass, redtop, Italian ryegrass, and common lespedeza).....	Good stand, uncut (6 to 8 inches) (15 to 20 cm)	0.60
	Centipede grass.....	Very dense cover (average 6 inches) (15 cm)	
	Kentucky bluegrass.....	Good stand, headed (6 to 12 inches) (15 to 30 cm)	
E	Bermuda grass.....	Good stand, cut to 2.5-inch height (6 cm)	0.35
	Common lespedeza	Excellent stand, uncut (average 4.5") (11 cm)	
	Buffalo grass	Good stand, uncut (3 to 6 inches) (8 to 15 cm)	
	Grass-legume mixture-- fall, spring (orchard grass, redtop, Italian ryegrass, and common lespedeza).....	Good stand, uncut (4 to 5 inches) (10 to 13 cm)	
	Lespedeza sericea	After cutting to 2-inch height (5 cm) Very good stand before cutting	

$$1 \text{ lb/ft}^2 \times 47.87 = \text{N/m}^2$$

Table 10. Manning's roughness coefficients for selected geotextiles.(37)

Lining Category	Lining Type	n-Value		
		Depth Ranges		
		0-0.5 ft (0-15 cm)	0.5-2.0 ft (15-60 cm)	>2.0 ft (>60 cm)
Temporary	Woven Paper Net	0.016	0.015	0.015
	Jute Net	0.028	0.022	0.019
	Fiberglass Roving	0.028	0.021	0.019
	Straw With Net	0.065	0.033	0.025
	Curled Wood Mat	0.066	0.035	0.028
	Synthetic Mat	0.036	0.025	0.021

Table 11. Permissible shear stresses for selected geotextiles. (37)

Lining Category	Lining Type	Permissible
		<u>Unit Shear Stress</u>
		(lb/ft ²)
Temporary	Woven Paper Net	0.15
	Jute Net	0.45
	Fiberglass Roving:	
	Single	0.60
	Double	0.85
	Straw with Net	1.45
	Curled Wood Mat	1.55
Synthetic Mat	2.00	

$$1\text{b/ft}^2 \times 47.87 = \text{N/m}^2$$

suited for use on steep slopes. Morrison and Simmons' study is the most comprehensive, but only semiquantitative.⁽⁵⁷⁾ The water jet test used created a narrow jet of water impinging on the soil surface at about 20 ft/s. Several samples tested withstood this test with no erosion. The durability of several products in field tests indicated that maintenance requirements would be moderate. No values of permissible shear stress or velocity are available for this class of erosion protection.

d. Cements

There are good quantitative results on the allowable shear stress for cement stabilized soils. Stabilization of noncohesive soils can be accomplished by adding from 1 to 10 percent cement. In the range from 1 to 3 percent, the soils erodibility is greatly reduced. For the addition of more than about 4 percent cement the soil becomes essentially nonerodible, but other factors such as freeze-thaw or wet-dry cycles may gradually cause surface deterioration. Tests on roller-compacted concrete indicate that it is nonerodible. The addition of lime to certain types of clay soils can reduce their erodibility. The complex chemical aspects of clay soils make this a complex area of investigation. Table 12 summarizes permissible shear stress values for cement-stabilized soil with low cement content.

e. Concrete Blocks

Concrete blocks form a semi-rigid lining over the embankment surface. The joints between the blocks can allow for pressure fluctuations in the filter material beneath the blocks that can pump a granular filter out through the joints, or lift a fabric filter away from the soil surface allowing erosive flow near the soil surface. Little data exist on the hydraulic conditions that can lead to this type of damage underneath the liner. Given a proper filter bedding and/or geotextile, this product is practically nonerodible and therefore not subject to failure via shear-stress mechanisms. Potential failure relates to the ability of the system to maintain direct, intimate contact with the subsoil being protected. This

Table 12. Permissible shear stresses for cement-stabilized soil.(68)

Cement Percent	Permissible Unit Shear Stress	
	Uncycled Sample lb/ft ²	12 Freeze-Thaw Cycles lb/ft ²
3.0	No failure at 4.5	0.51
2.0	2.36	0.47
1.5	2.05	0.45
1.0	1.54	0.18

1b/ft² x 47.87 = N/m²

contact can be enhanced through system weight, root anchorage, and mechanical (helix or duck-bill) anchors.

A summary of the characteristics of concrete protection systems tested by CIRIA is given in table 13. Results of CIRIA's tests of concrete-reinforced grass channels are presented in the table 14.⁽³⁴⁾

f. Gabions

Tests conducted on gabion protected embankments have indicated that gabions effectively protect embankments from erosion caused by overtopping flows. However, the gabion material must be sized properly and the wire mesh must be anchored securely to the embankment. Additionally, the gabions must be tightly packed with close-fitting angular stone to minimize basket deformation and rock migration.

g. Riprap

Riprap has long been a viable erosion protection alternative for channel banks and around hydraulic structures. However, limited data are available concerning the feasibility of using riprap to protect steep embankments. Additional research could determine if existing riprap design procedures are applicable for protecting steep waterways. Available limiting values of shear stress are reported in table 15.

Table 13. Summary of characteristics of CIRIA-tested concrete protection systems.

System	Description	Thickness	Weight	Cabling
		in	lb/ft ²	
Dycel 100	Precast concrete block	3.94	29.4	longitudinal
Petraflex H41212(.)	Precast concrete block	3.74	32.8	lateral and longitudinal
Armorflex 140	Precast concrete block	3.35	27.7	longitudinal
Dymex	Precast concrete block	3.94	22.7	none
Grasscrete GC1	In situ concrete	3.94	30.7	none

in x 25.4 = mm

lb/ft² x 4.88 = kg/m²

Table 14. Summary of CIRIA tests on concrete-reinforced grass channels. (34)

Channel (1)	Run Numbers (2)	Date (3)	Duration (hour) (4)	Discharge ft ³ /s (5)	Velocity at Ch.15 ft/s (6)	Performance (7)
Dycel	1	6/17/86	0.75	8.1	14.8*	Good
	2	6/17/86	1.75	8.3	15.1	Good
	3	6/17/86	2.75	9.7	16.7	Good
	4,5,6	7/02/86	0.75, 1.50, 3	25.6	22.6	Limited Damage
	7a	7/16/86	0.25	33.5	24.9*	Further Damage
	7b,8,9	7/16/86	0.25, 1.5, 3	36.7	25.9	Further Damage
	10	7/16/86	1.0	36.7	25.9	Limited Damage
Petra- flex	1	6/16/86	0.75	6.1	13.1*	Good
	2	6/16/86	1.50	5.8	13.1	Good
	3	6/16/86	3	6.3	13.8	Good
	4,5,6	7/03/86	1, 1.75, 2.50	27.4	23.3	Good
	7	7/15/86	0.75	37.5	25.9	Good
	8,9	7/15/86	1.50, 3	38.7	25.9	Limited Damage
	10	7/18/86	1.75	4.8	11.5	Limited Damage
Armor- flex	1	6/19/86	1	12.2	15.4*	Good
	2	6/19/86	1.25	13.2	15.7	Good
	3	6/19/86	3	11.7	15.1	Good
	4	7/07/86	0.75	26.0	22.6*	Limited Damage
	5,6	7/08/86	2, 2.50	26.5	23.0	Limited Damage
	7,8,9	7/17/86	0.75, 2, 2.50	34.4	26.2	Further Damage
	10a&b	7/24/86	0.25, 0.25	35.6	26.6	Limited Damage
Dymex	1	6/18/86	0.75	5.8	13.1*	Good
	2	6/18/86	1.75	6.2	13.5	Good
	3a	6/18/86	1.50	4.9	12.8*	Good
	3b	6/18/86	0.50	5.8	13.1	Good
	3c	6/18/86	0.50	4.4	11.8*	Good
	4	6/27/86	1	10.6	14.8*	Limited Damage
	5	6/27/86	1.50	10.6	15.1*	Further Damage
6	6/27/86	2.50	14.3	16.4	Failed	

*Interpolated velocity

Table 14. Summary of CIRIA tests on concrete-reinforced grass channels
(continued).(34)

Channel (1)	Run Numbers (2)	Date (3)	Duration (hour) (4)	Discharge ft ³ /s (5)	Velocity at Ch.15 ft/s (6)	Performance (7)
Grass- crete	1	6/12/86	0.75	4.6	14.4	Good
	2,3	6/12/86	1.50, 3	6.5	15.1*	Good
	Trial	6/20/86	0.75	21.4	22.3	Good
	4,5,6	7/14/86	0.50, 0.75, 3	36.0	25.9	Slight Damage
	7,8	7/22/86	0.50, 0.75	36.3	26.2*	Further Damage
	9	7/23/86	3	33.9	25.6	Further Damage

*Interpolated velocity

$$\text{ft}^3/\text{s} \times 0.0283 = \text{m}^3/\text{s}$$

$$\text{ft}/\text{s} \times 0.3048 = \text{m}/\text{s}$$

Note: "Damage" refers to loss of soil and grass from voids.
 "Failure" refers to loss of subsoil.
 "Velocity at Ch. 15" refers to the velocity of flow at a point in the
 channel 15m (49 ft) downslope from the crest.

Table 15. Permissible shear stress for gravel and rock riprap.(37)

Category	Type (size) (in)	Permissible Unit Shear Stress (lb/ft ²)
Gravel	1	0.40
	2	0.80
Rock	6	2.50
	12	5.00

$1\text{b/ft}^2 \times 47.87 = \text{N/m}^2$

$\text{in} \times 25.4 = \text{mm}$

DESCRIPTION OF FULL-SCALE EMBANKMENT TESTING PROGRAM

1. General

The testing program consisted of 57 individual hydraulic tests with each test falling into one of eight general categories. Categories were defined by the type of bare soil or embankment protection system being tested. The general categories are referred to as test series one through eight, enumerated below:

1. Type II (CL).
2. Type I (SC-SM).
3. Soil cement.
4. Gabion mattresses.
5. Geoweb.
6. Enkamat (7020).
7. Enkamat (7020) with asphalt.
8. Cable-tied concrete block revetment systems.

The general testing procedure was similar for all test categories. A 6 ft (1.8 m) high embankment with a crest width of 20 ft (6.1 m) was constructed in the 4 ft (1.2 m) wide flume for each test. The embankment soil was compacted in accordance with U.S. Department of Transportation and U.S. Bureau of Reclamation procedures. The downstream slope of the embankment was constructed on either a 2H, 3H, or 4H:1V slope. The full-scale embankment constructed in the flume represents a 4 ft (1.2 m) long, 6 ft (1.8 m) high embankment with a 20 ft (6.1 m) wide crest and a total width of 32 to 44 ft (9.8 to 13.4 m) depending on the sideslope. For the tests involving an embankment protection system, the system was placed on the embankment per the manufacturer's suggested installation procedures.

Prior to testing, the initial embankment profile was determined. After establishing the initial bed profile, water was introduced to the flume and an overtopping depth of 1, 2, or 4 ft (0.30, 0.61, or 1.2 m) was established. Overtopping depths were measured and maintained in the headbox upstream of the inlet diffuser (figure 10). Hourly water-surface and bed elevations were measured at 2-ft (0.61 m) intervals along the centerline of the flume. Also, hourly velocity measurements were taken at 4-ft (1.2 m) stations along the centerline of the flume. In order to determine velocity

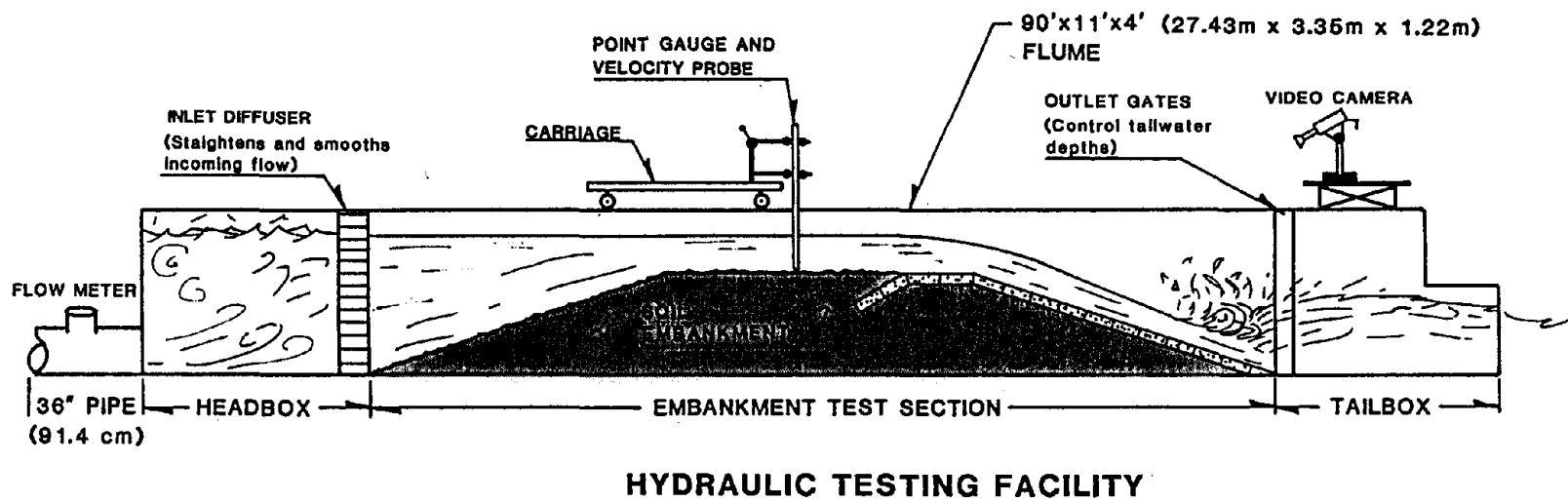


Figure 10. Profile of hydraulic testing facility.

profiles, three velocities were measured at each station. The velocities were measured at approximately 20, 60, and 80 percent of the total flow depth.

2. Data Collection Procedure

Data collected during testing included embankment and water-surface elevations, as well as flow velocities. Before introducing water to the flume, an initial embankment profile was taken using a point gauge attached to a carriage which moved along the length of the flume (along the width of the embankment). A diagram of the testing facility is shown in figure 10. The initial bed profile, as well as subsequent bed and water-surface profiles, were measured along the flume's centerline at 2-ft (0.61 m) intervals beginning at station 16 [approximately 20 ft (6.1 m) upstream of the embankment shoulder] and continuing downstream to the embankment toe. Once the embankment profile was determined, the overtopping depth was set at either 1, 2, or 4 ft (0.30, 0.61, or 1.2 m). After establishment of the overtopping depth, which typically required from 3 to 10 minutes, the tailwater condition was adjusted to achieve either a 1-ft (0.30 m) or a 2-ft (0.61 m) water-surface drop, or freefall (no tailwater). Adjustment of the tailwater gates, when required, typically required an additional 10 minutes. Immediately after establishing steady hydraulic conditions, the point gauge was used to measure water-surface elevations along the embankment to establish initial conditions, hereafter referred to as "hour 0." Also for hour 0, flow velocities were measured parallel to the embankment along the centerline, at 4-ft (1.2 m) intervals, beginning at station 16 and continuing downstream to the embankment toe. Velocities were measured at approximately 20, 60, and 80 percent of the flow depth below the water surface with a Marsh-McBirney Model 201 portable electromagnetic velocity meter.

Both embankment and water-surface elevations, as well as velocities, were measured hourly over the duration of each test. The velocities and flow depths determined in the data collection process defined the hydraulics for each test and allowed the calculation of water discharge, energy grade line,

shear stress, Darcy-Weisbach friction factor, and Manning's n . The determination of these parameters will be described in the section entitled, "Results of Full-Scale Embankment Testing Program."

The bed and water-surface elevations were entered into an IBM-PC-compatible microcomputer using R:base 5000, a relational data-base management software package. These data were placed in a data block within R:base named EMBANK. R:base was then employed to analyze the EMBANK data by computing flow depths, corrected flow depths (adjusted for the embankment slope), average velocities (based on corrected flow depths), and energy grade line elevations. An example of the results from the R:base analysis of EMBANK data is shown in figure 11. The figure shows partial results for test 49, for hour 0 and hour 1. This was a test of Petraflex-Vick concrete blocks on a 2H:1V embankment slope with a 4-ft (1.2 m) overtopping depth and freefall conditions. A plot of the results for test 49 is shown in figure 12. The energy associated with each measurement point is indicated in the figure by a circular symbol.

The velocity profiles, as measured with the portable water current meter, were also entered into R:base. These data were placed in a data block within R:base named VEL268. An example of the organization of these data is shown in figure 13. This figure contains velocity profile information for test 49, hours 0 and 1.

Overtopping depths, tailwater conditions, and embankment sideslopes for all tests are summarized in table 16.

3. Documentation of Test Conditions and Qualitative Assessment of Performance

The performance of bare soil embankments along with six types of embankment protection measures were investigated. Two different soils were tested to establish bare soil performance. The type I soil was classified as erodible, while the type II soil was considered nonerodible. The relative plasticity indices were the basis for these classifications. The eight test

Run Number : 49 Date of Test : 09-22-87 Start Time : 10:00 AM
 Soil Type : TYPE I, w/ PETRAFLEX Duration : 10 Hours End Time : 8:00 PM
 Overtopping Depth : 4.0 ft Water Surface Drop: FF Photographs: YES
 Side Slope : 2:1 Discharge : 96.0 CFS Video Tape : YES

Time (hr)	Station Number	Embankment Elev. (ft)	Water Surface Elev. (feet)	Meas Flow Depth (ft)	Corr Flow Depth (ft)	Ave Vel (ft/s)	EGL Elev (ft)
0.0	16.0	5.47	9.55	4.08	4.08	5.882	10.087
0.0	18.0	6.06	9.30	3.24	3.24	7.407	10.152
0.0	20.0	6.06	9.10	3.04	3.04	7.895	10.068
0.0	22.0	6.01	8.70	2.69	2.69	8.922	9.936
0.0	24.0	6.04	8.50	2.46	2.46	9.756	9.978
0.0	26.0	6.05	8.25	2.20	2.20	10.909	10.098
0.0	28.0	5.96	8.20	2.24	2.24	10.714	9.983
0.0	30.0	5.89	8.10	2.21	2.21	10.860	9.931
0.0	32.0	5.91	8.00	2.09	2.09	11.483	10.048
0.0	34.0	5.96	7.75	1.79	1.79	13.408	10.541
0.0	36.0	5.72	7.55	1.83	1.83	13.115	10.221
0.0	38.0	5.05	6.90	1.85	1.65	14.511	10.170
0.0	40.0	4.04	5.76	1.72	1.54	15.608	9.543
0.0	42.0	3.08	4.64	1.56	1.39	17.209	9.238
0.0	44.0	2.10	3.61	1.51	1.35	17.779	8.518
0.0	46.0	1.29	2.07	1.38	1.23	19.453	8.546
0.0	48.0	0.76	2.05	1.29	1.15	20.811	8.775
1.0	16.0	5.39	9.80	4.21	4.21	5.701	10.105
1.0	18.0	6.07	9.35	3.28	3.28	7.317	10.181
1.0	20.0	6.42	9.00	2.58	2.58	9.302	10.344
1.0	22.0	6.04	8.70	2.66	2.66	9.023	9.964
1.0	24.0	6.01	8.35	2.34	2.34	10.256	9.983
1.0	26.0	5.98	8.15	2.17	2.17	11.060	10.049
1.0	28.0	5.97	8.10	2.13	2.13	11.268	10.071
1.0	30.0	5.90	8.10	2.20	2.20	10.909	9.948
1.0	32.0	5.88	8.00	2.12	2.12	11.321	9.990
1.0	34.0	5.95	7.90	1.95	1.95	12.308	10.252
1.0	36.0	5.83	7.55	1.72	1.72	13.953	10.573
1.0	38.0	4.97	6.59	1.72	1.54	15.608	10.473
1.0	40.0	3.93	5.62	1.69	1.51	15.885	9.538
1.0	42.0	2.98	4.60	1.62	1.45	16.571	8.864
1.0	44.0	2.12	3.69	1.57	1.40	17.099	8.230
1.0	46.0	1.14	2.60	1.46	1.31	18.387	7.850
1.0	48.0	0.76	2.10	1.32	1.18	20.338	8.523

Note : A value of -0- indicates data point not taken.

Figure 11. Partial listing of EMBANK data and results for test 49.

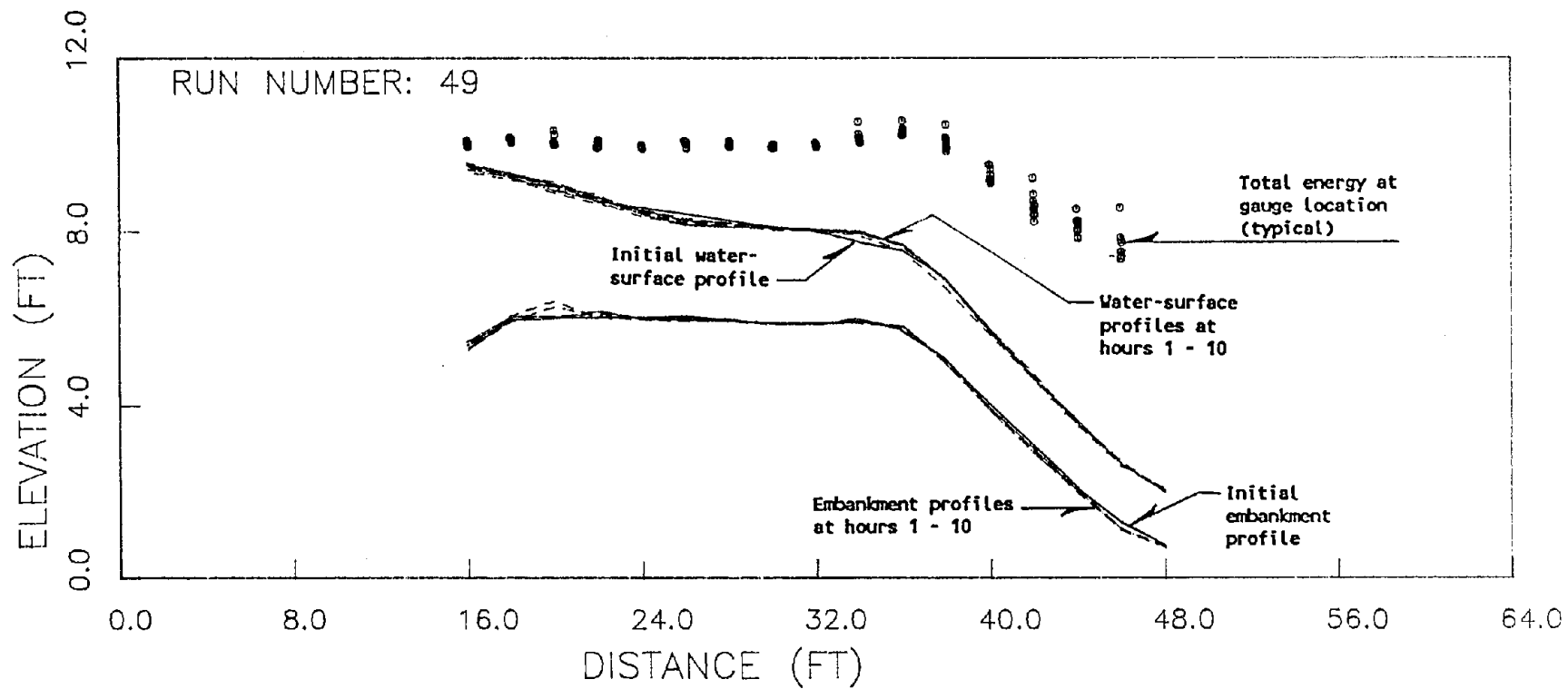


Figure 12. Embankment, water surface, and energy grade line profiles for test 49.

Run Number : 49 Date of Test : 09-22-87 Start Time : 10:00 AM
 Soil Type : TYPE I, W/ PETRAFLEX Duration : 10 Hours End Time : 8:00 PM
 Overtopping Depth : 4.0 ft Water Surface Drop: FF Photographs: YES
 Side Slope : 2:1 Discharge : 96.0 CFS Video Tape : YES

Time (hr)	Station Number	Velocity (ft/s)		
		0.2 depth	0.6 depth	0.8 depth
0.0	16.0	3.80	4.00	3.70
0.0	20.0	7.80	6.50	8.40
0.0	24.0	8.60	9.70	8.30
0.0	28.0	10.60	10.50	10.00
0.0	32.0	10.30	11.00	10.80
0.0	36.0	10.80	12.60	13.30
0.0	40.0	15.00	15.30	15.20
0.0	44.0	18.50	18.30	18.20
0.0	48.0	-0-	20.00	-0-
1.0	16.0	4.60	5.70	4.50
1.0	20.0	7.30	7.60	7.90
1.0	24.0	9.50	9.50	9.00
1.0	28.0	-0-	10.20	10.00
1.0	32.0	10.20	11.00	10.90
1.0	36.0	-0-	11.50	13.20
1.0	40.0	15.60	15.70	15.80
1.0	44.0	18.50	18.20	18.00
1.0	48.0	19.20	19.30	19.60
2.0	16.0	5.00	5.60	4.60
2.0	20.0	8.30	8.40	8.20
2.0	24.0	9.60	9.50	9.10
2.0	28.0	-0-	10.50	10.10
2.0	32.0	-0-	11.10	10.90
2.0	36.0	10.40	12.50	13.30
2.0	40.0	15.30	15.50	15.40
2.0	44.0	18.50	18.20	17.70
3.0	16.0	4.10	5.60	4.30
3.0	20.0	7.80	8.30	8.10
3.0	24.0	9.50	9.60	9.40
3.0	28.0	10.60	10.80	10.60

Note : A value of -0- indicates data point not taken

Figure 13. Partial listing of VEL268 data for test 49.

Table 16. Summary of hydraulic test conditions.

Test Series	Description	Test Number	Overtopping Depth (ft)	Water-Surface Drop (ft)	Initial Embankment Slope
1	Type II soil (CL)	1B	1	FF ¹	3:1
		2	2	FF	3:1
		3	2	FF	3:1
		4	2	1	3:1
		5	1	FF	4:1
		6	2	FF	4:1
		7	4	FF	4:1
		8	4	1	3:1
		9	4	2	3:1
		10	4	FF	3:1
3	Soil cement	11	1	FF	3:1
		12	2	FF	3:1
		13	4	FF	3:1
		14	1	FF	2:1
		15	2	FF	2:1
		16	4	FF	2:1
4	6-in thick gabion mattresses	17A	2	2	2:1
		17B	2	2	2:1
		18	4	2	2:1
		19	2	FF	2:1
		20	4	FF	2:1
		21	2	2	3:1
		22	4	2	3:1
		23	2	FF	3:1
24	4	FF	3:1		
2	Type I soil (SM-SC)	25	1	FF	3:1
		26	1	FF	4:1
		27	2	FF	4:1
		28	4	FF	4:1
		29	2	FF	3:1
		30	4	FF	3:1
		31	4	2	3:1
		32	4	1	3:1
		33	2	1	3:1

¹FF indicates freefall tailwater conditions.

Table 16. Summary of hydraulic test conditions (continued).

Test Series	Description	Test Number	Overtopping Depth (ft)	Water-Surface Drop (ft)	Initial Embankment Slope
5	4-in geoweb	34	1	FF ¹	2:1
		35	2	FF	2:1
		36	4	FF	2:1
6	Enkamat (7020)	37	2	2	2:1
		38	1	1	2:1
7	Enkamat (7020) w/3-in asphalt cover	39	2	2	3:1
		40	2	FF	3:1
		41	4	2	3:1
	Enkamat (7020) w/1-in asphalt cover	42	1	FF	2:1
43		1	1	2:1	
8	Armorflex concrete blocks	44	1	FF	2:1
		45	2	FF	2:1
		46	4	FF	2:1
		46A	4	FF	2:1
	Petraflex concrete blocks	47	1	FF	2:1
		48	2	FF	2:1
		49	4	FF	2:1
		49A	4	FF	2:1
		50	4	FF (hrs 0-2) 7/2.1 (hrs 2-6) 4/1.2 (hrs 6-8) 2/0.6 (hrs 8-10)	2:1
	50A	4	7/2.1	2:1	
6	Enkamat (7020)	51	0.5	FF	3:1
8	Dycel concrete blocks	52	1	FF	2:1
		53	1	FF	2:1
2	Type I soil	54	1	FF	3:1

ft x 0.3048 = m

¹FF indicates freefall tailwater conditions.

series were categorized according to soil type or protection system as described previously.

Embankment construction, protection system descriptions and installation procedures, and hydraulic test conditions for each test series are described in the following sections.

The embankment was not completely rebuilt between each test. For the protection system tests where erosion did not occur, the embankment was not reconstructed prior to the subsequent test. However, when erosion was observed, the partially eroded embankment was cut down to a subprofile 4 to 4.5 ft (1.22 to 1.37 m) high. Soil was then placed on the subprofile, as specified, to bring the embankment up to grade. An overcompacted soil core was formed as a result of not removing the embankment subprofile between tests. Consequently, embankment erosion during all tests (except test 54 where the embankment was completely reconstructed) was limited to the reconstructed shell of soil overlaying the subprofile.

a. Test Series 1: Type II Soil (CL)

Field and laboratory tests were conducted to determine the classification and engineering properties of this soil. Properties which were determined included Proctor density, permeability, Torvane shear strength, critical shear stress, Atterberg limits, grain-size distribution, and classification by both the Unified Soil Classification System (USCS) and the American Association of State Highway and Transportation Officials (AASHTO) system.

The standard Proctor test determined the maximum dry density to be 110 lbs/ft³ (17.3 kN/m³) at an optimum moisture content of 16.8 percent. The moisture-density curve is shown in figure 14. Permeability tests resulted in a range for hydraulic conductivity varying from 1.9×10^{-7} to 4.8×10^{-7} cm/s. The following Atterberg limits were determined: liquid limit--32.8 to 47.8, plastic limit--20.7 to 23.2, and plasticity index--11.6 to 24.6. The soil's grain-size distribution curve is given in figure 15. The D₅₀ for

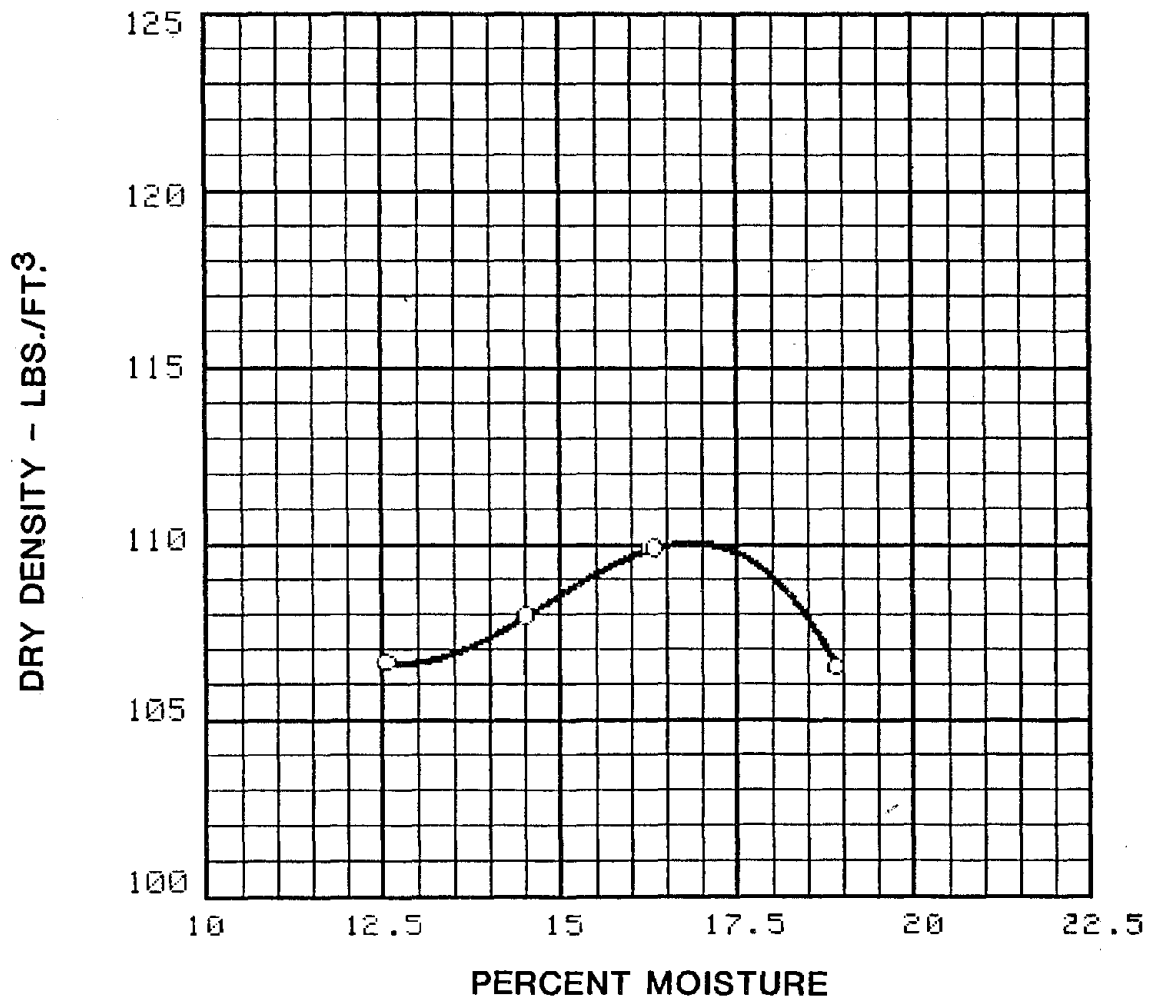


Figure 14. Moisture density curve for the type II soil.

CLAY	SILT	SAND			GRAVEL
		FINE	MEDIUM	CRSE	

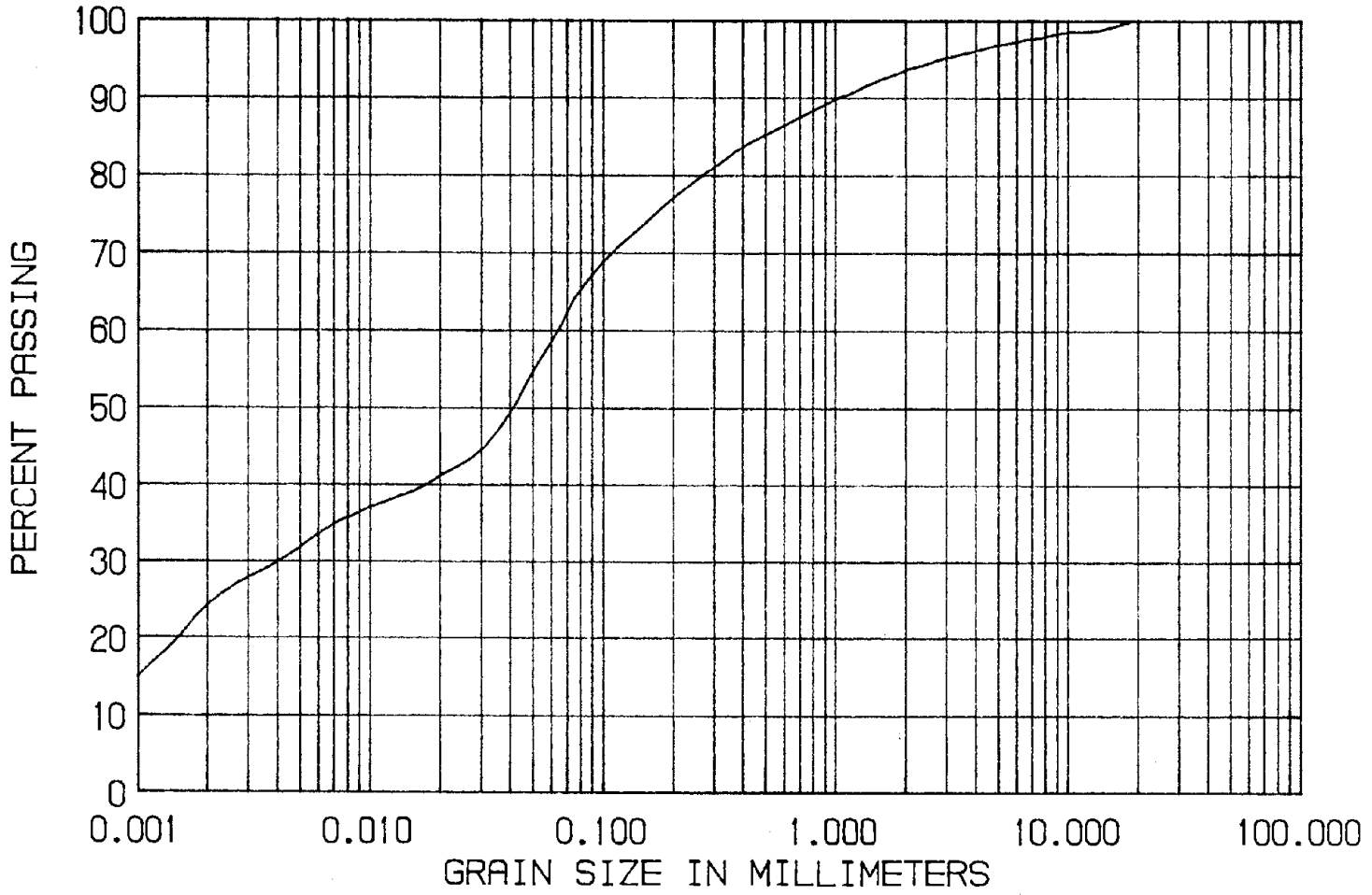


Figure 15. Grain size distribution curve for the type II soil.

this soil was 0.04 mm. The type II soil was classified as a clay of low plasticity (CL) by the USCS. The AASHTO classification for the soil is A-6. The Torvane test found the shear strength of the soil before saturation to be 2.5 tons/ft² (240 kN/m²). After saturation the shear strength ranged from 0.1 to 3.2 tons/ft² (10 to 310 kN/m²). The critical shear stress was determined to be 0.078 lb/ft² (3.7 N/m²). The soil consisted of approximately 40 percent sand and 60 percent silt and clay.

(1) Embankment Construction and Installation. The type II soil was placed in 8-in (20 cm) lifts and compacted to 95 to 100 percent of standard Proctor density. The soil was compacted with a jumping-jack style soil compactor using three passes per lift. The face of the embankment was prepared to a 3H:1V slope for tests 1B, 2, 3, 4, 8, 9, and 10, and a 4H:1V slope for tests 5, 6, and 7.

(2) Description of Hydraulic Test Conditions. The type II soil embankment was tested under several hydraulic conditions. Overtopping depths ranged from 1 to 4 ft (0.30 to 1.2 m). Downstream conditions varied from freefall to tailwater with as little as a 1-ft (0.30 m) water-surface drop. Refer to table 16 for a complete summary of test conditions.

(3) Qualitative Description of Type II Soil Performance. The type II bare soil embankment experienced considerable erosion for all but the least severe hydraulic conditions tested. The 1-ft (0.30 m) overtopping depth on the 3H:1V slope, and 1- and 2-ft (0.30 and 0.61 m) overtopping depths on the 4H:1V embankment did not cause substantial erosion. However, the erosion associated with higher discharges was significant. In general, tailwater conditions resulted in erosion of the crest and shoulder while the toe of the slope remained relatively stable. Conversely, freefall conditions tended to erode the toe of the slope to a greater degree than the crest and shoulder.

The duration of all type II bare soil embankment tests was 4 hours. For the lower discharges, the embankments had essentially stabilized by the end of the test with only minimal erosion occurring during the final hour.

However, the tests with 4-ft (1.2 m) overtopping depths and 3H:1V sideslopes were still experiencing considerable erosion at the end of the testing periods. In these cases, erosion would probably have resulted in a complete breach if the tests had continued.

b. Test Series 2: Type I Soil (SM-SC)

Field and laboratory tests were performed on this soil to determine its engineering properties and classification. Soil characteristics which were determined included Proctor density, permeability, Atterberg limits, grain-size distribution, and classification by the USCS and AASHTO system. The standard Proctor test determined the maximum dry density was 121.5 lb/ft³ (19.1 kN/m²) at an optimum moisture content of 11.9 percent. The moisture-density curve is shown in figure 16. The hydraulic conductivity for the type I soil was 7×10^{-8} cm/s at 95 percent of standard Proctor density. The following Atterberg limits were determined: liquid limit--21.5, plastic limit--16.6, and plasticity index--4.9. The grain-size distribution for the soil is given in figure 17. The D₅₀ for this soil was 0.045 mm. The Unified Soil Classification of this soil was silty clay to silty sand (SC-SM). The AASHTO classification was A-4(0).

(1) Embankment Construction and Installation. The type I soil was placed in the flume in 6- to 8-in (15 to 20 cm) lifts. A jumping-jack style soil compactor was used to compact the soil for tests 25 to 32. One pass per lift was required to achieve 95 to 100 percent standard Proctor density. Beginning with test 33, a vibrating plate compactor was used for compacting the embankments. Compaction of 89 to 93 percent of standard Proctor density was achieved with the vibrating plate. Prior to test 33, a jumping-jack compactor was used to compact the embankment. However, this method resulted in extremely high in-place densities, which were considered unrepresentative of actual field placement techniques. Therefore, the compaction method was changed to produce representative soil conditions. The downstream slope of the embankment was prepared to a 4H:1V slope for tests 26, 27, and 28, and a 3H:1V slope for tests 25, and 29 to 33.

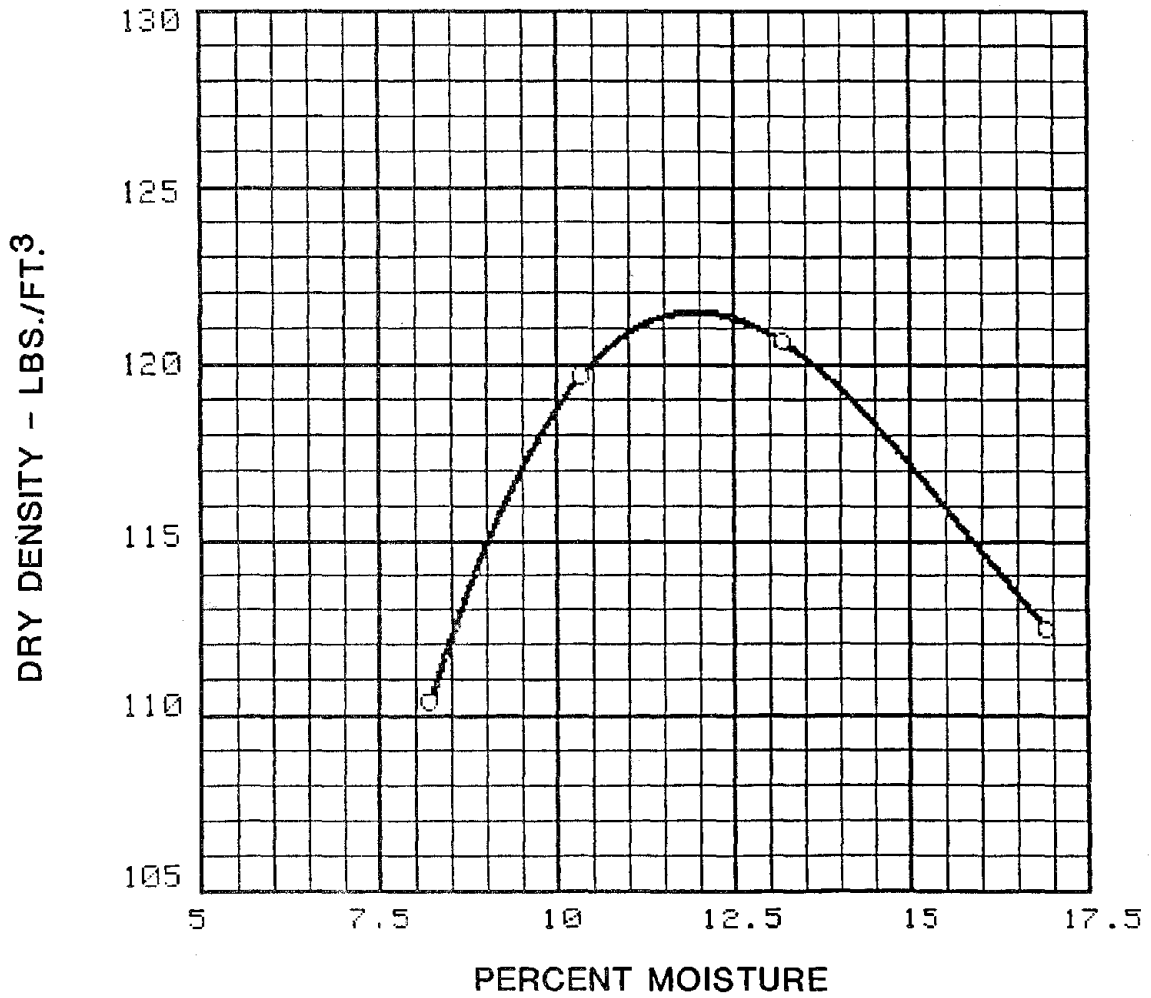


Figure 16. Moisture density curve for the type I soil.

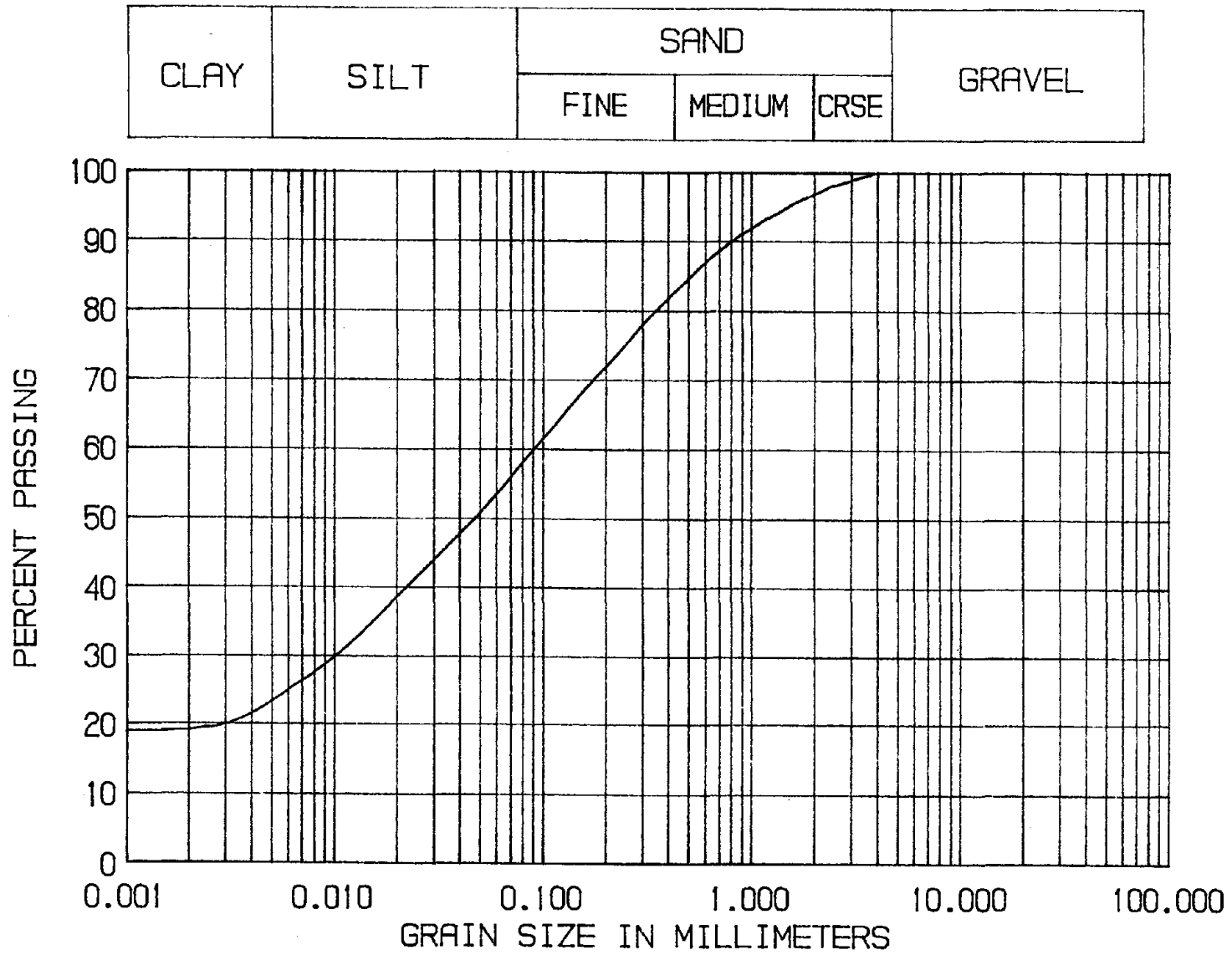


Figure 17. Grain size distribution curve for the type I soil.

(2) Description of Hydraulic Test Conditions. The type I soil embankment was tested under several hydraulic conditions. The overtopping depths varied from 1 to 4 ft (0.30 to 1.2 m). Downstream conditions varied from freefall to tailwater with a minimum water-surface drop of 1.0 ft (0.30 m). Refer to table 16 for a complete summary of test conditions.

(3) Qualitative Description of Type I Soil Performance. As with the type II soil, the type I bare soil embankment experienced significant erosion for all but the least severe hydraulic conditions tested. It was anticipated that the type II soil would be less erodible than the type I soil due to the relatively high plasticity index of the type II soil. The plasticity index for the type I soil was 4.9, whereas, for the type II soil, the index ranged from 11.6 to 24.6. However, the type I soil did not erode to the extent that the type II soil did.

The relative erodibilities of the type I and type II soils appeared to be more strongly correlated to in-place density rather than plasticity index. The type II soil, with a maximum Proctor density of 110 lb/ft³, required six passes of the jumping-jack compactor to achieve a compaction ratio of 95 to 100 percent. In contrast, the type I soil, with a maximum Proctor density of 121.5 lb/ft³, was easily compacted to 95 percent with only one pass of the jumping-jack compactor. Two or more passes resulted in an in-place density exceeding the maximum Proctor density. The high degree of compaction and resulting in-place density had a profound effect on the critical shear stress of the type I soil, increasing its effective resistance to erosion.

Previous studies have shown critical shear stress to be a function of plasticity index only (see equation 5). The results of this investigation suggest that in-place density should also be considered when estimating critical shear stress. An equation which includes both plasticity index and in-place density may be more appropriate for computing critical shear stress than the equations which have been previously developed.

The duration of all type I bare soil embankment tests was 4 hours. The embankments had mostly stabilized by the end of the tests without

significant erosion during the final hour. The only exceptions were tests 29 and 30, which were still eroding considerably during the fourth hour. These tests were performed on 3H:1V embankments with 2- and 4-ft (0.61 and 1.2 m) overtopping depths and freefall conditions. For this series of tests, these were the most severe hydraulic conditions considered. If the test durations had been extended, test embankments 29 and 30 would probably have experienced considerably more erosion.

c. Test Series 3: Soil Cement

Soil cement is a no slump mixture of Portland cement, soil, and water. The material is placed directly on the embankment soil and compacted using standard earth-working equipment to a specified field density, which is typically referenced to standard Proctor density laboratory results. Soil cement requires a curing period, generally specified as a minimum of 7 days. After curing, the soil cement results in a protection system with relatively low breaking strength, but exhibiting an extremely durable and erosion-resistant surface.

(1) Installation of Protection System. Type I soil was used to reconstruct the test embankment. The soil was placed in 4-in (10 cm) lifts and compacted to 95 to 100 percent of standard Proctor density. A jumping-jack style compactor was used to compact the embankment soil. One pass per lift was required to achieve the specified density. The downstream slope of the embankment was prepared in a stair-step fashion to a final 3H:1V side-slope for tests 11, 12, 13, and a 2H:1V sideslope for tests 14, 15, and 16.

The soil cement was mixed in a 6.0 ft³ (0.16 m³) portable cement mixer. The soil cement in this test series consisted of road base aggregate no larger than 3/4 in (1.9 cm), type II soil, no. 2 Portland cement, and water. The grain-size distribution curve for the soil cement aggregate (the blended road base and type II soil) is given in figure 18. The D₅₀ for the aggregate was 0.95 mm. The soil cement mixture contained 8 percent Portland cement by dry weight. The amount of water used in each batch was adjusted based on the field moisture content of the 3/4-in (1.9 cm) road base and type

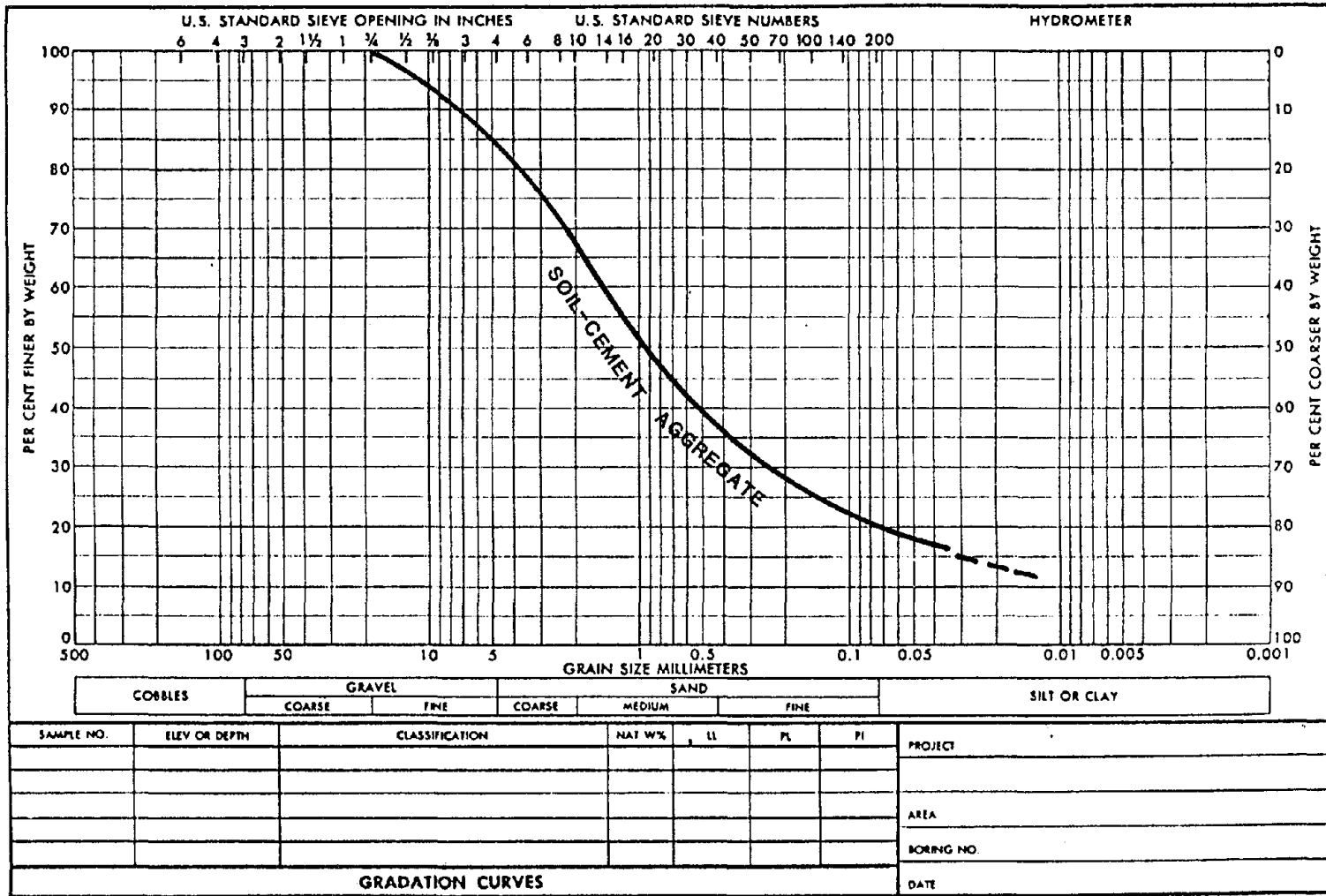


Figure 18. Grain size distribution curve for the soil cement aggregate (includes road base and type II soil).

ENG FORM 2087
1 MAY 63

PLATE V-2

II soil in order to achieve a final moisture content of 12 percent. A typical soil cement batch was mixed for a period of four minutes. The 28-day compressive break strength for the soil cement was 880 psi (6,070 kN/m²).

Except for the top and bottom steps, the soil cement was placed in 4-in (10 cm) lifts which were 3 ft (0.91 m) wide and 4 ft (1.2 m) long (spanning the entire width of the flume). The bottom step differed only in that it was 6 ft (1.8 m) wide. The top step included an 18-in (46 cm) deep, 12-in (30 cm) wide anchor trench. For the 3H:1V embankment, successive steps overlapped by 2 ft (0.61 m). The overlap distance for the 2H:1V embankment was 28 in (0.71 m). Figure 19 is a sketch of the 3H:1V soil cement embankment. The embankment profile including flume stationing is shown in figure 20.

For tests 11, 12, and 13 (3H:1V slopes), the soil cement was compacted to 95 percent of standard Proctor density with a hand tamping device. The soil cement for these tests was allowed to cure for 4 months (December 1986 through March 1987). During this time, the soil cement was exposed to several freeze-thaw and wet-dry cycles, which resulted in a loose, surficial flaking of the upper 3 to 5 mm. However, damage was limited to this surface layer, and no through-going cracks or disintegration was noted.

The soil cement for tests 14, 15, 16 (2H:1V slopes) was compacted to 95 percent of standard Proctor density with a vibrating plate compactor. This embankment included artificial cold joints at stations 40 and 44. A cold joint consisted of 12 mil (0.30 mm) black plastic placed between the soil cement lifts. Figure 21 is a sketch of the 2H:1V soil cement embankment with the cold joints at stations 40 and 44. The soil cement for this test series was allowed to cure for 7 days prior to testing. Figure 22 shows a completed soil cement installation.

(2) Description of Hydraulic Test Conditions. The two soil cement embankments were tested under six different hydraulic conditions with overtopping depths ranging from 1 to 4 ft (0.30 to 1.2 m) and freefall downstream conditions. The sideslopes tested included 3H:1V and 2H:1V. All

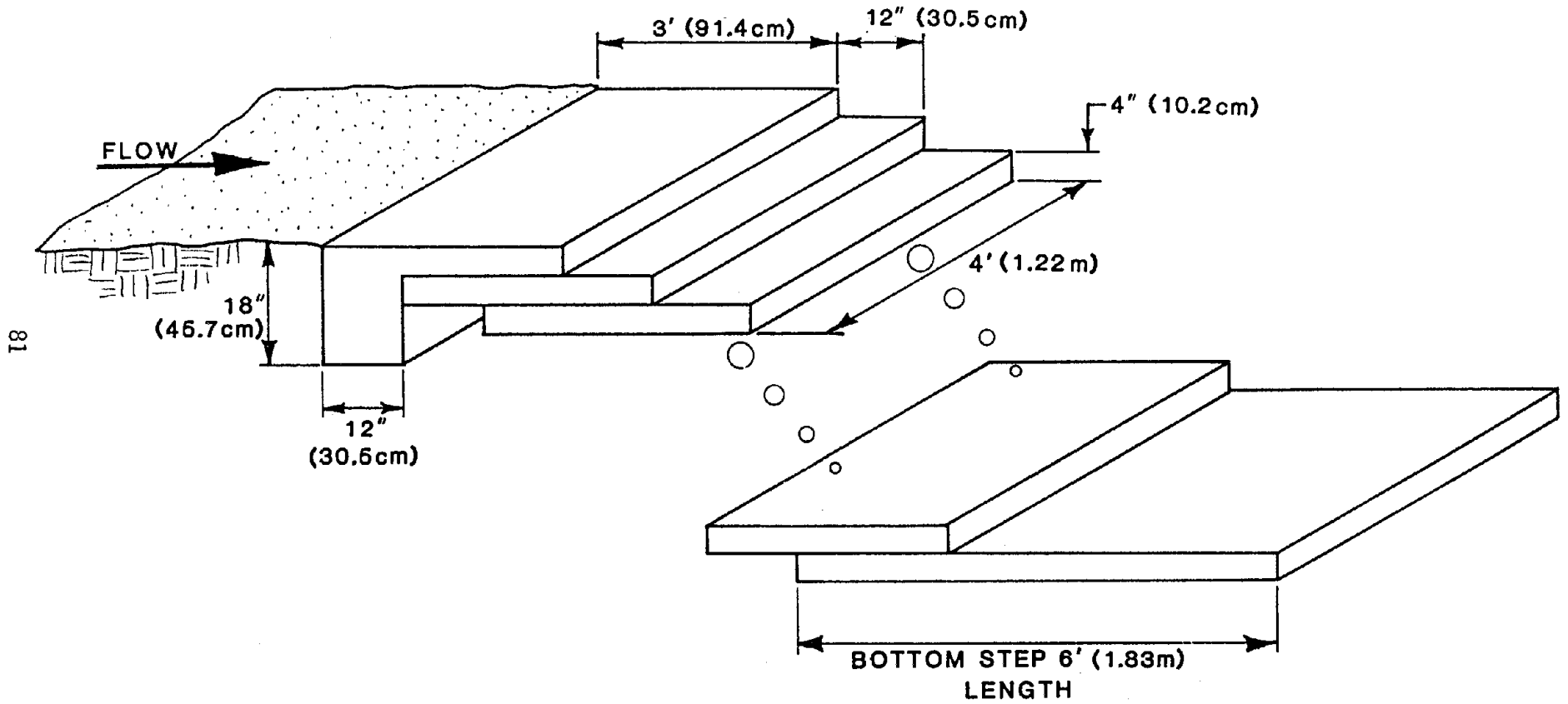
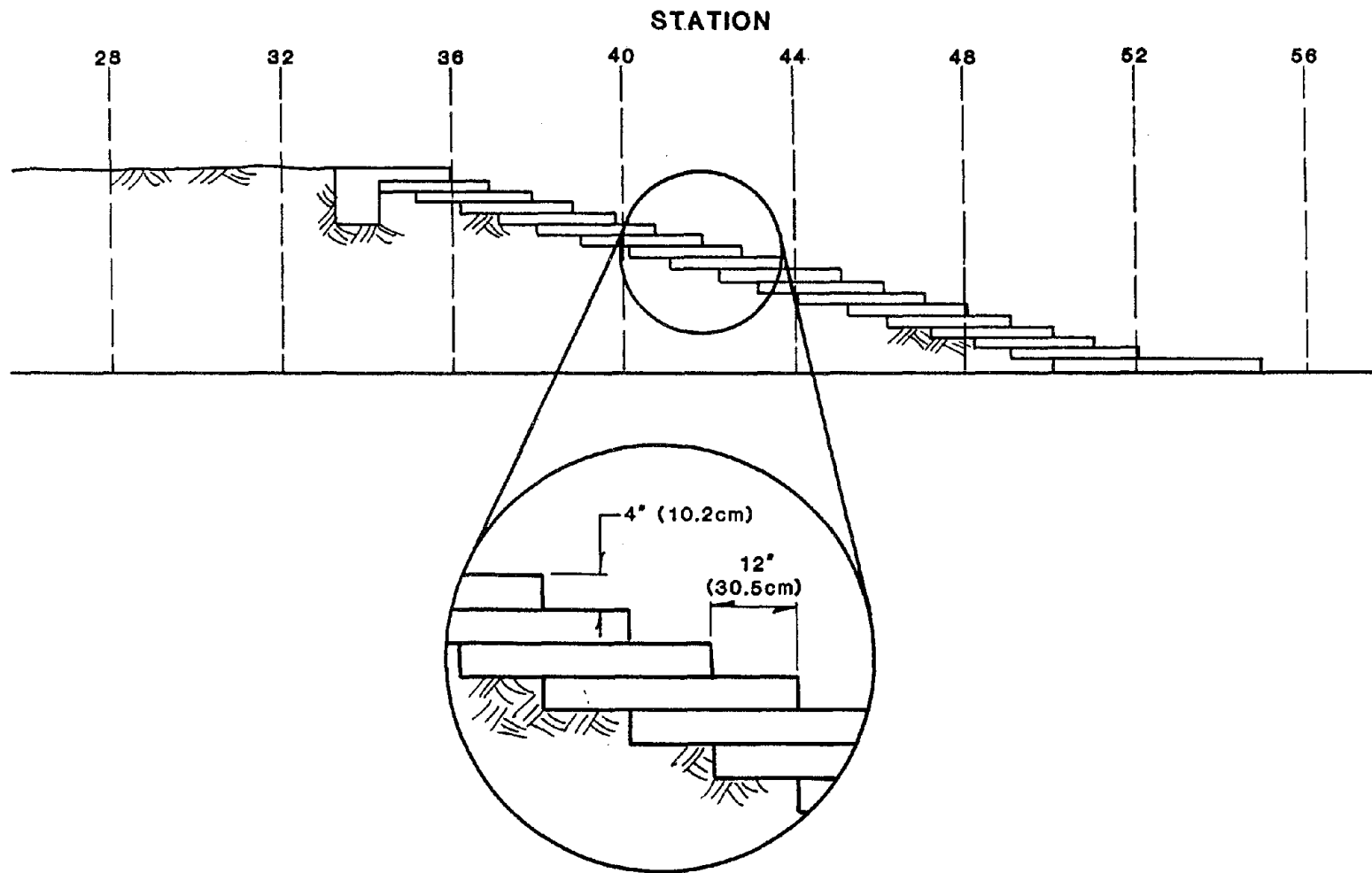
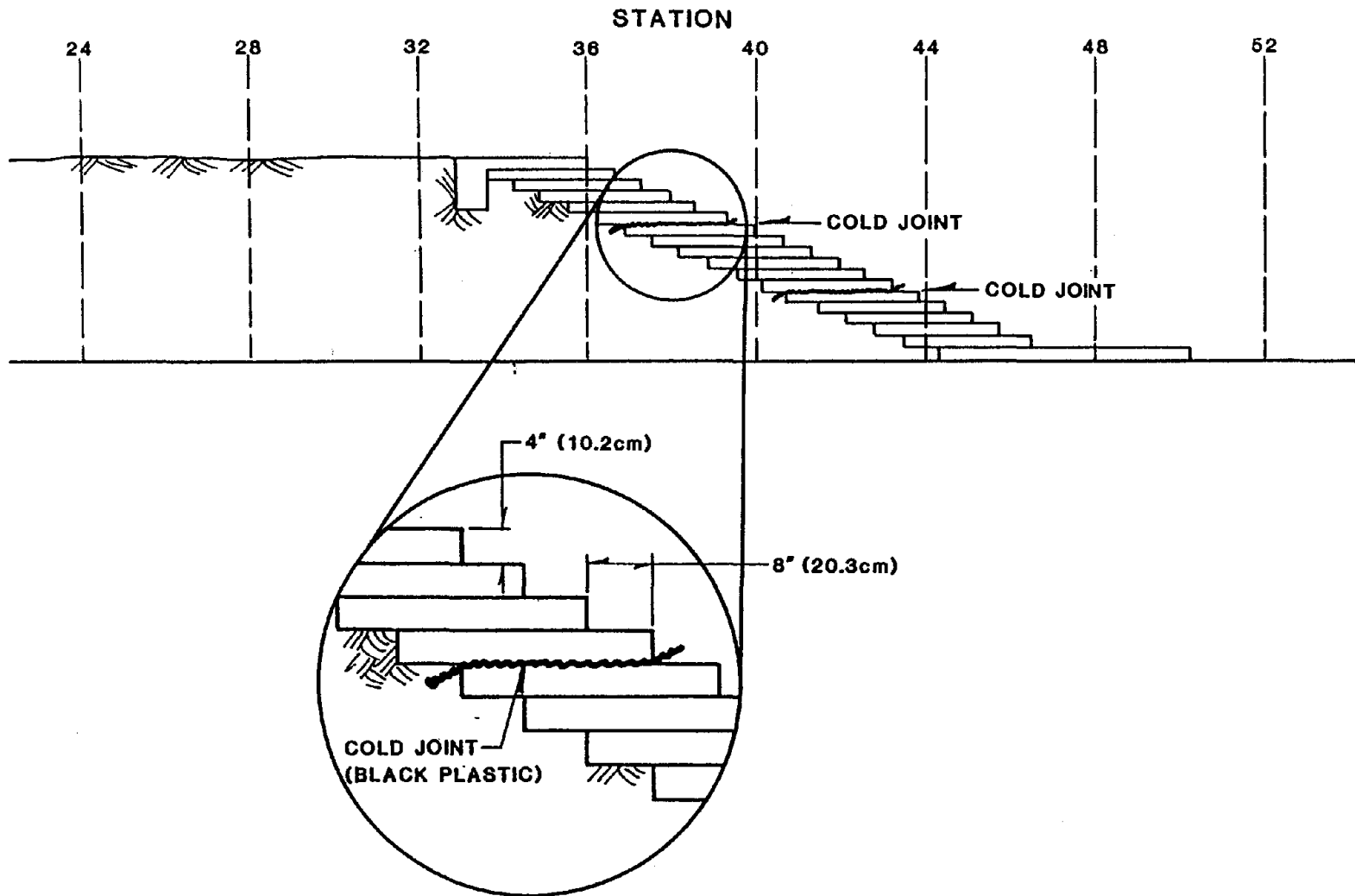


Figure 19. Sketch of the soil cement embankment (3H:1V slope).



82

Figure 20. Profile of the soil cement embankment (3H:1V slope).



83

Figure 21. Profile of the soil cement embankment (2H:1V slope).



a. Looking upstream



b. Looking downstream

Figure 22. Typical soil cement installation.

soil cement tests were conducted for a scheduled duration of 10 hours. Refer to table 16 for a complete summary of test conditions.

(3) Qualitative Description of Soil Cement Performance. Soil cement proved to be one of the most stable slope protection measures tested in this program. Although the unprotected portion of the crest degraded from 4 to 8 in (0.1 to 0.2 m) during the test, there was no indication of soil loss from beneath the protection system. Damage to the soil cement was limited to a "rounding off" of the edge of each stair step. Each test ran for the complete scheduled duration of 10 hours. Due to the limited amount of working space within the flume, it was quite labor-intensive to install the soil cement in the flume. However, a field application using the proper equipment could be very efficient.

d. Test Series 4: Gabion Mattresses

Gabion mattresses are rectangular baskets manufactured from galvanized steel wire mesh of triple-twist hexagonal weave. Each mattress is subdivided laterally, into three individual compartments. Typical mattress dimensions in this test series were 6 in (15 cm) deep by 8 ft (2.4 m) long by 4 ft (1.2 m) wide. Figure 23 shows a sketch of a typical gabion basket and lid. Tyvar 3401 filter fabric was used for the mattress underlayer. This material is a 4 oz (0.56 N) nonwoven geotextile made from spun-bonded fiber.

(1) Installation of Protection System. Type I soil was used to construct the test embankment. Soil was placed in 4- to 6-in (10 to 15 cm) lifts and compacted with a jumping-jack style compactor. One pass per lift was required to achieve 95 to 100 percent Proctor compaction density. The embankment was constructed to a 2H:1V slope for tests 17A, 17B, 18, 19, and 20, and a 3H:1V slope for tests 21, 22, 23, and 24. The crest of the embankment was constructed with a 6-in-deep notch to allow the gabion mattress to fit flush with the upstream soil embankment. The notch was located at station 32 for test 17A, but relocated upstream at station 28 for

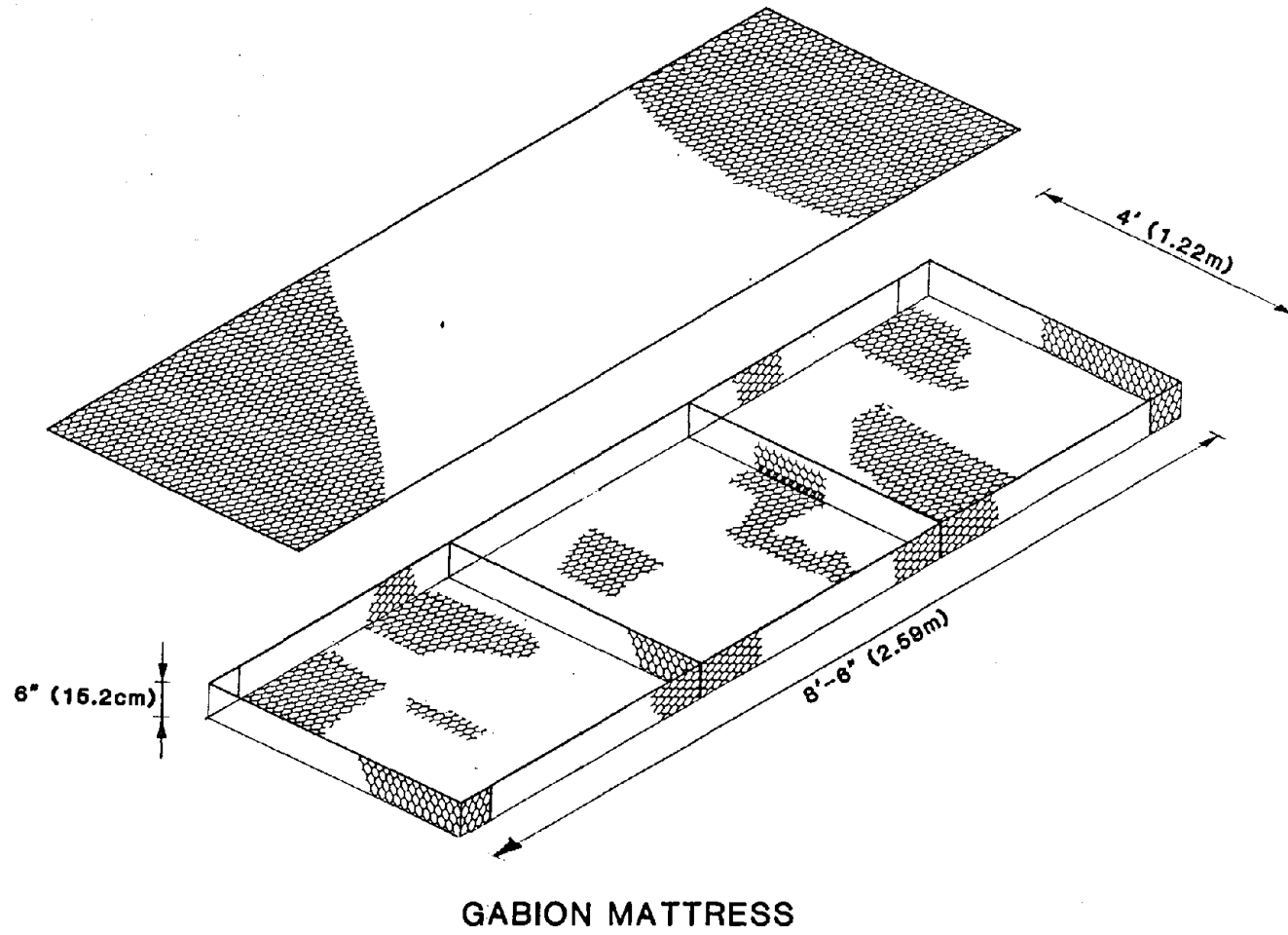


Figure 23. Sketch of 6-in (15.2 cm) gabion mattress and lid.

tests 17B to 24. Figure 24 is a sketch of a typical gabion mattress installation.

The Typar 3401 filter fabric was cut to a width of 60 in (152 cm) allowing the fabric to lap up 6 in (15 cm) on each flume wall. The fabric was keyed into the embankment crest at station 26, as shown in figure 24. The geotextile was then rolled out to station 52, 4 ft (1.2 m) beyond the toe of the slope.

The gabion mattresses and lids were cut from a width of 6 ft (1.8 m) to a final width of 4 ft (1.2 m). The mattresses were cut along their entire length and the pieces overlapped a distance of 1 ft (0.30 m). The manufacturer's recommended lacing pattern was used to wire the mattresses together.

The gabion mattresses were placed in the flume and wired together using a lacing pattern at each seam. The baskets were filled with 3- to 6-in (7.6 to 15 cm) rounded river rock. The gabion lids were then placed on the baskets and wired down. A solid steel bar was welded to each wall of the flume at station 48 to provide a system anchor at the toe of the slope. Figure 25 shows a picture of a completed gabion mattress installation.

(2) Description of Hydraulic Test Conditions. Gabion mattresses were tested under eight different hydraulic conditions. Test 17A had an overtopping depth of 2 ft (0.61 m) with a water-surface drop of 2 ft (0.61 m) and a 2H:1V sideslope. The scheduled duration of this test was 4 hours, but the system failed after 1 hour. The failure was attributed to loss of the crest anchor, caused when soil eroded from the upstream edge of the mattress allowing water under the gabions which washed the system off the embankment. Test 17B hydraulic conditions were identical to test 17A; however, the upstream edge of the mattress and geotextile anchorage was moved upstream to station 28 to avoid the effects of supercritical flow. This test was run for the scheduled duration of 4 hours and proved to be stable. Tests 18 through 23 were conducted under several different hydraulic conditions with overtopping depths ranging from 2 to 4 ft (0.61 to 1.2 m), 2H:1V to 3H:1V embankment sideslopes and downstream conditions varying from freefall

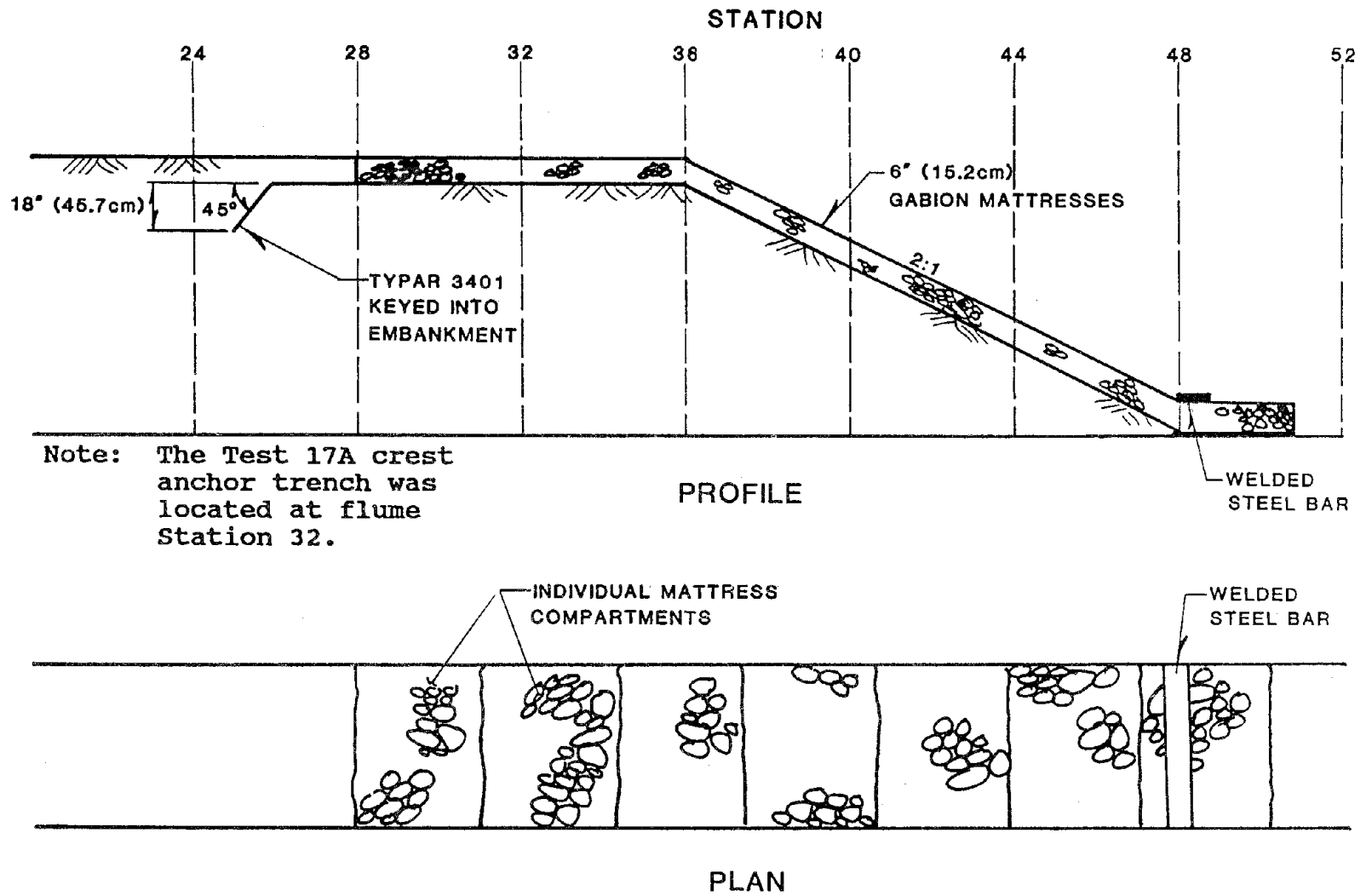


Figure 24. Sketch of typical 6-in (15.2 cm) gabion mattress system.



Figure 25. Typical 6-in (15.2 cm) mattress installation.

to tailwater with a 2-ft (0.61 m) water-surface drop. All of these tests were run for the scheduled 4 hr duration. Test 24 utilized a 4-ft (1.2 m) overtopping depth, freefall downstream condition and a 3H:1V sideslope. The duration of this test was scheduled to be 4 hours, but the system failed after 1 hour, again exhibiting loss of anchorage on the crest after the unprotected portion of the crest degraded sufficiently to allow the flow to impinge directly on the exposed face of the gabion mattress. See table 16 for a complete summary of test conditions.

(3) Qualitative Description of Gabion Mattresses Performance.

Gabion mattresses were found to be relatively stable under the hydraulic conditions investigated in this test series. Instabilities which arose for severe hydraulic conditions were mainly due to inadequacy of the crest anchoring system. Redesigning the crest anchor trench will improve the performance of the system under more severe hydraulic conditions. During these tests, the rocks which had been placed in the mattresses migrated to the downstream end of the individual baskets causing the baskets to deform slightly. At the end of each test, the rocks were redistributed within the baskets and the baskets returned to their original form. Tightly packing the rockfill using angular stones to increase the packing factor would help alleviate the problem of rock migration within the compartments. Reconditioning of the gabion system between tests also included bringing the embankment upstream of the mattresses back up to grade and recompacting it to 95 to 100 percent of standard Proctor density with a jumping-jack style compactor.

Figure 26 shows the failure exhibited by the gabion mattress system. This failure occurred during test 24 and was attributed to the loss of the crest anchor. Erosion of the embankment just upstream of the mattresses allowed water to impact the exposed mattress face and flow under the mattress system. This resulted in uplifting of the mattresses, causing the system to be rolled off the embankment.

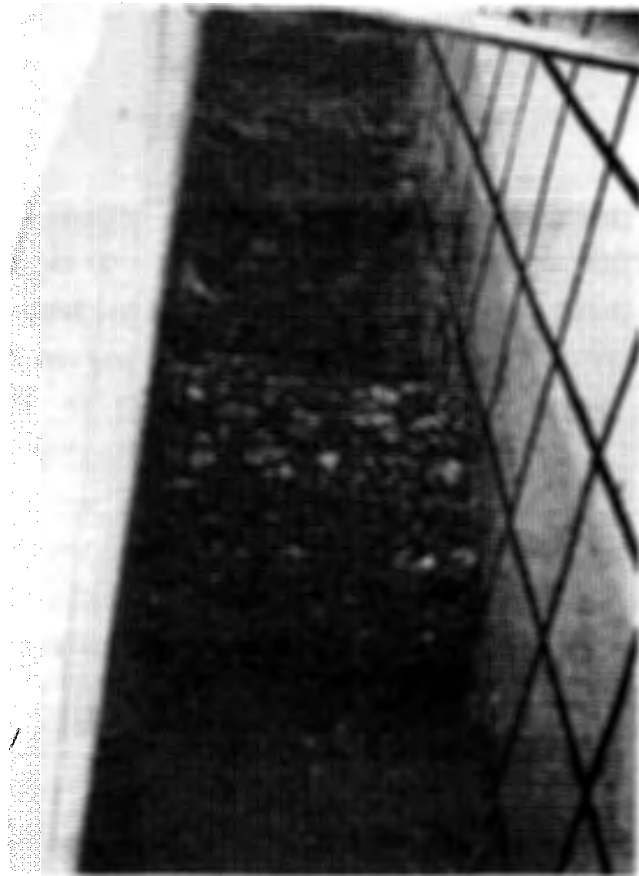


Figure 26. Failure of the gabion mattress system for test 24 (looking upstream).

e. Test Series 5: Geoweb

Geoweb is a grid confinement system made of high-density polyethylene. A typical section of geoweb used in this test series was 4 ft (1.2 m) long, 20 ft (6.1 m) wide, and 4 in (10 cm) deep, with a panel thickness of 0.047 in (1.2 mm). The open area of a single cell was 41 in² (6.4 cm²). Geoweb is delivered in a collapsed form and is expanded, in an accordion-like fashion, during installation. An example of geoweb, in both its collapsed and expanded forms, is shown in figure 27. Mirafi 1120N filter fabric was used for the geotextile underlayer for the geoweb system. This is a needle-punched, nonwoven fabric with a unit weight of 12 oz/yd² (2.0 N/m²), 120 mil (3.0 mm) thickness, and an effective opening sieve (EOS) of 100.

(1) Installation of Protection System. The embankment was constructed of type I soil, placed in 4- to 6-in (10 to 15 cm) lifts. Beginning with this test series, the jumping-jack style compactor was replaced with a vibrating plate compactor. Six passes per lift were required with a vibrating plate compactor to achieve 89 to 93 percent of standard Proctor density, a somewhat lower in-place density than that previously achieved with the jumping jack. The embankment was constructed at a 2H:1V slope for all three tests. Included in the construction of the embankment was an 18 in (46 cm) deep, 45° anchor trench located at station 28 for tests 34 and 35. The anchor trench was moved upstream to station 20 for test 36.

The Mirafi 1120N geotextile underlayer was cut to a 60-in (152 cm) width and anchored with 1/2-in (1.3 cm) diameter, 14-in (36 cm) long rebar staples to the bottom of the trench. The embankment was then covered with the underlayer from the trench to station 52 [4 ft (1.2 m) beyond the toe of the embankment].

The geoweb system was then placed in the flume in its collapsed form. The upstream edge of the geoweb was stapled at five locations in the anchor trench with 1/2-in (1.3 cm) diameter, 14 in (36 cm) long rebar staples. The geoweb was then expanded to cover the embankment and filter fabric. Geoweb is fabricated to a length of 20 ft (6.1 m), therefore, it was necessary to

SPECIFICATIONS

GEOWEB Structural Properties

- | | |
|-----------------------------------|-----------------------------|
| 1. Expanded Dimension | 8 ft. x 20 ft. x 8 or 4 in. |
| 2. Collapsed Dimension | 11 ft. x 5 in. 8 or 4 in. |
| 3. Panel Thickness Nominal | 0.047 in. |
| 4. Weight | 114 and 57 lbs. |
| 5. Cell Area | 41 in. ² |
| 6. Cell Seam Node Pitch | 13 in. |
| 7. Welds/Seam | 7 |
| 8. Seams Tensile Peel Strength | 300 lbs. |
| 9. Installation Temperature Range | -16°F to 110°F |

36

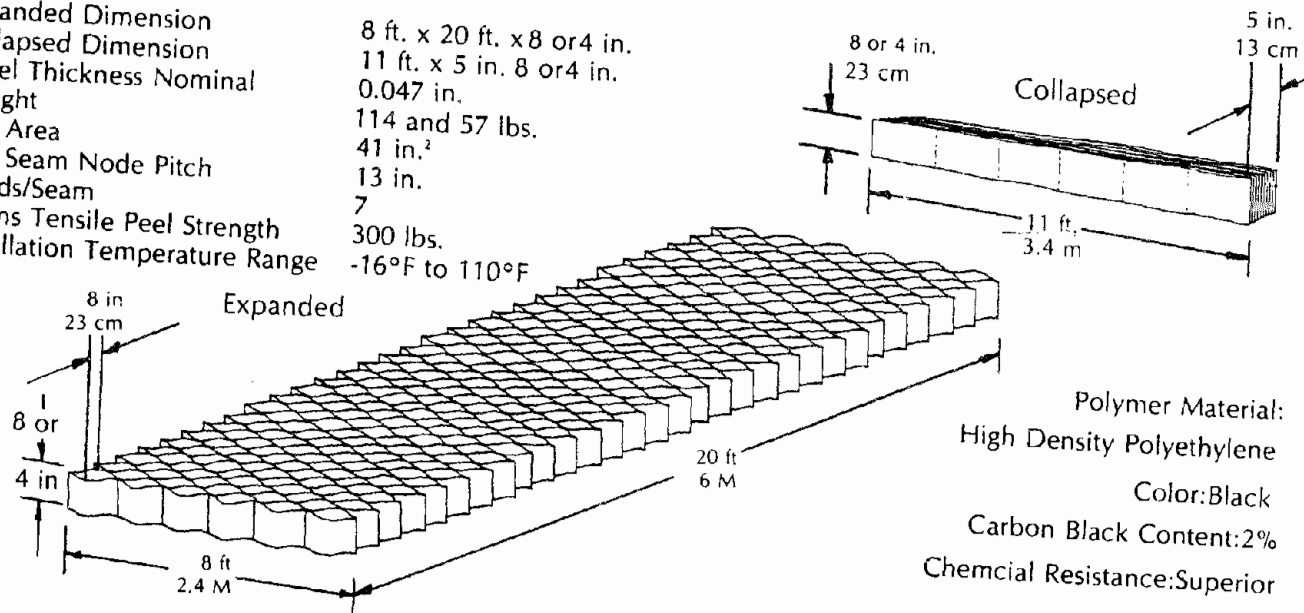


Figure 27. Geoweb grid confinement system.

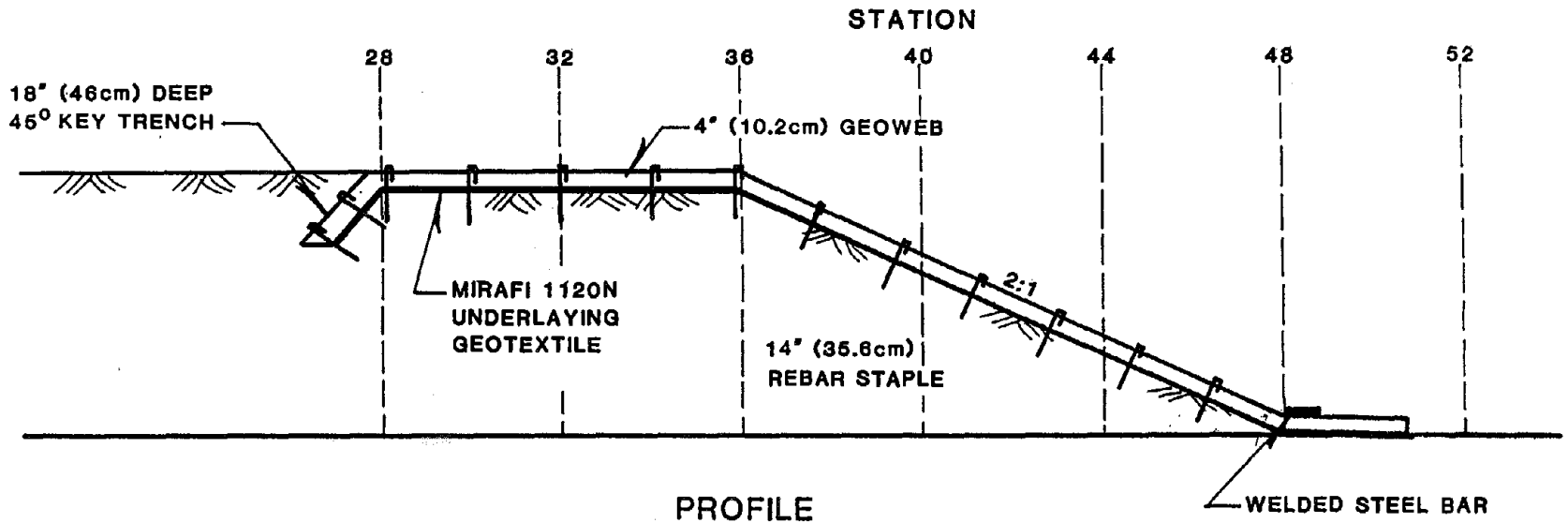
splice two sections in order to provide the necessary coverage. The geoweb was cut to allow the splice to be located at station 32. The geoweb sections were spliced by bolting adjacent cell walls together. Figure 28 is a sketch of the geoweb protection system. Rebar staples were placed at 2-ft (0.61 m) intervals along the width of the embankment to provide shear and pullout restraint. See figure 28 for the pattern of the shear and pullout restraint system.

The cells in the geoweb system were then filled with 1- to 2-in (2.5 to 5.0 cm) washed river rock. Figure 29 shows the fill material used in the geoweb system. Tenax netting was then placed over the rock-filled geoweb system and attached to each cell using commercial hog rings. Figure 30 shows the geoweb system with the Tenax netting in place. A steel bar was installed at station 48 to anchor the geoweb system at the toe of the downstream slope.

(2) Description of Hydraulic Test Conditions. Geoweb was tested under three different hydraulic conditions. Tests 34, 35, and 36 utilized 1-, 2-, and 4-ft (0.30, 0.61, and 1.2 m) overtopping depths, respectively. All three tests were conducted with freefall conditions. See table 16 for a complete summary of test conditions.

(3) Qualitative Description of Geoweb Performance. The geoweb protection system was stable for the 1-ft (0.30 m) overtopping depth (test 34), but failed under 2- and 4-ft (0.61 and 1.2 m) overtopping depths (tests 35 and 36). All tests were scheduled to last 10 hours, but test 35 failed within the first hour, and test 36 failed within 10 minutes as the 4-ft (1.2 m) overtopping flow was being established.

The failure of test 35 was attributed to the loss of the crest anchor which was located at station 28. This allowed water to flow under the system and lift it off the crest. When this occurred the entire system was flipped over and deposited at the toe of the slope. For test 36, the anchor trench was moved from station 28 upstream to station 20. This test failed within the first 10 minutes. Failure was caused by the geoweb material being



95

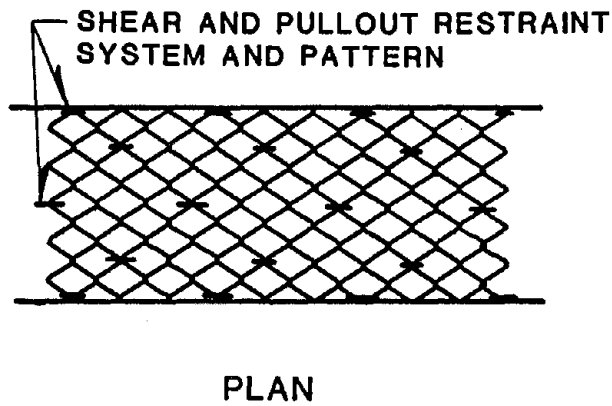


Figure 28. Sketch of the geoweb protection system.



a. Looking upstream from the toe of the slope



b. Looking downstream from the anchor trench.

Figure 29. Washed river rock [1 to 2 in (2.5 to 5.0 cm) diameter] used to fill the geoweb cells.



Figure 30. Geoweb protection system with Tenax netting in place (looking downstream).

stretched down the embankment, thereby pulling the system away from the flume walls and allowing soil to be washed from under the system.

Although the performance of the geoweb system was marginal, it was improved greatly over similar tests conducted for the FHWA from 1983 to 1985.(2) The improvement was due to the Tenax net covering. The net covering kept the fill material [1- to 2-in (0.30 to 0.61 cm) washed river rock] in the cells making the system heavier and more stable. It also minimized the impact of the water on the downstream edge of the cells, thereby reducing system deformation caused by stretching.

It should be noted that the cost effectiveness of this system may be diminished somewhat by the hand labor involved during installation as was performed for this series of flume tests. The process was very labor intensive and time consuming, particularly stapling the Tenax netting to the geoweb material by hand as instructed by the manufacturer. However, use of commercially available automatic stapling devices should alleviate this concern for field applications.

f. Test Series 6: Enkamat (7020)

Enkamat is a flexible soil reinforcement matting made from nylon monofilaments fused at their intersections. This matting system has a 90 percent open area which, when placed, is filled with a specified material. The enkamat is typically filled with soil and seeded with grass. Typar 3401 nonwoven geotextile was used for the underlayer.

(1) Installation of Protection System. Type I soil was used to construct the test embankment. The soil was placed in 4- to 6-in (10 to 15 cm) lifts and compacted with a vibrating plate compactor. Six passes per lift were required to achieve a compaction of 89 to 93 percent of standard Proctor density. The face of the embankment was prepared to a sideslope of 2H:1V for tests 37 and 38, and 3H:1V for test 51.

An 18 in (46 cm) deep, 45° anchor trench was prepared in the embankment at station 28 to provide a crest anchor for the enkamat system. Two pieces of the geotextile underlayer were cut to a width of 4 ft (1.2 m). The first piece was placed covering the embankment from station 34 to 52 for tests with a 2H:1V sideslope, and from station 34 to 56 for tests with a 3H:1V sideslope. The second piece of geotextile underlayer was then placed to cover the embankment and the first piece of underlayer from station 38 to the bottom of the anchor trench at station 28, thereby creating a 4-ft (1.2 m) overlap.

The enkamat material was cut to the required length and placed in the flume, covering the embankment from station 28 to 52 for tests with a 2H:1V sideslope (from station 28 to 56 for tests with a 3H:1V sideslope). Due to the fabricated width of 38 in (97 cm) it became necessary to splice the enkamat. This splice occurred 10 to 14 in (25 to 36 cm) from the left wall of the flume. Two types of stakes were used for shear and pullout restraint in this test series. For tests 37 and 38, wedge-shaped wooden stakes were placed along both walls at 3-ft (0.91 m) intervals. The stakes were also placed at 3-ft (0.91 m) intervals, halfway between the wall stakes, on the seam of the enkamat splice. For test 51, 12-in (30 cm) U-shaped rebar staples were used at the same locations as the wedge-shaped wooden stakes. The shear and pullout restraint system is shown in figure 30.

A solid steel bar was welded to each flume wall at station 48 for tests 37 and 38, and at station 54 for test 51 to provide a system anchor at the toe of the slope. Figure 31 is a sketch of the enkamat protection system. Figure 32 shows the completed installation of the enkamat system.

(2) Description of Hydraulic Test Conditions. Enkamat (7020) was tested under three different hydraulic conditions. Hydraulic conditions for test 37 (2H:1V slope) consisted of a 2-ft (0.61 m) overtopping depth with a 2-ft (0.61 m) water-surface drop. Test 38 (2H:1V slope) had a 1-ft (0.30 m) overtopping depth with a 1-ft (0.30 m) water-surface drop. Test 51 (3H:1V

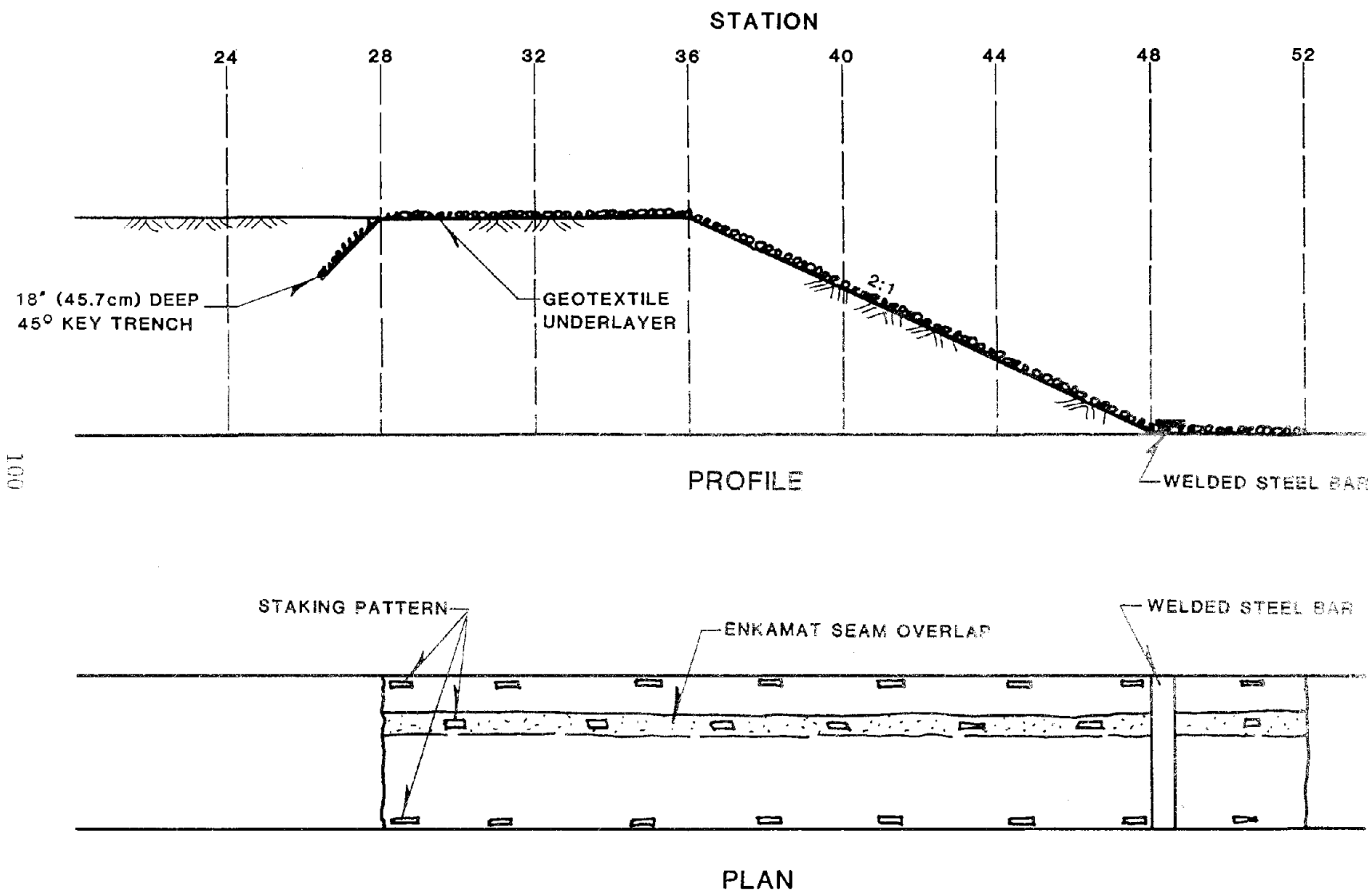
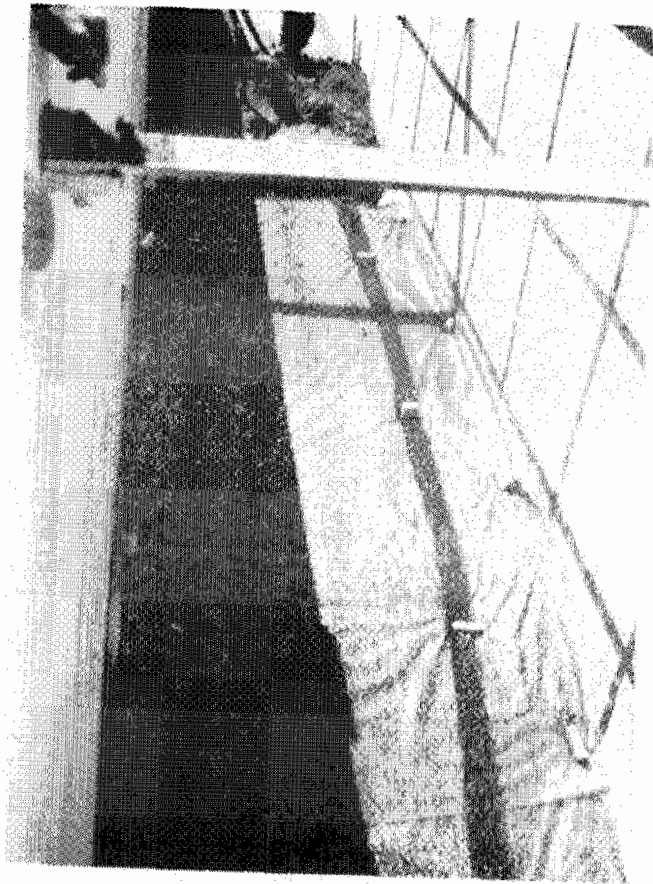
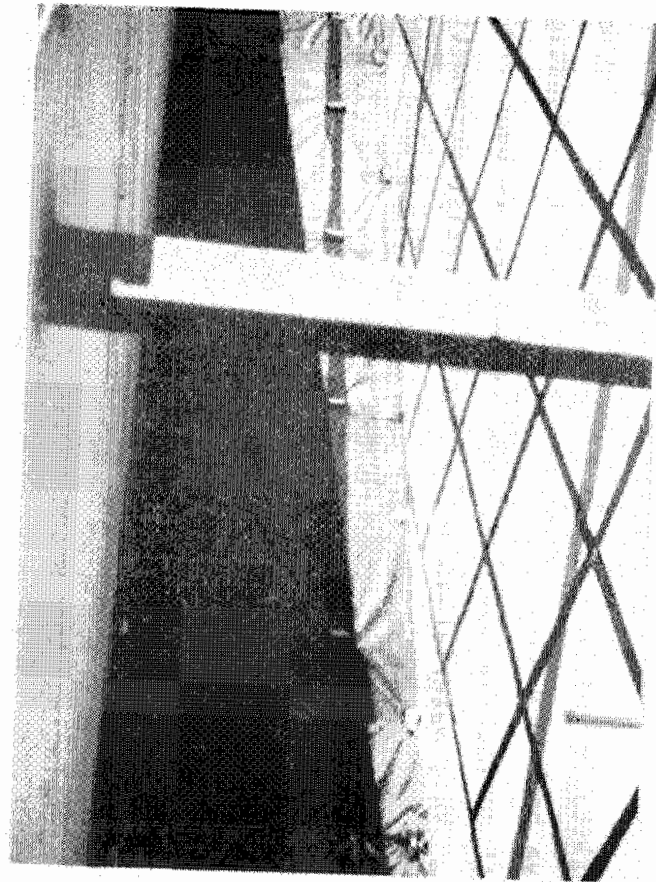


Figure 31. Sketch of Enkamat 7020 protection system.



a. Looking upstream at the embankment crest.



b. Looking upstream at the embankment slope.

Figure 32. Enkamat 7020 embankment protection system.

slope) used a 0.5-ft (0.15 m) overtopping depth with freefall conditions. See table 16 for a complete summary of test conditions.

(3) Qualitative Description of Enkamat Performance. Enkamat was the least effective bank protection system tested during this investigation. The unit weight of enkamat is too low to be considered as bank protection system by itself. This material is too flexible to resist deformation and retain embankment subsoil even at moderate overtopping flows when vegetation is not incorporated into the system.

The wooden, wedge-shaped stakes recommended by the system manufacturer tended to aggravate the already limited system stability. The enkamat material was torn when the stakes were driven through it. This weakened the matting and allowed the soil around the stakes (beneath the enkamat) to be locally eroded. Replacing the wedge-shaped stakes with U-shaped rebar staples improved the stability of the system slightly. These staples created smaller holes in the material and pinned a greater surface area per staple. However, the performance of this system was still unsatisfactory. For the 1- and 2-ft (0.30 and 0.61 m) overtopping depths, the tractive force of the flow was great enough to cause the enkamat to tear at the staked points.

g. Test Series 7: Enkamat (7020) With Asphalt

The enkamat used in this series of tests was the same as that used for the bare enkamat test series. Typar 3401 geotextile was again used as the underlayer. The asphalt used for this series of tests was prepared using a fine aggregate having a D_{50} of 0.7 mm. This aggregate was selected to ensure full penetration into the enkamat matrix. Figure 33 shows the grain-size distribution curve for the asphalt aggregate.

(1) Installation of Protection System. The embankment was constructed of type I soil placed in 4-to 6-in (10 to 15 cm) lifts. The compaction method utilized a vibrating plate compactor using 6 passes per

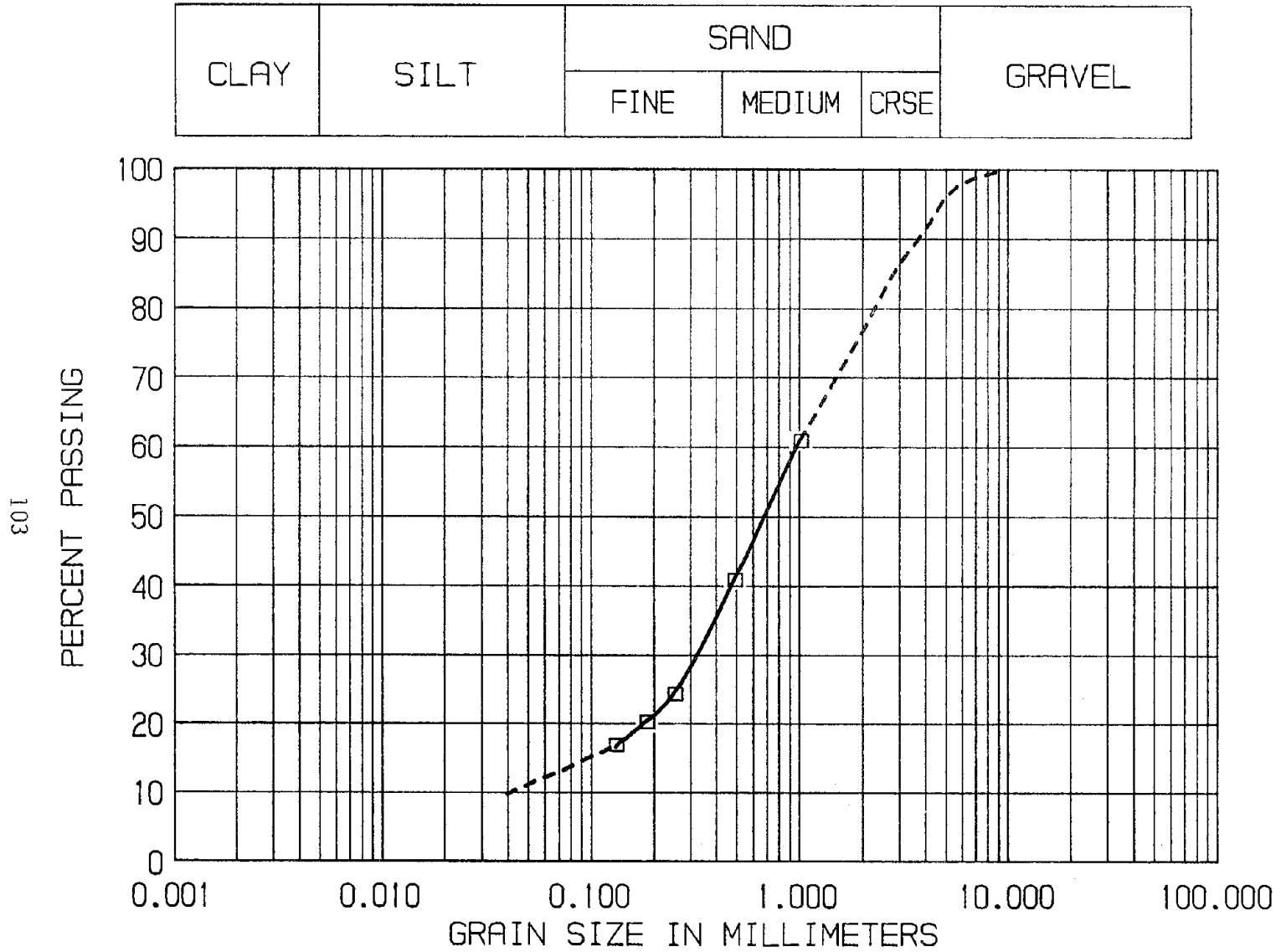


Figure 33. Grain size distributions curve for the asphalt aggregate.

lift to achieve 89 to 93 percent of standard Proctor density. For tests 39, 40, and 41, the enkamat and geotextile underlayer was installed in the same manner as for the bare enkamat tests. The sideslope for these tests was 3H:1V. The asphalt was then placed on the enkamat and the vibrating plate compactor passed over the asphalt six times to ensure proper compaction and penetration into the enkamat matrix. The final thickness of the asphalt for these tests was 3 in (7.6 cm).

For tests 42 and 43, the sideslope ratio was changed to 2H:1V. Also, a different staking system was used. Tests 39, 40, and 41 used the standard wooden stake recommended by the manufacturer, while tests 42 and 43 used a U-shaped rebar staple 8 in (20 cm) wide and 10 in (25 cm) long. The staking pattern used for the 3-in (7.6 cm) asphalt tests was identical to the pattern shown in figure 31 for the 1-in (2.5 cm) asphalt tests. The asphalt was then placed on the enkamat to a depth of 1 in (2.5 cm) and compacted with the vibrating plate compactor. Satisfactory penetration of the enkamat was achieved; however, compaction and smoothing of the thin layer of asphalt was difficult.

For both the 1- and 3-in (2.5 and 7.6 cm) asphalt-impregnated enkamat systems, a solid steel bar was welded to the flume walls across the toe of the slope to provide anchoring for the system. Figures 34 and 35 are sketches of the enkamat with 3- and 1-in (7.6 and 2.5 cm) asphalt cover, respectively. Figure 36 shows the completed enkamat with 1-in (2.5 cm) asphalt installation.

(2) Description of Hydraulic Test Conditions. The enkamat with 3 in (7.6 cm) of asphalt was tested under three different hydraulic conditions. Test 39 utilized a 2-ft (0.61 m) overtopping depth and a water-surface drop of 2-ft (0.61 m). Test 40 had a 2-ft (0.61 m) overtopping depth with freefall. Test 41 utilized a 4-ft (1.2 m) overtopping depth with a water-surface drop of 2 ft (0.61 m). The scheduled duration of these three tests was 4 hours. The enkamat with 1 in (2.5 cm) of asphalt was tested under two different conditions. Test 42 had a 1-ft (0.30 m) overtopping depth with

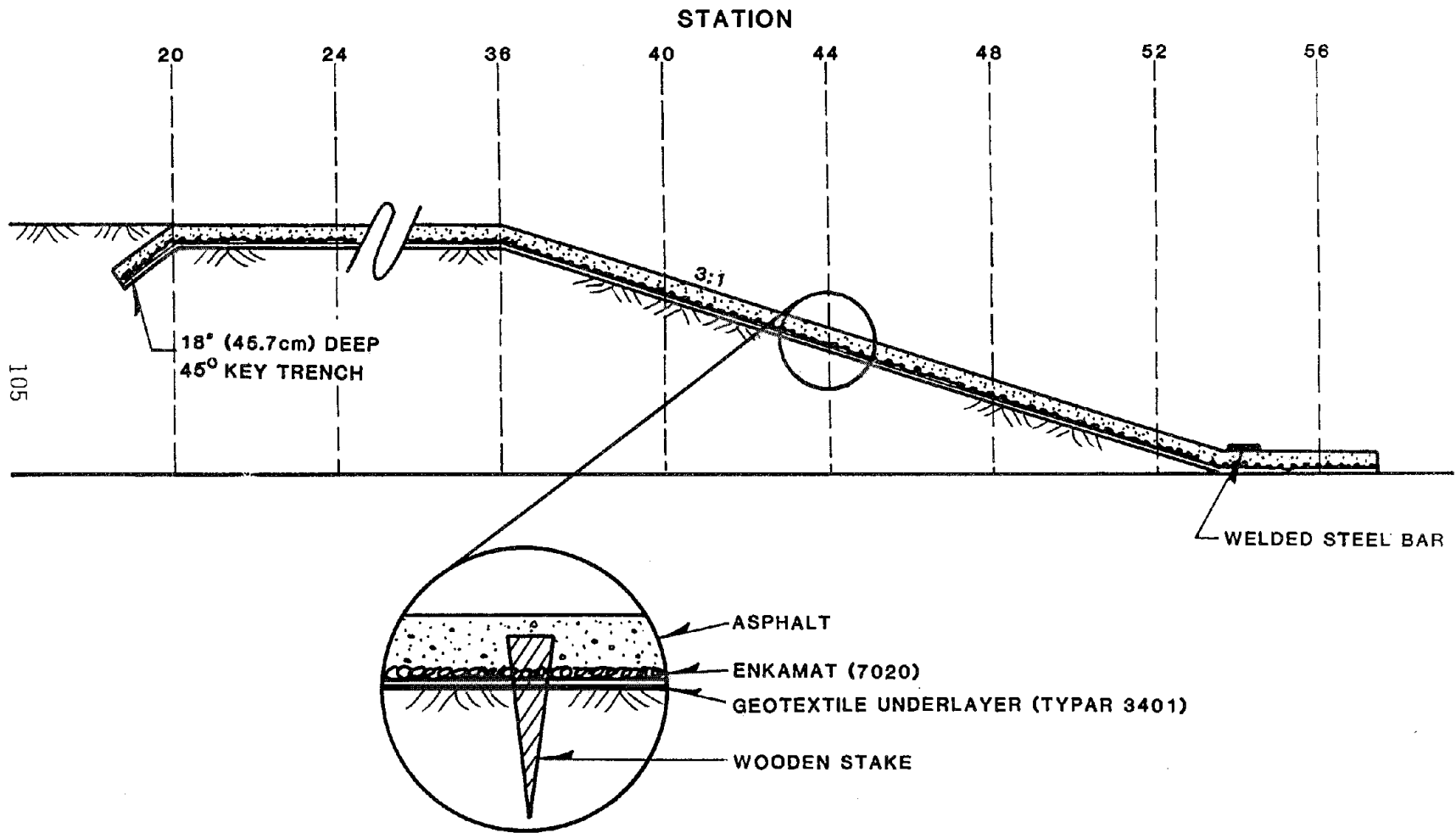


Figure 34. Sketch of Enkamat 7020 with 3-in (7.6 cm) asphalt cover.

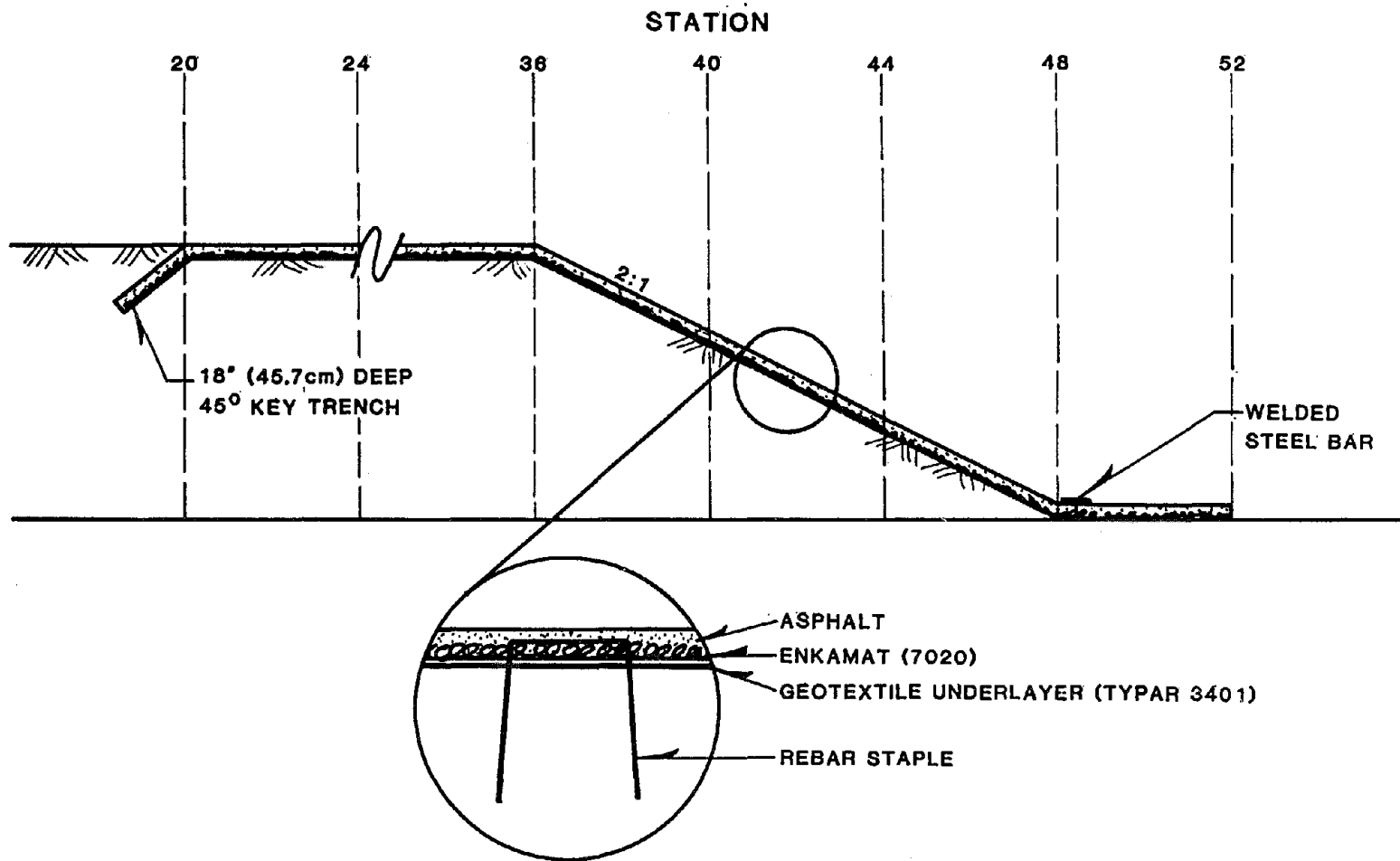


Figure 35. Sketch of Enkamat 7020 with 1-in (2.5 cm) asphalt cover.



a. Looking upstream.



b. Looking downstream.

Figure 36. Enkamat with 1-in (2.5 cm) asphalt cover embankment protection system.

freefall conditions. The scheduled test duration was 4 hours. Test 43 utilized a 1-ft (0.30 m) overtopping depth with a 1-ft (0.30 m) water-surface drop. The scheduled test duration was 4 hours. See table 16 for a complete summary of test conditions.

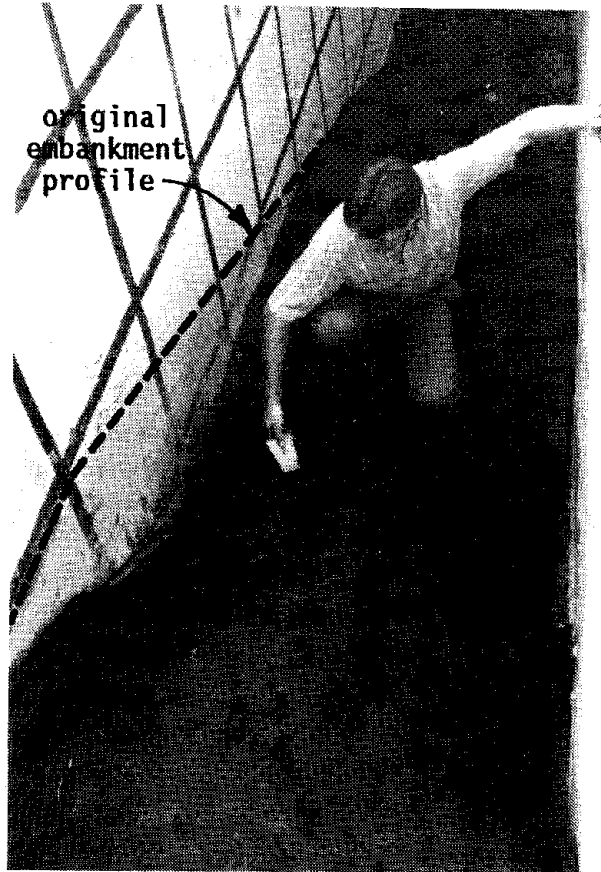
(3) Qualitative Description of Enkamat-With-Asphalt Performance.

The enkamat with 3 in (7.6 cm) of asphalt cover was stable for the two tests involving 2-ft (0.61 m) overtopping depths and varying tailwater conditions. The system failed after 1 hour under an overtopping depth of 4 ft (1.2 m). However, it was not obvious whether the performance of the enkamat or the asphalt was being tested. Due to the thickness of the asphalt, it was felt the performance of the enkamat was being masked and the asphalt was actually being tested, although the enkamat provided a reinforcing matrix which prevented chunks of asphalt from breaking away when failure occurred.

The enkamat with 1 in (2.5 cm) of asphalt cover was tested under a 1-ft (0.30 m) overtopping depth with both freefall and 1-ft (0.30 m) water-surface drop tailwater conditions. In both instances, the system failed. The failure which occurred for freefall conditions happened within the first one-half hour of the test and is shown in figure 37. The failure associated with the 1-ft (0.30 m) water-surface drop was significant, but not as extreme as shown in figure 37. In both cases, failure was the loss of intimate contact between the protection system and embankment. This resulted in the system being lifted off the embankment and significant erosion of the embankment soil.

h. Test Series 8: Cable-tied Concrete Block Mattresses

Cable-tied concrete block revetment systems consist of interlocking blocks with stabilizing cables running through each block. The three systems tested in this program differed in their plan areas, interlocking features, block weights, and cabling methods. All three types of blocks tested had approximately 20 percent open area. Sketches of each of the three blocks are shown in figure 38. In all three cases, the systems selected for

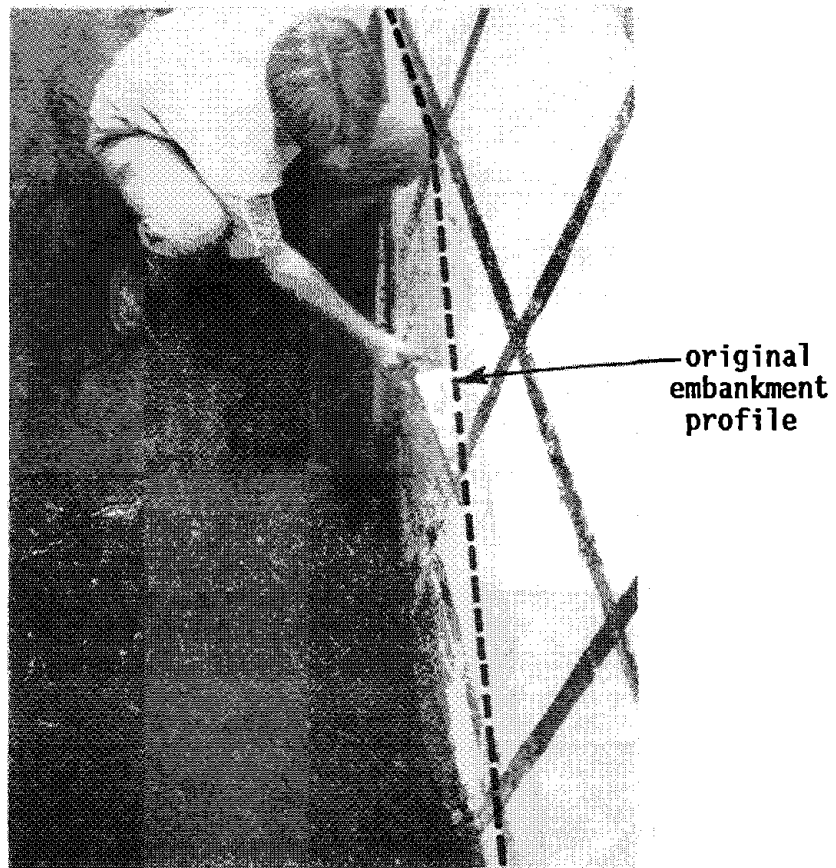


a. Looking downstream at the embankment slope. Note severe loss of subsoil and corresponding system deformation near shoulder.



b. Looking downstream at the embankment crest. Note deformation of system near right wall.

Figure 37. Failure of the enkamat with 1-in (2.5 cm) asphalt cover protection system.



c. Looking upstream at the embankment shoulder. Note deterioration of asphalt surface.

Figure 37. Failure of the enkamat with 1-in (2.5 cm) asphalt cover protection system (continued).

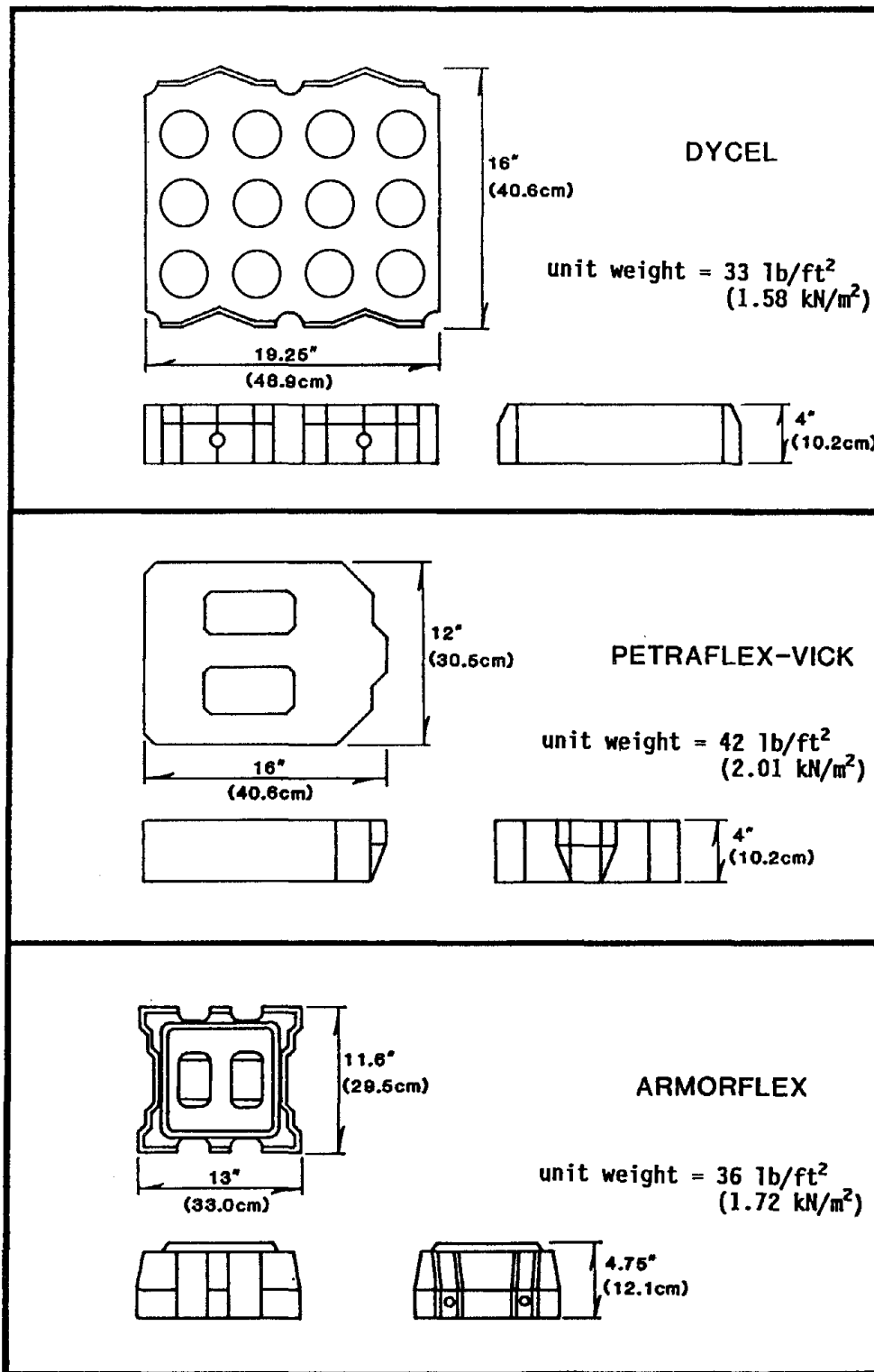


Figure 38. Sketches of the three types of concrete blocks tested.

testing were the lightest standard blocks available from each manufacturer. Heavier systems are fabricated, but were not tested in this program. A typical configuration of a concrete block revetment system is shown in figure 39. All concrete-block protection systems were tested on 2H:1V embankment slopes.

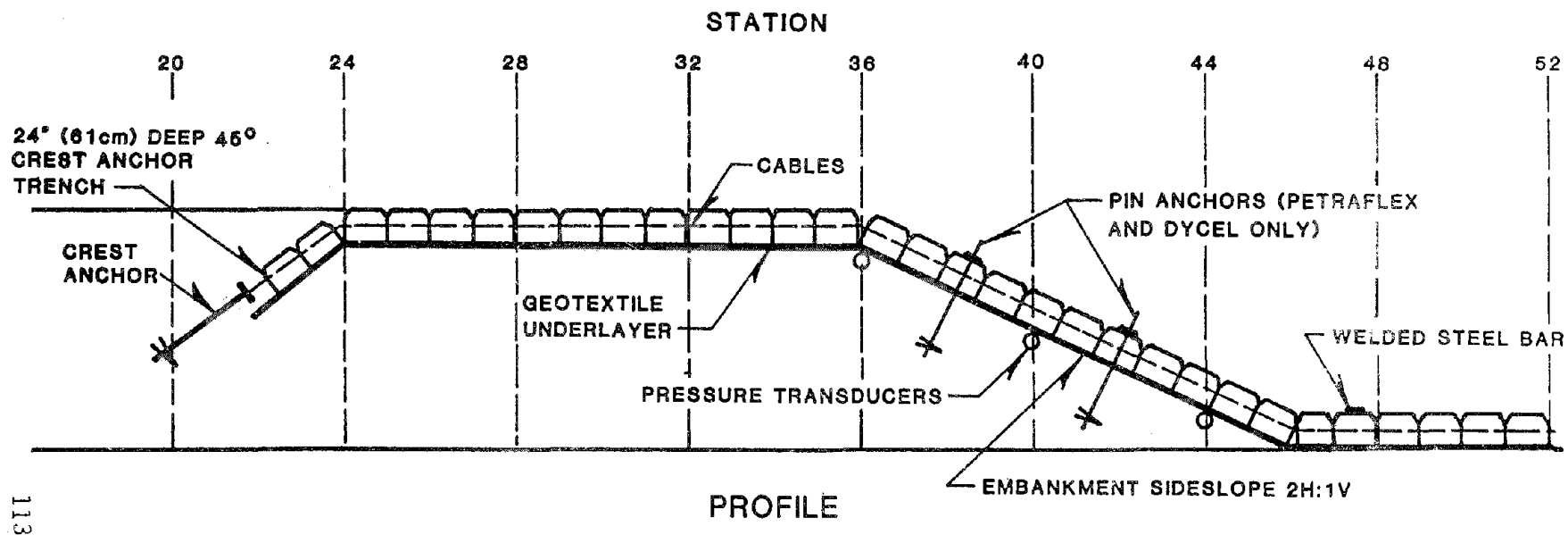
(1) Description of the Armorflex Product. Armorflex systems consist of interlocking concrete blocks reinforced with longitudinal cables running through each block (in the direction of flow) to enhance system stability. The Armorflex class 30 system used in the testing program is an open-cell block having a unit weight of 36 lb/ft² (1.72 kN/m²).

Nicolon 70/06 fabric was used as the geotextile underlayer for the Armorflex test series. This geotextile underlayer is a woven fabric with an effective opening sieve (EOS) of 70, a unit weight of 6.6 oz/yd² (2.19 N/m²), and a 2 to 8 percent open area.

(2) Installation of the Armorflex System. Type I soil was used to construct the test embankment. The soil was placed in 4- to 6-in (10 to 15 cm) lifts and compacted with a vibrating plate compactor to 89 to 93 percent of standard Proctor density. The downstream slope of the embankment was prepared at a 2H:1V sideslope.

A 24-in (61 cm) deep anchor trench was prepared at a 45° angle at station 24 [12 ft (3.7 m) upstream of the embankment shoulder]. The geotextile underlayer was cut to a width of 56 in (142 cm) and placed in the anchor trench. It was then rolled out covering the embankment to station 54. Two helix anchors were placed in the bottom of the anchor trench.

The Armorflex blocks were placed starting at station 52 and continuing over the entire embankment to the anchor trench at station 24. Each concrete block was placed in its interlocking position allowing the reinforcing cables to be passed through the cable tunnels. Each block had two parallel cable tunnels. During the placement of each row of blocks, the cables were pushed through the two cable ducts in each block leaving a loop in each cable at the



113

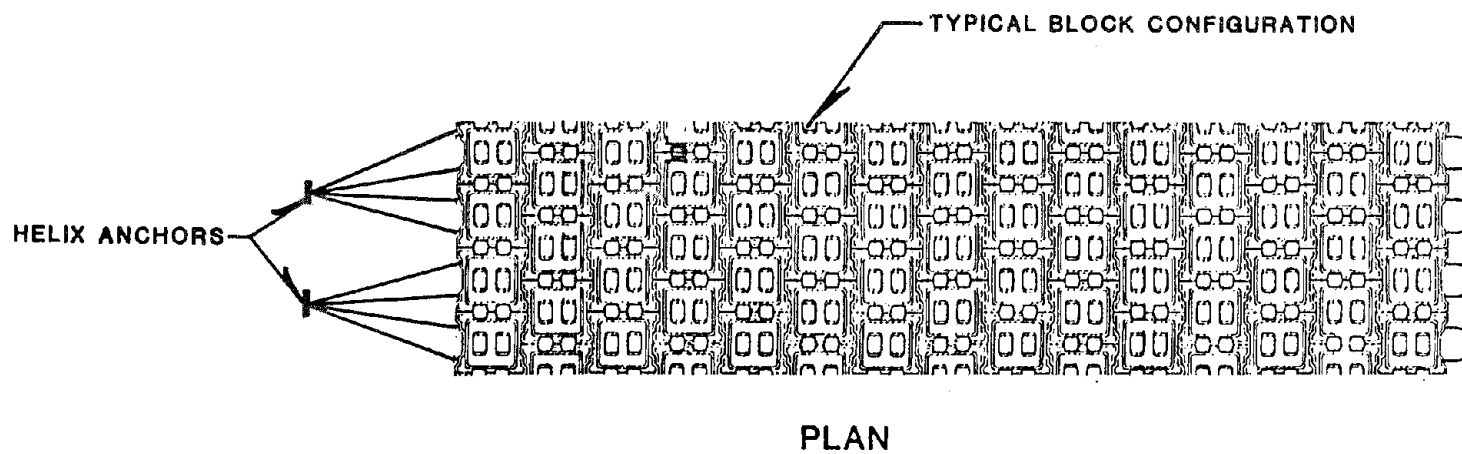


Figure 39. Typical concrete revetment system configuration.

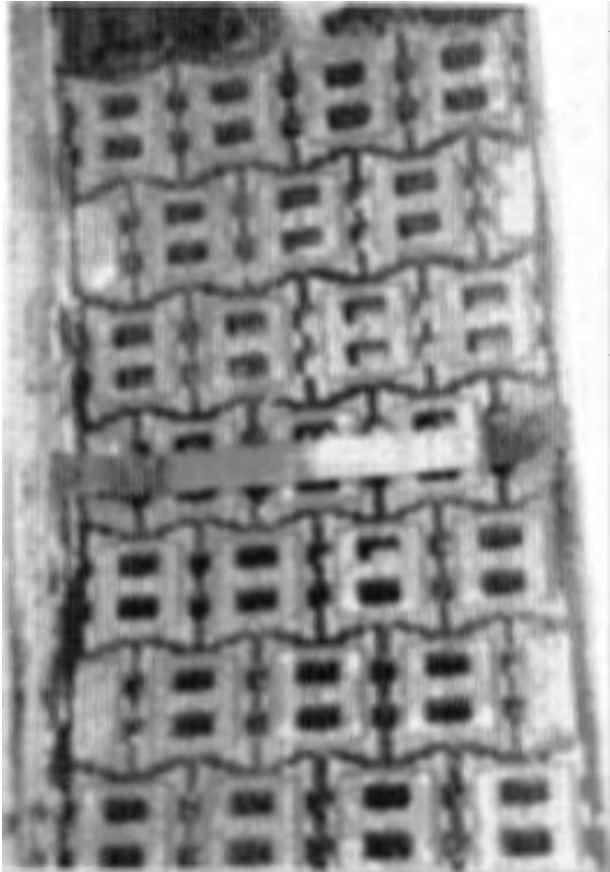
downstream end of the mattress. Once block placement was complete, the cable ends were fastened to the helix anchors in the anchor trench. The open cells in the Armorflex mattress were filled with 3/4-in (1.9 cm) crushed gravel. A steel bar was installed at station 48 to provide a toe anchor for the system. Figure 40 shows the completed Armorflex embankment protection system. A gap about 1/2 in (1.3 cm) existed between the block system and the flume wall after installation, which was also filled with crushed rock.

Prior to testing, angular crushed rock sized between 1/4 and 3/4 in (6 to 19 mm), was broomed into the voids between blocks and into the open cells.

(3) Description of Armorflex Hydraulic Test Conditions. The Armorflex block system was subjected to three different hydraulic conditions. Tests 44, 45, and 46 investigated 1-, 2-, and 4-ft (0.30, 0.61, and 1.2 m) overtopping depths, respectively, all with freefall conditions. A fourth tests, test 46a, was also conducted using a 4-ft (1.2 m) overtopping depth. This test was different from test 46, in that rebar was placed in the 1-1/2 in gap between the flume wall and the adjacent concrete blocks. In all cases, nearly complete loss of the gravel in-fill on the downstream slope was observed. Partial gravel loss from the system occurred on the crest. See table 16 for a complete summary of test conditions.

(4) Description of the Petraflex-Vick System. The Petraflex-Vick system consisted of interlocking concrete blocks reinforced with both longitudinal and lateral cables running through each block to enhance system stability. Each block had a unit weight of 42 lb/ft² (2.0 kN/m²). Two pairs of helix anchors were installed to anchor the system on the downstream face of the embankment, and two more helix anchors were used to secure the longitudinal cables within the anchor trench.

Polyfilter GB and Tensar (geonet) DNI were used as geotextile underlayers for this test series. Polyfilter GB is a woven fabric made of polypropylene monofilament fibers. This geotextile underlayer has an effective opening sieve of 40 to 50, a 20 to 30 percent open area and a unit weight of 6 oz/yd² (1.0 N/m²). Tensar DNI has a mesh structure made of



a. Looking downstream at the embankment toe.



b. Looking upstream at the embankment crest.

Figure 40. Completed Armorflex embankment protection system prior to placement of crushed rock infill.

polyethylene and consists of two sets of parallel strands which provide multiple drainage channels. The material thickness is 0.25 in (0.64 cm) and has a unit weight of 0.161 lb/ft² (7.71 N/m²).

(5) Installation of the Petraflex-Vick Product. Type I soil was used to construct the test embankment. The soil was placed in 4- to 6-in (10 to 15 cm) lifts and compacted with a vibrating plate compactor to 89 to 93 percent of standard Proctor density. The embankment was prepared at a 2H:1V sideslope.

A 24-in (61 cm), 45° anchor trench was constructed at station 26. A pressure transducer was installed beneath the geotextile underlayers at station 40 to provide hydraulic pressure data. The Polyfilter GB was cut to a width of 60 in (152 cm). The Tensar DN1 was cut to a width of 48 in (122 cm). The geotextile underlayers were then placed in the trench and rolled out covering the embankment to station 52, 4 ft (1.2 m) beyond the toe of the embankment. The Tensar drainage net was placed between the Polyfilter GB and the block mattress. Three helix anchors were used to hold the geotextile underlayers in place. The anchors were installed in the trench 6 in (15 cm) from the upstream edge of the underlayers.

The Petraflex-Vick concrete blocks were cabled together in rows of three using lateral cables. Blocks were placed in the flume starting at station 52 and ending at station 26 in the anchor trench. During the placement of each row of blocks, the longitudinal cables were pushed through the two cable ducts in each block leaving a loop in each cable at the downstream end of the mattress. Once block placement was complete, the cable ends were fastened to the helix anchors located in the anchor trench.

Two pieces of 1/2-in (1.3 cm) rebar were placed between the edges of the blocks and the flume walls between stations 26 and 48. The rebar was installed to hold the underlayers in place and minimize boundary effects on the system, as a 2-in (5 cm) gap between the block system and each flume wall existed when placement was complete.

The geotextile underlayers were cut to allow placement of a pair of helix anchors at station 37 and an additional pair of anchors at station 42. After placement of the 4 helix anchors, the geotextile underlayers were sealed with patches of Polyfilter GB and tar. Steel plates were then placed over the threaded top of each anchor and secured with washers and nuts. Figure 41 shows the Petraflex-Vick anchoring system.

Washed river rock 1 to 1-1/2 in (2.5 to 3.8 cm) in diameter was placed in the open cells of the concrete block mattress. A steel bar was welded to the flume walls at station 48 to provide a toe anchor for the system. Figure 42 shows the completed Petraflex-Vick embankment protection system. It should be noted that the rockfill was not placed between individual blocks, but only in the cells of each block. This is due to the three-dimensional geometry of the mechanical interlock. Separating individual blocks to allow gravel in-fill was felt to be counterproductive to this interlock.

(6) Description of Petraflex-Vick Hydraulic Test Conditions. The Petraflex-Vick system was tested under three different hydraulic conditions. Overtopping depths of 1, 2, and 4 ft (0.30, 0.61, and 1.2 m) were investigated, all with freefall conditions. These three tests (47, 48, and 49) were run for the scheduled duration of 10 hours. The embankment proved to be stable for these tests. As a result of the observed stability, three additional tests were run.

Test 49A had a 4-ft (1.2 m) overtopping depth with freefall conditions and a scheduled duration of 4 hours. Prior to the start of this test the slope anchors were removed. Test 50 used a 4-ft (1.2 m) overtopping depth with changing tailwater conditions. Hours 0 to 2 had a freefall tailwater condition, hours 2 to 6 had a 3-ft (0.91 m) tailwater depth, and hours 6 to 8 had an 8-ft (2.4 m) tailwater depth. Tailwater depth was measured from the bottom of the flume. Test 50A had a 4-ft (1.2 m) overtopping with a 7-ft (2.1 m) tailwater depth. Prior to starting test 50A, the toe anchor was removed. This test was run for a scheduled duration of 4 hours. All three additional tests were stable. See table 16 for a complete summary of test conditions.



Figure 41. Anchoring system for the Petraflex-Vick revetment.



a. Looking upstream.



b. Looking downstream (the Armorflex in foreground provided protection for the upstream embankment only).

Figure 42. Completed Petraflex-Vick concrete block embankment protection system.

Reproduced from
best available copy.

(7) Description of the Dycel Product. The Dycel system consisted of interlocking concrete blocks with longitudinal cables running through each block to enhance system stability. The block type used in this test series was Dycel 100. This block has a unit weight of 33 lbs/ft² (1.6 kN/m²). UCO-SG 34/34 and Polyfilter GB were the geotextile underlayers used for tests 52 and 53, respectively. UCO-SG 34/34 is a woven geotextile consisting of polypropylene monofilaments. This geotextile is 0.80 mm thick with an effective opening sieve (EOS) of 120. It has a unit weight of 0.12 oz/ft² (0.36 N/m²). For test 53, the Tensar DN1 drainage mesh was also used, similar to the Petraflex-Vick system.

(8) Installation of the Dycel System. Type I soil was used to construct the test embankment for this test series. This soil was placed in 4- to 6-in (10 to 15 cm) lifts and compacted to 89 to 93 percent of standard Proctor density. The embankment was constructed at a 2H:1V sideslope. An anchor trench was prepared at station 24. This trench was 26 in (66 cm) deep and oriented at a 45° angle.

Pressure transducers were placed along the centerline of the flume at stations 36, 40, and 42. These transducers were installed to provide hydraulic pressure data during each test.

The UCO-SG 34/34 geotextile underlayer was cut to a length of 28 ft (8.5 m) and width of 56 in (142 cm). For test 52, the underlayer was placed in the trench and rolled out covering the embankment from station 24 to 52. The Polyfilter GB was cut and placed in the same manner for test 53.

For tests 52 and 53, the Dycel blocks were placed individually starting at station 52 covering the embankment to the bottom of the anchor trench. During the block placement the longitudinal cables were pushed through the cable ducts in each individual block. The cables were placed allowing them to be looped at the downstream end of the mattress. Upon completion of the block placement, the cable ends were secured to helix anchors located at the bottom of the anchor trench. A steel bar was welded to the flume walls at

station 48 to provide a system anchor at the toe of the slope. Figure 43 shows the completed Dycel 100 system.

Two slope anchors were installed at both stations 37 and 42 on the face of the embankment to provide system stability for test 53. Figure 44 shows the slope anchoring system used on the Dycel 100 block mattress.

(9) Description of Dycel Hydraulic Test Conditions. The Dycel 100 concrete block mattresses were subjected to one hydraulic condition--a 1-ft (0.30 m) overtopping depth with freefall conditions. Tests 52 and 53 were conducted using this hydraulic condition. Both tests failed the block system within 1-1/2 hours of testing. See table 16 for a complete summary of test conditions.

(10) Qualitative Description of Cable-Tied Concrete Block Mattress Performance. The effectiveness of the cable-tied concrete block mattresses varied substantially from system to system. The Dycel 100 [33 lb/ft² (1.58 kN/m²)] system was unstable for all hydraulic conditions. The Armorflex class 30 [36 lb/ft² (1.72 kN/m²)] system was effective for 1- and 2-ft (0.30 to 0.61 m) overtopping flows, but failed under a 4-ft (1.2 m) overtopping depth. The Petraflex-Vick [42 lb/ft² (2.01 kN/m²)] system remained stable for all hydraulic conditions and test durations.

The Dycel 100 mattress was tested twice with a 1-ft (0.30 m) overtopping depth. In both instances, the system failed within the first 1-1/2 hours. This was at least partially due to block geometry and low unit weight. The combination of relatively large surface area per block and low unit weight apparently proved counterproductive to stability. Individual Dycel blocks have over 60 percent more surface area than either of the other blocks. In addition, the unit weight of these blocks is 8 and 21 percent lower than the Armorflex and Petraflex-Vick blocks, respectively. These two factors appear to make the Dycel system more vulnerable to hydraulically induced uplift forces which act on the embankment in the vicinity of the shoulder. In theory, the uplift forces result from a zone of negative pressure which



Figure 43. Completed Dycel concrete block embankment protection system (looking downstream).

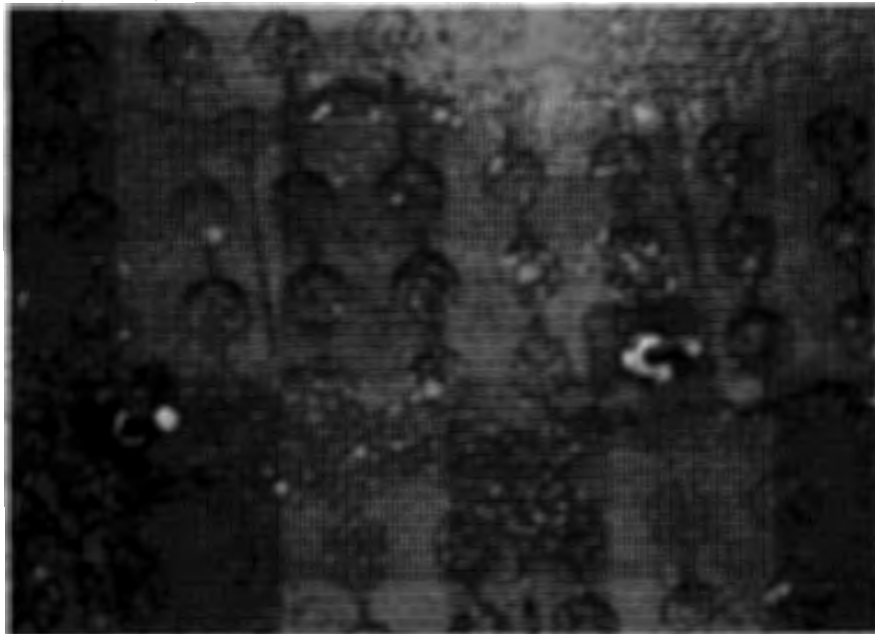


Figure 44. Anchoring system for the Dycel 100 revetment.

results from overtopping flow. Figure 45 shows the displacement of the Dycel blocks due to uplift forces.

By lifting the blocks off the embankment, excessive amounts of water were apparently allowed under the system which caused the underlying soil to become saturated. Buffeting of the Dycel mattress by the high-velocity flow evidently caused the saturated embankment soil to liquefy, resulting in a considerable amount of soil in the shoulder region to slide as a shallow-seated surface slip and settle at the toe, thereby causing the mattress to deform. It is evident the helix anchor system on the embankment face during test 53 was inadequate for preventing failure. Failure of the embankment due to the above-described process is shown in figure 46. Note the redistribution of soil beneath the mattress from the shoulder area to the toe.

The Armorflex class 30 system was stable for low- to mid-range flows, but failed under a 4-ft (1.2 m) overtopping depth. As with the Dycel system, the Armorflex failed due to an apparent shallow-seated liquefaction of the embankment soil. Although the exposed surface area of the Armorflex blocks is less than the other two blocks, their unit weight is only slightly greater than the Dycel blocks and 14 percent less than the Petraflex-Vick blocks. Consequently, the Armorflex system was vulnerable to uplift forces at high flows. Figure 47 illustrates the failure of the Armorflex system.

After failures of both the Armorflex and Dycel systems, the edges of individual blocks were observed to have been randomly lifted (see figures 45 and 47). This displacement was the mechanism which allowed water under the mattresses, eventually resulting in failure of the systems. The lack of lateral cables (across the embankment) and the lack of a vertical mechanical interlock of the blocks may have contributed to the threshold instability of these systems, as well as their lower unit weights compared to the Petraflex-Vick system.

The Petraflex-Vick concrete block mattress was tested under six different hydraulic conditions and suffered no significant damage. The system was subjected to a total of 48 hours of testing with 28 hours at



a. Looking downstream at the embankment shoulder.

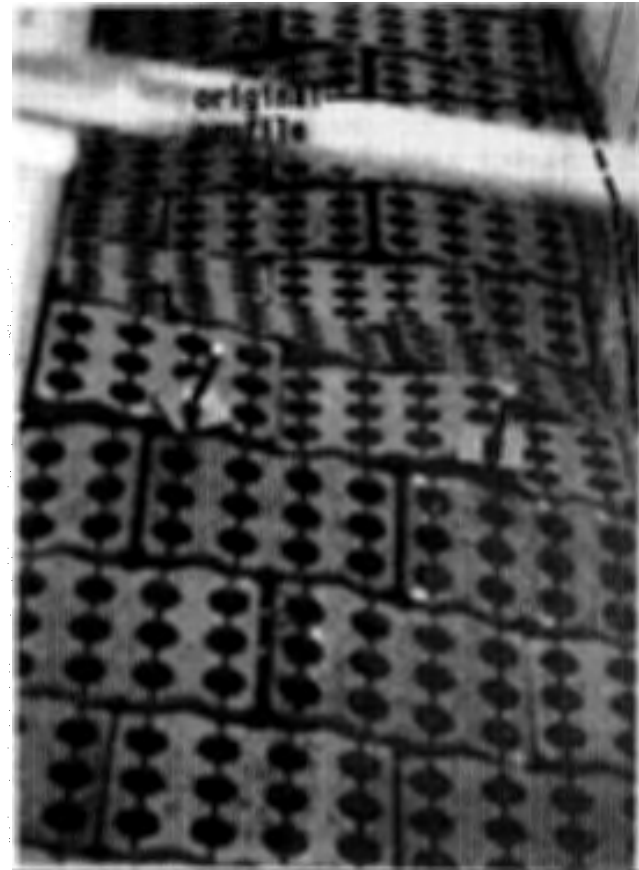


b. Block displacement due to uplift forces.

Figure 45. Dycel block system after failure, showing displacement of individual blocks.



a. Looking upstream at the embankment toe.



b. Looking upstream at the embankment shoulder.

Figure 46. Dycel block system after failure, showing deformation of embankment.



area of
subsoil loss

Figure 47. Localized failure exhibited by the Armorflex system.

maximum flow [4-ft (1.2 m) overtopping depth]. System weight, mechanical interlock and the installation of lateral cables and slope anchors all appeared to contribute to the better performance of this system.

The Petraflex-Vick blocks were significantly heavier [42 lb/ft² (2.0 kN/m²)] than the Dycel 100 [33 lb/ft² (1.6 kN/m²)] and Armorflex class 30 blocks [36 lb/ft² (1.7 kN/m²)]. Installing two geotextile underlayers with this system may have relieved some of the hydraulic uplift pressure on the Petraflex-Vick system and seemed to have minimized soil saturation by channeling water down the embankment under the blocks but over the filter fabric. The Polyfilter GB used with this system had a larger effective opening sieve (EOS) than the UCO-SG 34/34 (Dycel 100) and Nicolon 7006 fabric (Armorflex class 30). This underlayer design may also have contributed to the success of the Petraflex-Vick system, although the same design did not prevent the second failure of the Dycel system. It was felt the lateral cables and vertical interlocking feature of the Petraflex-Vick blocks also contributed to the system's stability. Figure 48 illustrates the Petraflex-Vick system after testing.

Finally, for all three systems, it should be noted that the crushed rock infill placed in the open cells and between the blocks was washed away rapidly in the first minutes of each test on the downstream slope. Preventing this loss of infill material may significantly enhance system stability.



a. Looking downstream.



b. Detail of the embankment toe.

Figure 48. Petraflex-Vick concrete block mattress after testing.

Reproduced from
best available copy.

RESULTS OF FULL-SCALE EMBANKMENT TESTING PROGRAM

Embankment and water-surface elevations were taken at 2-ft (0.61 m) intervals across the crest and down the face of the embankment. In addition, velocity profiles were determined every 4 ft (1.2 m) using a Marsh-McBirney Model 201 electromagnetic velocity meter. These data were collected hourly. For the concrete block protection systems, pressure transducers were used to measure pressure profiles beneath the systems. This section will discuss the methodologies used to analyze the data and the results of the analyses.

1. Determination of Test Discharges

Velocity measurements taken on the embankment slope were not always consistent due to turbulence and air entrainment, and therefore not considered in computing discharges. Across the crest, however, the velocities were reasonably consistent. For each test, the crest velocities and measured flow depths were averaged and the average discharge estimated using the velocity-area method. The velocity-area discharges were verified by computing average discharges with the broad-crested weir equation. This equation is

$$Q = C L H^{3/2} \quad (7)$$

where L is the embankment length [4 ft (1.2 m)], H is the total head on the crest, and C is a coefficient determined by figure 2 for use with English units. Generally, this comparison resulted in two discharge estimates which agreed reasonably well. The 1-, 2-, and 4-ft (0.30, 0.61, and 1.2 m) overtopping depths corresponded to approximately 14, 34, and 96 ft³/s (0.4, 1.0, and 2.7 m³/s), respectively.

2. Computation of Hydraulic Parameters

The embankment and water-surface elevation data were entered into R:base 5000, a relational data base management software package. This process was explained in the previous chapter. R:base was used to compute flow depths and corrected flow depths. The corrected depths account for the embankment

slope and are always oriented perpendicular to the direction of flow. The velocity area method was then used to determine the average flow velocity at each station from the known discharge and corrected depth. Finally, total energies were computed using measured water-surface elevations and computed velocities.

Embankment and water-surface profiles, along with energy grade lines, were plotted for each test. An example of these plots was given in figure 12. The profile plots were useful for several reasons. First, they were examined in order to identify errors in data collection or entry. The profile plots were also useful for determining the friction slope along the downstream slope of the embankment. For tests where the energy data defined a reasonably straight line between the shoulder and toe, the friction slope was calculated by linear regression. When the energy data contained a significant number of anomalies, which made linear regression impractical, the friction slope was determined graphically. Finally, the profile plots provided a convenient means for identifying locations of soil erosion and protection system failure. This was particularly useful when identifying control volumes for computing bed shear for bare soil tests.

3. Analysis Methodology for Freefall Conditions

The mode of failure for all bare soil embankments and protection systems, except the enkammat with asphalt and concrete block systems, was related to shear stress acting on the slope of the embankment. Consequently, determining bed shear on the embankment slope was one of the primary goals of the analysis. In addition, flow resistance on the downstream slope of the embankment was computed.

The failure mechanism for both concrete block and enkammat with asphalt systems was lifting of the protection system off the embankment by a hydraulically induced zone of negative pressure downstream of the crest. Discussion of the subatmospheric pressure zone and the resulting uplift phenomenon will be presented later in this chapter.

a. Computation of Bed Shear Stress

The tests which involved freefall conditions were analyzed using the principles of conservation of momentum. The embankment and water-surface profile plots were evaluated and a control volume on the embankment slope was identified for each test. The control volumes were generally located between stations 38 and 44. However, when embankment changes due to erosion or faulty protection system performance adversely affected hydraulics at either station 38 or 44, an alternative location for the control volume was chosen. An attempt was made to define control volumes at least 6 ft (1.8 m) long. This was achieved for all but three tests. An example of a typical control volume, the control volume for test 49, is shown in figure 49.

The principle of the conservation of momentum may be expressed as

$$\Sigma F = \Delta(\rho VQ) \quad (8)$$

where ΣF is the sum of the forces acting on the control volume in the direction of flow, Q is the discharge, ρ is the density of water, and V is the flow velocity parallel to the embankment. The right-hand side of equation 8 is the change in momentum across the control volume. Figure 50 is a schematic of a typical control volume which indicates the parameters used in this analysis. By considering a control volume of unit width and inserting all appropriate terms, equation 8 becomes:

$$W \sin \theta + P_1 - P_2 - \tau_0 L = \rho q V_2 - \rho q V_1 \quad (9)$$

where W is the weight of water in the control volume, P_1 and P_2 are the forces due to pressure, τ_0 is the bed shear stress, L is the length of the control volume, θ is the embankment slope, and q is the unit discharge. The shear stress term did not include wall shear because of the relative smoothness of the flume walls. Flow resistance due to the walls was assumed to be negligible. This assumption was verified by computing the contribution to total shear due to the walls, which indicated that wall shear was less than 1 percent of bed shear. By expanding equation 9 and solving for the shear stress, the following equation results:

$$\tau_0 = \frac{\gamma}{2} (d_1 + d_2) \sin \theta + \frac{1}{L} \left[\frac{\gamma}{2} (d_1^2 - d_2^2) \cos \theta - \rho q^2 \left(\frac{1}{d_2} - \frac{1}{d_1} \right) \right] \quad (10)$$

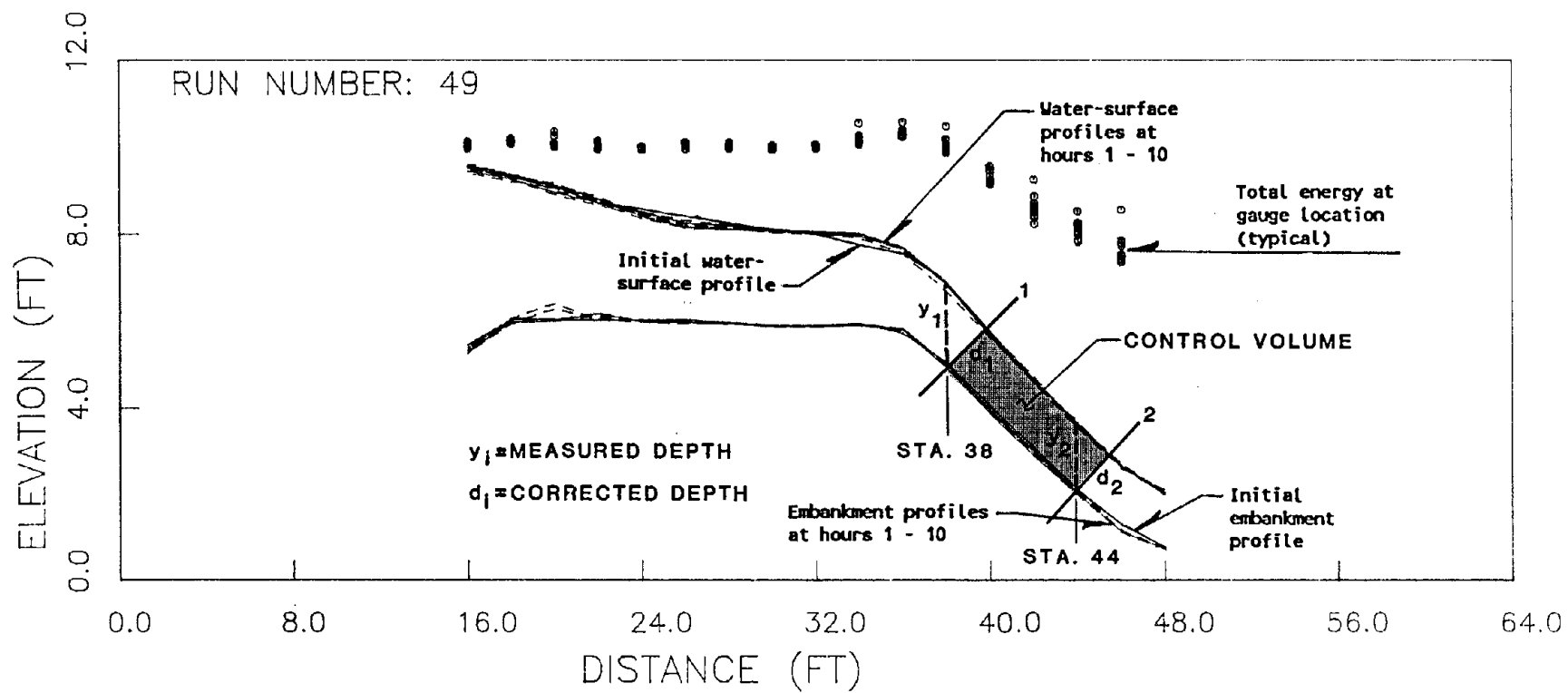


Figure 49. Control volume for test 49.

where γ is the specific weight of water and the remaining parameters are defined in figure 50. The bed shear τ_0 is easily computed as it is the only unknown in the equation. Using this equation, the average bed shear across the control volume was computed for each hour of all freefall tests.

b. Computation of Flow Resistance

Flow resistance on the embankment slope was quantified with both the Darcy-Weisbach friction factor and Manning's roughness coefficient. A Darcy-Weisbach friction factor was calculated for each hour for every freefall test using the computed bed shear, measured flow velocity, and the equation:

$$f = \frac{8 \tau_0}{\rho V^2} \quad (11)$$

where τ_0 is the bed shear computed using the momentum equation, ρ is the density of water, and V is the average velocity across the control volume.

Manning's roughness coefficients were computed using Manning's equation in the form:

$$n = \frac{1.49}{V} d^{2/3} S_f^{1/2} \quad (12)$$

where V is the flow velocity, d is the depth of flow, and S_f is the average friction slope for a single test. Two values for Manning's n were determined for each test. These values were computed for the hydraulic conditions at the upstream and downstream limits of the control volumes. The average depth and velocity at these locations, for the duration of each test, were used as input to equation 12. Again, wall shear was assumed to be negligible. This was incorporated in equation 12 by replacing the hydraulic radius with the flow depth.

4. Results for Freefall Conditions

Results of the quantitative analysis for freefall conditions, including average velocities, friction slopes, shear stresses, Darcy-Weisbach friction

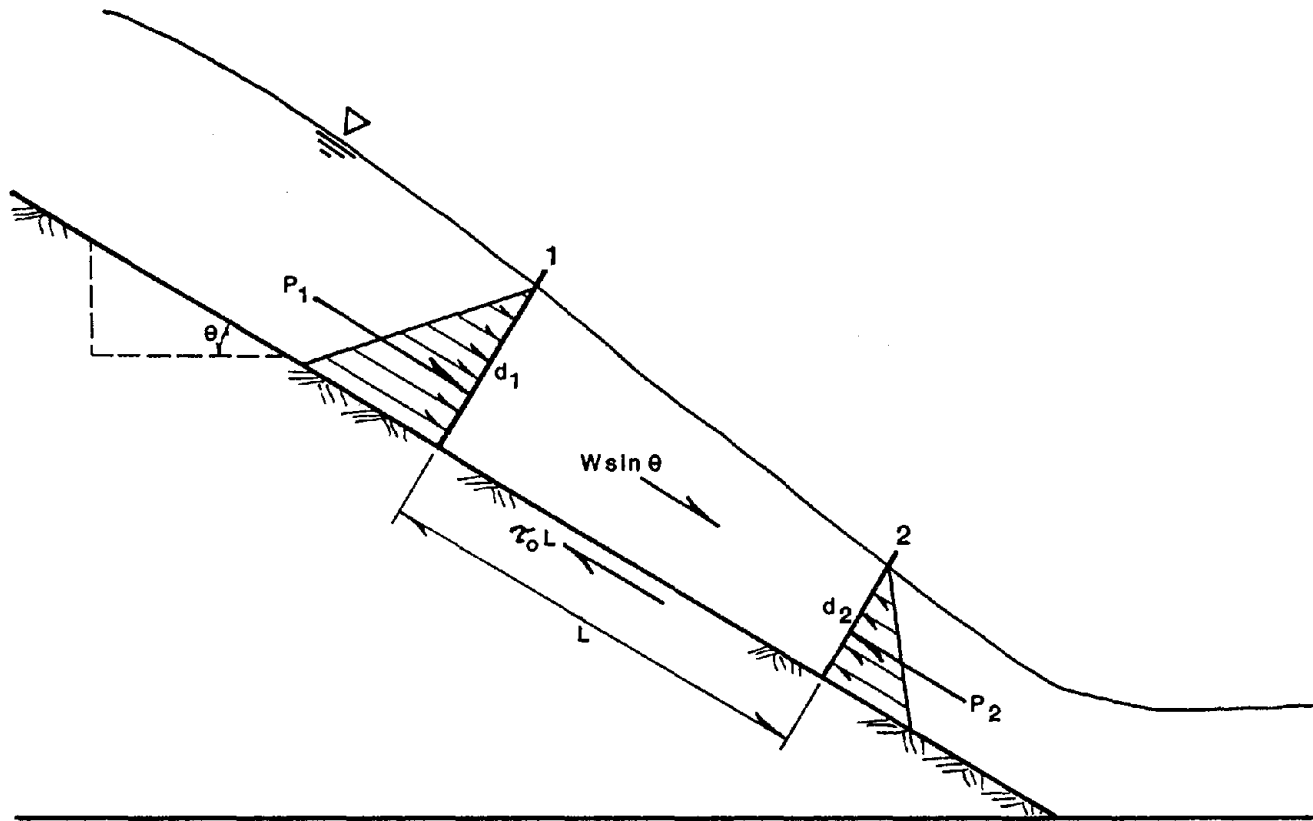


Figure 50. Typical control volume with momentum equation parameters.

factors, and Manning's roughness coefficients, are summarized and discussed in this section.

a. Bare Soil Embankments

Results of hydraulic analyses for the bare soil embankments are given in table 17. Time-averaged bed shear, flow velocity, and flow depth are plotted against unit discharge in figures 51, 52, and 53, respectively. The tendency of these three parameters to increase with increasing unit discharge is indicated. It was anticipated that shear stresses would be smaller for 4H:1V than 3H:1V embankment slopes. However, shear stress did not appear to be a function of embankment slope for the bare soil tests. Lack of correlation between bed shear and embankment slope was probably due to nonuniform erosion of the embankment for each individual test as well as from one test to another. Furthermore, varying erosion patterns were probably the reason for not being able to identify relationships between hydraulic parameters and embankment erosion. Both type I and II soils experienced erosion for all test conditions. Erosion was considerably more severe for the 2- and 4-ft (0.61 and 1.2 m) overtopping depths than for the 1-ft (0.30 m) tests. In general, erosion depths for the lower discharges did not exceed 1.0 ft (0.30 m) and averaged less than 0.5 ft (0.15 m). The 2- and 4-ft (0.61 and 1.2 m) tests resulted in more severe erosion. Erosion depths for the type II soil embankments ranged up to approximately 2.5 ft (0.76 m) and averaged over 1.5 ft (0.46 m). At the higher discharges, the maximum erosion depth for the type I soil embankments was 1.6 ft (0.49 m) with an average depth of approximately 1.0 ft (0.30 m). An exception to this discussion was test 54, an additional bare soil embankment test. Test 54 will be described later in this section.

It should be noted that the duration of all bare soil tests was 4 hours. For the lower discharges, the embankments had essentially stabilized by the end of the test with only minimal erosion occurring during the final hour. However, several tests with 2- and 4-ft (0.61 and 1.2 m) overtopping depths were still eroding considerably after 4 hours. Erosion would probably have been increasingly more severe if the tests had continued.

Table 17. Shear stress and bed roughness analysis results for bare soil embankments under freefall conditions.

Soil Type	Test No.	Embankment Sideslope (Run/Rise)	Depth of OT (ft)	Q (ft ³ /s)	Hydraulic Analysis (Stations 38 to 44)					Comments
					τ_o (lb/ft ²)	f	V_{ave} (ft/s)	S_f	n	
Type II	18 ^a	3:1	1	14	10-13	1.15 - 2.00	5.7 - 5.9	0.32	0.101 - 0.108	
	3 ^b	3:1	2	37	15-18	0.48 - 0.63	10.5 - 11.2	0.33	0.068 - 0.075	
	5 ^c	4:1	1	18	6-8	0.17 - 0.35	10.4 - 11.2	0.25	0.036 - 0.041	
	6 ^c	4:1	2	38.5	12-15	0.25 - 0.40	12.7 - 14.3	0.25	0.040 - 0.049	
	7 ^d	4:1	4	93.5	22-31	0.54 - 0.95	11.6 - 12.7	0.19	0.077 - 0.090	
Type I	25 ^e	3:1	1	13.5	7-9	0.19 - 0.55	8.4 - 10.3	0.33	0.039 - 0.055	
	26 ^f	4:1	1	14	5-8	0.25 - 0.41	8.7 - 9.5	0.24	0.040 - 0.046	
	27 ^g	2:1*	2	31.5	18-29	0.35 - 0.75	11.1 - 14.8	0.31	0.037 - 0.060	
	28	3:1*	4	92.5	34-41	0.77 - 0.94	13.4 - 13.9	0.32	0.085 - 0.090	
	29	2:1**	2	34.5	23-24	0.88 - 1.00	10.0 - 10.2	0.50	0.092 - 0.095	
	30	3:1	4	96	25-30	0.42 - 0.48	15.2 - 15.9	0.27	0.064 - 0.069	

a: Stations 34-44
 b: Stations 38-46
 c: Stations 44-54
 d: Stations 36-48
 e: Stations 40-46
 f: Stations 40-44
 g: Stations 42-48

*Approximate slope after erosion; original slope = 4:1
 **Approximate slope after erosion; original slope = 3:1

ft x 0.3048 = m
 ft³/s x 0.0283 = m³/s
 lb/ft² x 47.87 = N/m²

- Note:
1. Friction slope S_f determined by linear regression and verified by graphical average of energy grade line over the downstream embankment slope for the duration of test.
 2. Bed shear τ_o determined by momentum equation between stations 38 and 44 (except where noted) for each measurement period; typical range reported.
 3. Average velocity V_{ave} determined over duration of test between stations 38 and 44 (except where noted).
 4. n determined by Manning's equation: $n = \frac{1.49}{V} d^{2/3} S_f^{1/2}$
 5. f determined by equation: $f = 8\tau_o/\rho V^2$ for each measurement period; typical range reported.

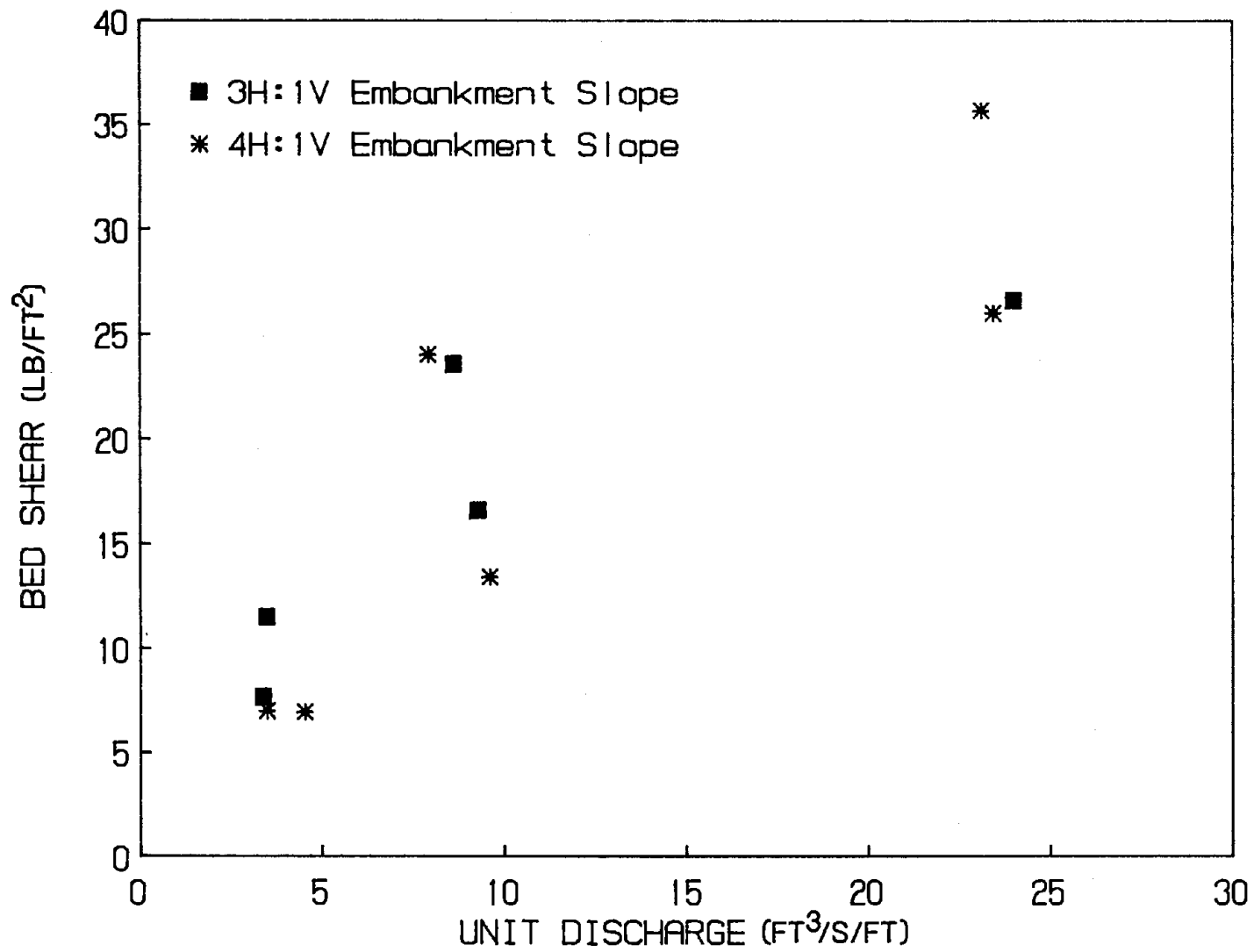


Figure 51. Bed shear versus unit discharge for bare soil freefall tests.

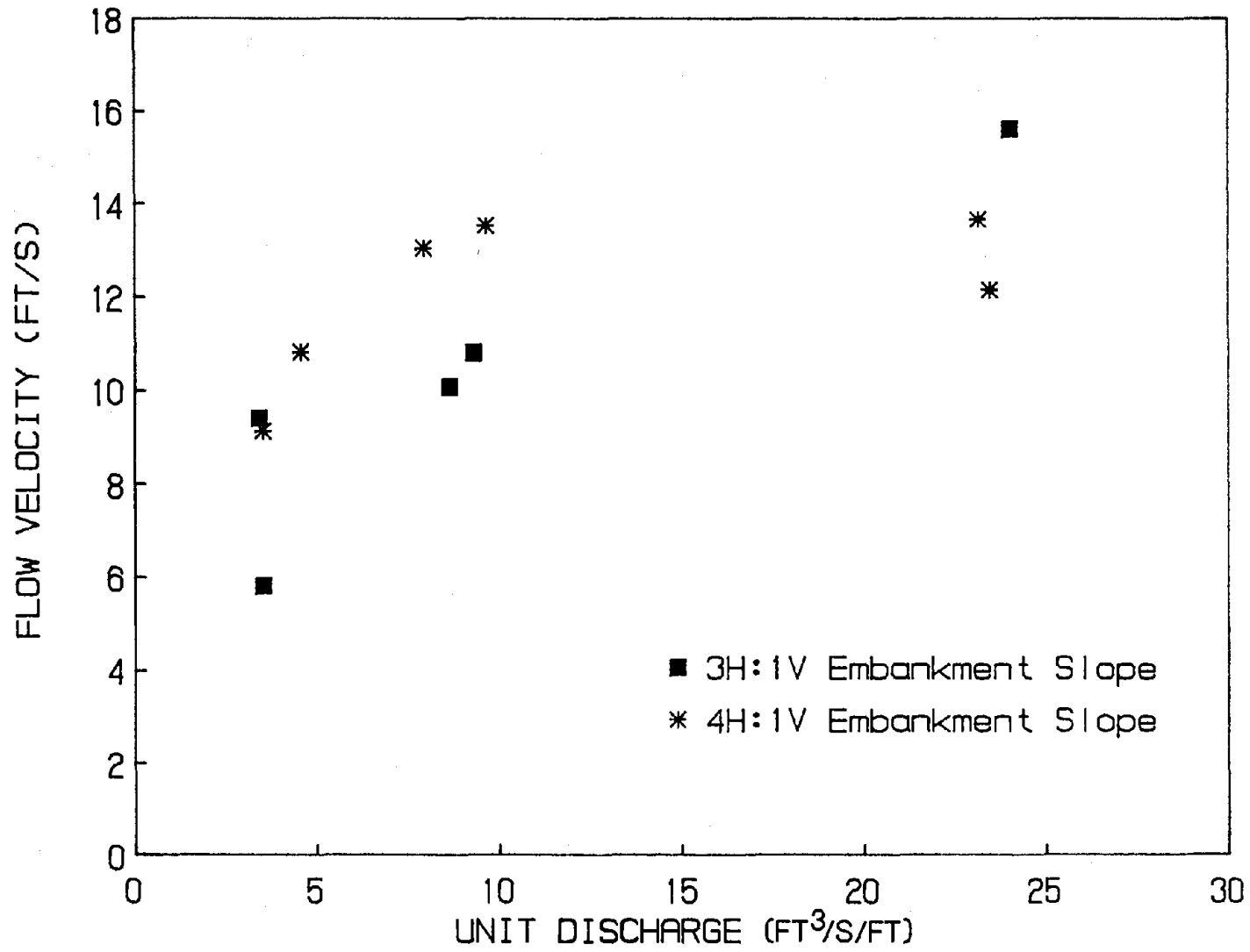


Figure 52. Flow velocity versus unit discharges for bare soil freefall tests.

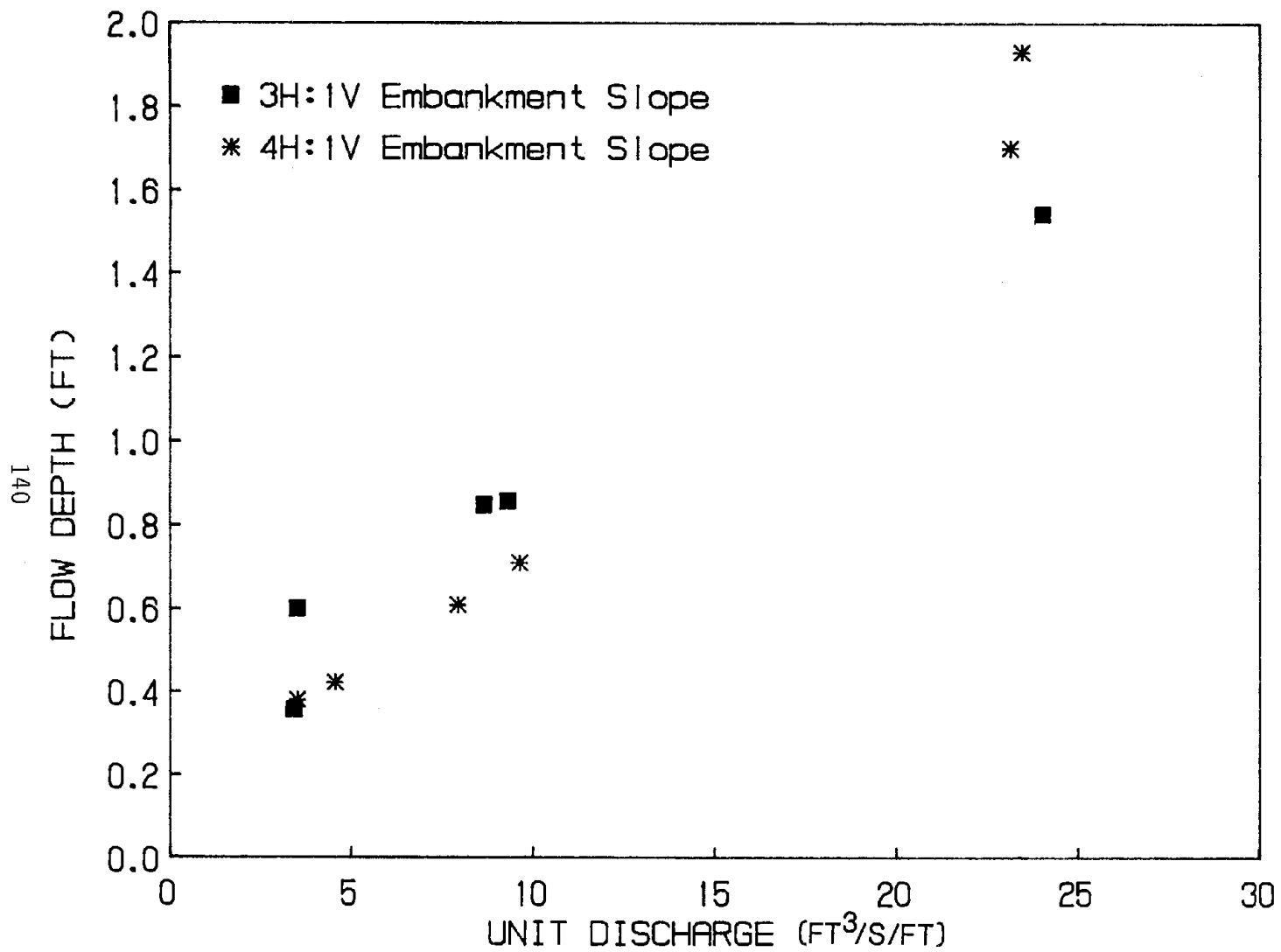


Figure 53. Flow depth versus unit discharges for bare soil freefall tests.

Two different erosion patterns were observed for freefall and tailwater conditions. Freefall conditions resulted in erosion being concentrated at the toe of the embankment. Figure 54 illustrates the erosional behavior of a type I bare soil embankment under freefall conditions and a 2-ft (0.61 m) overtopping depth (test 29). In contrast, tailwater conditions caused erosion of the crest and shoulder while soil loss at the toe was minimal. An example of this behavior for a type I bare soil embankment with a 1-ft (0.30 m) water-surface drop and 2-ft (0.61 m) overtopping depth (test 33) is shown in figure 55. Erosion rates for the bare soil tests were computed for the three regions: crest (stations 24 to 30), shoulder (station 34 to 40), and toe (station 44 to end). Hourly erosion rates are summarized in table 18. Hourly rates for each region for tests 29 and 33 are shown in figure 56. The figure clearly shows the regions where erosion was concentrated for these tests.

One additional bare soil test (test 54) was conducted using the type I soil. The embankment for this test was completely reconstructed and compacted to 89 to 93 percent of standard Proctor density using a vibrating plate compactor. This differed from the other bare soil embankments which consisted of an approximately 18-in-deep (46 cm) reconstructed shell of soil overlaying an overcompacted soil core. The test 54 embankment was subjected to a 1-ft (0.30 m) overtopping depth and freefall conditions. Even with this low-flow condition, erosion was severe, with the entire embankment being washed out within 20 minutes. The average erosion rate over this period was approximately $600 \text{ ft}^3/\text{hr}/\text{ft}$ ($55.7 \text{ m}^3/\text{hr}/\text{m}$). The changes in embankment profile with time are indicated in figure 57. Data collection during test 54 was difficult due to the rapid erosion rate. However, the profiles shown in figure 57 are reasonably representative of changes to the embankment over the short duration of this test.

The bed shear stresses reported in table 17 indicate that, for identical soils and embankment slopes, bed shear increases with increasing discharge. Because flow is nearly uniform across the control volume, these two trends were anticipated. When flow is uniform, pressure forces acting on the

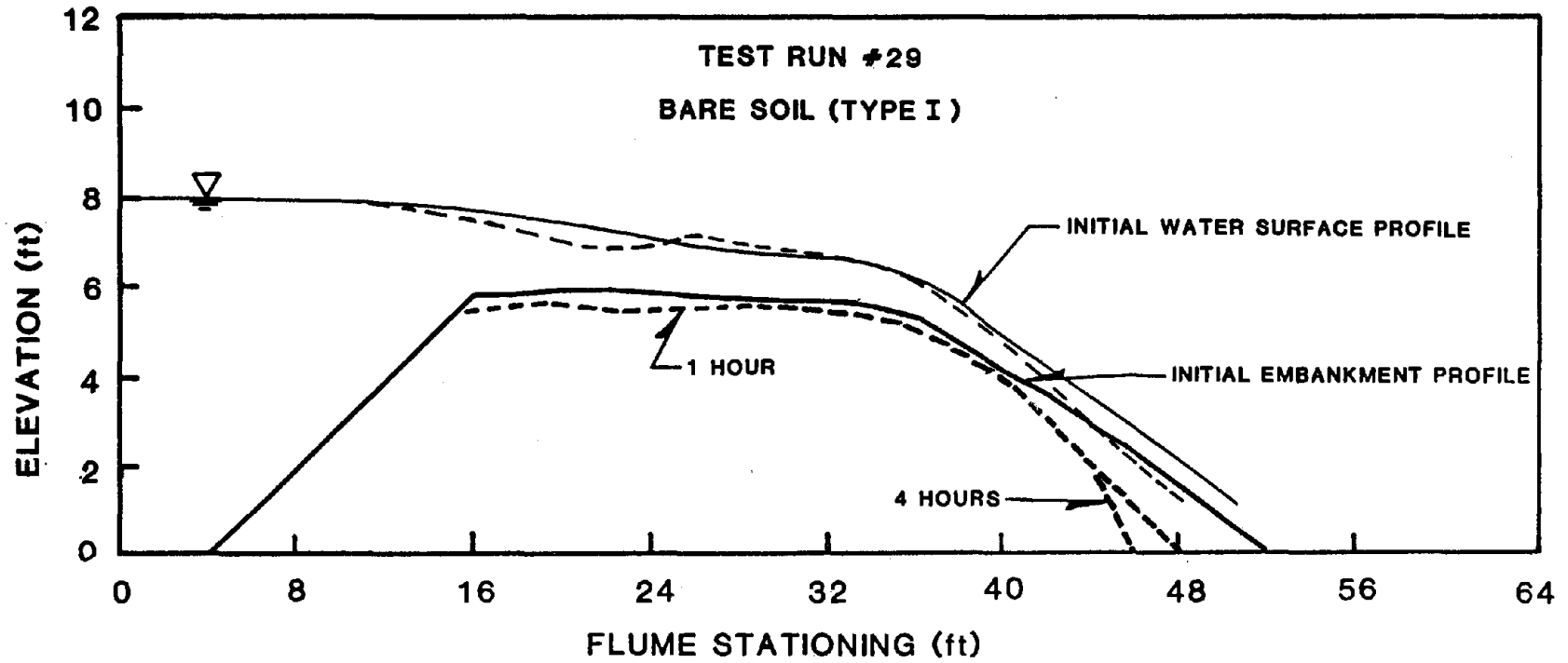
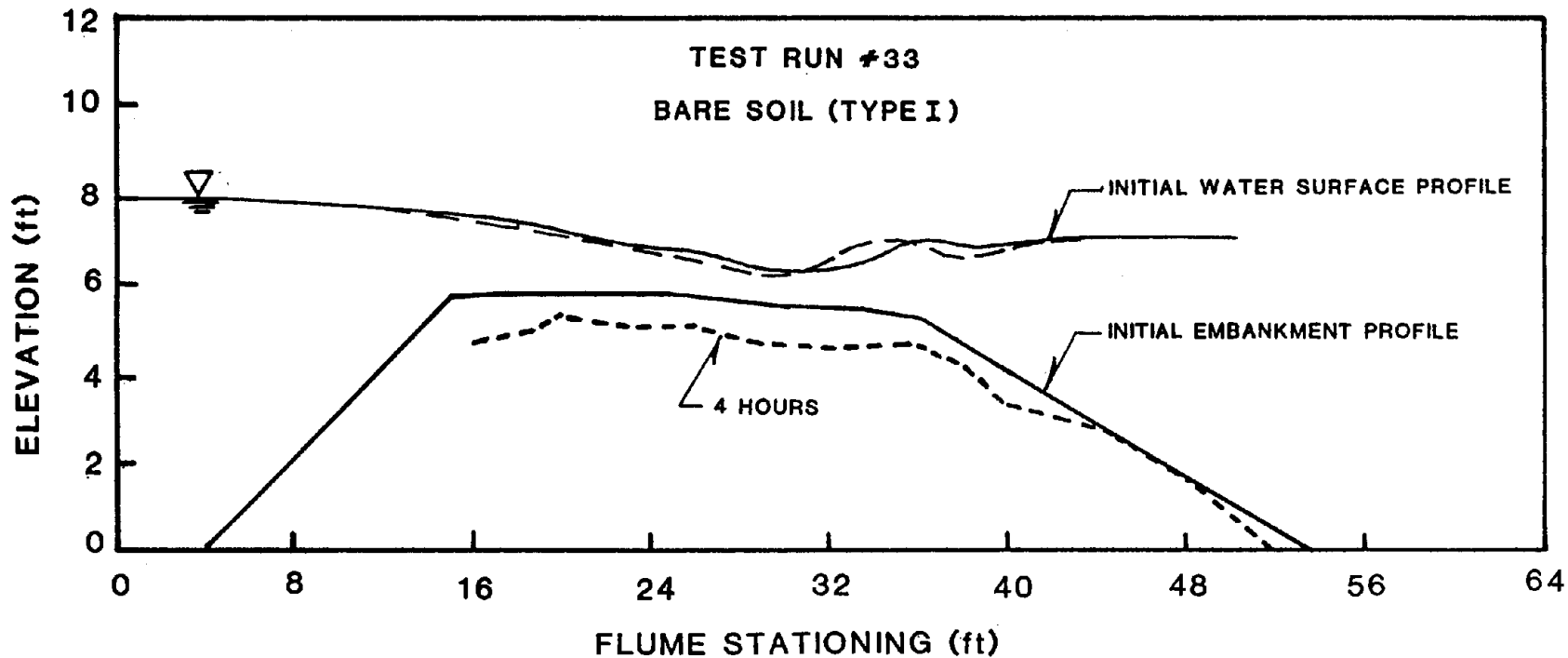


Figure 54. Erosion pattern for the test 29 bare soil embankment under freefall conditions [2-ft (0.61 m) overtopping depth].



143

Figure 55. Erosion pattern for the test 33 bare soil embankment under tailwater conditions [2-ft (0.61 m) overtopping depth with a 1-ft (0.30 m) water surface drop].

Table 18. Measured erosion rates for bare soil embankment tests.

Soil Type	Test No.	Over-topping Depth (ft)	Tail-water	Crest Sta 24 - 30				Shoulder Sta 30 - 40				Toe Sta 44 - end			
				1 hr	2 hrs	3 hrs	4 hrs	1 hr	2 hrs	3 hrs	4 hrs	1 hr	2 hrs	3 hrs	4 hrs
				(ft ³ /hr/ft)				(ft ³ /hr/ft)				(ft ³ /hr/ft)			
II	1b	1	FF	1.16	0.32	0.00	0.20	3.32	0.04	-0.60	0.48	-0.3	6.2	-1.2	3.7
	2	2	FF	0.50	0.54	1.02	0.02	1.81	0.29	0.24	0.72	1.13	-0.08	0.12	0.34
	3	2	FF	0.35	0.55	0.58	0.29	2.11	1.27	0.49	0.29	3.01	1.15	0.30	-0.03
	4	2	1 ft	0.50	0.22	0.18	0.00	0.88	-0.12	0.09	0.13	2.62	-0.24	-0.57	0.29
	5	1	FF	0.74	0.06	0.10	-0.06	-1.02	1.16	0.04	0.04	0.65	0.07	-0.20	0.16
	6	2	FF	0.74	-0.20	0.31	-0.04	0.24	0.09	0.50	0.20	0.12	0.43	-0.11	0.06
	7	4	FF	3.63	0.21	0.04	0.01	6.88	0.02	-0.30	0.05	8.40	-1.92	1.70	0.10
	8	4	1 ft	0.26	-0.07	0.11	0.06	0.79	0.13	0.75	0.41	2.95	0.85	0.44	0.74
	9	4	2 ft	1.38	0.80	0.75	1.00	2.58	1.62	1.37	2.52	4.40	1.49	4.15	0.44
	10	4	FF	-0.08	8.36	7.24	9.36	4.56	8.92	12.12	26.60	6.2	19.4	18.5	20.6
I	25	1	FF	0.86	0.05	0.00	0.05	2.12	-0.01	0.15	-0.03	1.49	0.40	0.00	0.15
	26	1	FF	0.37	0.09	-0.01	0.04	2.05	0.86	0.08	0.10	1.80	7.34	-0.82	0.03
	27	2	FF	0.41	0.12	0.08	0.13	2.09	0.22	0.14	-0.21	2.50	2.28	1.70	0.34
	28	4	FF	0.62	0.13	-0.02	0.08	2.25	0.38	0.11	0.08	4.48	1.34	-0.57	0.52
	29	2	FF	0.84	0.09	0.59	0.13	0.47	0.37	0.43	0.08	6.33	0.08	2.26	-0.03
	30	4	FF	0.18	0.12	0.38	0.37	0.33	0.06	0.03	0.15	0.88	0.65	0.72	0.22
	31	4	2 ft	0.52	0.99	-0.10	0.26	0.31	0.55	0.96	0.72	8.21	0.21	0.87	0.10
	32	4	1 ft	0.22	0.58	0.52	0.03	1.12	0.25	-0.02	0.47	0.48	0.19	-0.08	0.22
	33	2	1 ft	4.26	-0.26	0.07	0.05	3.43	-0.51	0.08	0.08	-0.82	-0.99	0.42	-0.05
	51*	1	FF	EROSION RATE WAS APPROXIMATELY 600 FT ³ /HR PER FOOT WIDTH											

* Entire embankment compacted to 89 to 93 percent of standard Proctor density with vibrating plate compactor.

ft x 0.3048 = m

ft³/hr/ft x 0.0929 = m³/hr/m

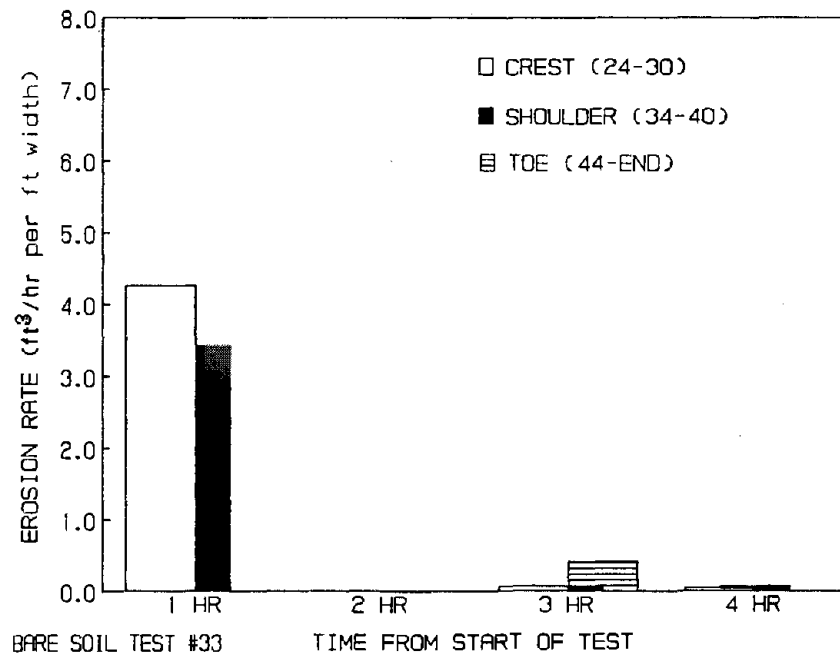
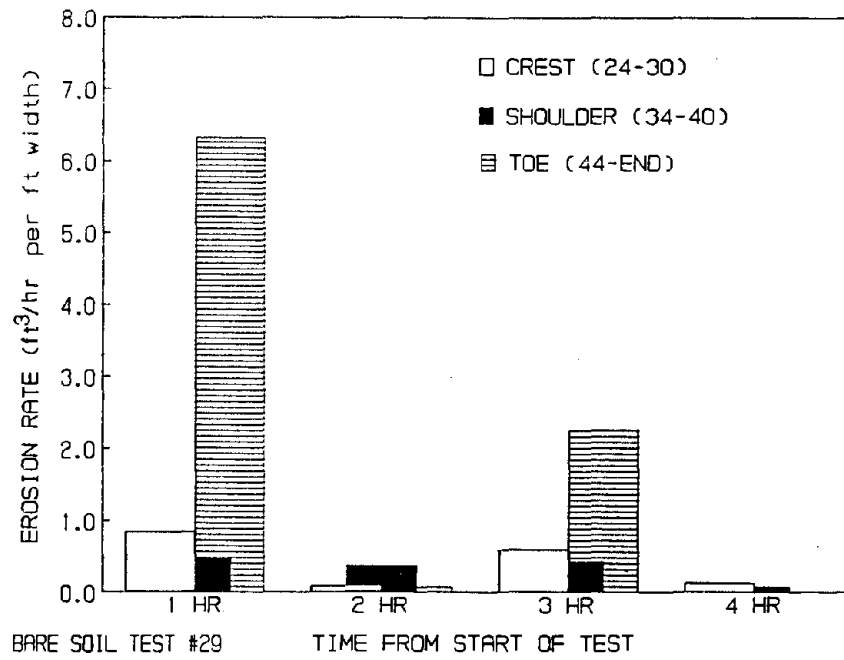


Figure 56. Hourly rates for tests 29 and 33.

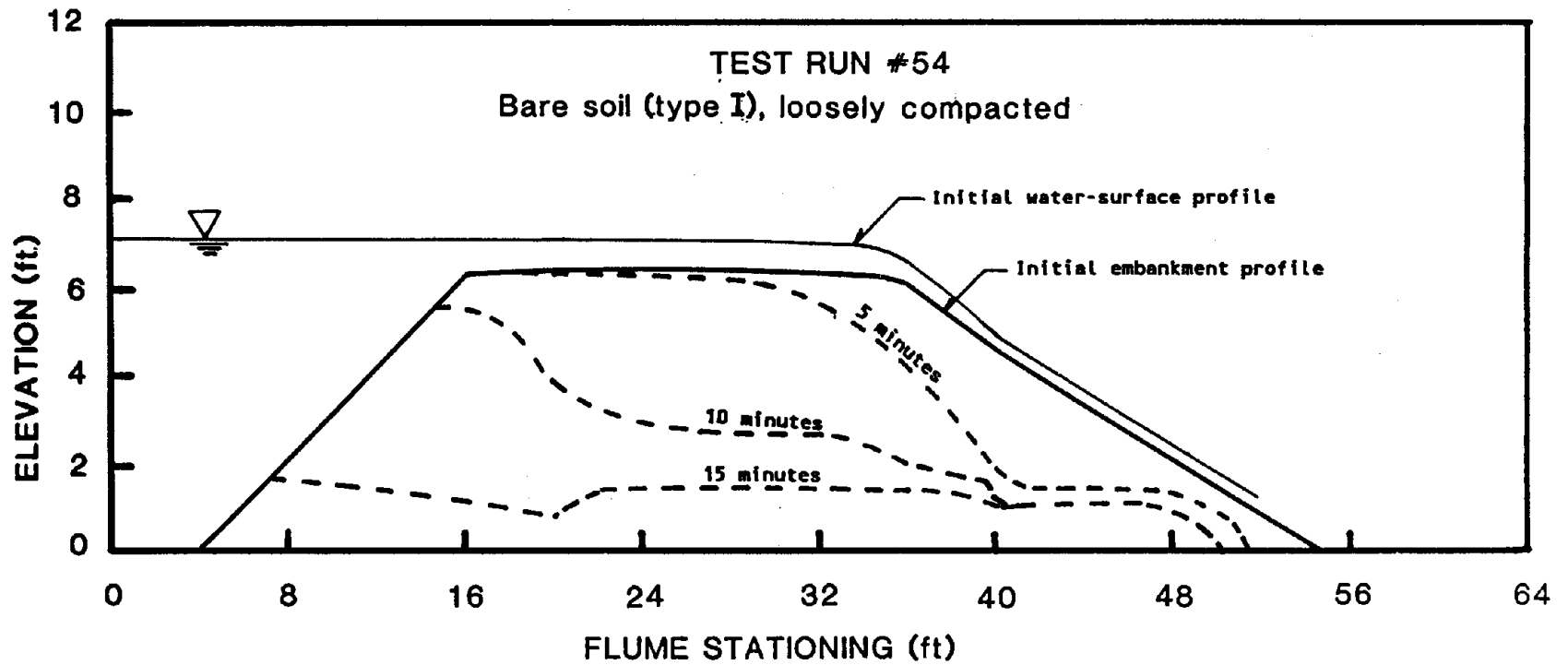


Figure 57. Erosion pattern for the test 54 bare soil embankment, loosely compacted, under freefall conditions [1-ft (0.30 m) overtopping depth].

control volume are in equilibrium, the change in momentum is zero and equation 9 reduces to

$$\tau_0 = \frac{W}{L} \sin\theta \quad (13)$$

As discharge is increased, the volume of water within the control volume and therefore the body force also increases. In addition, an increase in embankment slope corresponds to a larger component of body force in the direction of flow. By correlating erosion with bed shear, it was observed that while all test conditions caused significant erosion, it did not become severe until bed shear exceeded 10 to 15 lb/ft² (0.48 to 0.72 kN/m²).

A consistent relationship did not emerge when friction factors were compared to discharges and embankment slopes. This is partially due to the conflicting dependencies of friction factor on bed shear and flow velocity; parameters which both increase with discharge. The Darcy-Weisbach friction factor is directly proportional to bed shear, but inversely proportional to flow velocity (see equation 11). Another factor which may have contributed to the lack of correlation between friction factor and embankment slope during the bare soil tests was the nonuniform erosion of the embankment. This was particularly evident for tests with 2- and 4-ft (0.61 and 1.2 m) overtopping depths. Due to freefall conditions, the toe of a bare soil embankment generally eroded more rapidly than any other portion of the embankment. This headcut phenomenon resulted in an increase of embankment slope with time, particularly for higher discharges. In cases where slope changes were substantial, an approximate slope which more accurately defined actual conditions was used in the calculation of shear stress. This procedure was necessary for tests 27, 28, and 29. The estimated slopes for these tests are given in table 17.

It was also found that Manning's roughness coefficients could not be correlated to either discharge or embankment slope. It is probable this was the result of the same phenomena which kept trends between friction factor and discharge or slope from emerging.

Detachment rate equations of the form

$$E = K (\tau - \tau_c)^a \quad (14)$$

where E is the erosion rate in $\text{ft}^3/\text{s}/\text{ft}$, τ is the measured shear stress in lb/ft^2 , τ_c is the critical shear stress of the soil, and K and a are constants for the soil, were developed for both type I and type II soils using the measured erosion rates and shear stresses.

Based on the measured shear stress values for the bare soil tests, it was found that critical shear stresses for the type I and type II soils were typically less than 2 percent of the bed shear stress due to the high-velocity flow. Therefore, this parameter was neglected in the regression equations developed for these tests, with the resulting equation used for analysis:

$$E = K\tau^a \quad (15)$$

As with the Phase I FHWA study, the parameters K and a were determined by regressing local erosion rates during the first hour of testing with the average shear stresses over the same period. Detachment rate equation parameters were computed using data from freefall tests only. These data are plotted on figure 58 along with the regression equations. These parameters, as well as the soil characteristics, are compared with those for the Phase I FHWA study in table 19. Discrepancies between detachment rate parameters are attributed to different methodologies used to determine shear stress. Shear stresses computed in the Phase I FHWA study were derived from theoretical relative roughness estimates of the friction factor f , while the current study utilized shear stresses computed directly from measured data.

b. Embankment Protection Measures

Results of the analysis for the embankment protection measures are given in tables 20 and 21. Bed shear, flow velocity, and flow depth are plotted

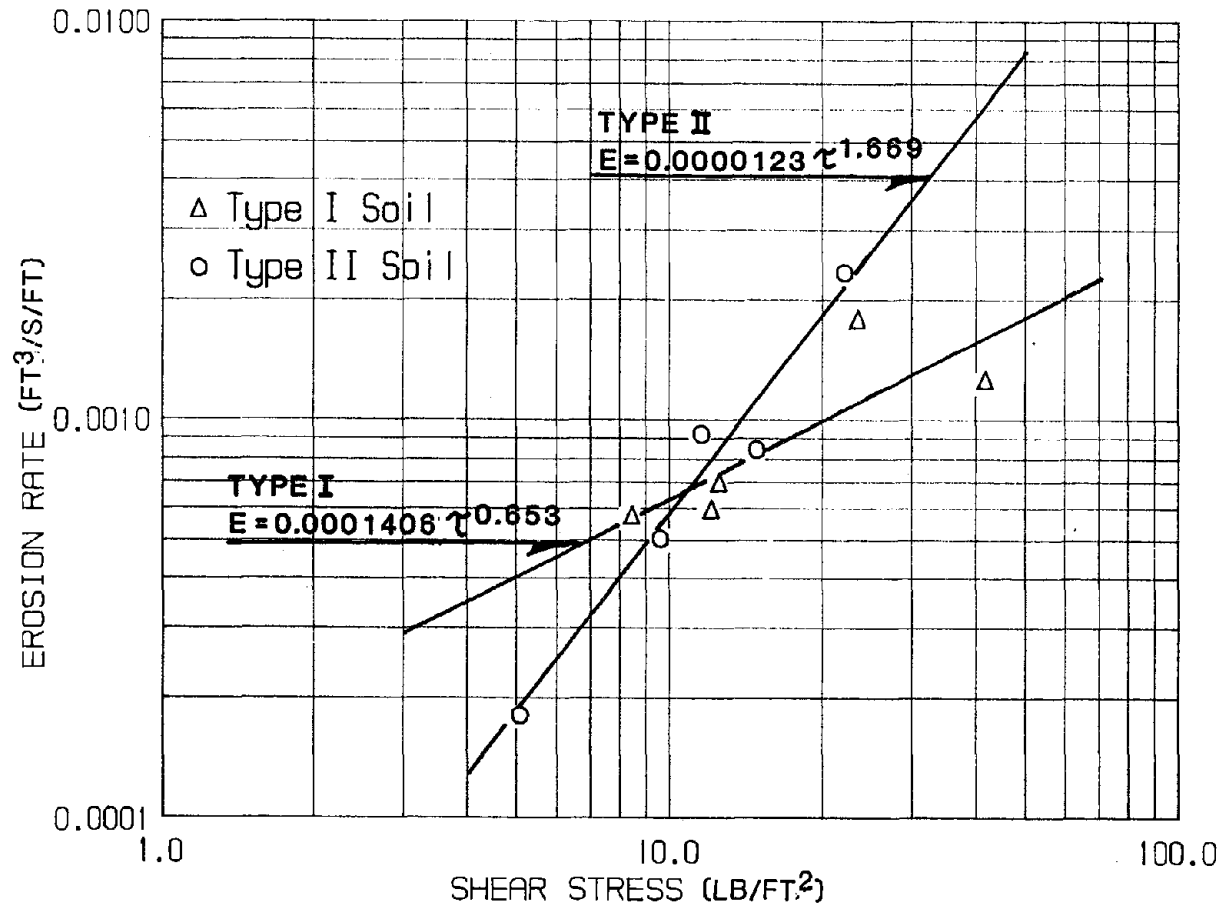


Figure 58. Detachment rate regression equations for soil types I and II.

Table 19. Comparison of FHWA phase I and FHWA phase II soil characteristics and detachment rate equations parameters.

Source	Soil Type	Plasticity Index	D ₅₀ (mm)	Proctor Density (lb/ft ³)	Percent of Max. Proctor Density	Detachment Rate Equation Parameters ^a	
						k	a
FHWA Phase I Study (ref. 2)	Noncohesive	--	--	--	--	0.00324	1.30 ^b
	Cohesive (High PI)	11.7-15.7	0.04	106	92-95	0.000086	0.91 ^b
	Cohesive (Low PI)	5.7	0.10	113	95	0.00022	0.43 ^b
FHWA/BOR Phase II Study (current study)	Cohesive (Type II)	11.7-15.7	0.040	110	95-100	0.000012	1.669 ^c
	Cohesive (Type I)	4.9	0.045	121	95-100	0.00014	0.653 ^c
	Cohesive (Type I - Loosely Compacted) ^d	4.9	0.045	121	89-93	--	--

^aDetachment rate relationship of the form: $E = K (\tau - \tau_c)^a$.

^bParameters determined based on shear stresses computed from estimated friction factors and measured erosion rates.

^cParameters determined based on shear stresses computed from measured data only and measured erosion rates.

^dParameters could not be determined as only one data point was available for this condition and a regression analysis could not be performed.

Table 20. Shear stress and bed roughness analysis results for soil cement, gabion mattress, and geoweb protection systems under freefall conditions.

Product	Test No.	Embankment Sideslope (RUN/RISE)	Depth of Over-topping (ft)	Q (ft ³ /s)	Hydraulic Analysis (stations 38 to 44)					Comments
					τ_o (lb/ft ²)	f	V _{ave} (ft/s)	S _f	n	
Soil Cement	11	3:1	1	12	7-9	0.40 - 0.60	8.0 - 8.2	0.31	0.052 - 0.054	Stable
	12	3:1	2	34	9-13	0.20 - 0.40	11.9 - 13.2	0.33	0.049 - 0.057	Stable
	13	3:1	4	96	18-27	0.30 - 0.50	14.2 - 16.0	0.18	0.052 - 0.063	Stable
	14 ^a	2:1	1	15	14-15	1.15 - 1.30	6.8 - 7.1	0.50	0.096 - 0.105	Stable
	15	2:1	2	39	23-27	0.75 - 0.95	10.9 - 11.0	0.46	0.085 - 0.087	Stable
	16	2:1	4	98	44-47	0.85 - 0.95	14.0 - 14.7	0.38	0.089 - 0.096	Stable
6-in Gabions	19 ^b	2:1	2	35	26-30	1.00 - 1.10	9.0 - 11.7	0.49	0.073 - 0.114	Stable, Basket Deformation
	20 ^c	2:1	4	96	30-40	0.55 - 0.85	13.9 - 14.8	0.23	0.067 - 0.074	"
	23 ^d	3:1	2	30.5	14-17	0.60 - 0.95	8.4 - 9.4	0.28	0.073 - 0.087	"
	24	3:1	4	96	15-25	0.26 - 0.50	13.9 - 16.8	0.20	0.051 - 0.069	Failure at Crest Anchor
4-in Geoweb	34 ^e	2:1	1	14	9-11	0.35 - 0.50	9.5 - 9.9	0.47	0.052 - 0.055	Stable
	35 ^e	2:1	2	34	18-25	0.70 - 0.95	9.8 - 10.2	0.44	0.086 - 0.092	Failure

151

- a: Stations 36-40
 b: Stations 38-46
 c: Stations 38-42
 d: Stations 38-48
 e: Stations 40-46

$$\text{ft} \times 0.3048 = \text{m}$$

$$\text{ft}^3/\text{s} \times 0.0283 = \text{m}^3/\text{s}$$

$$\text{lb}/\text{ft}^2 \times 47.87 = \text{N}/\text{m}^2$$

- Note: 1. Friction slope S_f determined by linear regression and verified by graphical average of energy grade line over the downstream embankment slope for the duration of test.
2. Bed shear τ_o determined by momentum equation between stations 38 and 44 (except where noted) for each measurement period; typical range reported.
3. Average velocity V_{ave} determined over duration of test between stations 38 and 44 (except where noted).
4. n determined by Manning's equation: $n = \frac{1.49}{V} d^{2/3} S_f^{1/2}$
5. f determined by equation: $f = 8\tau_o/\rho V^2$ for each measurement period; typical range reported.

Table 21. Shear stress and bed roughness analysis results for enkamat with asphalt and concrete-block mattress protection systems under freefall conditions.

Product	Test No.	Embankment Sideslope (Run/Rise)	Depth of Over-topping (ft)	Q (ft ³ /s)	Hydraulic Analysis (stations 38 to 44)					Comments
					τ_o (lb/ft ²)	f	V _{ave} (fps)	S _f	n	
Enkamat with 3-in asphalt	40	2:1	2	34	13-16	0.40 - 0.50	9.7 - 13.1	0.22	0.041 - 0.066	Stable
Enkamat with 1-in asphalt	42	2:1	1	12	5-9	0.25 - 0.40	8.6 - 9.9	0.29	0.037 - 0.046	Failure
Armorflex	44	2:1	1	13.8	4-7	0.10 - 0.25	10.1 - 12.9	0.36	0.029 - 0.044	Stable
	45	2:1	2	34.0	9-12	0.25 - 0.35	9.7 - 15.1	0.24	0.035 - 0.073	Stable
	46	2:1	4	90.5	32-36	0.55 - 0.60	14.6 - 16.2	0.22	0.054 - 0.064	Failure*
Petraflex	47	2:1	1	13.5	8-10	0.31 - 0.44	9.7 - 10.0	0.48	0.050 - 0.053	Stable
	48	2:1	2	34.0	10-12	0.27 - 0.32	9.8 - 14.7	0.25	0.035 - 0.068	Stable
	49	2:1	4	96.0	26-32	0.44 - 0.56	14.3 - 16.9	0.30	0.061 - 0.080	Stable
	49A	2:1	4	93.0	25-26	0.44 - 0.48	13.6 - 16.9	0.26	0.055 - 0.080	Stable
Dycel	52 ^e	2:1	1	12.0	7-10	0.45 - 0.60	7.3 - 9.9	0.39	0.043 - 0.071	Failure**
	53 ^b	2:1	1	12.0	7-10	0.45 - 0.64	7.8 - 8.3	0.40	0.058 - 0.064	Failure**

a: Stations 36-40
 b: Stations 38-46
 c: Stations 38-42
 d: Stations 38-48
 e: Stations 40-46

*After 5 hours
 **After 1 hour

ft x 0.3048 = m
 ft³/s x 0.0283 = m³/s
 lb/ft² x 47.87 = N/m²

- Note:
1. Friction slope S_f determined by linear regression and verified by graphical average of energy grade line over the downstream embankment slope for the duration of test.
 2. Bed shear τ_o determined by momentum equation between stations 38 and 44 (except where noted) for each measurement period; typical range reported.
 3. Average velocity V_{ave} determined over duration of test between stations 38 and 44 (except where noted).
 4. n determined by Manning's equation: $n = \frac{1.49}{V} d^{2/3} S_f^{1/2}$
 5. f determined by equation: $f = 8\tau_o/\rho V^2$ for each measurement period; typical range reported.

against unit discharge in figures 59, 60, and 61, respectively. The tendency of these three parameters to increase with increasing unit discharge is indicated. Figure 59 illustrates the correlation between bed shear and embankment slope. The increase of the component of body force in the direction of flow with increasing embankment slope results in higher bed shear. As with the bare soil tests, bed shear was directly proportional to discharge for identical protection system and geometric conditions. Bed shear was also directly proportional to embankment slope. Friction factors and Manning's roughness coefficients could not be correlated to either discharge or embankment slope for the hydraulic tests with the protection systems. It is believed a simple relationship between roughness and either discharge or slope was not observed due to the relatively complex inter-relationship of shear stress, flow velocity, and flow depth.

(1) Soil Cement. Soil cement was one of the most stable slope protection measures tested. For even the most severe hydraulic conditions, there was no indication of erosion or surface damage. This result was significant, particularly since the embankment experienced shear stresses up to nearly 50 lb/ft^2 (2.4 kN/m). The stair-step fashion in which the soil cement was placed resulted in a relatively rough surface on the downstream slope of the embankment. The roughness of the stair-step embankment was manifested in relatively high friction factors and Manning's roughness coefficients. This was particularly true of the 2H:1V embankment. For this scenario, Darcy-Weisbach friction factors ranged from 0.75 to 1.30 while Manning's roughness coefficients varied from 0.085 to 0.105. These values were significantly higher than those for both bare soil embankments and other protection systems.

(2) Gabion Mattresses. Gabion mattresses were relatively stable during testing, but experienced problems with deformation of the wire-mesh baskets. Basket deformation was caused by the gradual migration of the rockfill to the downstream end of each basket compartment. This behavior was observed for 2- and 4-ft (0.61 and 1.2 m) overtopping depths on both 2H and 3H:1V slopes. Therefore, movement of mattress rocks and basket deformation occurred at shear stresses as small as 14 lb/ft^2 (0.67 kN/m). Test 24, a

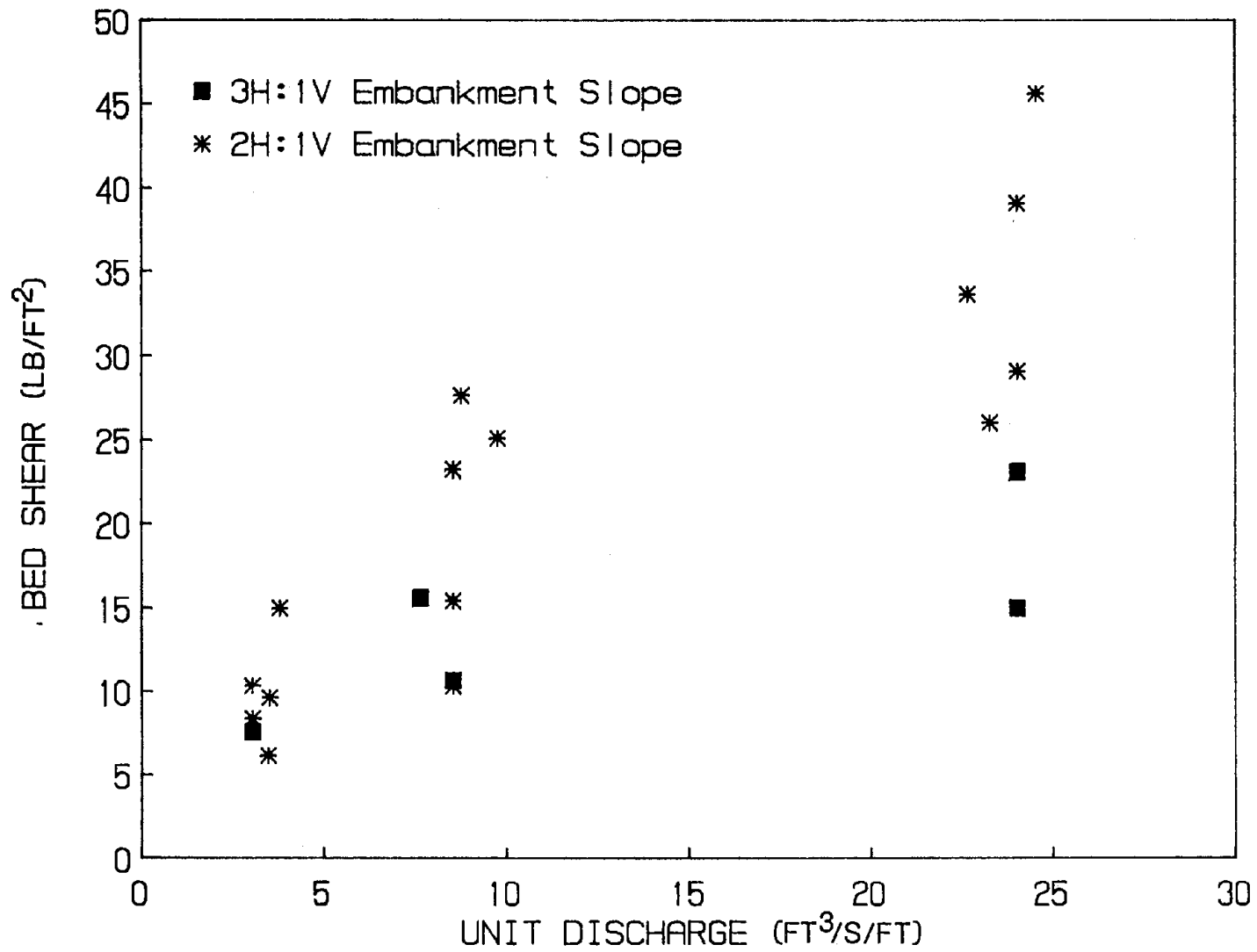


Figure 59. Bed shear versus unit discharge for protection system freefall tests.

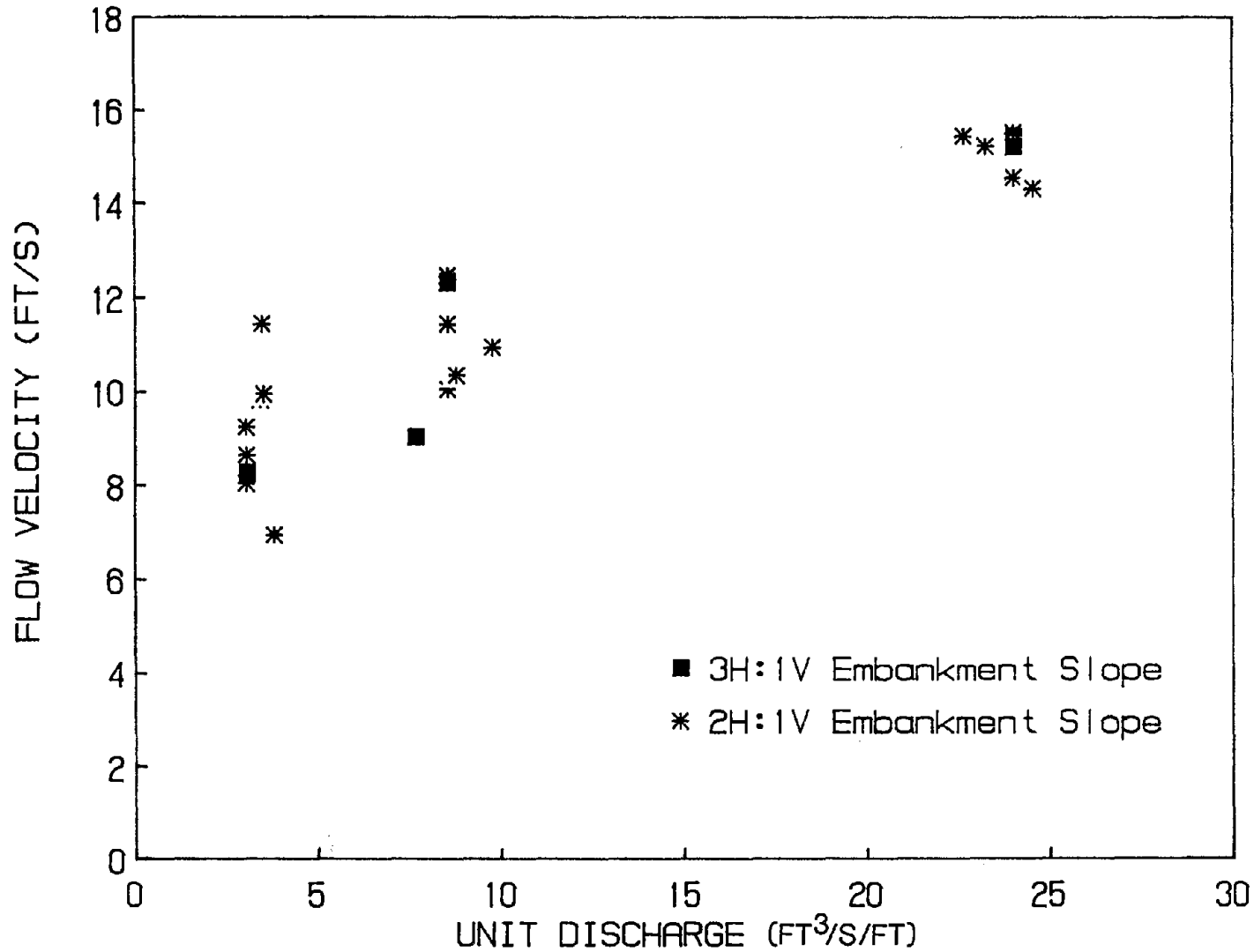


Figure 60. Flow velocity versus unit discharge for protection system freefall tests.

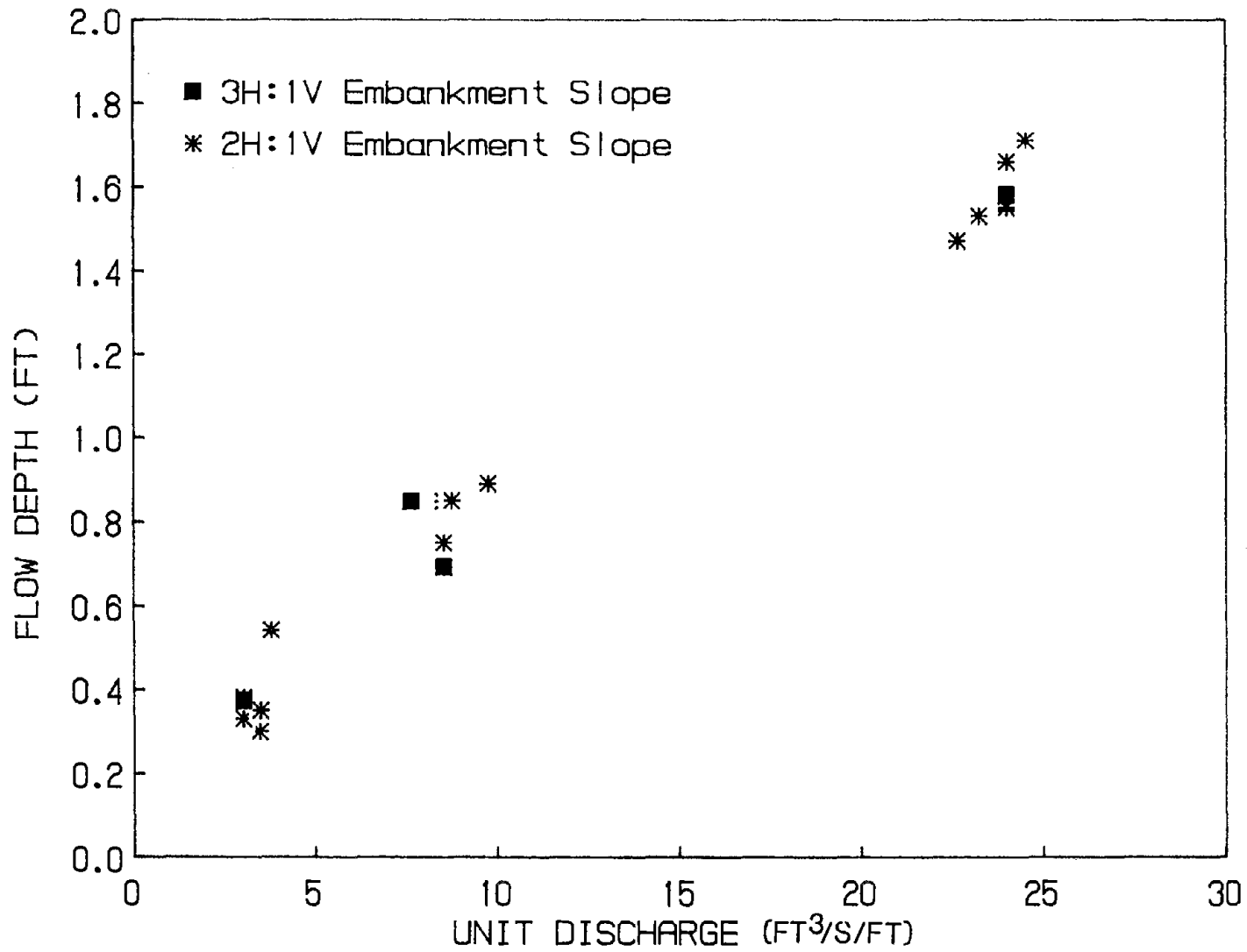


Figure 61. Flow depth versus unit discharge for protection system freefall tests.

4-ft (1.2 m) overtopping depth and 3H:1V slope test, failed due to loss of the crest anchor. This was caused by erosion of the crest upstream of the mattresses, eventually allowing water under the system which rolled the gabions down the embankment. Another 4-ft (1.2 m) test, test 20, did not fail the crest anchor. It is probable that test 24 failed, while test 20 did not, due to the embankment erosion/reconstruction cycles which preceded test 24. During the gabion tests, erosion of the crest occurred to varying degrees and required patching and recompacting of the embankment. It was concluded that, while test 20 did not fail, it may have been at the threshold of failure and subsequent embankment repairs left the crest somewhat unstable and subject to failure under similar hydraulic conditions.

Friction factors for the gabions ranged from 0.26 to 1.10 while Manning's roughness coefficients varied from approximately 0.05 to 0.09. These values are relatively high, being exceeded only by those computed for soil cement. The relatively high roughness parameters were at least partially due to the variable-height bed surface which resulted when mattress rocks shifted and deformed the baskets. Because loss of the crest anchor was the observed failure mechanism for gabions, redesigning the anchor would undoubtedly enhance the performance of this system.

(3) Geoweb. Results of the geoweb tests were mixed. The system was stable for 1-ft (0.30 m) overtopping depths, but was otherwise unstable. Test 35, the only 2-ft (0.61 m) test with freefall conditions, failed within the first hour. The failure mechanism was loss of the crest anchor due to shear stress exerted by the flow on the system. The presence of significant shear stresses was observed, particularly for medium and high flows, by the geoweb being stretched in the direction of flow. The 2-ft (0.61 m) overtopping condition of test 35 resulted in shear stresses of 18 to 25 lb/ft² (0.86 to 1.20 kN/m²) which were sufficient to cause crest anchor failure by pulling the geoweb out of the 18-in-deep (46 cm), 45° anchor trench.

Friction factors for the geoweb varied from 0.35 to 0.95. Manning's roughness coefficients ranged from approximately 0.05 to 0.09. These values

are similar to those computed for gabions and somewhat less than the roughness values for soil cement.

(4) Enkamat. Bare enkamat was the least stable embankment protection system investigated. A single freefall test was conducted, which used a 0.5-ft (0.15 m) overtopping depth, but resulted in failure of the system within 10 minutes. The discharge for this test was estimated to be less than 5 ft³/s (0.14 m³/s). Although data collection was minimal due to the rapid failure, it was estimated that tractive stresses at failure did not exceed 3 lb/ft² (0.14 kN/m²). Failure was caused by stretching of the enkamat, causing separation from the flume walls which allowed liquefaction of the subsoil due to rapid ingress of water beneath the system to occur.

(5) Enkamat with Asphalt. The enkamat with asphalt tests indicated that stability improved with asphalt thickness, thereby suggesting the performance of the asphalt, rather than the enkamat, was being tested. However, the system was relatively unstable. Enkamat with 1 in (2.5 cm) of asphalt was extremely unstable with failure occurring after 30 minutes under a 1-ft (0.30 m) overtopping depth. Although the failure mechanism was not related to shear stress, bed shear at the time of failure was approximately 5 to 9 lb/ft² (0.24 to 0.43 kN/m²). The cause of failure was hydraulically induced uplift forces due to negative pressure at the embankment shoulder. This phenomenon will be described in detail later in this chapter. The enkamat with 3 in (7.6 cm) of asphalt performed more satisfactorily and was stable for a 2-ft (0.61 m) overtopping depth with shear stresses ranging from 13 to 16 lb/ft² (0.62 to 0.77 kN/m²).

Because the asphalt surface of this protection system was relatively smooth, computed roughness parameters were significantly smaller than those for all bare soil embankments and protection measures except the concrete-block mattresses. Friction factors varied from 0.25 to 0.50 while Manning's roughness coefficients ranged from approximately 0.035 to 0.065.

(6) Articulating Concrete-Block Revetment Systems. Performance of the concrete-block systems differed from product to product. The Dycel

system failed for even the lowest flows while the Petraflex-Vick system was stable for all hydraulic conditions. Armorflex system performance fell between these two extremes by failing under high flows, but showing stability for low- and mid-range flows. As with the enkamat with asphalt systems, the mode of failure for the concrete-block systems was uplift due to negative pressure near the embankment shoulder. Shear stresses at the time of failure for the Dycel system were 7 to 10 lb/ft² (0.34 to 0.48 kN/m²) while the Armorflex system failed at bed shears of 32 to 36 lb/ft² (1.5 to 1.7 kN/m²). The Petraflex-Vick system remained stable at shear stresses exceeding 30 lb/ft² (1.4 kN/m²).

Roughness parameters for the concrete-block mattresses were comparable to the enkamat with asphalt parameters, but substantially less than values for other protection measures and bare soil embankments. Armorflex friction factors ranged from 0.10 to 0.60 and Manning's roughness coefficients varied from approximately 0.03 to 0.07. For the Petraflex system, friction factors were 0.27 to 0.56 while the approximate range of Manning's roughness coefficients was 0.04 to 0.08. Because only low-flow conditions were imposed on the Dycel mattresses, roughness parameters were less variable. Friction factors varied from 0.45 to 0.64 while Manning's roughness coefficients ranged from 0.04 to 0.07.

5. Uplift Forces and the Subatmospheric Pressure Zone

The mode of failure for the enkamat with asphalt and concrete-block mattress systems was lifting of the protection system off the soil embankment. This allowed water to flow under the system, causing rapid saturation of the embankment soil to occur with subsequent failure by liquefaction. Failure of the enkamat with asphalt resulted in deformation, cracking, and partial loss of the system as shown in figures 34, 35, and 36. While the concrete-block system failures appeared to be less dramatic they were no less significant. Loss of intimate contact between the protection system and the subsoil allowed considerable amounts of water under the system. Once this happened, the soil embankment quickly become saturated to a depth sufficient for liquefaction to occur. The combination of saturated soil and cyclic

loading of the embankment due to turbulent pressure fluctuations caused liquefaction. This resulted in soil sliding down the embankment from the shoulder to the toe, thereby causing deformation of the system. This failure is illustrated in figures 37 and 46.

Hydraulically induced uplift forces are the result of negative pressure at the shoulder caused by separation of the nappe from the embankment at the downstream edge of the crest. Water traveling horizontally across the crest follows a path defined by projectile motion equations from the edge of the crest until the path intersects the embankment, at which time the nappe is deflected along the downstream slope of the embankment. An illustration of this behavior is given in figure 62. The zone of subatmospheric pressure is located between the points of separation and reattachment.

The nappe profile is defined by the equations governing projectile motion. When the grade break at the edge of the crest is taken as the origin and the crest is horizontal, these equations reduce to

$$y = \frac{-gx^2}{2V_0^2} \quad (16)$$

where g is the acceleration due to gravity, V_0 is the flow velocity at the origin, and x and y are distances from the origin along the respective coordinate axes. Given the flow velocity, the shape of the underside of the nappe is defined by equation 16. By subtracting equation 16 from the embankment profile equation and multiplying by the specific weight of water (γ), the following equation for computing the negative pressure profile results:

$$P = \gamma \left(\frac{gx^2}{2V_0^2} - \frac{x}{z} \right) \quad (17)$$

where P is the pressure at location x , and z is the number of horizontal units per vertical unit for the embankment slope. The variation of pressure with distance from the crest, for a 4-ft (1.2 m) overtopping depth, for both 2H and 3H:1V embankment slopes is shown in figure 63. The measured flow velocity at the edge of the crest for this condition was approximately 13.1

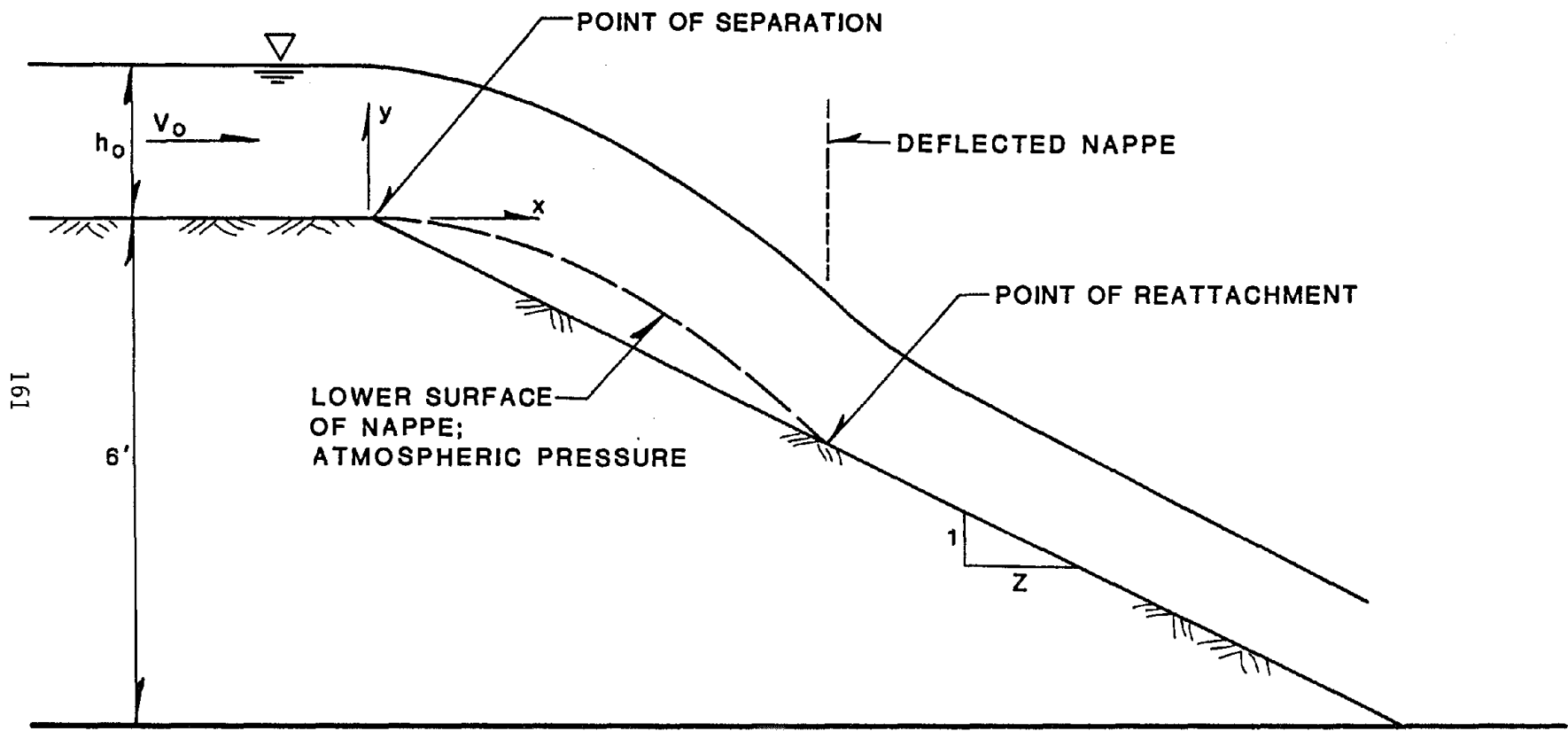


Figure 62. Profile of water nappe and theoretical subatmospheric pressure zone.

ft/s (4.0 m/s). The location of theoretical maximum negative pressure was determined by taking the derivative of equation 16 with respect to x and setting it equal to zero. Solving for x yields the equation

$$x' = \frac{V_0^2}{gz} \quad (18)$$

where x' is the x -location of maximum negative pressure. The maximum negative pressure is computed by substituting equation 18 for x in equation 17 and simplifying. The equation for maximum negative pressure becomes

$$P_{\max} = \frac{-\gamma V_0^2}{2gz^2} \quad (19)$$

where all terms have been previously defined. The theoretical maximum negative pressures for 1-, 2-, and 4-ft (0.30, 0.61, and 1.2 m) overtopping depths for both 2H and 3H:1V embankment slopes are shown in figure 64. Hydraulic parameters used to compute these pressures were taken from the test data. Results of pressure calculations for test 49 are illustrated in figure 65. Test 49 consisted of a Petraflex-Vick concrete-block system with 4-ft (1.2 m) overtopping depth and freefall conditions. For this test, the flow depth and velocity at the edge of the crest were 1.8 ft (0.55 m) and 13.1 ft/s (4.0 m/s), respectively.

Pressure transducer readings from instruments installed beneath the geotextile underlayer were collected for several concrete-block tests. Pressure data were taken at stations 36, 40, and 44. These locations were selected to represent the shoulder, mid-slope, and toe regions, respectively. Pressure readings for test 46A, Armorflex with a 4-ft (1.2 m) overtopping depth and freefall condition, are shown in figure 66. Note the sudden drop in pressure at 14 minutes into the test which correspond to sudden failure of the system. Pressure readings for the Dycel system with a 1-ft (0.30 m) overtopping depth and freefall condition (test 52) are shown in figure 67. Negative pressures were not measured because the transducers were located below the geotextile. The negative pressure zone due to overtopping flow

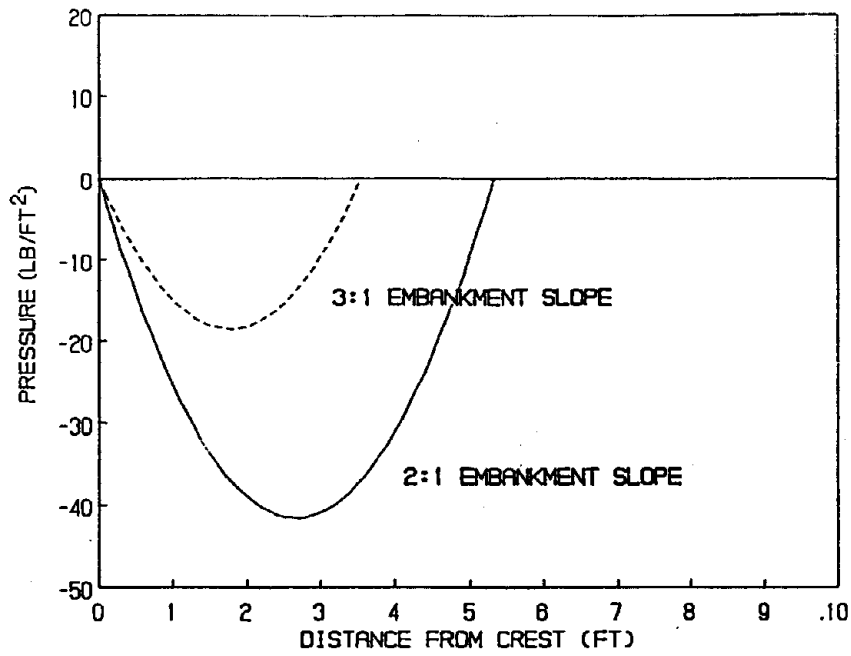


Figure 63. Theoretical pressure variation with distance from crest for 4-ft (1.2 m) overtopping depth.

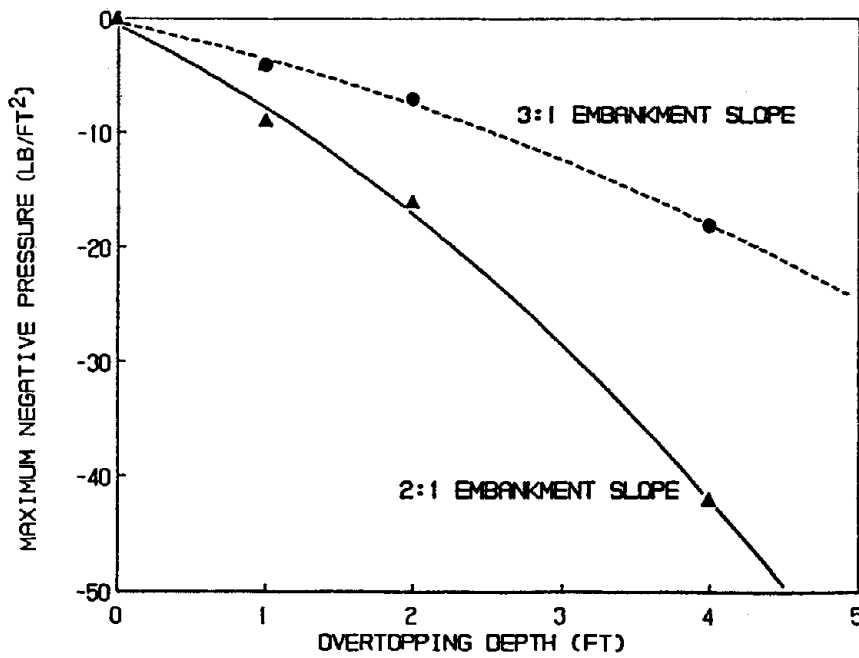


Figure 64. Theoretical maximum negative pressure variation with overtopping depth.

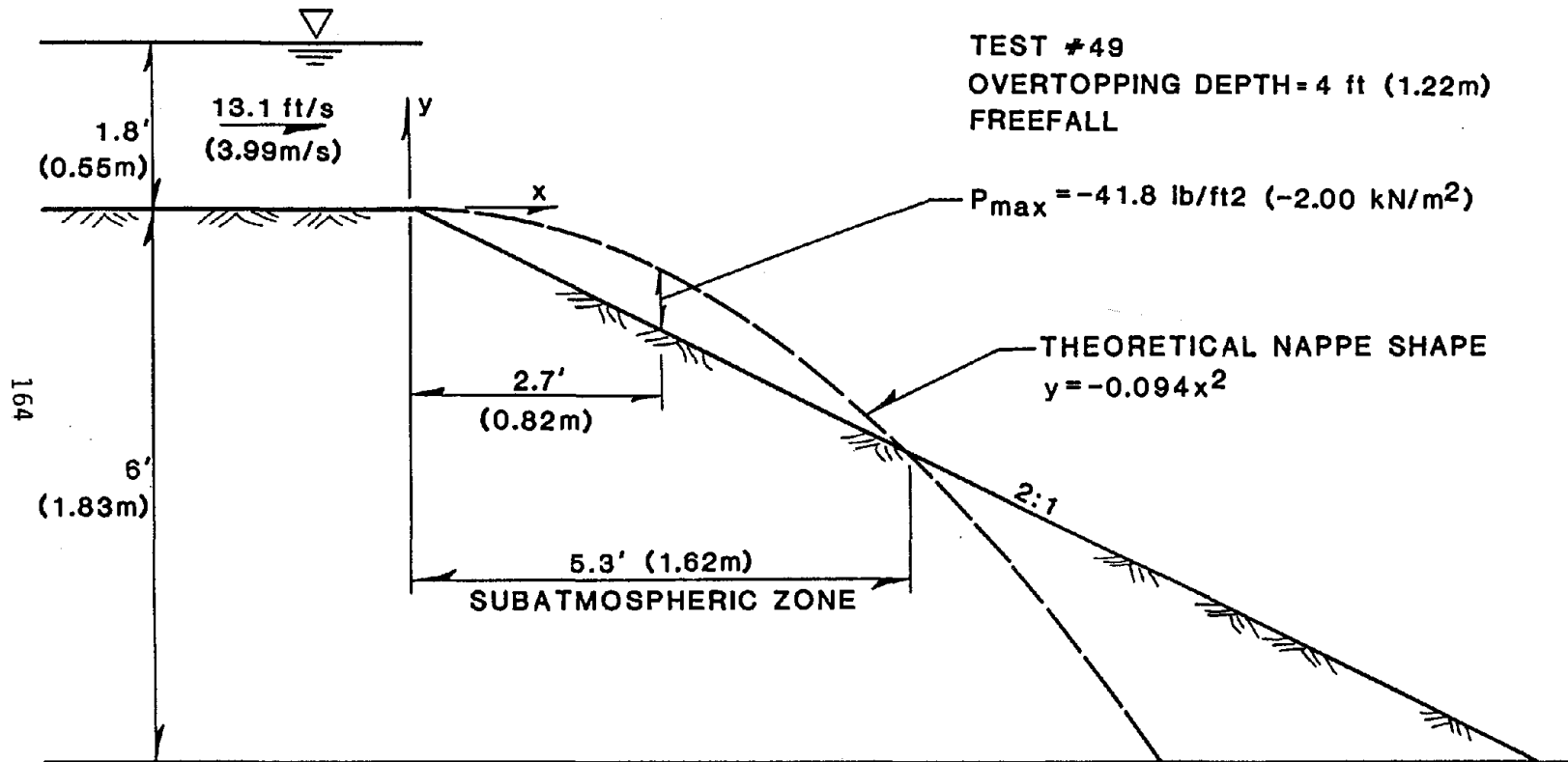


Figure 65. Theoretical negative pressure profile for test 49.

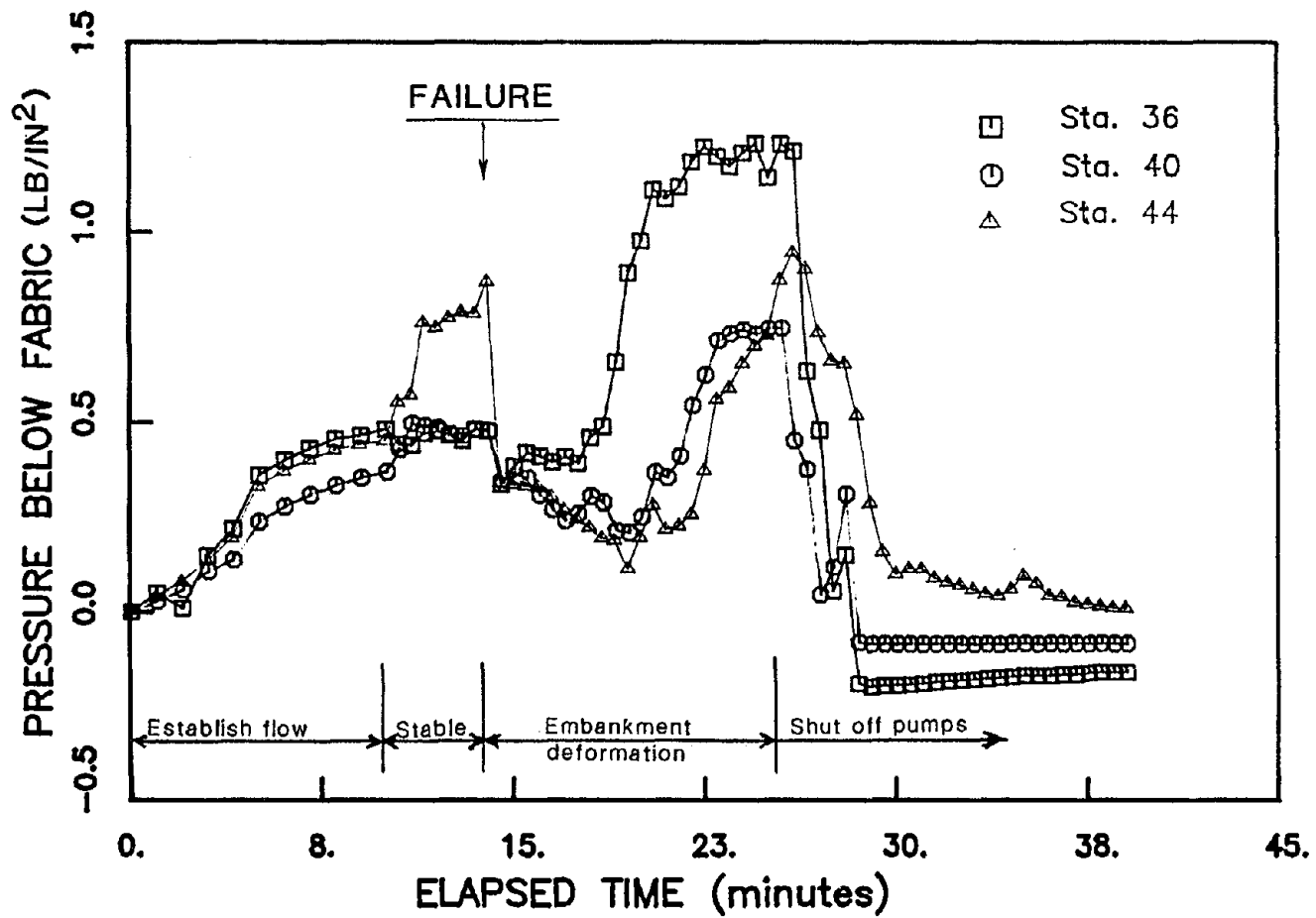


Figure 66. Pressure transducer readings taken during test 46A [4-ft (1.2 m) overtopping depth, freefall conditions, Armorflex block system]. Note the failure at 14 minutes into test.

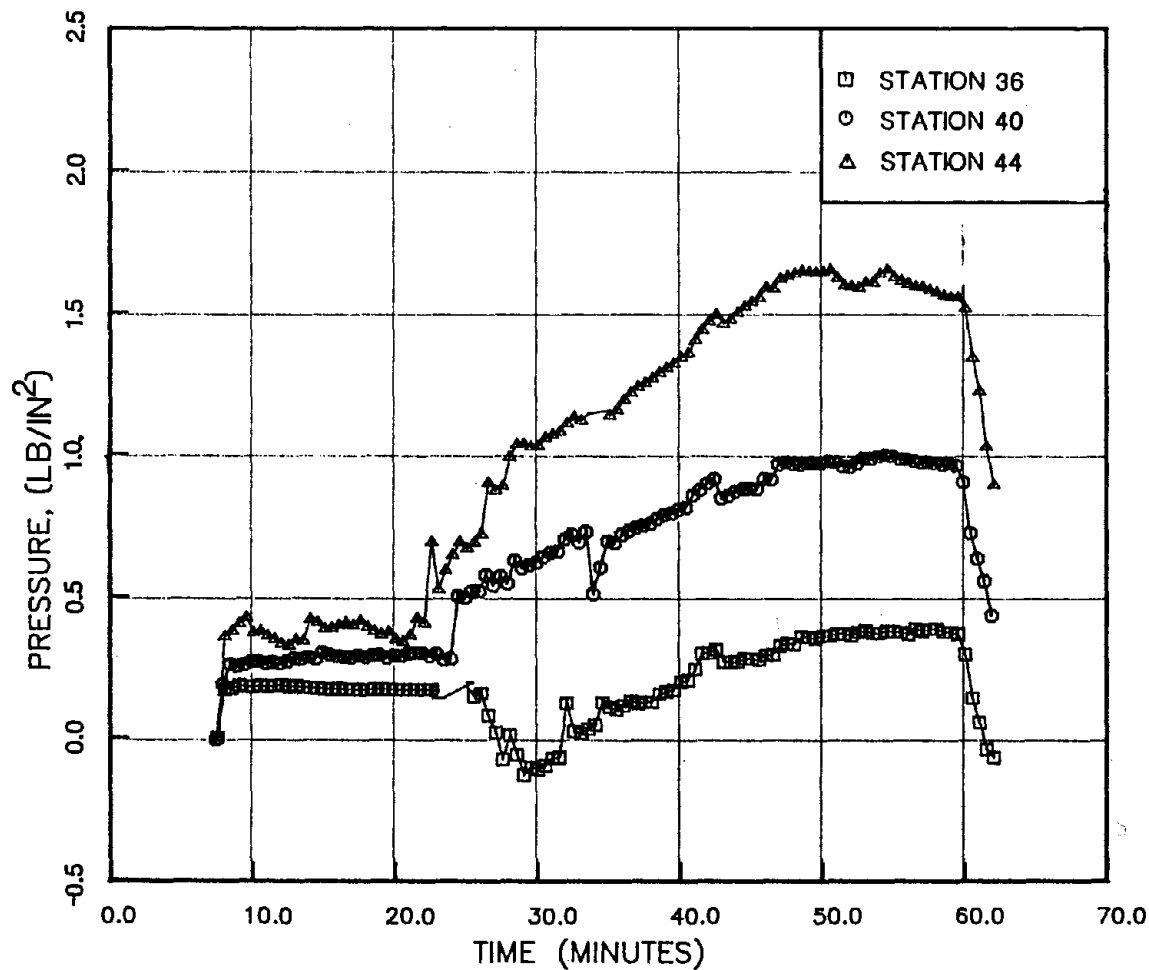


Figure 67. Pressure transducer readings taken during test 52 [1-ft (0.30 m) overtopping depth, freefall conditions, Dycel block system].

exists above the blocks while positive pressures are seen below the geotextile due to accretion of water beneath the protection system. The time of failure for test 52 cannot definitely be determined from the pressure data. However, the period of stability at the beginning of the test (minutes 8 through 23) is thought to correspond to the time during which water was effectively precluded from flowing beneath the system. Beyond 23 minutes, the transducer data reveal a gradual buildup of pressure beneath the geotextile, corresponding to the accumulation of water beneath the blocks.

Figures 66 and 67 are examples of pressure data from system failures. Figure 68, on the other hand, is an example of pressure data for a stable system. The data were collected at station 40 during test 47, which was a 1-ft (0.30 m) overtopping depth with freefall condition test for the Petraflex-Vick system. Pressure readings were stable for the entire duration of the test. Note the pressure readings for test 47 are approximately equal to those for test 52 at station 40 during the period of stability (see figure 67).

Ogee crest nomographs provided by the U.S. Bureau of Reclamation define a nappe profile which is similar to that determined by projectile motion equations.⁽⁸⁹⁾ However, the nomographs are applicable for upstream embankment slopes ranging from 45° to vertical which are significantly different than the broad-crested configuration used for this study. The conditions for which the nomographs apply support a vertical velocity component whereas test conditions do not. The ogee nomographs could be used for determining the nappe profile and, ultimately, the negative pressures acting on the embankment, although their use is not recommended due to the above considerations.

Theoretical maximum negative pressures were computed for the enkamats with asphalt and concrete-block mattress freefall tests. The results are summarized in table 22. The enkamats with asphalt systems were extremely vulnerable to uplift and failed with calculated maximum negative pressures of -10 and -17 lb/ft² (-0.48 and -0.81 kN/m²) for 1 and 3 in (2.5 and 7.6 cm) of asphalt, respectively. This was partially due to the lightweight nature

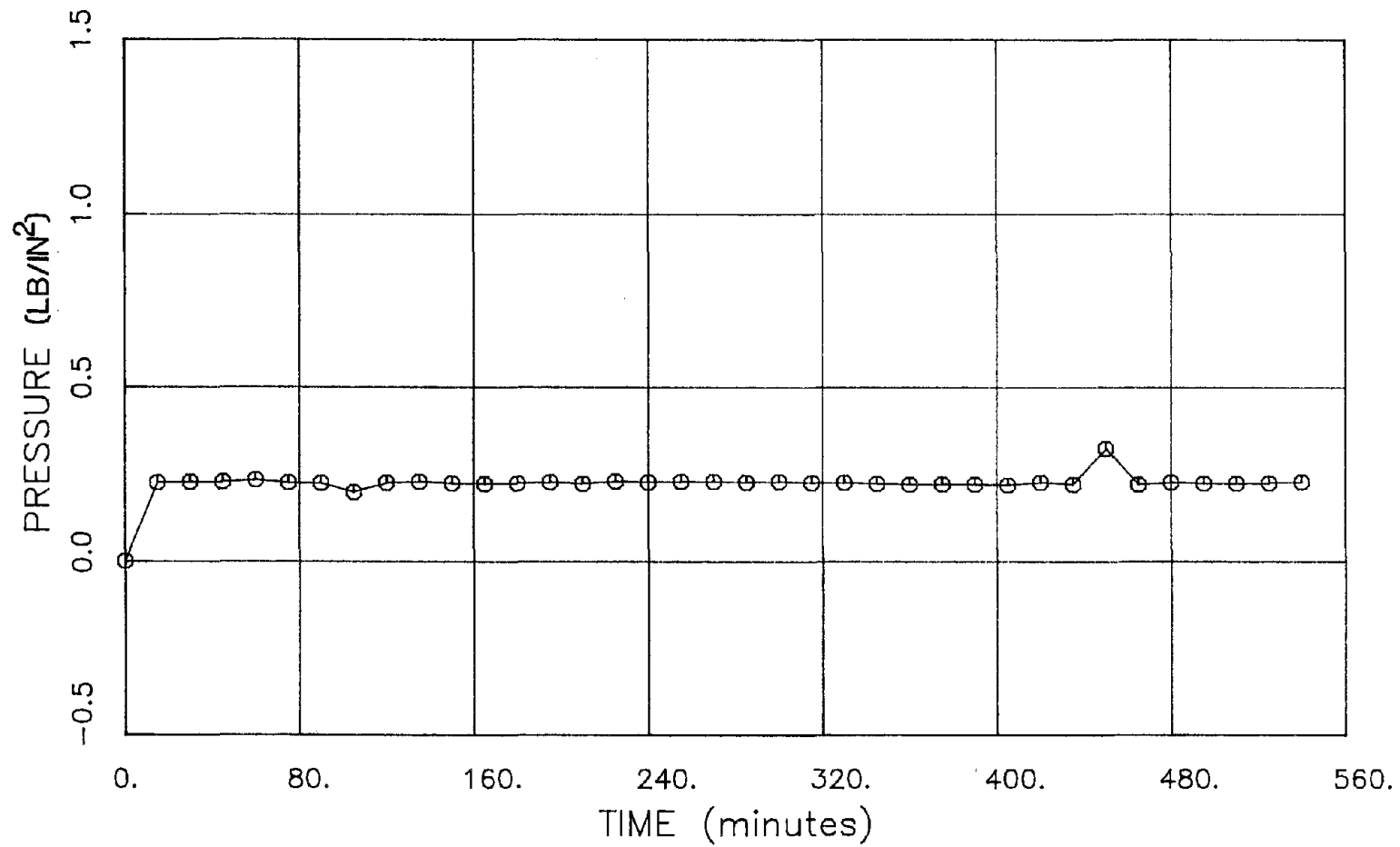


Figure 68. Pressure transducer readings taken at station 40 during test 47 [1-ft (0.30 m) overtopping depth, freefall conditions, Petraflex-Vick block system].

Table 22. Subatmospheric pressure analysis for enkamat with asphalt and concrete-block mattress protection systems under freefall conditions.

Product	Test No.	Discharge (ft ³ /s)	Flow Depth ^a (ft)	Velocity (ft/s)	Maximum Calculated Negative Pressure (lb/ft ²)
Enkamat with 3-in asphalt	40	34	1.02	8.3	-16.8
Enkamat with 1-in asphalt	42	12	0.48	6.3	- 9.5
Armorflex	44	13.8	0.50	7.0	-11.8
	45	34	1.00	8.5	-17.6
	46	90.5	1.77	12.8	-39.7
Petraflex	47	13.5	0.53	6.3	- 9.7
	48	34	1.04	8.2	-16.3
	49	96	1.83	13.1	-41.8
	49A	93	1.88	12.4	-37.1
Dycel	52	12	0.39 ^b	7.7	-14.3
	53	12	0.51 ^b	5.9	- 8.4

^aDepth at the edge of the crest (station 36).

^bAverage depth prior to failure.

$$\text{ft} \times 0.3048 = \text{m}$$

$$\text{ft}^3/\text{s} \times 0.0283 = \text{m}^3/\text{s}$$

$$\text{lb}/\text{ft}^2 \times 47.87 = \text{N}/\text{m}^2$$

of the systems. The enkamat with 1 and 3 in (2.5 and 7.6 cm) of asphalt had unit weights of 10 and 30 lb/ft² (0.48 and 1.4 kN/m²), respectively. Probably more important was the inability of the pull-out restraint system to keep the enkamat and asphalt in intimate contact with the embankment. Once this contact was lost, water was allowed under the edges of the system resulting in erosion along the flume walls and failure of the protection system.

The Dycel mattresses were also prone to failure at low negative pressures. This system failed at a calculated maximum negative pressure as low as -8 lb/ft² (-0.38 kN/m²). As explained in the previous section, failure was attributed to the blocks' low unit weight, and lack of lateral cables and vertical interlocking capabilities. Without lateral cables and vertical interlocking, the blocks are not sufficiently restrained to eliminate flutter. This phenomenon apparently allows water under the system resulting in liquefaction and failure of the protection system. Dycel blocks may be particularly vulnerable to flutter due to their relatively low height to surface area ratio. This geometric shape appears to be more susceptible to pressure differentials and random flow patterns exhibited by turbulent conditions. Another feature of the Dycel and Armorflex systems which adversely affected performance was the open joint at the crest/slope grade break. Apparently, the joints for these two systems contributed to liquefaction of the embankment by allowing water under the systems.

The Armorflex mattresses were more resistant to uplift forces and failed only under a 4-ft (1.2 m) overtopping depth. The maximum negative pressure calculated for this condition was -40 lb/ft² (-1.9 kN/m²). Overtopping depths of 1- and 2-ft (0.30 and 0.61 m), tests for which the system was stable, resulted in maximum negative pressures of -12 and -18 lb/ft² (-0.57 and -0.86 kN/m²), respectively. Greater unit weight and favorable geometric characteristics both contributed to increased stability. Armorflex blocks had a relatively high depth to surface area ratio which apparently tended to reduce flutter. Geometric conditions and weight were the factors which significantly improved stability, but were unable to safely protect the embankment under severe flow conditions.

The Petraflex-Vick system was stable for all test conditions, which included maximum calculated negative pressures up to -42 lb/ft^2 (-2.0 kN/m). Relatively high unit weight, both lateral and longitudinal cables, and the three-dimensional interlocking characteristic of the blocks all contributed to the stability of this system. The lateral and longitudinal cables, along with the vertical interlocking feature, minimized flutter and caused the system to behave as a continuous mattress rather than as individual blocks. This was important in preventing significant ingress of water under the system. The result was insufficient water to saturate the embankment to the extent required to cause liquefaction and resulted in stability of the system up to the maximum flow capacity of the testing facility.

COMPARISON OF CURRENT TEST PROGRAM RESULTS TO OTHER INVESTIGATIONS

1. General

The current test program described in the previous sections of this report is the second of two studies performed under contract to the FHWA. Several other embankment stability test programs have been conducted by various agencies, notably CIRIA in the United Kingdom, the USBR, and the FHWA. (34,89,2)

The CIRIA test program focused on grass as both primary and supplemental protection for steep slope channels. (34,38) See tables 5 and 10 for a summary of the CIRIA test program. The program investigated full-scale channels protected with enkamat filled with topsoil and seeded with grass, enkamat with asphalt fill seeded with grass, concrete block revetment systems with voids and interstices filled with topsoil and seeded with grass, and other geotextile-reinforced grass systems. A plain grass channel was also tested as a "control" against which the performance of the other systems was compared. All tests were conducted on a 33 ft (10 m) high embankment on a 2.5H:1V slope. CIRIA tests did not include overtopping conditions; water was released directly onto the protected embankment slope rather than being allowed to flow across the crest and down the embankment. Without overtopping, test conditions are less severe due to the lack of the subatmospheric pressure zone which is established when overtopping conditions exist. Furthermore, erosion of the crest upstream of protection systems is not investigated when true overtopping conditions are not imposed.

The USBR test program was not as comprehensive as the other programs and focused on bare soil embankments along with riprap and gabion embankment protection systems. Tests were conducted in a laboratory-scale flume on either 6H:1V or 4H:1V slopes and included overtopping conditions. Although the embankments were not as steep as in some field applications, testing of the overtopping condition was significant in determining the protection provided by these systems. Results of the USBR test program are summarized in table 6.

The first FHWA test program investigated embankments protected with grass only, soil cement, gabions, geoweb, bare enkammat, and enkammat filled with topsoil and seeded with grass.⁽²⁾ Tests were conducted on a 6 ft (1.8 m) high embankment, at slopes ranging from 4H:1V to 2H:1V, constructed in a 3 ft (0.91 m) wide flume. Overtopping conditions were imposed by ponding water behind the embankment to establish various overtopping depths on the crest of the embankment.

The current study performed for the FHWA was conducted under conditions similar to the first FHWA test program. Tests were completed in a 4 ft (1.2 m) wide flume on a 6 ft (1.8 m) high embankment constructed at 4H:1V to 2H:1V slopes. The protection measures investigated were soil cement, gabions, geoweb, bare enkammat, enkammat filled and covered with asphalt, and several concrete block revetment systems. This section provides a comparison of the performance of similar protection systems in each test program.

2. Nonreinforced Grass Protection

Grass-lined channels, without artificial reinforcement, were not investigated in the current study but were tested by CIRIA and the FHWA phase I program.^(34,2)

The grass-lined channels constructed for the CIRIA test program exhibited uniform vegetative coverage and a well-developed root system. The grass was established and maintained for approximately 18 months prior to testing. Local damage was observed at flow velocities of 9.2 ft/s (2.8 m/s). Damage was limited to the removal of individual grass plants and the subsequent development of small scour holes. Failure of the grass lining occurred at flow velocities of 12.1 ft/s (3.7 m/s). This was characterized by the loss of significant numbers of grass plants, erosion of large scour holes, uplift and bulging due to the ingress of water under the root mat, and stripping of relatively large sections of turf from the subsoil.

The FHWA phase I nonreinforced grass embankment tests were conducted on a 3H:1V slope with overtopping depths varying from 0.5 to 4 ft (0.15 to 1.2

m) and velocities ranging up to 14 ft/s (4.3 m/s). The grass for this program was not as well-developed as for the CIRIA tests. Uniform coverage was not achieved and the root system was not fully established. Performance of the grass covering was satisfactory for low-flow velocities and overtopping depths [0.5 ft (0.15 m)]. Loss of grass plants, local scour, and severe toe erosion was observed for more severe hydraulic conditions [overtopping depths of 2 and 4 ft (0.61 and 1.2 m)].

The FHWA phase I grass embankment protection did not show the degree of stability exhibited by the CIRIA grass-lined channels. This was probably primarily due to the relative level of establishment of the root systems. The underdeveloped vegetation in the FHWA phase I program gave protection for low flows only, while mid-range flows did not cause significant damage to the fully established CIRIA system. The CIRIA results were probably not significantly biased by a lack of true overtopping conditions since the failure mechanism for this system was related to bed shear stress in the high velocity flow field, as opposed to uplift near the downstream shoulder.

3. Soil Cement Protection Systems

Soil cement was tested as an embankment protection system by the current test program (FHWA phase II) and the FHWA phase I study.

For the FHWA phase II program, soil cement was placed on the downstream embankment slope in horizontal lifts, resulting in a stair-stepped embankment surface. The soil cement mixture contained eight percent by weight Portland no. 2 cement. Downstream slopes were constructed at 3H:1V and 2H:1V slopes and subjected to 1- to 4-ft (0.30 to 1.2 m) overtopping depths with flow velocities up to 20 ft/s (6.1 m/s). The protection system was stable with no damage to the embankment for even the most severe hydraulic conditions.

The FHWA phase I test program also placed soil cement parallel to the embankment slope with a total thickness of 12 in (0.3 m). The embankment was constructed at a 2H:1V embankment slope. Tests were performed for 1- to 4-ft (0.30 to 1.2 m) overtopping depths with flow velocities ranging up to

19 ft/s (5.8 m/s) on the embankment slope. As was the case with the other programs, the embankment was stable and did not experience surface damage for any hydraulic condition.

The two test programs which considered soil cement as an embankment protection measure each found it an extremely effective system for providing protection against overtopping. Of particular interest was the determination that simulated cold joints between lifts (intended to reflect poor construction practices) did not affect the stability of this type of system. Performance of the systems was determined to also be unaffected by the orientation of soil cement placement as both the stair-step placement and placement parallel to the slope gave no indication of instability. However, practical considerations must be addressed when using soil cement. Placement orientation may be dictated by embankment geometry. Parallel placement requires less material than stair steps, but can be difficult to install on steep slopes.

4. Gabion Mattress Protection Systems

Performance of gabion mattresses was investigated by the current test program (FHWA phase II), the USBR, and phase I of the study for the FHWA.

FHWA phase II tests were conducted on 3H:1V and 2H:1V embankments for 2- and 4-ft (0.61 and 1.2 m) overtopping depths with velocities ranging up to 19 ft/s (5.8 m/s). The gabion mattresses were generally stable, but basket deformation occurred due to migration of the rockfill to the downstream end of each basket. This movement of the rockfill was also detrimental in that it exposed the underlying filter fabric which increased the potential for embankment erosion. Failure of the system did occur for an overtopping depth of 4 ft (1.2 m). The mode of failure was loss of anchorage at the crest due to erosion of the unprotected portion of the crest upstream of the gabions, which exposed the upstream face of the system to direct impact by the flow.

The USBR conducted a laboratory flume study of gabions on 6H:1V and 4H:1V embankment slopes. The scaled gabion mattresses represented a

prototype system with angular rock up to 12 in (30 cm) in diameter. The laboratory fill corresponded to material larger than the 3- to 6-in (8 to 15 cm) diameter rockfill used by the FHWA phase II program. However, results were similar to those for the current test program; the system was generally stable, but basket deformation was observed, caused by migration of the fill material within individual basket compartments.

Tests of gabion mattresses in the FHWA phase I program were conducted on embankment slopes of 3H:1V and 2H:1V. Overtopping depths varied from 1 to 4 ft (0.30 to 1.2 m) with a maximum flow velocity of 19 ft/s (5.8 m/s). Results concurred with those for the other test programs. Basket deformation occurred due to shifting of the rockfill, but the systems were otherwise stable. Embankment erosion was not observed, but the underlying filter fabric was exposed subsequent to migration of the fill material.

The three test programs gave similar results for gabion mattress systems. If adequate anchoring is provided, gabions will remain in place but the rockfill will migrate to the downstream end of the individual baskets resulting in basket deformation and exposure of the underlying filter fabric. This behavior was observed for all geometric and hydraulic conditions. The best available mitigation of this behavior is to tightly pack the baskets with angular stone to minimize void spaces, and to decrease inter-compartmental spacing by adding additional panel dividers.

5. Geoweb Protection Systems

Geoweb systems were tested by each of the two phases of the test program for the FHWA. The major difference between protection system configurations for the programs was the addition of Tenax netting over the geoweb for phase II.

The phase I study investigated stability of 8-in-thick (204 mm) geoweb on 3H:1V embankments under 1- and 2-ft (0.30 and 0.61 m) overtopping depths where flow velocities ranged up to 12 ft/s (3.7 m/s). The system performed poorly primarily due to the gravel-fill being eroded from individual cells

thereby subjecting the embankment to direct erosion. All test conditions resulted in failure of the system.

Geometric and hydraulic conditions were more severe for the phase II program. An embankment slope of 2H:1V was used along with 1- to 4-ft (0.30 to 1.2 m) overtopping depths with a maximum flow velocity of 14 ft/s (4.2 m/s). The phase II system included the installation of Tenax netting over 4-in-thick (102 mm) geoweb. The netting was wired to the top of the geoweb cells to halt the loss of gravel-fill from the cells. This configuration was successful in stopping the gravel from boiling out of the geoweb. The system was stable for a 1-ft (0.30 m) overtopping depth, but failed when subjected to 2- and 4-ft (0.61 and 1.2 m) depths. For the 2-ft (0.61 m) overtopping test, failure occurred when the unprotected portion of the crest eroded to a depth which allowed the geoweb to be pulled out of the anchor trench. For the 4-ft (1.2 m) overtopping test, the anchor trench was positioned nearer the upstream edge of the crest, and failure occurred due to stretching of the geoweb under the tractive force of the flow.

In general, geoweb can provide adequate embankment protection provided the material which fills the cells remains stable and shear stresses are less than 10 lbs/ft² (0.48 kN/m²). Phase II tests indicated stability for low flows, while phase I tests resulted in failure for all hydraulic conditions. The difference in performance was attributed to maintaining the gravel-fill within the geoweb cells. Loss of gravel-fill in the phase I program was averted in the phase II tests by covering the system with Tenax netting. Consequently, direct erosion of the embankment was avoided in the second phase. Failure due to loss of the crest anchor can be prevented by improved anchoring techniques and providing shear and pullout restraint throughout the system. Both testing programs indicated stretching of the material by flow-induced shear stress. This caused the system to separate from the flume walls which resulted in erosion occurring along the walls. Installing shear and pullout restraint along the edges of the individual geoweb panels may improve stability.

6. Enkamat Protection Systems

Bare enkamat was tested by both phase I and II of the FHWA study. In addition, FHWA (phase I) and CIRIA investigated enkamat which had been filled with topsoil and seeded with grass.

The FHWA (phase II) bare enkamat tests used an embankment slope of 2H:1V and overtopping depths of 0.5 to 2 ft (0.15 to 0.61 m). Failure occurred rapidly for all hydraulic conditions, including the 0.5-ft (0.15 m) overtopping test. The failure mechanism was bed shear stress which caused the fabric to stretch, thereby exposing the embankment soil along the flume walls. Erosion along the walls resulted in failure of the system. Also contributing to instability was the enkamat being ripped at staked restraint points which resulted in local turbulence and soil loss.

Bare enkamat tests for phase I used 3H:1V embankment slopes and 0.5- to 2-ft (0.15 to 0.61 m) overtopping depths with a maximum velocity of 16 ft/s (4.9 m/s). As with the phase II program, failure of all tests was the result of stretching or ripping of the material and excessive embankment erosion, including local scour near the shear restraint staples.

FHWA (phase I) tests of enkamat with grass used a 3H:1V embankment slope and 0.5- to 4-ft (0.15 to 1.2 m) overtopping depths which resulted in a maximum velocity of 15 ft/s (4.6 m/s). The system provided reasonable protection for overtopping depths up to 1 ft (0.30 m). Failure was observed for the 2- and 4-ft (0.61 and 1.2 m) overtopping depths. A large number of grass plants were quickly removed by the flow. Once this occurred, the system failed in the same manner as bare enkamat. Loss of vegetation was exacerbated by the relatively short growth period which resulted in an inadequate root system and nonuniform coverage of the enkamat.

The CIRIA test program investigated enkamat-with-grass channels on a 33 ft (10 m) high embankment at a 2.5H:1V slope for velocities up to 23 ft/s (7.0 m/s). The channels suffered limited erosion at velocities approaching 17 ft/s (5.2 m/s). Failure occurred after 1.5 hours of testing at 23 ft/s

(7.0 m/s) due to uplift and bulging caused by ingress of water under the system, which allowed the considerable kinetic energy of the flow to be converted to a stagnation pressure within the bulge.

The test programs concurred that bare (unvegetated) enkammat does not provide adequate embankment protection for even low-flow overtopping conditions, even when underlain by a geotextile. Bed shear stresses which develop on steep slopes are too great to be resisted by anchoring and shear restraint staking systems. However, performance was significantly improved when the enkammat was filled with topsoil and seeded with grass provided the grass was allowed to become sufficiently established. All test programs indicated stability for enkammat with grass protection for low flows with failure occurring under high-flow conditions. Performance for mid-range flows was not as clearly defined. The FHWA phase I program indicated instability, but this may have been the result of a poorly developed stand of grass. Conversely, CIRIA tests showed stability for mid-range flows when the root system was well developed.

7. Enkammat-with-Asphalt Protection Systems

This protection measure was tested in the FHWA phase II program by installing bare enkammat and filling and covering it with either 1 or 3 in (25 or 76 mm) of asphalt. Similar tests were conducted by CIRIA, but these involved factory-produced enkammat filled with bitumen-bound gravel chippings which was subsequently topsoiled and seeded.

The FHWA phase II study tested enkammat with asphalt on a 2H:1V embankment slope with 1- and 2-ft (0.30 and 0.61 m) overtopping depths which resulted in velocities ranging up to 16 ft/s (4.8 m/s). Failure of the system with 1 in (25 mm) of asphalt occurred for the 1-ft (0.30 m) overtopping depth and maximum velocity of 14 ft/s (4.2 m/s). The mode of failure was uplift at the shoulder which allowed water underneath the system. The enkammat with 3 in (76 mm) of asphalt was stable for the 2-ft (0.61 m) overtopping test with a maximum velocity of 16 ft/s (4.8 m/s). It is clear that in this case, the system's stability was enhanced due to the weight and

protective integrity of the asphalt, with the enkamat providing a physical reinforcing matrix.

The asphalt-filled enkamat used for the CIRIA study was lighter than the FHWA system and was not a completely solid material. The voids remaining in the enkamat were filled with topsoil and seeded with grass. The CIRIA system was tested at velocities ranging up to 21 ft/s (6.5 m/s). The asphalt-filled enkamat was stable at flow velocities of 13 ft/s (3.9 m/s), but failed at 18 ft/s (5.5 m/s). The mode of failure was uplift due to water under the system which forced the enkamat and root matrix to bulge and separate from the subsoil.

Direct comparison of the two systems is difficult due to differences in the physical make-up of the protection measures. The failure mechanism for the FHWA 1-in (25 mm) asphalt and CIRIA systems was similar, although during FHWA tests the failure occurred at less severe hydraulic conditions. The heavier enkamat with 3 in (76 mm) of asphalt system performed much like the lighter CIRIA system with a well developed stand of grass. These two systems provided reasonable protection for low- and mid-range flows, while the 1-in (25 mm) asphalt system was not stable for even minimal overtopping depths.

8. Concrete Block Protection Systems

Several concrete block systems were tested by both the current test program and the CIRIA program. Common to both studies was the investigation of Dycel, Armorflex, and Petraflex-Vick blocks. The major differences between the physical character of the installation and testing of these products during these studies was that the CIRIA investigations included a well established grass growth within the block matrix and did not establish a flow field which truly overtopped the embankment. Both of these conditions result in enhanced stability; therefore, the FHWA program is considered to have tested these products under more severe conditions for a given depth of flow.

a. Dycel Blocks

The FHWA phase II program tested Dycel 100 blocks on a 2H:1V embankment slope with an overtopping depth of 1 ft (0.30 m) and a maximum velocity of 13 ft/s (3.9 m/s). Failure was observed for this hydraulic condition due to liquefaction of the embankment soil with a resulting shallow-seated slip surface. Liquefaction occurred as the result of rapid saturation of the embankment soil following ingress of water under the system. Block flutter and uplift of the system in the subatmospheric pressure zone at the shoulder were apparently responsible for allowing water under the system.

The voids and interstices of the Dycel blocks tested by CIRIA were filled with topsoil and seeded with grass prior to testing, allowing a well-developed root system to form. The system was substantially more resilient than the FHWA system as it suffered only limited damage for flow velocities of up to 26 ft/s (8.0 m/s).

The FHWA Dycel system could not withstand low-flow overtopping conditions while the CIRIA system was stable for all hydraulic conditions tested, including relatively high flows. Establishment of a well developed grass root system significantly enhanced the Dycel system performance. However, system stability may have been overestimated since the CIRIA test program did not impose true overtopping conditions which cause uplift due to negative pressures. This phenomenon was instrumental in causing failure of the FHWA Dycel system.

b. Armorflex Blocks

The Armorflex class 30 protection system was tested on a 2H:1V embankment slope for phase II of the FHWA study. Hydraulic conditions included 1- to 4-ft (0.30 to 1.2 m) overtopping depths with flow velocities ranging up to 19 ft/s (5.8 m/s). The system exhibited stability for 1- and 2-ft (0.30 and 0.61 m) overtopping depths. Failure due to liquefaction of the embankment soil was observed for the 4-ft (1.2 m) overtopping case in a manner identical to the Dycel failures. Apparent uplift of the system due to

negative pressure at the shoulder and block flutter allowed water under the system. This resulted in saturation of the embankment soil and, ultimately, liquefaction of the embankment with failure by shallow slippage.

The CIRIA Armorflex system had the advantage of a well developed stand of grass established in the topsoil-filled block voids and interstices. The system proved to be stable for all hydraulic conditions tested, including flow velocities up to 26 ft/s (8.0 m/s). Minor damage occurred in the form of local loss of grass plants, which was limited and did not appear to adversely affect stability.

Both the FHWA and CIRIA test programs indicated the Armorflex system was stable for low- and mid-range flows. It appears that grass is not necessary to provide adequate protection for these conditions. However, the establishment of a well-developed grass root system is essential for stability at high flows. This became apparent when the nongrassed FHWA system failed under high-flow conditions while the grassed CIRIA system was stable. It should be noted that the CIRIA system was not subjected to true overtopping conditions and therefore was not subjected to uplift forces in the zone of negative pressure. Furthermore, the CIRIA tests were conducted on channels having a trapezoidal cross section whereby the protection systems could be anchored on the sideslopes above the water surface. This aspect of test geometry may have improved system stability when compared to the FHWA tests conducted in a straight-walled flume.

c. Petraflex-Vick Blocks

The FHWA phase II study tested Petraflex-Vick concrete blocks on a 2H:1V embankment slope for 1- to 4-ft (0.30 to 1.2 m) overtopping depths with flow velocities ranging up to 21 ft/s (6.4 m/s). The system was extremely sound and did not give any indication of instability during any of the tests. It is believed this behavior was due to the larger unit weight, the three-dimensional interlocking characteristic of the blocks, the presence of both lateral and longitudinal cables, and the use of two geotextile underlayers.

Grass was established in the topsoil-filled block voids and interstices of the CIRIA Petraflex block system. As with the Armorflex system, this protection measure was stable for all hydraulic conditions with only minor damage occurring due to local loss of individual grass plants.

Performance of both the FHWA and CIRIA Petraflex-Vick systems was outstanding with no instability indicated for any of the test conditions. Grass was not necessary for stability at flow velocities less than or equal to 21 ft/s (6.4 m/s). Although the nongrassed FHWA system was not tested at velocities greater than this, it did not fail during 28 hours of testing at maximum hydraulic conditions.

9. Summary and Conclusions

In general, results from the various test programs agreed reasonably well. Where differences in performance were noted, they could be accounted for by differences in the protection systems or hydraulic conditions, i.e., anchoring, overtopping versus steep slope flow conditions, and the presence or absence of grass cover.

The CIRIA tests generally indicated greater stability than other test programs. This was attributed to the establishment of well-developed stands of grass on all CIRIA protection measures and the lack of true overtopping conditions. To truly assess the benefit of incorporating grass into embankment protection measures, the systems should be tested with overtopping flow imposed as in the FHWA test program. However, it is apparent that grass significantly enhances the performance of embankment protection measures and results of testing with overtopping conditions may not differ substantially from those determined by CIRIA.

The results of FHWA's current study confirm the conclusion reached by the CIRIA investigators: "The effectiveness of all systems depends on establishing a composite construction with intimate contact between the component parts." Once intimate contact is lost, a system's ability to protect against erosion and uplift is significantly compromised. Therefore,

it is paramount when selecting, designing, and installing an embankment protection system that the design goal is to achieve uniform, intimate contact with the embankment subsoil. Furthermore, this contact must be maintained areally for the entire duration of the overtopping event.

For ease in comparing the limiting values of velocity and/or shear stress for the various protection measures discussed in this report, available data on limiting values have been summarized and are provided in table 23.

Table 23. Summary of critical velocity and shear stress for various protection measures.

Source	Protective Cover	Underlying Soil	V_c (ft/s)	T_c (lb/ft ²)	
ARS (see table 8)	Class A Vegetation	Erosion Resistant	6-8	3.7	
		Erodible	4-6	3.7	
	Class B Vegetation	Erosion Resistant	5-7	2.1	
		Erodible	3-5	2.1	
	Class C Vegetation	Erosion Resistant	4-5	1.0	
Erodible		3-4	1.0		
Class D Vegetation	Erosion Resistant	3.5	0.60		
	Erodible	2.5	0.60		
Class E Vegetation	Erosion Resistant	3.5	0.35		
	Erodible	2.5	0.35		
	FHWA phase I study (see table 11)	Woven Paper		N/A	0.15
		Jute Net		N/A	0.45
		Single Fiberglass		N/A	0.60
Double Fiberglass			N/A	0.85	
Straw w/Net			N/A	1.45	
Curled Wood Mat			N/A	1.55	
	Synthetic Mat		N/A	2.00	
CIRIA (see figure 9)	Plain Grass, Good Cover	Clay	7-15*	N/A	
	Plain Grass, Average Cover	Clay	5-12*	N/A	
	Plain Grass, Poor Cover	Clay	3-10*	N/A	
	Grass, Reinforced w/Nylon Mat	Clay	14-19*	N/A	
CIRIA (see table 14)	Dycel w/Grass	Clay	23-26	N/A	
	Petraflex w/Grass	Clay	>26	N/A	
	Armorflex w/Grass	Clay	23-26	N/A	
	Dymex w/Grass	Clay	15	N/A	
	Grasscrete	Clay	26	N/A	
FHWA phase II study (see table 20)	Dycel w/o Grass	Type I	<7.3	<7.0	
	Petraflex w/o Grass	Type I	>17	>32	
	Armorflex w/o Grass	Type I	12-15	12-20	
	Enkamet w/3 in Asphalt	Type I	13	13-16	
	Enkamet w/1 in Asphalt	Type I	<8.6	<5	
FHWA phase I study (see table 15)	Gravel				
		D ₅₀ = 1 in	N/A	0.40	
	D ₅₀ = 2 in	N/A	0.80		
	Rock				
D ₅₀ = 6 in		N/A	2.50		
D ₅₀ = 12 in	N/A	5.00			
FHWA phase II study (see table 19)	6 in Gabions	Type I	17	35	
	4 in Geoweb	Type I	9-10	10	
	Soil Cement	Type I	>16.0	>45	
	(8% Cement)				

*Critical velocity is dependent on test duration (see figure 9).

$$\text{ft/s} \times 0.3048 = \text{m/s}$$

$$\text{lb/ft}^2 \times 47.87 = \text{N/m}^2$$

DESIGN AND INSTALLATION CONSIDERATIONS

This section presents information on the design and installation of protection systems for minimizing embankment damage due to overtopping flow. Implicit throughout the following discussion is the recognition that the ultimate goal of any protection system is to maintain direct, intimate contact with the embankment subsoil under the design hydraulic conditions. Loss of contact at any point in the system may lead to rapid exploitation by destabilizing hydraulic forces, causing local scour or uplift which may then propagate through the system.

1. Hydraulic Considerations

- **Peak discharge:** The inflow design flood, or portion thereof, which is to pass the embankment must first be determined so that the peak discharge of the outflow hydrograph can be calculated. Reservoir storage and attenuation characteristics must be considered where appropriate.
- **Peak unit discharge:** In many cases, the designer may have considerable latitude in choosing the length of embankment which can be designated for overtopping. By increasing the length of the overtopping region from L_1 to L_2 , the unit discharge will decrease proportionately, and the overtopping head will be decreased by the ratio

$$\frac{H_2}{H_1} = \left(\frac{L_1}{L_2}\right)^{2/3} \quad (20)$$

Although the total area of embankment requiring protection will increase as a result of lengthening the overflow section, the decrease in overtopping head will decrease the velocity, shear stress, and uplift pressures such that a more cost-effective system might be selected.

- **Velocity and depth:** The maximum, or terminal, flow velocity will be attained on the embankment slope downstream of the zone of acceleration,

where uniform supercritical flow exists. The velocity in this zone can be computed using Manning's equation:

$$v = \frac{1.49}{n} d^{2/3} S_0^{1/2} \quad (\text{English units}) \quad (21)$$

where v = velocity (ft/s)
 n = Manning's roughness coefficient
 d = uniform depth of flow (ft)
 S_0 = embankment slope (dimensionless)

Recommended values of the Manning's roughness coefficient for overtopping conditions are listed in table 24 for various protection systems. When both depth and velocity are unknown, a Manning's n should be chosen and an iterative solution technique adopted based on the continuity principle:

$$q = V \cdot d \quad (22)$$

where q = discharge per unit width, and
the other terms as previously defined.

- **Bed shear stress:** The bed shear stress τ_0 should be computed using both the maximum velocity and the maximum depth computed for uniform flow, from the representative range of Manning's n values reported in table 23.

Based on the maximum depth of flow, the computed shear stress is given by

$$\tau_0 = \gamma d_m S_0 \quad (23)$$

where γ = unit weight of water
 d_m = maximum depth at uniform flow
 S_0 = embankment slope

Using the maximum velocity method, the shear stress is computed by

$$\tau_0 = \frac{1}{8} f \rho V_m^2 \quad (24)$$

Table 24. Recommended values of the Manning's roughness coefficient for various protection systems during overtopping flow.

Protection System	Manning's n Values	
	Unvegetated(2) (*)	Vegetated(34)
<u>Soil Cement</u>		
a. Parallel to Slope	0.017 - 0.035	N/A
b. Stair-Step 2H:1V	0.085 - 0.100	N/A
3H:1V	0.050 - 0.065	N/A
<u>Gabions</u>		
a. Parallel to Slope	0.050 - 0.090	N/A
b. Stair-Step	0.085 - 0.115	N/A
<u>Geoweb</u>		
a. Parallel to Slope	0.050 - 0.090	Not Available
<u>Asphalt</u>		
a. Parallel to Slope	0.030 - 0.090	N/A
<u>Concrete Blocks</u>		
a. Parallel to Slope	0.035 - 0.080	0.025 - 0.045
<u>Geotextile (meshes and mats)</u>		
a. Parallel to Slope	N/A	0.018 - 0.030 (or use SCS retardance curves)

N/A = Not Applicable (not recommended)

*Use lower value to compute maximum velocity at uniform flow.

**Use higher value to compute maximum depth at uniform flow.

Note: Values in this table subject to change with additional research.

where f = Darcy friction factor
 ρ = unit mass of water
 V_m = maximum velocity at uniform flow

Representative values of the Darcy friction factor f are given in table 25. Values of bed shear derived from each of the above equations should be compared, and the larger of the two adopted for design calculations. Based on results of the current study, limiting values of shear stress for each of the protection systems investigated for the FHWA are reported on table 26. It is emphasized that the values reported in this table are derived from the installation and testing conditions as described in previous sections of this report. Values of maximum permissible shear stress may be increased where vegetation is well and reliably established, or where enhanced shear and pullout restraint is provided beyond that utilized in the current study. Additionally, it is emphasized that several of the protection systems exhibited failure mechanisms which were not primarily associated with tractive forces, e.g., asphalt and concrete block systems. Therefore, the values in this table represent the observed shear stress at the time of failure and do not necessarily imply that shear stress alone was the causative factor leading to failure.

- **Hydraulic uplift:** As detailed in earlier sections of this report, subatmospheric pressure near the downstream shoulder can result in uplift pressures which can lead to separation of the protection system from the embankment subsoil, allowing the destructive ingress of water beneath the system.

With a relatively impermeable embankment, the maximum uplift head is due to subatmospheric pressure and for a horizontal crest is calculated as

$$P_{\max} = \frac{V_0^2}{2gZ^2} \quad (25)$$

where P_{\max} = maximum uplift head normal to embankment slope in ft of water (meters of water) due to subatmospheric pressure
 V_0 = velocity at crest/slope transition in ft/s (m/s)

Table 25. Recommended values of the Darcy friction factor f for various protection systems during overtopping flow.

Protection System	Darcy friction factor f	
	Unvegetated(2)	Vegetated
a. Parallel to slope	0.40	N/A
b. Stair-step 2H:1V	1.00	N/A
3H:1V	0.50	N/A
<u>Gabions</u>		
a. Parallel to slope	0.85	N/A
b. Stair-step	1.30	N/A
<u>Geoweb</u>		
a. Parallel to slope	0.75	Not Available
<u>Asphalt</u>		
a. Parallel to slope	0.45	N/A
<u>Concrete Blocks</u>		
a. Parallel to slope	0.55	See Note 1
<u>Geotextile (meshes and mats)</u>		
a. Parallel to slope	N/A	See Note 1

N/A = Not Applicable (not recommended)

Notes: 1. Convert Manning's n using $f = 116 \frac{n^2}{d^{1/3}}$ (English units)

2. Values in this table subject to change with additional research.

Table 26. Limiting values of shear stress observed for the FHWA embankment testing program for various protection systems.

Protection System	<u>Limiting value of shear stress</u> lbs/sq ft
Soil cement (8 percent)*	>45
Gabions (6-in thick)	35
Geoweb (4-in thick)	10
Enkamat with 1-in asphalt	< 5
Enkamat with 3-in asphalt	15
Armorflex class 30 blocks	15
Petraflex-Vick blocks*	>30
Dycel 100 blocks	< 7

*Maximum capacity of testing facility was reached with no indication of failure.

g = acceleration due to gravity in ft/s^2 (m/s^2)
 Z = dimensionless embankment slope ZH:1V

Because the zone of subatmospheric pressure is relatively limited in size (typically confined to the first 5 to 10 ft (2 to 3 m) downstream of the shoulder) providing a short chamfer or rounding the downstream shoulder can reduce this component considerably. However, when the embankment is relatively permeable such that the full reservoir head could be transmitted through seepage, for example, through a gravel base course beneath a roadway, then the calculation of total uplift head P_{tot} should include both seepage and subatmospheric terms. This can be estimated as

$$P_{\text{tot}} = (1/3) H_0 + P_{\text{max}} \quad (26)$$

where P_{tot} = total uplift head normal to embankment slope in ft of water (meters of water)

H_0 = total overtopping head in ft (m)

P_{max} = maximum uplift due to subatmospheric pressure in ft (m)

Multiplying the uplift head by the unit weight of water yields the uplift pressure. The unit weight of the system in the region of the downstream shoulder should exceed this value. When grass can be relied upon to provide uniform root penetration into the underlying subsoil, pullout resistance of approximately 40 lb/ft^2 (2 kN/m^2) can be assigned to the vegetative component, based on studies performed by CIRIA.⁽³⁴⁾ Additionally, mechanical anchorage can be provided by helical or duck-bill soil anchors; however, care must be taken to ensure that the system between the anchor points is restrained in the vertical dimension. In the case of concrete blocks, this implies that a stack-bonded mechanical interlock is necessary to prevent movement of individual blocks in the vertical dimension when system weight is less than the total uplift pressure.

- Tailwater:** Downstream channel conditions will determine the presence or absence of a hydraulic jump on the embankment slope. When tailwater is present such that submergence of the crest occurs, the calculated discharge must be decreased by the submergence correction factor, and a

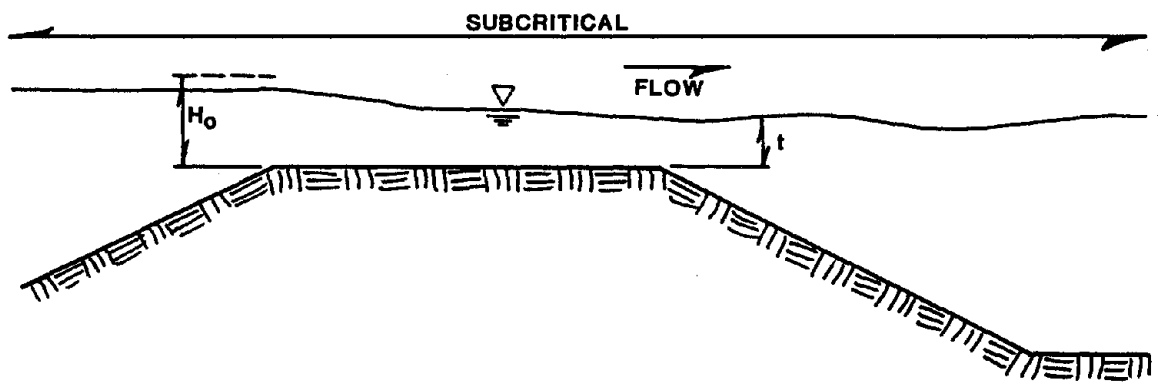
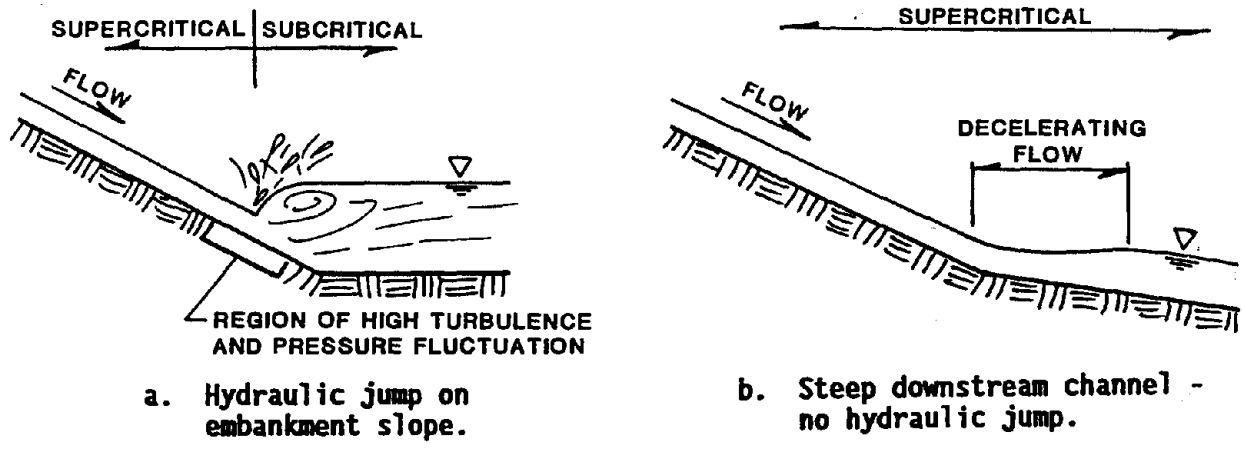
hydraulic jump will not form since critical depth is not achieved. A tailwater rating curve for the downstream channel must be determined so that jump or submergence characteristics can be calculated.

It is usually desirable to stabilize the position of the jump by means of a hydraulic control and to contain the jump within a stilling basin. For structures designed to overtop on a relatively frequent basis, this approach is recommended. However, for structures where overtopping protection is provided for extremely rare occurrences, it may be more cost effective to toe the protection system into the foundation and allow local scour to occur downstream from the toe of the embankment, provided slope stability is not compromised.

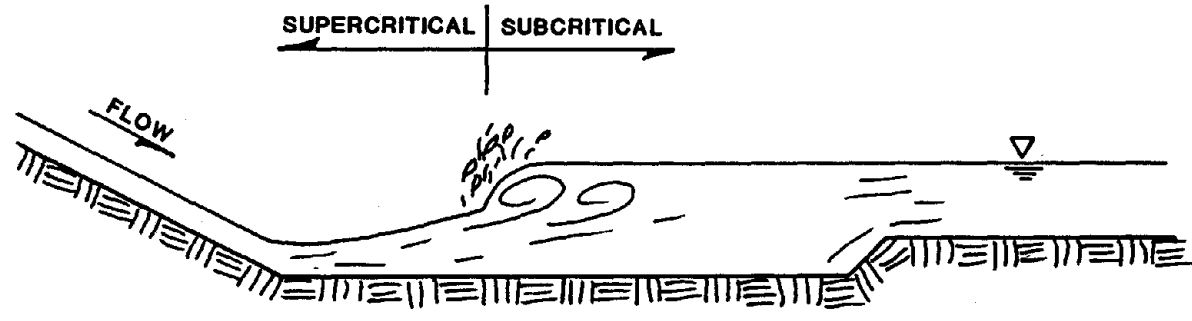
When tailwater conditions dictate that the hydraulic jump will occur on the embankment slope, it is advisable to provide heavier protection and/or anchorage in the critical zone where the front of the jump intersects the slope. This is because the turbulent energy dissipation occurring at the front of the hydraulic jump gives rise to a strongly two-dimensional flow pattern causing increased turbulence and dynamic pressure fluctuations in this zone. Typical tailwater and hydraulic jump conditions are shown in figure 69.

2. Installation Considerations

- **General**: Protection systems must be installed so that an even, uniform distribution of overtopping flow is achieved. Local concentrations of flow must be avoided, as well as areas of increased turbulence (trees, power poles) or changes in momentum (slope discontinuities, bends). Particular attention must be paid to termination details of the crest, toe, and sides of the protection system. Areas which are vulnerable to destructive ingress of water include the crest termination, open joints at slope transition points, and joints at seams or panel edges. Drainage at the toe of the protection system must also be provided so that saturated embankment soils or filter bedding can be relieved of hydrostatic pressure shortly after flow over the waterway ceases.



c. Submergence, $t/H_0 > 0.75$
no hydraulic jump



d. Hydraulic jump contained in stilling basin downstream of embankment slope.

Figure 69. Typical tailwater conditions.

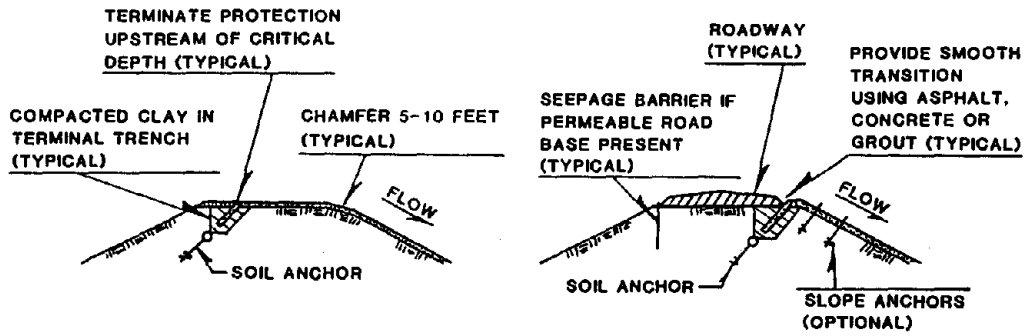
Systems should be installed far enough upstream so as to allow termination in the zone of subcritical flow. Where the crest of the embankment is to be used as a roadway, this may be impractical. In this case, the protection system should be terminated beneath the road surface and a seepage barrier installed on the upstream shoulder to prevent seepage through the base course.

- **Crest details:** The upstream end of the protection system must be designed to provide two important functions:
 1. To preclude ingress of water. Water can enter beneath the system through excessive seepage or through open joints at the crest termination.
 2. To provide continuous anchorage for resisting tractive forces arising from shear stress on the downstream portion of the protection system.

In addition, the region of the crest near the downstream shoulder must be protected from destabilization due to uplift forces. This becomes increasingly important for embankment slopes steeper than 3H:1V.

Typical crest details are provided in figure 70 which illustrate various ways of accomplishing the required performance on this portion of the embankment.

- **Side Details:** The flow which overtops an embankment must be confined to the protected portion by providing a sunken invert, side berms, or both. Total depth of the constructed waterway should equal the maximum expected depth of flow plus freeboard allowance, which may include calculation of superelevation and height of standing waves where a curvature in planform cannot be avoided. The protection system should be carried up the full height of the waterway sides and anchored in a terminal trench or by liberal use of soil anchors and shear pins, as shown in figure 71.

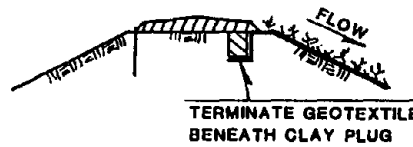


a. Cabled block crest detail (no roadway).

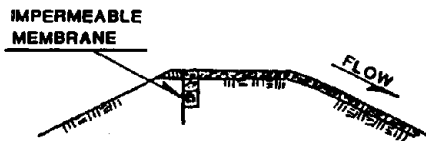
b. Cabled block crest detail (roadway present).



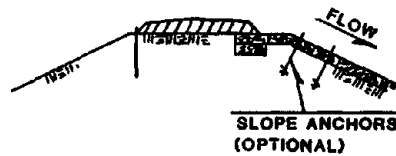
c. Vegetated geotextile mat (no roadway).



d. Vegetated geotextile mat (roadway present).

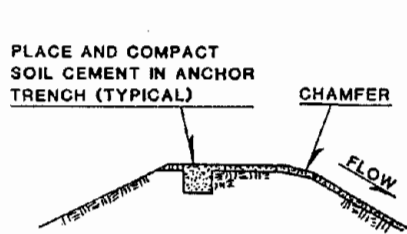


e. Gabions (no roadway).

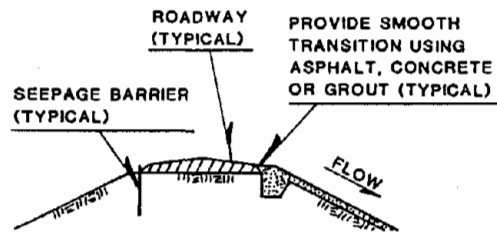


f. Gabions (roadway present).

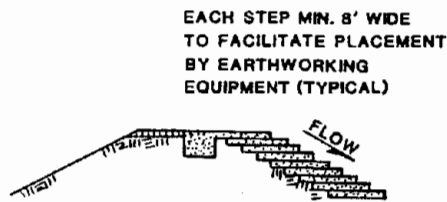
Figure 70. Typical crest details for selected protection systems.



g. Soil cement parallel to slope (no roadway).



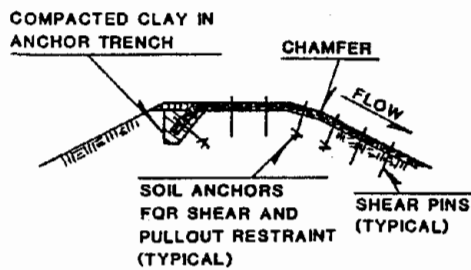
h. Soil cement parallel to slope (roadway present).



i. Stair-stepped soil cement (no roadway).



j. Stair-stepped soil cement (roadway present).



k. Geoweb (no roadway).



l. Geoweb (roadway present).

Continued

Figure 70. Typical crest details for selected protection systems. (continued).

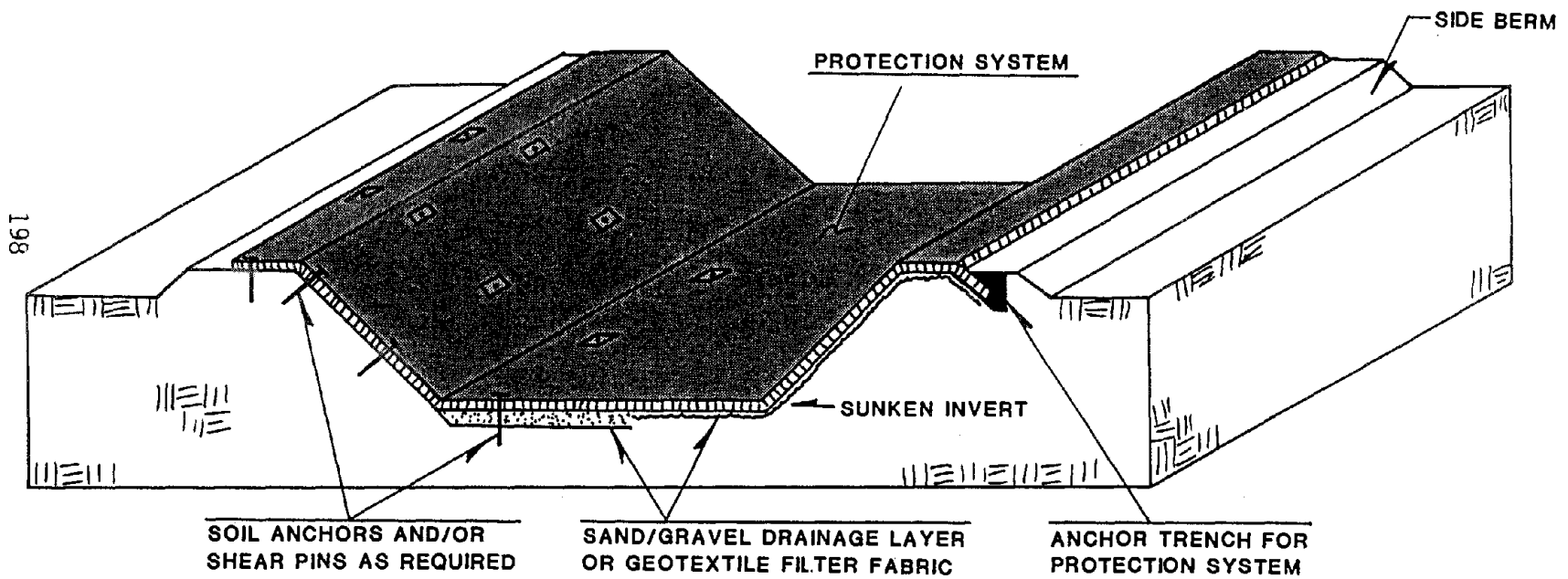


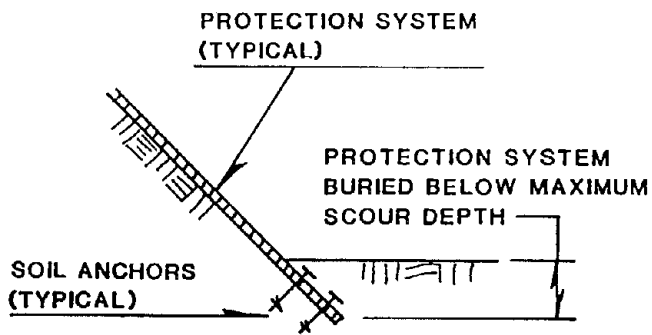
Figure 71. Typical cross section through protected waterway showing side termination options.

When the overtopping zone must intersect abutment groin areas, heavier protection should be considered due to flow concentration and deflection in these zones. Expansions or contractions of the width of the waterway should be avoided due to unfavorable hydraulic conditions and the difficulty in constructing the complex geometries of warped transition sections using many of the standard protection systems.

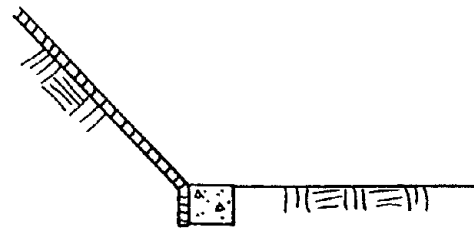
- **Toe Details:** Termination of the protection system at the toe of the embankment slope is important to prevent undermining and progressive headcutting. When overtopping is expected to occur only during an extremely rare event, some scour at the toe may be acceptable provided the protection system is entrenched below the maximum depth of local scour and that geotechnical slope stability is not compromised by the scour hole. For fairly frequent operation of the waterway, it is advisable to carry the protection system downstream of the toe a safe distance, or terminate the protection system by providing a stilling basin to force a stable hydraulic jump. Selection of the toe termination method will depend to a large degree on the nature of the tailwater condition at the design flow. Figure 72 illustrates some typical toe termination methods.
- **Well-Grassed Conditions:** For installations where a dense, well-maintained grass stand will provide an integral part of the protection system, considerable shear restraint and uplift resistance can be relied upon to enhance system stability. Detailed design considerations using well established vegetation are beyond the scope of this report; however, excellent design and installation guidelines for these systems can be found in the CIRIA Report No. 116, "Design of Reinforced Grass Waterways."⁽³⁴⁾ The reader is encouraged to consult this report when considering a vegetative-based protection system.

3. Cost Considerations

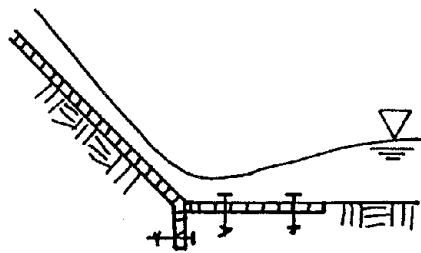
The in-place costs for various protection systems will vary from project to project, depending on site-specific characteristics. Availability of



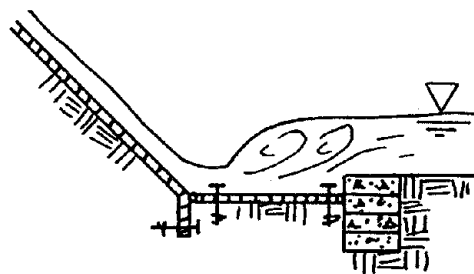
a. Burial below depth of scour.



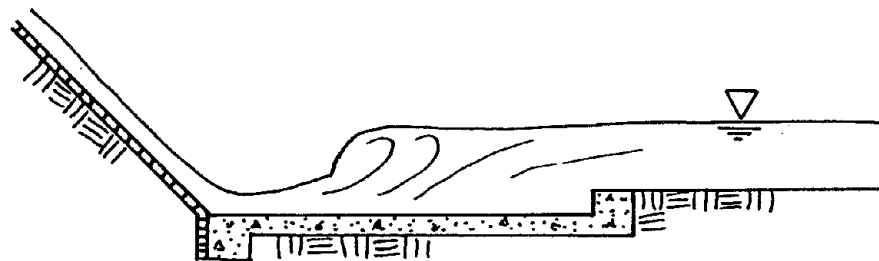
b. Termination behind concrete or gabion block.



c. Extended downstream protection.



d. Extended downstream protection with gabion berm.



e. Provision of concrete stilling basin.

Figure 72. Examples of typical toe termination details.

local materials will play a large part in determining the cost effectiveness of many of the protection systems investigated in this study. For example, if a local source of appropriately sized durable rock required for gabion fill is not available, costs will be directly affected by the haul distance involved. Similarly, soil cement suitability requires that the gradation characteristics of the soil aggregate fall within a specified range of percentages for the various grain-size categories, which sometimes dictates that blending materials from several sources is required. Access considerations are important when large construction equipment is required for system placement.

As part of this study, various manufacturers, distributors, and designers were polled to determine a representative range of in-place costs for selected protection systems. Table 27 presents the results of this poll, with most cost values based on actual bid documents for large-scale field projects where site conditions were favorable for the particular system being polled. The information presented in table 27 was obtained during the fall of 1986, and is considered representative, in that a reasonable range of costs was obtained for various placement techniques. However, this information should be considered only for general comparison purposes and should not be used for cost estimation. Designers are encouraged to contact manufacturers directly for assistance in estimating costs for a particular project.

Table 27. Representative costs of various protection systems.

Protection System	Condition	Installed cost ranges
		(\$/ft ²)
Soil cement	8-ft wide stair-step configuration	
	3H:1V	1.40 - 3.00
	1H:1V	3.00 - 6.00
Gabions	9-in thick reasonable haul	2.75 - 3.00
Geoweb	4-in thick, concrete filled	2.50 - 2.75
	4-in thick, rock filled	1.50 - 2.00
	8-in thick, rock filled	2.50 - 3.00
Enkamat	Soiled and seeded	0.75 - 1.15
Cable-tied Concrete blocks	Lighter weight systems Soiled and seeded	2.50 - 3.00
Roller-compacted concrete	8-ft wide stair-step configuration	
	3H:1V	1.85 - 4.60
	1H:1V	4.00 - 10.00

Note: Costs based on informal poll, fall 1986. Subject to vary considerably based on individual project site characteristics.

GLOSSARY OF TERMS

ANCHOR An object placed in the subsoil which is designed to provide restraint against separation of the protection system from the subgrade.

ASPHALT Bitumen-bound admixture consisting of tar, oil, and granular soil aggregate commonly used for the surface of roadways.

ANGLE OF REPOSE Angle of slope formed by noncohesive soil or rock at the critical equilibrium condition of incipient sliding.

AUXILIARY SPILLWAY A secondary spillway designed to operate only during exceptionally large floods.

COMPACTION A decrease in the volume of voids within a soil matrix, yielding an increase in density.

CREST The horizontal or near-horizontal top of an embankment.

CRITICAL DEPTH Depth of flow where the combined kinetic and potential energies are at a minimum. For this condition the ratio of inertial forces to gravitational forces is equal to unity.

DEPTH OF FLOW The distance from the channel bed to the water surface measured normal to the direction of flow.

DEPTH OF OVERTOPPING The head of water above an embankment crest as measured vertically from the crest to the water surface in the upstream pool.

DISCHARGE The volume of water passing a given cross section in a specified length of time, e.g. cubic feet per second.

DESIGN DISCHARGE The discharge at a specific location to be used for design purposes, usually associated with a specified return period or frequency of occurrence.

EMBANKMENT A raised mound of soil or rock typically used for elevating a roadway or impounding water. Embankments are generally characterized by a length dimension many times greater than either the height or width dimensions.

EROSION In the context of this report, the uncontrolled detachment and removal of soil from an embankment by the action of flowing water.

FABRIC A woven or nonwoven geotextile.

FAILURE In the context of this report, the loss of direct and intimate contact between protection system and subgrade whereby the retention of subgrade soils against the action of flowing water cannot be guaranteed.

FILTER BLANKET One or more layers of graded, permeable noncohesive soil material placed between the subsoil and the protection system to prevent soil loss by piping or washout while permitting drainage and pressure relief to occur.

FILTER FABRIC A permeable geotextile used between the subsoil and the protection system to achieve the same results as a filter blanket.

FREEBOARD Vertical distance from the water surface to the top of the protection system at the design discharge.

FREEFALL In the context of this report, the hydraulic condition which exists on the downstream embankment slope whereby supercritical flow reaches the toe of the embankment unconstrained by tailwater.

GABION Compartmented rectangular containers made of galvanized steel hexagonal mesh and filled with stone.

GEOTEXTILE A synthetic fabric specifically designed to be used as a construction material, typically in conjunction with soil placement and compaction in civil engineering applications. Primary purposes include filtration, separation, drainage, soil reinforcement, and erosion control.

HYDRAULIC JUMP Transition zone from supercritical to subcritical flow characterized by turbulent, non-uniform flow with associated head loss due to change from kinetic to potential energy.

HYDRAULIC LOADING The discharge-related parameters of flow which have a bearing on the potential failure of a protection system. These parameters include velocity, depth, duration, shear stress, pressure, and frequency of immersion.

HYDRAULIC RADIUS Cross-sectional area of flow divided by the wetted perimeter.

HYDRAULIC RESISTANCE A measure of channel roughness and form resistance encountered by flowing water, typically described by the Manning's n value.

HYDROSTATIC PRESSURE Pressure at a depth below the water surface for flow at constant, unidirectional velocity or at rest.

INCIPIENT MOTION The threshold of movement for a given particle of soil or rock under the action of flowing water.

LINING, FLEXIBLE Channel protection material or system which exhibits deformability such that adjustment to subgrade settlement can occur. Materials are typically porous in nature to allow infiltration and exfiltration to occur.

LINING, PERMANENT Lining designed for long-term use.

LINING, RIGID Lining material with no capacity to adjust to subgrade settlement. Typically constructed of nonporous material with a smooth finish that provides a large conveyance capacity (e.g., concrete, soil cement).

LINING, TEMPORARY Lining designed for short term utilization, typically to assist in the establishment of a permanent vegetative lining.

MAT A three-dimensional flexible geotextile typically greater than 10 mm thick.

MESH A two-dimensional geotextile made of two sets of parallel strands which intersect at a constant angle, typically 0.5 to 5 mm thick with an opening size greater than 2 mm.

NAPPE The shape of the underside of an aerated overfall jet of water, for example as occurring over a sharp-crested weir.

NORMAL DEPTH Depth of flow under uniform flow conditions. See UNIFORM FLOW.

OGEE A particular spillway surface geometry which approximates the shape of an aerated nappe at the design discharge.

PERMEABILITY Property of a soil or geotextile that enables water or air to move through it under an applied gradient.

PROTECTION SYSTEM In the context of this report, a channel lining designed to resist erosion by high velocity flows.

RETARDANCE CLASSIFICATION Qualitative description of the resistance to flow exhibited by various types of vegetation.

REVTMENT A facing of erosion-resistant material which protects the underlying material from erosion damage. This term is typically used to describe heavier, non-vegetated systems or products.

RIPRAP Broken rock, cobbles, or boulders placed on the sides and/or bottom of channels for erosion protection. Often used in conjunction with filter blankets or filter fabrics.

RIPRAP, GROUTED Riprap with all or part of the interstices filled with Portland cement mortar.

RIPRAP, WIRE-ENCLOSED See GABIONS.

ROLLER-COMPACTED CONCRETE (RCC) A no-slump mixture of sand, gravel, portland cement and water placed and compacted by standard earth-working equipment.

SHEAR STRESS Frictional force developed on the wetted area of the channel in the direction of flow; force per unit area.

SHEAR STRESS, PERMISSIBLE Maximum allowable shear stress for a given soil or protection system. Shear stresses exceeding this value invite system failure and erosion damage.

SIDESLOPE Slope of the channel sides, customarily reported as a ratio of the amount of run to the amount of rise, e.g., 3H:1V.

SOIL CEMENT A no-slump mixture of (native) soil and portland cement placed and compacted by standard earthworking equipment. Differs from RCC in that a higher percentage of fines (silts and clays) are present in the mix, resulting in less cement by weight and a correspondingly lower compressive strength.

SUBCRITICAL FLOW Tranquil flow characterized by a flow depth greater than critical depth.

SUBGRADE The soil which comprises the embankment underlying the channel, and which is to be protected from erosion by the protection system.

SUBMERGENCE The presence of tailwater above the embankment crest such that the unit discharge is decreased to a value less than that for freefall conditions.

SUPERCritical FLOW Rapid flow characterized by flow depths less than critical depth.

TAILWATER The elevation of the water surface in the channel downstream from the embankment toe.

TOE The intersection of the downstream embankment slope with the foundation or valley floor.

TRANSDUCER, PRESSURE An electronic instrument whose voltage output is directly related to the pressure at its sensing tip.

UNIFORM FLOW The condition of flow where the rate of energy loss due to frictional resistance is equal to the bed slope of the channel. Where uniform flow exists, the slopes of the energy line, the water surface, and the channel bed are identical.

VELOCITY, MEAN Discharge divided by the cross-sectional area of flow.

VELOCITY, LOCAL Velocity at a specific point within the flow region. May be defined as a direction-dependent vector quantity, e.g., V_x , V_y , V_z .

VELOCITY, PERMISSIBLE Maximum allowable mean velocity for a soil or protection system. Velocities exceeding this value invite system failure and erosion damage.

REFERENCES

1. C. E. Kindsvater, "Discharge Characteristics of Embankment-Shaped Weirs." Studies of Flow of Water Over Weirs and Dams, USGS Water-Supply Paper 1617-A, 1964.
2. Y. H. Chen and B. A. Anderson, Development of a Methodology for Estimating Embankment Damage Due to Flood Overtopping. Federal Highway Administration and Forest Service, Report No. FHWA/RD-86/126, Washington, D.C., 1986.
3. J. N. Bradley, Hydraulics of Bridge Waterways. Hydraulic Design Series No. 1, U. S. Department of Transportation, Federal Highway Administration, 1973.
4. C. T. Yang, "Unit Stream Power Equation for Gravel." Journal of Hydraulics Division, American Society of Civil Engineers, Vol. 110, No. 12, December 1984.
5. E. T. Smerdon and R. P. Beasley, "Relation of Compaction and Other Soil Properties to Erosion Resistance of Soils." Trans. American Society of Civil Engineers, Vol. 8, 1959.
6. E. T. Smerdon, and R. P. Beasley, "The Tractive Force Theory Applied to Stability of Open Channel in Cohesive Soils." Research Bulletin 715, University of Missouri, College of Agricultural, Agr. Exp. Station, October 1959.
7. J. C. McWhorter, T. G. Carpenter, and R. N. Clark, Erosion Control Criteria for Drainage Channels. Prepared for the Mississippi State Highway Department in cooperation with U. S. Department of Transportation, Federal Highway Administration, by Agricultural Experiment Station, Mississippi State University, State College, Mississippi, March 1968.
8. J. M. Wiggert and D. N. Contractor, "A Methodology for Estimating Embankment Failure." An unpublished paper presented to Water Resources Engineers, Inc., Springfield, VA, Department of Civil Engineering, Virginia Polytechnic Institute and State University, Blacksburg, VA 24060, no date, written around 1969.
9. E. A. Cristofano, "Method of Computing Erosion Rate for Failure of Earthfill Dams." Unpublished memorandum, Engineering and Research Center, Bureau of Reclamation, Department of the Interior, Denver, CO, April 1965.
10. R. Ariathurai and K. Arulanandan, "Erosion Rates of Cohesive Soils." Journal of Hydraulics Division, ASCE, Vol. 104, No. HY2, pp. 279-283, February 1978.

11. S. P. Chee, Design of Erodible Dams. In proceedings of International Conference of Water Resources Engineering, Asian Institute of Technology, Bangkok AIT, Vol. 1, pp. 105-113, 1978.
12. S. Fortier and F. C. Scobey, Permissible Canal Velocities. Trans. American Society of Civil Engineers, Vol. 89, pp. 940-956, 1926.
13. E. W. Lane, Design of Stable Channels. Trans. American Society of Civil Engineers, Vol. 120, pp. 1234-1260, 1955.
14. M. B. Cox, "Tests on Vegetated Waterways." Oklahoma Agricultural Experimental Station, Technical Bulletin T-15, 1942.
15. M. B. Cox and V. J. Palmer, "Results of Tests on Vegetated Waterways and Method of Field Applications." Oklahoma Agricultural Experiment Station, Misc. Pub. No. MP-12, pp 43, 1948.
16. W. O. Ree, "Hydraulic Characteristics of Vegetation for Vegetated Waterways." Agricultural Engineering, Vol. 30, pp. 184-187, 189, 1949.
17. W. O. Ree and V. J. Palmer, Flow of Water in Channels Protected by Vegetative Linings. U. S. Department of Agricultural Technical Bulletin 967, pp 115, 1949.
18. M. B. Cox, "Tests on Vegetated Waterways." Oklahoma Agricultural and Mechanical College Agricultural Experiment Station Technical Bulletin No. T-15, pp. 23, 1962.
19. W. I. Eastgate, "Vegetated Stabilization of Grassed Waterways and Dam Dywashes." M. Eng. Sc. Thesis, Department of Engineering, University of Queensland, St. Lucia, Queensland, Australia, 1966.
20. K. C. Yong, "Scour Resistance of Farm Spillways with Grass Dormant." University of New South Wales Research Laboratory, Report 104, 1968.
21. K. C. Yong and D. M. Stone, "Resistance of Low-Cost Surfaces for Farm Dam Spillways." University of New South Wales Water Research Laboratory, Report 95, 1968.
22. W. O. Ree, F. R. Crow, and W. W. Huffine, "Annual Grasses for Temporary Protection of Earth Spillways." Trans. American Society of Agricultural Engineers, Vol. 20(5), pp. 934-939, 1977.
23. N Kouwen and T. E. Unny, "Flow Retardance in Vegetated Channels." American Society of Civil Engineers, J. Irr. and Drainage Div. Vol. 95(IR2), pp. 329-342, 1969.
24. D. K. McCool, "Effect of Vegetal Length and Spatially Varied Flow on Velocity Distribution Coefficients." Trans. American Society of Agricultural Engineers, Vol. 13(5), pp 603-607, 1970.

25. G. T. Thompson and J. A. Robertson, "A Theory of Flow Resistance for Vegetated Channels." Trans. American Society of Agricultural Engineers, Vol. 19(2), pp. 288-293, 1976.
26. D. T. Y. Kao and B. J. Barfield, Predictions of Flow Hydraulics for Vegetated Channels. Trans. American Society of Agricultural Engineers, Vol. 21(3), pp 489-494, 1978.
27. N. Kouwen and R. M. Li, Biomechanics of Vegetative Channel Linings. American Society of Civil Engineers, J. Hydraulic Division Vol. 106(HY6), pp. 1085-1103, 1980.
28. N. Kouwen, R. M. Li, and D. B. Simons, "Flow Resistance in Vegetated Waterways." Trans. American Society of Agricultural Engineers, Vol. 24(3), pp. 684-690, 698, 1981.
29. D. M. Temple, "Flow Retardance of Submerged Grass Channel Linings." Trans. American Society of Agricultural Engineers, Vol. 25(5), pp. 1300-1303, 1982.
30. United States Department of Agriculture, Soil Conservation Service, Handbook of Channel Design for Soil and Water Conservation, SCS-TP-61, pp. 34, 1947 (revised 1954).
31. D. M. Temple, "Tractive Force Design of Vegetated Channels." Trans. American Society of Agricultural Engineers, Vol. 23(4), pp. 884-890, 1980.
32. D. M. Temple, "Design of Grass-lined Open Channels." Trans. American Society of Agricultural Engineers, Vol. 26(4), pp. 1064-1069, 1982.
33. D. M. Temple, R. M. Ahring, A. G. Davis, and K. M. Robinson, Handbook for Stability Design of Grass-Lined Open Channels, U.S. Department of Agriculture, Draft Copy., 1985.
34. H. W. M. Hewlett, L. A. Borman, M. E. Bramley, "Design of Reinforced Grass Waterways." Construction Industry Research and Information Association, Report 116, London, United Kingdom, 1987.
35. A. L. Cox, R. C. Adams, and T. B. Lawson, "Erosion-Control Study, Final Report Part II, Roadside Channels." Louisiana Department of Highways Research and Development Section in cooperation with U. S. Department of Transportation, Federal Highway Administration, 1971.
36. U. S. Geological Survey, "Performance of Temporary Ditch Linings." Prepared for the Federal Highway Administration at the U. S. Geological Survey Gulf Coast Hydrosience Center, Bay St. Louis, Mississippi, 1985.

37. Y. H. Chen and G. K. Cotton, "Design of Roadside Channels with Flexible Linings." Hydraulic Engineering Circular No. 15, Report No. FHWA-IP-86-5, Washington, D.C., Federal Highway Administration, 1986.
38. H. W. M. Hewlett, L. A. Boorman, M. W. Bramley, and E. Whitehead, "Reinforcement of Steep-Grassed Waterways." Construction Industry Research and Information Association, Technical Note 120, Storey's Gate, Westminster, London, SW1P 3AU, 1985.
39. G. L. Williams, "Performance Testing of Landglas-Fiberglass for Erosion Control." Owens Corning Fiberglass Technical Report TC/T&I/77-1, 1977.
40. North Dakota Department of Transportation, Erosion-Control Matting put to the Test. Public Works Journal 111(10), pp. 77-79, 1980.
41. G. L. Hoffman and R. Adamsky (Pennsylvania Department of Transportation), "Nylon Erosion-Control Mat." Transportation Research Board, Record No. 859, 1982.
42. C. S. Kemic, "Enkamat Matting." American Enka Company, Technical Information, Update IY 81-23, Enka, North Carolina, 1981.
43. D. W. White, "Evaluation of Membrane-Type Materials for Streambank Erosion Protection." U. S. Army Engineers Waterways Experiment Station Geotechnical Laboratory, Misc. Paper GL-84-4, 1981.
44. G. M. McNitt, "The Use of Three-Dimensional Nylon Mat for Erosion Control on the Angeles National Forest." U. S. Forest Service, 1982.
45. Arkansas State Highway and Transportation Department, "Product Evaluation, Enkamat Erosion-Control Fabric." Materials and Research Division, Research Section, 1983.
46. Missouri Highway and Transportation Department, "Investigation of Erosion-Control Materials for Ditches in Highway Corridors in Missouri." Study Number 81-3, Division of Materials and Research, 1983.
47. Burgess L. Kay, "Mulch and Chemical Stabilizers for Land Reclamation in Dry Regions." Chapter 26 of Reclamation of Drastically Disturbed Lands. ASA-CSSA-SSSA, Madison, Wisconsin, 1978a.
48. Burgess L. Kay, "Mulches for Erosion Control and Plant Establishments on Disturbed Sites." Agricultural Experiment Station, University of California, Davis, Agronomy Progress Report No. 87, 1978b.
49. L. J. Goodman, "Effectiveness of Various Soil Additives for Erosion Control." Highway Research Board Bulletin No. 69, 1952.

50. D. Gabriels and M. DeBoodt, "Erosion Reduction Factors for Chemically Treated Soils: Laboratory Experiment." Soil Science Society of America, Soil Conditioners, pp. 95-102. SSSA Special Publication No. 7, Madison, Wisconsin, 1975.
51. H. A. Sultan and H. Liu, "Rainfall Erosion Control of Compacted Soils Using Chemical Stabilizers." Arizona Conference on Roads and Streets Proc. (22nd) pp. 169-181, 1973.
52. H. A. Sultan, "Soil Erosion and Dust Control on Arizona Highways: Part II, Laboratory Testing Program." Arizona Department of Transportation, ADOT-RS-10-141-II, 1974a.
53. H. A. Sultan, "Soil Erosion and Dust Control on Arizona Highways: Part III, Progress Report - Field Testing Program." Arizona Department of Transportation, ADOT-RS-10-141-III, 1974b.
54. H. A. Sultan, "Soil Erosion and Dust Control on Arizona Highways: Part IV, Final Report - Field Testing Program." Arizona Department of Transportation, ADOT-RS-10-141-IV, 1976a.
55. H. A. Sultan, "Chemical Stabilization for Control of Dust and Traffic Erosion." Transportation Research Board, Record No. 593, pp. 34-40, Washington, D. C., 1976b.
56. R. A. Forsyth, "Use of Waste Materials and Soil Stabilization." Transportation Research Board, Record No. 593, Washington, D. C., 1976.
57. Morrison, W. R. and L. R. Simmons, "Chemical and Vegetative Stabilization of Soils." Engineering and Research Center, Bureau of Reclamation, REC-ERC-76-13, 1977.
58. Department of the Interior, Bureau of Reclamation, "Mix Design Investigation of Asphaltic Concrete for Dam Facing - Glen Elder Dam Missouri River Basin Project." Kansas, Report No. CHE-42, 1965.
59. G. DeGroot, "Bonding Study on Layered Soil Cement." Bureau of Reclamation, Engineering and Research Center, Report No. REC-ERC-76-16, 1976.
60. P. J. Nussbaum and B. E. Colley, "Dam Construction and Facing with Soil Cement." Portland Cement Assoc. R&D Lab. Bulletin, No. Rd010.01W, 1971.
61. F. J. Davis, E. W. Gray, and C. W. Jones, "The Use of Soil Cement for Slope Protection." International Commission on Large Dams, de Wagram 22 et 30 75008, Paris, France, 1973.
62. H. H. Duval and J. H. Alexander, "Procedure for Economic Development of Soil-Cement Mix Design (abridgement)." Transportation Research Board, Record No. 501, pp. 28-34, 1974.

63. W. G. Holtz and K. D. Hansen, "The Use of Compacted Soil Cement in Water-Control Structures." Portland Cement Association by Woodward-Clyde Consultants, Report No. RP228.01W, 1976.
64. Portland Cement Association, "Soil Cement for Water Control: Laboratory Tests." Report No. 15166.012W, Skokie, Illinois, 1976.
65. Portland Cement Association, "Suggested Specification for Soil-Cement Slope Protection for Embankments." Report No. 15052.03W, Skokie, Illinois, 1976.
66. L. L. Litton and R. A. Lohnes, "Soil Cement for Use in Stream Channel Grade-Stabilization Structures." Transportation Research Board, Record No. 839, pp. 33-38, 1982.
67. L. L. Litton and R. A. Lohnes, "Attrition Rates of Soil Cement Subjected to Water Jets." Transportation Research Board, Record No. 941, pp. 18-23, 1982.
68. M. R. Akky, "The Erodibility of Cement Stabilized Soil." Ph.D. Dissertation, University of California at Davis, Davis California, 1974.
69. K. L. Saucier, "Roller-Compacted Concrete for Use in Mass Concrete Construction." U.S. Army Corps of Engineers, Waterways Experiment Station, Technical Report SL-84-17, Vicksburg, Mississippi, 1984.
70. S. Diamond, "Soil Stabilization for Erosion Control." Purdue and Indiana State Highway Commission JHRP, Purdue University, West Lafayette, Indiana, 1975.
71. Kawamura, Mitsunore, Diamond, and Signey, "Stabilization of Clay Soils Hydrology in the Small Computer Age, Vol. 2, Proceedings of Hydraulics Division Speciality Conference, American Society of Civil Engineers, 1985.
72. G. Machan, Stabilization of Soils for Erosion Control on Construction Sites. JHRP-75-4, 1975.
73. G. Machan, S. Diamond, and E. Leo, "Laboratory Study of the Effectiveness of Cement and of Lime Stabilization for Erosion Control." Transportation Research Board, Record No. 641, 1977.
74. J. L. Perry, "Lime Treatment of Dams Constructed with Dispersive Clay Soils." Transactions of the American Society of Agricultural Engineers, pp. 1093-1099, 1977.
75. T. N. McDaniel and R. S. Decker, "Dispersive Soil Problem at Los Esteros Dam." American Society of Civil Engineers, Journal of Geotechnical Engineering Div. 105(GT9), 1979.

76. A. K. Howard and J. P. Bara, "Lime Stabilization on Friant-Kern Canal." Bureau of Reclamation, Engineering and Research Center, Report REC-ERC-76-20, Denver, Colorado, 1976.
77. C. R. Styron, "Evaluation of Rigid and Flexible Materials for Bank Protection." Investigation Report 2, Section 32 Program Streambank Erosion-Control Evaluation and Demonstration Work Unit 4 - Research on Soil Stability and Identification of Causes of Streambank Erosion, Geotechnical Laboratory, U. S. Army Engineer Waterways Experiment Station, Vicksburg, Mississippi, 1979.
78. Delft Hydraulics Laboratory, "Stability of Armorflex Block Slope Protection Mats Under Wave Attack." Report on model investigation, Delft Hydraulics Laboratory, Report M1910, the Netherlands, May 1983.
79. Tetra Tech, Inc., "Wave Tests of Armorflex Block Slope Protection Mats." Technical Report TC-3475, Pasadena, California, 1981.
80. M. P. Keown, "Utilization of Filter Fabric for Streambank Protection Applications." U. S. Army Engineer Waterways Experiment Station, Technical Report HL-80-12, Vicksburg, Mississippi, 1980.
81. G. R. Powledge and R. A. Dodge, "Overtopping of Small Dams - An Alternative for Dam Safety," Hydraulics and Hydrology in the Small Computer Age, Vol. 2, Proceedings of Hydraulics Division Speciality Conference, American Society of Civil Engineers, 1985.
82. F. Hartung and H. Scheuerlein, "Design of Rockfill Dams." International Conference of Large Dams, 10th Congress, Montreal, 1970.
83. J. Knauss, "Computation of Maximum Discharge at Overflow Rockfill Dams," International Conference on Large Dams, 13th Congress, New Delhi, 1979.
84. J. R. Dunn, E. Simantob, and H. Y. Ko, "Centrifuge Modeling of Earth Dam Overtopping." Engineering Mechanics in Civil Engineering, Proceedings of the 5th Engineering Mechanics Division Speciality Conference, American Society of Civil Engineers, Laramie, Wyoming, 1984.
85. H. Y. Ko, J. R. Dunn, and E. Simantob, "Feasibility Study of Centrifuge Modeling of Earth Dam Overtopping." Report to U. S. Army Corps of Engineers Waterways Experiment Station, Vicksburg, Mississippi, 1983.
86. H. Y. Ko, J. R. Dunn, and E. Simantob, "Study of Embankment Performance During Overtopping and Throughflow." Report to U. S. Army Corps of Engineers Waterways Experiment Station, Vicksburg, Mississippi, 1984.

87. S. P. Miller, H. Y. Ko, and R. J. Dunn, "Embankment Overtopping." Hydraulics and Hydrology in the Small Computer Age, Vol. 2, Proceedings of Hydraulics Division Speciality Conference, American Society of Civil Engineers, 1985.
88. H. Y. Ko, R. J. Dunn, and T. Hollingsworth, "Study of Embankment Performance During Overtopping-Prototype Modeling and Dimensional Verification." Report to U. S. Army Corps of Engineers Waterways Experiment Station, Vicksburg, Mississippi, 1985.
89. U.S. Department of the Interior, Bureau of Reclamation, Design of Small Dams. U.S. Government Printing Office, Washington, D.C., 1974.
90. E. W. Lane, "Progress Report on Results of Studies on Design of Stable Channels," U.S. Bureau of Reclamation, Hydraulic Laboratory Report No. HYD-352, June 1952.